The University of Adelaide

Thesis submitted for the degree of Doctor of Philosophy in Theoretical Physics

Department of physics
and
Special research centre for the subatomic structure of matter

Hadrons and Quarks in Dense Matter: From Nuclear Matter to Neutron Stars

Author:
Daniel L. Whittenbury

Supervisors:
Prof. A. W. Thomas
Prof. A. G. Williams
Dr R. Young

November 10, 2015

Contents

List of Tables

List of Figures

Signed Statement

I certify that this work contains no material which has been accepted for the award of any other degree or diploma in my name, in any university or other tertiary institution and, to the best of my knowledge and belief, contains no material previously published or written by another person, except where due reference has been made in the text. In addition, I certify that no part of this work will, in the future, be used in a submission in my name, for any other degree or diploma in any university or other tertiary institution without the prior approval of the University of Adelaide and where applicable, any partner institution responsible for the joint-award of this degree.

I give consent to this copy of my thesis, when deposited in the University Library, being made available for loan and photocopying, subject to the provisions of the Copyright Act 1968.

I also give permission for the digital version of my thesis to be made available on the web, via the University's digital research repository., the Library Search and also through web search engines, unless permission has been granted by the University to restrict access for a period of time.

SIGNED: ..... DATE: .....

Acknowledgements

It is with immense gratitude that I acknowledge the support and help of all those who have helped me in one way or another throughout my PhD studies. The research presented in this thesis would not have been possible without them.

First of all, I would like to single out my supervisor Anthony W. Thomas. Despite having many graduate students, he manages to make time for all of us. He has been an incredible teacher and I have benefited greatly from his constant support, patience and guidance.

In addition, I would also like to express my gratitude to my collaborators Kazuo Tsushima, Jonathan D. Carroll, Jirina Rikovska-Stone and Hrayr Matevosyan. Their help during the early stages of my PhD studies was invaluable to my development and I am indebted to them for all their efforts.

I must also thank Parada T. P. Hutauruk and Manuel E. Carrillo-Serrano for their friendship and helpful conversations both related to physics and not. They have been a great help.

Last but certainly not least, I would like to thank Sunny (Yuan Yang Sun) for her love, support and for just being Sunny. Somehow she has managed to put up with me throughout the duration of my PhD studies and has kept me sane, which are by no means easy feats.

Dedication

This thesis is dedicated to the memory of my mother Meredith Anne Kite (1960–2009) who impressed upon me from an early age the importance of education.

Abstract

The underlying theme of this thesis is an investigation of the equation of state of strongly interacting matter and the modelling of cold neutron stars. Particular emphasis is placed on the influence of quark degrees of freedom, which we investigate by using relativistic quark level models. More precisely, we study the equation of state for QCD matter in the zero temperature limit, from the confined hadronic phase to the deconfined quark phase.

We begin by exploring the equation of state for nuclear matter in the quark-meson coupling model, including full Fock terms. The comparison with phenomenological constraints can be used to restrict the few additional parameters appearing in the Fock terms which are not present at Hartree level. Because the model is based upon the in-medium modification of the quark structure of the bound hadrons, it can be readily extended to include hyperons and to calculate the equation of state of dense matter in beta-equilibrium. This leads naturally to a study of the properties of neutron stars, including their maximum mass, their radii and density profiles.

Next, we study deconfined quark matter using the three flavour Nambu–Jona-Lasinio model based on one-gluon exchange. The model is implemented by employing Schwinger's covariant method of proper time regularisation. Comparisons are made with the more commonly used three momentum regularised model with the t' Hooft determinant term. Hybrid equations of state are constructed using the developed Hartree-Fock quark-meson coupling and Nambu–Jona-Lasinio models. We consider the possibility that deconfinement may be a crossover transition. Using the resulting hybrid equations of state, the properties of hybrid stars are then calculated.

List of Publications

- Whittenbury, D.L., Matevosyan, H. H., Thomas, A.W. *Hybrid Stars using the Quark-Meson Coupling and Proper Time NJL Models* (in preparation)
- Whittenbury, D.L., Carroll, J.D., Thomas, A.W., Tsushima, K., Stone, J.R. *Quark-Meson Coupling Model, Nuclear Matter Constraints and Neutron Star Properties*, Phys. Rev. C **89** 065801 (2014).
- Thomas, A.W., Whittenbury, D.L., Carroll, J.D., Tsushima, K., Stone, J.R.*Equation of State of Dense Matter and Consequences for Neutron Stars*, EPJ Web Conf. **63** (2013) 03004.
- Whittenbury, D.L., Carroll, J. D., Thomas, A. W., Tsushima, K., and Stone, J.R. *Neutron Star Properties with Hyperons*, arXiv:1204.2614 [nucl-th] (unpublished).

1 Introduction

Many scientists, too many to name or even count, have contributed to our current understanding of the universe. Over the past 100 years or so, scientific research has intensified culminating in the knowledge that our universe, at its most basic level, is made up of a few fundamental building blocks governed by four fundamental forces—electromagnetic, gravitational, strong nuclear and weak nuclear. The determined struggle to make sense of these has been a long journey on a winding path paved with numerous theories and fascinating discoveries. At present, the fundamental particles and three of the four known forces can be neatly packaged in the so called standard model of particle physics. This model formulates the electromagnetic, strong nuclear and weak nuclear forces between the fundamental particles as a quantised gauge field theory. The standard model is well tested and has satisfied nearly all tests, but it is far from the last word and there are still many open problems.

Unlike the other forces, gravity has proved too difficult to incorporate into the same framework. A quantum theory of gravity is still lacking and is likely to be so for some time. In most circumstances in particle physics, this is not a concern as its influence on the particles is negligible. Thus gravity can generally be safely ignored. It typically only becomes necessary to consider gravity on macroscopic scales. However, there are places in our universe where all four fundamental forces play an important role, an example of such a place is inside neutron stars. These are fascinating objects where matter interacts under remarkably extreme, yet stable conditions. They will play a starring role in this thesis.

Classically, gravity appears to be reliably described by the general theory of relativity. Among other things, this force is responsible for shaping galaxies. However, the theory has only been rigorously tested on the scale of the solar system. Early last century observational data indicated a deviation from expected galactic rotation curves. This led to the development of two contrasting ideas, namely non-luminous (dark) matter and modified theories of gravity. Both have been suggested as a solution to the problem. Since, there has been a large amount of observational evidence in

support of the existence of dark matter, it has also been interpreted by some that our theory of gravity may need to be modified (or possibly even both). In direct detection experiments so far, no beyond the standard model dark matter candidates have been found but the search is far from over. In 2015 the Large Hadron Collider (LHC) is gearing up for another run at even higher energies. The discovery of beyond the standard model physics at the LHC would be ground breaking, it could potentially shed light on long standing open problems in particle physics, astronomy and cosmology. The physics community is eagerly waiting to see what they ferret out.

In this thesis we will not consider extensions of the standard model or modifications of gravity. We will be interested in systems described by the strongly interacting sector of the standard model, particularly at finite density. We also assume that for macroscopic extrapolations of such systems that general relativity is adequate in describing their gravitational interaction.

Quantum Chromodynamics (QCD) describes the strongly interacting sector of the standard model. Developing a complete and rigorous understanding of this perplexing theory, including all of its emergent phenomena, is by far the most challenging problem confronting nuclear and particle physicists today. Its solution has thus far proved extremely difficult to deduce, even more complex than Quantum Electrodynamics (QED). The only first principles approach to study QCD is Wilson's lattice gauge theory, where QCD is simulated on a Euclidean space-time lattice. Much has been learnt using this approach, but its application to systems at finite density is still problematic, because of the notorious fermion sign problem. This problem originates from the fermion determinant not giving rise to a positive definite probability, essentially rendering standard Monte Carlo simulation techniques useless. There have been some attempts to extend the simulations by expanding about zero baryonic chemical potential, but only very limited progress has been achieved in this direction.

The force carrier of QCD, the gluon, carries colour charge unlike the photon in QED which is charge neutral. This seemingly simple difference is at the heart of the additional complexity of QCD. The non-linear interactions which ensue from the gluon carrying colour charge are responsible for asymptotic freedom, whereby at large momentum transfer or equivalently short distances the coupling parameter becomes small. The perturbative techniques which were instrumental in the predicative success of QED only become applicable in this limit. At lower energies the coupling grows and quarks and gluons become confined in colour neutral bound states. The exact way in which this occurs is unclear. These hadrons are the smallest level of structure and in experiment they are what we actually detect.

Despite quarks and gluons being confined and never seen directly in experiment their existence has been inferred in Deep Inelastic Scattering (DIS) experiments. At CERN in 1982, the European Muon Collaboration (EMC) performed DIS experiments to determine the $F_2(x)$ structure function of iron. They found, contrary to conventional reasoning at the time, that it significantly deviated from the $F_2(x)$ structure function of the deuteron, indicating that quark structure of the nucleons is sensitive to the nuclear environment. This revelation begs the question, if quarks are affected by the nuclear environment, to what extent do quarks and gluons influence traditional nuclear physics? This spurred considerable experimental and theoretical research aimed at

linking conventional nuclear physics with QCD.

When presented with a new form of matter determining its thermodynamic behaviour is of central importance. This includes exploring and characterising its phase diagram and ascertaining its Equation of State (EoS). The phase diagram of QCD matter[1] is commonly characterised by its temperature, T, and baryonic chemical potential, μ, or in some cases by the pressure, P. This two dimensional phase space has been extensively studied using different methods from lattice QCD to phenomenological models. Yet it is still not very well understood. Only portions of the diagram are satisfactorily described by theory and accessible to experiment. In particular, the area where dense matter resides is largely unknown.

The phase diagram is meant to show what distinct phases occur in thermal equilibrium under certain physical conditions. As alluded to above, what we have observed in experiment, are quarks and gluons confined to hadrons such as mesons and baryons. However, as temperature and density increase, hadronic matter may transition to a deconfined phase in concordance with asymptotic freedom.

The EoS, on the other hand, is a thermodynamic relation between state variables describing a state of matter under a set of physical conditions. It is essential input and completely indispensable for understanding processes which occur in heavy ion collision experiments, the evolution of the early universe just after the big bang, core collapse supernovae and the properties of neutron stars.

Quantum chromodynamics exhibits complicated emergent phenomena, confinement is one, Dynamical Chiral Symmetry Breaking (DCSB) is another. Most notably, the latter is responsible for the majority of mass seen in our universe. These two phenomena can be used to define several distinct phases. At low temperature and density, we know quarks and gluons are confined. This defines the hadronic phase. If at some point in the QCD phase diagram they become deconfined, forming a quark-gluon plasma, this defines a second phase. Here the effective degrees of freedom define two distinct phases. This is not to say they cannot coexist in a mixed phase. Likewise chiral symmetry can be used to define two distinct phases, the broken phase and the restored (or approximately restored) phase. Chiral and deconfinement transitions may not coincide and other phases, such as superconducting phases of matter, may also exist.

Lattice QCD has been instrumental in understanding the low density region ($\mu \sim 0$) of the phase diagram. A chiral transition has been supported by a number of different simulations performed by various groups. These numerical studies have indicated that the restoration of chiral symmetry is not an actual phase transition, but rather a crossover. They find at high temperature and low density, that the quark condensate, i.e., the order parameter of chiral symmetry, rapidly and continuously approaches zero. The consensus is that a transition occurs at high temperature $T_c \sim 155$ MeV. However, as it is a crossover transition, the exact location of the transition is somewhat ambiguous.

On the opposite end of the scale, at low temperature and finite density, where we do

[1] In using the term *QCD matter*, we wish to make it clear that, we use it as a collective term for strongly interacting matter, which has as its most elementary degrees of freedom quarks and gluons. As such, it not only refers to quarks and gluons, but also to finite nuclei and a hypothetical form of matter called nuclear matter.

not have asymptotic freedom, the situation is very complicated. However, this portion is experimentally accessible, allowing us to develop effective and phenomenological models. Making comparisons to experimental data allows us to improve upon them.

Given the complicated nature of QCD, hadrons have been used to develop effective and phenomenological models of QCD. Nuclear physics employed these degrees of freedom long before the advent of QCD, amassing an incredible wealth of knowledge about the strong interaction at low and intermediate energies. In contrast to lattice studies, it is found at finite density using different phenomenological models that the chiral transition is first order. It is commonly thought that in the interior of the QCD phase diagram there will be a critical end point, where the transition to the chirally restored phase becomes second order. The location and existence of such a critical point is extremely model dependent. For example, in the NJL model with vector interaction, it is found that on increasing the vector coupling the critical point is shifted closer to the μ axis, i.e., to lower temperature.

Experimentally, nuclear structure experiments give us information at low temperature and density, mostly around the saturation density ($\rho_0 = 0.16\ \mathrm{fm}^{-3}$). The only way to probe the higher densities in a laboratory setting is in Heavy Ion Collisions (HIC), where nuclei collide, momentarily forming very hot and dense matter. The matter formed in these experiments only has enough time to develop equilibrium with respect to the strong interactions, but not weak equilibrium. The only place in the universe where complete thermal equilibrium is likely to form (or at least approximately) is in the interior of neutron stars. Signatures of a deconfinement phase transition have been searched for in heavy ion collisions at CERN and RHIC, but the findings have so far been inconclusive. With the commissioning of new rare isotope beam facilities, probing higher densities and greater isospin asymmetries will occur yielding further information on the high density behaviour of strongly interacting matter. This will provide crucial information on the density and isospin dependence of nuclear forces.

Experimentally accessing dense matter at low temperature is not currently possible. Knowledge of this region of the phase diagram would allow for a more complete understanding of QCD and the strong nuclear force. Neutron stars provide us with access to this region, their densities are far greater than what we are currently capable of maintaining here on Earth in a laboratory. They can be thought of as a kind of laboratory which can be used to test, constrain and understand effective and phenomenological models of QCD. They can easily be used in this way as neutron stars have observables such as mass, radius, photon red-shift, temperature, cooling rate, angular velocity and moment of inertia, which can be observed (or inferred) and then compared to a calculated value within a chosen model.

In this approach, one starts with models which are constrained by experimental evidence at low density and extrapolate out to higher densities. Caution needs to be taken when extrapolating a chosen model out to higher densities, possibly pushing it out of its range of validity. This is where astrophysical observations become important. The idea is not to just compare calculations with observations to either support or refute them, but rather to use these observations to try and understand the physics involved in dense matter. That is, to understand how the strong force works in dense matter.

As matter is compressed, the fundamental degrees of freedom become increasingly more important. It is commonly thought that the densities reached in the inner core of neutron stars may be sufficient to produce a phase transition to some form of deconfined quark matter. Neutron stars are incredibly complex and a complete understanding has not yet been achieved. In their study one must draw upon many branches of physics, the most important of which are nuclear physics and general relativity.

Moreover, neutron stars are fascinating objects in their own right, containing matter under extreme conditions. As such they warrant in-depth study. With the development of new radio astronomy facilities, such as the Square Kilometre Array (SKA); and gravitational wave detectors, such as LIGO, advanced LIGO and VIRGO; it is important to maintain theoretical research efforts to complement and inform observation. These future tools will provide new information on neutron stars and hence also QCD.

Throughout this thesis, we will focus on the calculation of the EoS of dense QCD matter at zero temperature. In this region of the phase diagram, QCD is too difficult to solve exactly. Without some new deep physical insight allowing a simplification of the QCD equations, we must resort to effective and phenomenological models. As phenomenological approaches have proved useful in the past, we will be using this approach.

A realistic model should be inspired by QCD, incorporating its key symmetries, emergent phenomena and of course encompassing the great wealth of empirical information obtained through over 100 years of nuclear physics research. Ideally it should be derived from or have as much in common with QCD as possible. To this end we develop and employ two different models. Both models embody QCD in different asymptotic limits, one in the confined hadronic region and the other in the deconfined quark region.

We use an improved version of the Quark-Meson Coupling (QMC) model for modelling hadronic matter. Previous versions of this model have had impressive success in predicting properties of nuclear matter, finite nuclei and neutron stars. The QMC model is one of the most realistic phenomenological models available—it is relativistic, includes quark degrees of freedom, and incorporates confinement by modelling hadrons with a bag model. The version of the QMC model that will be used in this thesis will include the effects of hyperons and the four lightest mesons (σ, ω, ρ and π), Fock terms, form factors and the effect of the tensor interaction of the vector mesons. Baryons will be modelled using the one gluon exchange version of the bag model, which has been shown to be important for hyperon hyperfine mass splitting.

In the quark phase, we employ a three flavour Nambu–Jona-Lasinio (NJL) model incorporating a vector interaction. The NJL model is an effective low energy model of QCD, where gluons are integrated out leaving quarks to interact locally in a four Fermi like contact interaction. It incorporates many of the symmetries of QCD, such as chiral symmetry and its breaking, but it is much easier to calculate with than QCD. However, the NJL model is not in general confining[2], although it is covariant and incorporates DCSB. In this way, the QMC and NJL models are complementary to each other. In this thesis, Schwinger's proper time method is chosen to covariantly

[2]An NJL model incorporating an infra-red cut-off allows for a crude definition of confinement, see Ch. 6 and references cited therein.

regularise the model. For comparative purposes, we also consider the extensively used three momentum regularised model with t' Hooft determinant term.

This thesis extends previous work on the EoS of strongly interacting matter by considering the role of quark degrees of freedom at finite density, using the models mentioned above, and studying the properties of neutron stars. This thesis is organised as follows: In Ch. 2, we prepare the reader for subsequent chapters by reviewing the main results of nuclear physics and QCD relevant to the problem at hand. A quick run-through of the properties of the NN interaction as determined from early nuclear physics through to modern day experiment and theory. The underlying ideas and features of QCD are summarised. Then we introduce the hypothetical and idealised form of matter called nuclear matter. A brief discussion of experimental and theoretical knowledge of its EoS is presented. Finally, we introduce Quantum-Hadrodynamics (QHD) and the QMC model, and define their Mean Field Approximation (MFA). In Ch. 3. the application of general relativity to neutron stars and their connection to the EoS is discussed.

In Ch. 4, we begin the main part of this thesis by considering the hadronic phase, exploring the equation of state for nuclear matter in the QMC model, including full Fock terms, i.e., both the Dirac and Pauli terms are taken into account. We include a full derivation of the Fock terms and explain in detail all approximations used. We then investigate the EoS of symmetric and asymmetric nuclear matter. The comparison with phenomenological constraints can be used to restrict the few additional parameters appearing in the Fock terms which are not present at Hartree level. Because the model is based upon the in-medium modification of the quark structure of the bound hadrons, it can be readily extended to include hyperons, allowing hyperon optical potentials and the EoS of dense matter in beta-equilibrium to be calculated. This leads naturally to a study of the properties of neutron stars in Ch. 5, including their maximum mass, their radii and density profiles. We take the point of view that the uncertainty in modelling neutron stars resides in the EoS and not in the form of a modified theory of gravity. To calculate the properties of neutron stars we solve the Tolman-Oppenheimer-Volkoff equations as derived within the framework of general relativity from Einstein's equation. Moreover, even though neutron stars are far from being at zero temperature their temperature has a negligible effect on their properties. The matter of a typical neutron star is considered to be insensitive to the temperature, because it is small in comparison to the chemical potentials of the constituent particles.

In Ch. 6, we introduce the NJL model, discuss its main features and its connection to QCD. A simple explanation of the MFA for the NJL model is discussed. A Fierz invariant NJL Lagrangian is derived based on one-gluon exchange. The MFA to the Fierz invariant NJL model is presented in the path integral formalism, deriving the NJL effective potential and gap equation. Pion phenomenology is used to constrain the few model parameters and then numerical results are presented for pure quark matter as function of chemical potential, flavour symmetric quark matter and quark matter in beta-equilibrium with leptons. In Ch. 7, we investigate the possibility of a phase transition between the Hartree-Fock QMC and NJL models developed in earlier chapters. We conclude in Ch. 8 with a summary and a discussion of possible future work in this field of research.

Considering the multidisciplinary nature of this area of research we have as an additional aim of this thesis, strived to write in a pedagogical manner, including sufficient background, detail and numerous references to both textbooks and relevant research papers. This was done in the hope that it will be useful to future students that wish to enter this field of research.

2

From Nuclear Physics to QCD and Back Again

This chapter contains a short and concise review of relevant information in the literature pertaining to nuclear physics and Quantum Chromodynamics (QCD). In the next chapter its application and relevance to neutron stars will be discussed. Here we present well known material, preparing the reader for the following chapters. Its aim is to place this dissertation in the correct context.

We start by reviewing the basic notions of early nuclear physics and the properties of the nucleon-nucleon (NN) two-body interaction. Emphasis will be placed on nuclear physics in the era of Quantum Chromodynamics (QCD). In particular, the mean-field approach to the non-perturbative regime of QCD (i.e. nuclear physics) will be reviewed.

2.1 NN Interaction and Early Nuclear Physics

The field of nuclear physics has now been around for over 100 years. It began with Rutherford studying the emitted particles of radioactive substances [1]. His research was directed mostly towards the nature and properties of alpha particles, eventually proving them, with Royds, to be helium nuclei [2]. Once he obtained an understanding of these particles he used them to probe the structure of atoms, ultimately proposing in 1911 [3] the existence of a positively charged nucleus based on the experimental results of Geiger and Marsden [4], who scattered alpha particles off metal foils. From the scattering experiments it was determined that the nucleus must be small, and that the range of the strong interaction is of the order of a few fermis. Since those early days, a great deal has been learnt about nuclei and the strong nuclear force holding them together. Despite not being completely understood, that is possessing a complete, coherent and theoretically satisfying formulation and still an on-going avenue of intense research, nuclear theory and its experimental techniques have been applied to many

diverse areas with applications to: studies of fundamental interactions, compact stars, and the beginning of the universe—just after the big bang; diagnosis and therapy for cancer patients; power generation and sadly the development of weapons of mass destruction.

We wish to stress the most important features of the strong nuclear force. The majority of the early knowledge of the strong nuclear force was obtained by analysing the low energy scattering of two nucleons and by experiments involving light nuclei. The purpose of these studies was to develop a potential description of the two-body NN interaction, which could be used to understand nuclear systems at a more fundamental level. The experimental information on the two-body interaction that was available mostly consisted of cross sections and empirically extracted phase shifts of various partial waves for NN scattering and the bound state properties of the deuteron. A potential description extracted from this two-body information can then be used in describing the few-body systems such as triton, helion and helium nuclei. In this way one can try to determine to what degree one can ignore the three-, four- and in general many-body forces. Discrepancies between calculations of few-body systems and experimental results can indicate a need for either an improved potential or inclusion of many-body forces. From experiment it was learnt that the strong nuclear force has the following features: strong intermediate range attractive force with a short ranged repulsive core, charge conjugation C, parity P and time reversal T invariant, approximate charge symmetry[1], approximate charge independence[2], spin dependent[3], and many-body forces are important. We will now elucidate these features in more detail. It is important to note that, almost all of the early attempts to describe the strong nuclear force were phenomenological. In this approach, one tries to develop a mathematical form for the force that satisfies the known empirical properties.

The constituents of the nucleus, now known to be protons and neutrons, differ in charge and quark structure. If one neglects their structure, the electromagnetic interaction and the small mass difference between them, they can be interpreted as two degenerate states of the same particle, the nucleon N. This nucleon was originally proposed by Heisenberg who described its two states using Pauli's spin matrices, in what would become known as isospin formalism. This is possible, because of the approximately equal masses and approximate charge independence of the strong force. This symmetry, which essentially counts the number of charge states that are equivalent under the influence of the nuclear force, is known as isotopic, isobaric or isospin symmetry, in analogy with spin. The approximate charge symmetry and independence of the nuclear force is translated into this isospin symmetry. A convenient description of symmetries is provided by group theory in which the corresponding symmetry group is $SU(2)$. It is not a fundamental symmetry, but rather an approximate one, which is very well realised in nature and has far reaching consequences in all of hadronic physics. A system with isospin symmetry means that the strength of the interaction is invariant under rotations in the abstract isospin space. This means that the interaction

[1]Excluding the electromagnetic interaction, the force between pp is the same as between nn.

[2]Excluding the electromagnetic interaction, the force between pp is the same as between nn and also np.

[3]Tensor and spin-orbit contributions are important.

between nucleons is independent of whether it is between neutrons and neutrons (nn), or protons and protons (pp) or even neutrons and protons (np). This interaction has an attractive component as can be inferred by the observational fact nuclei are bound systems of these nucleons, which indicates the nuclear force must be attractive in some range.

Theoretical arguments and experimental support for charge symmetry and independence came in the mid 1930s. Among the earliest suggestions was from Young [5] who argued on the basis of nuclear binding and the number theory properties of stable nuclei that not only np bonds are important, but also nn and pp are as well. He argued that the binding energy is proportional to A not Z and that strong attractive interactions exist between neutrons and to maintain balance within the nucleus they must also exist between protons.

The deuteron is a very important piece of the two nucleon interaction puzzle. It is the only bound two nucleon system and thus demonstrates that the np interaction must be attractive. Furthermore, the deuteron has a non-zero quadrupole moment [6] of positive sign indicating a prolate spheroidal charge distribution. The non-zero quadrupole moment implies that the NN interaction is not central. Through arguments based on angular momentum and parity of the deuteron ($J^\pi = 1^+$), the ground state of the deuteron must be an admixture of ${}^3S_1$ and ${}^3D_1$ states. A tensor component in the NN interaction can account for such an admixture and is generally a significant component of most modern NN potentials.

The pp scattering experiments of White [7] and the improved experiments of Tuve *et al* [8, 9] indicated that there was an attractive pp interaction at close distances ($< 5 \times 10^{-13}$m) deviating from the repulsive electromagnetic interaction. The data from the latter experiment was analyzed further by Breit *et al* [10] and showed that for the ${}^1S$ state pp and pn interactions were the same within the experimental error.

It was during this period (1935) that Yukawa [11], made his famous mesotron (meson) hypothesis. His hypothesis was that a massive particle of mass intermediate between the electron and the proton was mediating the strong interaction, like the photon for the electromagnetic interaction. Yukawa realised that the range of the interaction was correlated with the mass of the exchanged particle and estimated it's mass to be around $\sim 200m_e$. The meson hypothesised was a scalar and it was later realised by Pauli [12] that it needed to be of pseudo-scalar nature to give the correct sign for the deuteron quadrupole moment, which was later confirmed by experiment (spin and parity measurement). This was the first really fundamental idea to appear in nuclear physics and in 1937 the muon was discovered in cosmic radiation observations [13, 14] and misinterpreted as Yukawa's meson. Ten years passed and the real pion was eventually found in cosmic background radiation [15, 16] and then soon after in experiment at Berkeley [17] and Bristol [18]. This brought support for the idea that the strong interaction was mediated by a massive particle and for the following decade the pion played the starring role.

The following decade (1950s) saw the development of pion theories concentrating on one and two pion exchange. The strong force appeared to be considerably more complicated than other forces previously studied. To handle the additional complexity

Long range: "Outer" or "Classical" $r \gtrsim 2$ fm

Intermediate range: "Dynamical" 1 fm $\lesssim r \lesssim 2$ fm

Short range: "Core" or "Phenomenological" $r \lesssim 1$ fm

Figure 2.1.1: Division of configuration space into three regions.

Taketani *et al* [19] advocated a division of the range of the nuclear force into two separate regions, the inner region to be treated phenomenologically due to the complicated nature and many contributing effects; and the outer region treated by meson exchange. The subdivision was later extended to three regions [20], which has proved to be very useful and is still in use today. This division is summarised in Fig. 2.1.1.

As the deuteron is a weakly bound system, it is mostly affected by the outer region. Thus subsequent works studied the properties of the deuteron ground state and low energy np scattering, finding that a pseudo-scalar pion potential described the experimental data rather well and that the one-pion exchange (OPE) is dominant in the outer region [19–28]. It has also been established that two-pion exchange becomes important in the intermediate region. For the innermost region, presumably many effects become important, such as multi-pion; heavy meson; quark and gluon exchanges. The two-pion exchange which becomes important in the intermediate region, contains difficulties and ambiguities which led to conflicting results. The two different approaches, of Taketani *et al* [24] and Brueckner and Watson [29] developed at the same time are discussed in [30] and [31].

Around this time NN scattering was being analyzed indicating that a strong, short–range spin-orbit interaction was also necessary to describe the experimental data [32–34], particularly in accurately describing polarization data. Two-pion exchange could not provide a sufficiently large spin-orbit potential required by the analyses. Gammel and Thaler suggested that this short range spin-orbit potential may originate from the exchange of a meson heavier than the pion. Subsequently, it was proposed by several authors that a heavy neutral vector meson arising from 3π exchange could be the natural explanation for the spin-orbit potental and short range repulsion. Not long after in 1961, the omega (ω) meson was discovered [35] followed by the rho (ρ) meson [36] the following year. The experimental discovery of vector heavy mesons, spurred the beginning of one boson exchange (OBE) models. These models assumed that the multi-pion exchanges could be well represented as resonances from multi-pion scattering, drastically simplifying calculations and indicating why multi-pion exchange theories of the 1950's did not do well, the absence of correlated (resonant) pion exchange [37].

More and more particles (K, Roper,...) were being discovered in particle accelerators and bubble chambers. It was eventually deemed that not all of these particles could be fundamental. Quark and parton models were appearing and the stage was being set for the appearance of a new more fundamental theory, Quantum Chromodynamics (QCD). The description of the strong nuclear force was changing to a description of

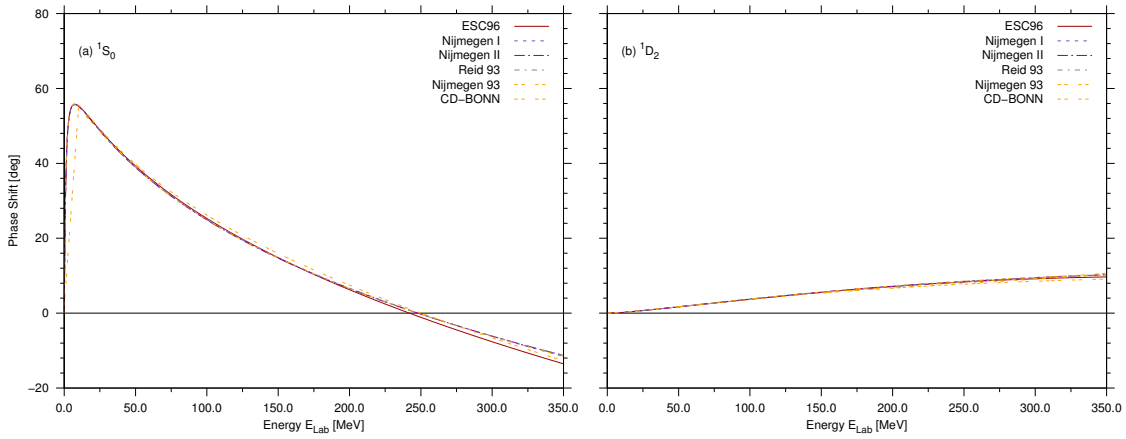

Figure 2.1.2: Phase shifts versus energy for (a) $^1S_0$ and (b) $^1D_2$ partial waves. Data obtained through NN-Online [40] and INS DAC [41] on 7/2/2014.

quark and gluon dynamics where the residual interaction between between hadrons can be viewed as a kind of Van der Waals force in analogy to molecular interactions. The first steps in this direction were by Gell–Mann [38] and Zweig [39], with the development of the eightfold way and constituent quark models. QCD which was developed by Gell–Mann and others as a local gauge theory of colour has now become the leading theory for describing the strong interaction, relegating all meson exchange theories to the status of phenomenological models. The formidable task of describing the NN interaction from the underlying quark and gluon dynamics is of great importance, but without some new deep physical insight to handle the QCD equations of motion one must seriously consider effective and phenomenological models, especially those which preserve the most important underlying features of the theory. Limited progress has been achieved from first principles in the non-perturbative regime. QCD will be reviewed in Section 2.2.

Over time massive amounts of data have been collected from pp and pn scattering experiments. Low energy data is well suited to partial wave analysis, because fewer partial waves are needed. Analysis of this data in terms of phase shifts of partial waves has lead to the conclusion that at low energies the NN potential is attractive, this is easily seen in Fig. 2.1.2 as the S-wave phase shift is positive. At higher energies the potential becomes repulsive as the phase shift changes sign at about 250 MeV. This is followed by many higher partial waves at even higher energies indicating a repulsive core.

The repulsive core was suggested by Jastrow [42–44] to explain the isotropy seen in pp scattering cross section between 20°–90°. His interaction potential was the only one at that time that was consistent with the charge independence hypothesis. The S-wave state is most influenced by the introduction of a repulsive core because of the absence of angular momentum barrier. The hard core causes a change in sign of the phase shift. The higher partial waves are relatively unaffected until higher energies are reached. The D-wave and other even parity states will still mostly be influenced by

the attractive part of the potential in the 0–350 MeV energy range and hence their phase shifts remain positive. The cancellation between these phases decreases the anisotropy seen without the repulsive core. It was suggested that the attractive part was associated to the pion and the repulsive part with a heavier meson. Unfortunately, detailed information about the repulsive core is unavailable because of the limited data above $\sim$ 350 MeV and the absence of an unambiguous determination of the phase shifts.

Much more can be learnt about the NN potential from partial wave analysis besides the appearance of a repulsive core at short distances. One can also infer spin-orbit and tensor contributions to the nuclear potential. The spin-orbit interaction is particularly evident when considering the ${}^3P_{0,1,2}$ partial waves. If the force was purely central then ${}^3P_{0,1,2}$ would be essentially the same and would not reproduce the observed splitting. An attractive spin-orbit force can give the correct splitting in these partial waves producing repulsion for ${}^3P_1$ and attraction for ${}^3P_2$ [30]. To accurately reproduce these phase shifts the tensor interaction is also required [30].

In the 1960s deviations from charge symmetry and independence were beginning to be studied by Wong and Noyes [45], Heller *et al* [46], Henley and Morrison [47] and Biswas *et al* [48]. Wong and Noyes concluded that measurement of the nn scattering length (a_{nn}) would give a sensitive quantitative test of charge symmetry, because in a charge symmetric theory $a_{nn} = a_{pp}$ and a charge independent theory $a_{nn} = a_{pp} = a_{pn}$. Studies during this period indicated that charge symmetry was better realised in nature than charge independence.

Various phenomenological potentials were developed throughout the decades to understand the nuclear force. Model parameters were constrained by analyzing two-body NN scattering data with kinetic energies in the range 0–350 MeV along with the properties of light nuclei. That is, the NN potential was inferred from this information by performing a fit. There are numerous phenomenological potentials ranging from early attempts to modern day potentials which are very accurate, being fitted to large sets of NN scattering data and deuteron properties, achieving a χ^2 per degree of freedom of about 1. A few of the more historically significant and modern potentials are: Gammel–Thaler [49], Hamada–Johnston [50], Yale [51], Paris [52], Reid [53], Argonne V14 [54], V18 [55], Nijmegen [56], Bonn [37], and its charge dependent variation CD-BONN [57].

Ambiguity in the determination of the NN interaction is emphasised by the existence of a number of very accurate and essentially phase shift equivalent potentials, each of which has a rather different origin, —see, for example, the phase shifts for partial waves ${}^1S_0$ and ${}^1D_2$ in Fig. (2.1.2). The potentials which utilise a meson exchange picture of the NN interaction, like the Bonn, Nijmegen or Paris potentials, deserve a special mention, as even with the advent of QCD, meson exchange potentials can be well motivated from the point of view of effective field theory. In this context, the nucleons and mesons, the low-energy degrees of freedom, are being used to describe the low-energy physics. Meson exchange models provide a convenient way to describe many of the features of the strong interaction in an effective way. For instance from direct analogy with QED, the ω meson, a massive neutral vector meson, would produce a short range (due to its mass) spin-orbit potential. The spin-orbit force in the NN

interaction is considerably stronger than that felt by an electron in an atom and in nuclei it is strongest near the surface [58]. It is strongest near the surface, because a nucleon in the interior of the nucleus feels an equal number of spin up and spin down nucleons all around it, except near the surface [58]. Thus, it is important for finite nuclei but of little importance for infinite nuclear matter where surface contributions are ignored. The latter form of matter will be the focus of this thesis. The tensor interaction comes predominately from the π and ρ meson exchanges with very little from the ω meson.

As discussed previously, pions being the lightest mesons describe the outer region, whereas the heavier mesons describe the intermediate and short range regions. However, as one probes shorter and shorter distances by increasing the scattering energy there is a need to describe the inner hard core of the potential more accurately. As the scattered nucleons approach one another they can overlap and one is then faced with the conceptual problem of going from a purely meson exchange model where the hadrons are treated as point particles to incorporating both the quark substructure of the hadrons and their short range interactions within and between the colliding nucleons as arising from the underlying quark-gluon dynamics. The inner region is generally handled either entirely phenomenologically or by artificially suppressing meson exchanges using form factors. The suppression of the meson exchanges is motivated by the finite extent of the nucleon. In NN scattering one-gluon and quark exchange effects have been considered by some [59–62], but their effects are generally neglected even in high precision potentials and are assumed to be incorporated phenomenologically into the parameters of the model. Only when considering Δ excitations and particularly the extension of the two-body interaction to three-, four- and more generally many-body interactions is nucleon substructure considered in more detail. Conventionally, one uses a two-body potential possibly supplemented with a model for the three- or more-body forces as input into a many-body formalism such as Dirac–Brueckner–Hartree–Fock (DBHF) [63–65], Brueckner–Hartree–Fock (BHF) [66–72], variational methods [73, 74], correlated basis function methods [75, 76], self consistent (SCGF) models [77, 78], quantum Monte Carlo techniques [79–83] and chiral effective field theory [84, 85].

Many-body forces have been shown in a number of studies to be important to the description of nuclear systems. As a particular example, a Green's function Monte Carlo method with the Argonne AV18 two-body potential supplemented with a three-body force derived from pion exchange was used by Pieper *et al* in Ref. [86]. In this work, nucleon substructure was minimally included in the form of Δ excitations. They demonstrated the importance of these three-body forces for producing the correct binding in nuclei. More specifically, nuclei were found to be underbound, with their underbinding increasing with mass number. The three-body force was found to be a significant factor in predicting the experimental value. Moreover, it has been stressed that many-body forces can result in increased pressure in pure neutron matter [87]. The latter is an important first approximation to the material in the core of neutron stars. These additional contributions from three-body forces can have important consequences for the stability of neutron stars.

Mean-field methods offer an attractive alternative to the above methods presenting several desirable characteristics, particularly their computational simplicity and

applicability to larger systems. In fact, the mean-field approximation becomes more reliable with increasing density [58]. Both non-relativistic and relativistic mean-field models have been developed. Two of the most notable non-relativistic mean field models are the Skyrme and Gogny interactions, the former employs an instantaneous zero range contact interaction, whereas the latter incorporates a finite range. As for the relativistic models, one begins with an effective Lagrangian and uses it directly. In this thesis we will use this methodology to investigate the properties of nuclear matter and neutron stars. A relativistic quark level model, which treats baryons as a colour–singlet, confined cluster of three quarks, will be utilised. Moreover, this model naturally incorporates many-body forces through the in–medium modification of the internal structure of the baryons. The calculations will be performed at a level of approximation such that the effects of pions and the tensor interaction as arising from the exchange of vector mesons will be incorporated.

2.2 Basic Notions of Quantum Chromodynamics

In this section, we wish to review the essential background material regarding quantum chromodynamics (QCD) with emphasis on its place in the standard model of particle physics and its gauge and chiral symmetries. We refer the interested reader to more complete discussions of QCD, particularly Ref. [88] and [89].

QCD is one of three components comprising the standard model of particle physics. It is the component which describes the strongly interacting sector and is responsible for the majority of mass seen in our universe. The remaining two components of the standard model are described by electroweak theory, which is the amalgamation of quantum electrodynamics (QED) with the Glashow-Weinberg-Salam theory of the weak interactions. This "standard model" has been around for forty odd years and has passed every experimental test to date.

The Lagrangian of the standard model has the local gauge symmetry $SU_c(3) \otimes SU_L(2) \otimes U_Y(1)$ and has approximately 19 parameters. Even with the experimental successes of the standard model, at a fundamental level it cannot be considered complete. The standard model is not fully satisfying as a theory due to several deficiencies. The most self-evident deficiency is that it does not include a quantum theory of gravitation. Moreover, it is formulated in a rather cut and paste manner. In particular, it must be extended to explain massive neutrinos and their oscillations; and the scalar boson (Higgs) sector, so crucial to electroweak theory is also included in a rather ad hoc manner in contrast to the gauge bosons, which arise from gauge principles. As it stands today, it is a very accurate theory, but there is certainly more interesting physics and mathematics lurking beyond this model. Many suggestions for physics beyond the standard model are littered throughout the literature, but we will not discuss these possibilities.

QED is the archetypical quantum field theory. It was developed during the period 1927 to around 1950 by Feynman, Dyson, Schwinger and Tomonaga. It predates QCD by several decades and was a fruitful template for developing the more intricate quantum field theories making up the standard model. In fact, to go from QED to QCD no fundamentally new principles are needed, just the familiar requirements of

Property	Up	Down	Strange	Charm	Bottom	Top
Symbol	u	d	s	c	b	t
Q	2/3	-1/3	-1/3	2/3	-1/3	2/3
B	1/3	1/3	1/3	1/3	1/3	1/3
I_3	1/2	-1/2	0	0	0	0
Mass	0.002–0.008	0.005–0.015	0.1–0.3	1.0–1.6	4.1–4.5	180 ± 12

Table 2.2.1: Quark properties [91], masses are in units of GeV.

causality, unitarity, gauge invariance and renormalizability.

Agreement between experiment and QED is impressive. The anomalous magnetic moment of the electron is known to agree with theory to many significant figures. It does not get much better than this for a confirmation of a theory. There are other tests of this theory that have also had impressive results, such as the Lamb shift and the quantum Hall effect in condensed matter. The theory of QED is tried and tested and its impressive successes are well known. This is an ideal template to use as a starting place to describe the strong nuclear force.

2.2.1 QCD Lagrangian and its Symmetries

QCD is based on the same guiding principles as QED—causality, unitarity, gauge invariance, and renormalizability. It is the theory describing the dynamics of coloured quarks and gluons, as proposed by Gell-Mann [38], Zweig [39], Neeman [90] and others during the 1960s–1970s. The starting point for gauge field theories, such as QCD, is to construct a Lagrangian density which is invariant under the local gauge group such that it preserves the above mentioned requirements. The gauge group of QCD describing colour is the non-Abelian group $SU(3)_c$. Its non-Abelian nature introduces new complications absent in QED leading to fascinating emergent phenomena. We will not delve too deeply into the historical developments of QCD here, instead we wish to simply review its formulation in terms of quarks and gluons, followed by a discussion of its symmetries and emergent phenomena.

Quarks are spin–1/2 fermions and come in 6 flavours: up, down, strange, charm, bottom and top. They are massive and carry fractional baryonic and electromagnetic charge. Their properties are summarised in Table 2.2.1. Gluons on the other hand are massless vector bosons—one associated to each generator of the gauge group. Both quarks and gluons carry colour charge, so in contrast to photons in QED, gluons interact with each other. This is due to the fact that the gauge group is non-Abelian. In the case of the resonance $\Delta^{++} = |u\uparrow u\uparrow u\uparrow\rangle$ the additional colour degree of freedom allows for the preservation of the Pauli principle in the quark model, without which it would be violated.

To construct the QCD Lagrangian density, we need a covariant kinetic term for quarks and gluons and a mass term for the quarks. The quarks are in the fundamental representation of the colour gauge group and the gluons are in the adjoint representation. In contrast to electroweak theory the gauge group is not broken, so the gluons remain massless. The fermionic quark field $q = (q_{fc})$ has a flavour index $f \in (u,\ d,$

s, c, b, t), and a colour index $c \in (r,\ g,\ b)$. Each q_{fc} is a 4-component Dirac spinor. Explicitly,

$$q = (q_{fc}) = \begin{pmatrix} q_{uc} \\ q_{dc} \\ q_{sc} \\ q_{cc} \\ q_{bc} \\ q_{tc} \end{pmatrix} = \begin{pmatrix} q_{fr} \\ q_{fg} \\ q_{fb} \end{pmatrix} \quad . \tag{2.2.1}$$

This quark field transforms under the gauge group as

$$q(x) \to q\,'(x) = \Omega(x) q(x) \quad , \quad \Omega(x) \in SU(3)_c \ . \tag{2.2.2}$$

To define a gauge invariant kinetic term for the quarks, we define a covariant derivative

$$D_\mu = \partial_\mu - igA_\mu(x) \ , \tag{2.2.3}$$

where g is a dimensionless coupling. For the gauge field $A_\mu(x)$ we can choose a basis $\{T^a\}_{a\in(1,\ldots,8)}$ such that $A_\mu(x) = \sum_{a=1}^{8} A^a_\mu(x) T^a$, where T^a are the generators of the gauge group and are usually given in terms of the Gell-Mann matrices $T^a = \dfrac{\lambda^a}{2}$. The gauge fields $A_\mu(x)$, like the Gell-Mann matrices, are 3×3 traceless hermitian matrices, which transform under the gauge group as

$$A_\mu(x) \to \Omega(x) A_\mu(x) \Omega^{-1}(x) + \frac{1}{ig} (\partial_\mu \Omega(x)) \Omega^{-1}(x) \ . \tag{2.2.4}$$

We also need a covariant kinetic term for the gluons, if we define the field strength tensor

$$G_{\mu\nu}(x) = \frac{i}{g} \left[D_\mu, D_\nu\right] = \partial_\mu A_\nu(x) - \partial_\nu A_\mu(x) - ig \left[A_\mu(x), A_\nu(x)\right] \tag{2.2.5}$$

then the field strength tensor will transform as

$$G_{\mu\nu}(x) \to \Omega(x) G_{\mu\nu}(x) \Omega^{-1}(x) \ . \tag{2.2.6}$$

With this definition for the field strength tensor, we have that $\mathrm{Tr}_c\, G_{\mu\nu} G^{\mu\nu}$ is gauge invariant. We can now put it all together with a quark mass term to construct the local gauge invariant QCD Lagrangian with an explicit quark mass term,

$$\mathcal{L}_{\mathrm{QCD}} = \bar{q}(i\gamma^\mu D_\mu - \mathbf{M}) q - \frac{1}{2} \mathrm{Tr}_c \left[G^{\mu\nu} G_{\mu\nu}\right] \tag{2.2.7}$$

$$= \bar{q}_f (i\gamma^\mu D_\mu - m_f) q_f - \frac{1}{4} G^{\mu\nu}_a G^a_{\mu\nu} \quad , \tag{2.2.8}$$

where Einstein summation notation and the standard normalization convention is assumed. The flavour index is $f \in (u,\ d,\ s,\ c,\ b,\ t)$ and $a \in (1, \ldots, 8)$ is the group index. If we consider only the strong interaction the mass matrix is $\mathbf{M} = \mathrm{diag}\,(m_u, m_d, m_s, m_c, m_t, m_b)$.

Decomposition into subgroups

$$U_{L,R}(3) \simeq SU_{L,R}(3) \otimes U_{L,R}(1)$$

Spontaneous Chiral Symmetry Breaking of $SU_A(3)$

$$SU_L(3) \otimes SU_R(3) \simeq SU_V(3) \otimes SU_A(3) \longrightarrow SU_V(3)$$

Anomalous Breaking of $U_A(1)$

$$U_L(1) \otimes U_R(1) \simeq U_V(1) \otimes U_A(1) \longrightarrow U_V(1)$$

Flavour Symmetry ($m_u = m_d = m_s \neq 0$)

$$SU_V(3) \longrightarrow SU_F(3)$$

Figure 2.2.1: Summary of symmetries and their breaking.

For convenience we will drop the flavour and colour indices on the quark Dirac spinor q_{fc}, which is a 4-component spinor made of two 2-component spinors, Weyl spinors. The two Weyl spinors transform irreducibly under the Lorentz group, whereas the Dirac spinor is a reducible representation of the Lorentz group. That is

$$q = \begin{pmatrix} q_R \\ q_L \end{pmatrix},$$

where $q_{R,L}$ will not mix under Lorentz transformations.

The flavour index corresponds to a global symmetry $SU(N_{\rm F})$, where $N_{\rm F}$ is the number of quark flavours, in the limit of equal quark masses; whereas the colour index corresponds to the local gauge symmetry $SU(3)_c$. From the above Lagrangian one can easily see that the non-Abelian nature of the gauge group gives rise to three- and four-gluon vertices.

The QCD Lagrangian is constructed to be invariant under the local gauge group $SU(3)_c$, but is also invariant under a number of discrete and global continuous symmetries. The Lagrangian is invariant under charge conjugation C, parity P, time reversal T and in the massless limit it also has scale invariance and the chiral symmetry $U(N_{\rm F})_{\rm L} \otimes U(N_{\rm F})_{\rm R}$. Chiral symmetry and its breaking is very important for QCD and hence nuclear physics. Fig. (2.2.1) summarises the symmetries of QCD and their breaking.

Using the projection operators, $P_{L,R} = (1 \pm \gamma_5)/2$, we can decompose a Dirac spinor into the left– and right–handed components. In terms of these Weyl spinors, the free Dirac Lagrangian for a single quark flavour is

$$\mathcal{L} = \bar{q}_L(i\gamma^\mu\partial_\mu - m)q_L + \bar{q}_R(i\gamma^\mu\partial_\mu - m)q_R - m(\bar{q}_L q_R + q_R q_L) \quad . \tag{2.2.9}$$

As can be seen in Eq. (2.2.9) only the mass term couples the left and right handed Weyl spinors. Only in the chiral limit ($m \to 0$) do they decouple and can be treated

as independent fields. In this limit, this Lagrangian is invariant under $U_L(1) \otimes U_R(1)$. More generally, for $N_{\rm F}$ quark flavours we have $U(N_F)_{\rm L} \otimes U(N_{\rm F})_{\rm R}$. These are known as chiral symmetries. What is meant by this is that the symmetry group is broken up into left and right components and the left and right spinors transform independently under the left and right symmetry groups. Chiral symmetries are broken by the inclusion of a mass term. Scale invariance is also lost because of the inclusion of a mass term.

It is possible to decompose chiral symmetries into a vector and axial-vector symmetry. The vector symmetry treats the left and right spinors equally, whereas the axial-vector symmetry does not. More precisely, if $g \in U_V(1)$ then $g = e^{i\alpha}$, where $\alpha \in \mathbb{R}$ is the same for both the left and right spinors. For the axial-vector symmetry if $g \in U_A(1)$ then $g = e^{i\alpha\gamma_5}$, where $\alpha \in \mathbb{R}$ is the same for both the left and right spinors, but because of the appearance of γ_5 the transformation is different for the left and right projected spinors.

Later we wish to study nuclear matter and the matter in the interior of neutron stars. For both we will make the assumption that they are at zero temperature. Thus it will be sufficient to consider QCD with just the 3 lightest flavours: up, down and strange—as these are the only relevant flavours at the densities and temperatures of interest to us. With this simplification the QCD Lagrangian has the global symmetry $U(3)$ which can be decomposed in the chiral limit as follows

$$\begin{aligned} U(3) &\simeq SU(3) \otimes U(1) \\ &\simeq SU_L(3) \otimes U_L(1) \otimes SU_R(3) \otimes U_R(1) \\ &\simeq SU_V(3) \otimes U_V(1) \otimes SU_A(3) \otimes U_A(1) \ . \end{aligned}$$

The $U_A(1)$ axial symmetry does not survive the classical to quantum transition and is said to be anomalously broken. This is known as the $U_A(1)$ problem as there is no ninth meson seen, so it cannot have been spontaneously broken. The symmetry group is further broken spontaneously and also explicitly by current quark masses. The symmetry $SU_{\rm A}(3)$ is clearly broken as this symmetry implies the appearance of degenerate parity partners. For the nucleon this would correspond to the $N(1535)$, which is obviously not degenerate. The spontaneous breaking of $SU_A(3)$,

$$SU_L(3) \otimes SU_R(3) \simeq SU_V(3) \otimes SU_A(3) \longrightarrow SU_V(3),$$

is apparent in the particle spectrum through the appearance of 8 pseudo-scalar mesons $\pi^{\pm,0}, K^{0,+}\bar{K}^{-,0}$ and η. These pseudo-scalar mesons have anomalously low masses and a mass gap exists between them and the other mesons. The light masses and the existence of a mass gap can be explained by spontaneously breaking $SU_A(3)$ and interpreting the pseudo-scalar mesons as the Goldstone modes associated with the breaking of 8 group generators. The other mesons are then interpreted as ordinary massive mesons. The explicit breaking of the axial symmetry is the reason why the pseudo-scalar mesons have finite masses. Even though they are not massless they are still called Goldstone modes or pseudo Goldstone modes.

Non-zero current quark masses break the axial symmetry explicitly, but only break the vector symmetry if they are non-degenerate. If the three lightest quarks: up, down and strange were degenerate in mass, then the vector symmetry $SU_V(3)$ would

be preserved and called flavour symmetry, denoted $SU_F(3)$. The two lightest quark flavours have approximately the same masses, but the strange quark mass is considerably larger, see Table 2.2.1, so the flavour symmetry is explicitly broken, but still generally regarded as a good first approximation. The resulting quantum theory is invariant under

$$SU_c(3) \otimes U_V(1) \quad .$$

Goldstone modes associated with spontaneously broken symmetries are massless, whereas the actual meson octet is not. Let's consider why this is so for the case of pions. Similar arguments hold for the remaining members of the meson octet. At low energy the weak decay of pions to leptons can be described by a current–current interaction, where the current can be broken up into a hadronic and leptonic part, $J_\mu = J_\mu^{\mathrm{H}} + J_\mu^{\mathrm{L}}$. The T–matrix associated to the decay is then [92]

$$T^{(\pi \to \mu\nu)} \sim \langle \mu\nu \left| J_\mu J^\mu \right| \pi(q) \rangle = \left\langle \mu\nu \left| J^{\mu,\mathrm{L}} \right| 0 \right\rangle \left\langle 0 \left| J_\mu^{\mathrm{H}} \right| \pi(q) \right\rangle \quad . \tag{2.2.10}$$

The hadronic portion is the part of interest. As the pions are pseudo-scalars, the hadronic current is given by the axial vector current A_μ^a (Note axial current not the gauge field). The relevant matrix element can be put in the form

$$\left\langle 0 \left| A_\mu^a(x) \right| \pi^b(q) \right\rangle = i f_\pi q_\mu \delta_{ab} e^{-iq\cdot x} \quad , \tag{2.2.11}$$

where a, b are flavour group indices. Taking the divergence of Eq. (2.2.11),

$$\left\langle 0 \left| \partial^\mu A_\mu^a(x) \right| \pi^b(q) \right\rangle = f_\pi q^2 \delta_{ab} e^{-iq\cdot x} = m_\pi^2 \delta_{ab} e^{-iq\cdot x} \ , \tag{2.2.12}$$

leads to the Partially Conserved Axial Current (PCAC) relation,

$$\partial^\mu A_\mu^a(x) = f_\pi m_\pi^2 \pi_a(x) \quad . \tag{2.2.13}$$

From Eq. (2.2.13) we see that in the limit $m_\pi \to 0$ the axial current is conserved, or conversely if the axial current is not conserved then pions are massive.

2.2.2 Asymptotic Freedom and Perturbation Theory

QED calculations are performed using perturbation theory. One assumes that the interacting theory is a small perturbation away from the free theory which can be solved. Physical quantities of interest like cross sections are given in terms of a power series expansion of the QED coupling (or equivalently the fine structure constant). The QED calculations that have agreed so well with experiment use this perturbative expansion, which is usually represented pictorially by a growing succession of Feynman graphs. The number of graphs at each order grows quickly. For this theory to make meaningful predictions each term of the perturbation series should be finite and the series must converge. Naively one would expect each term in the perturbation series to be finite and for the whole series to converge due to the very small coupling in QED. It was realised early on that higher order corrections, corresponding to graphs with loops, were divergent. These divergences that plagued the theory were resolved through the process of renormalization. The process of renormalization is not unique

to quantum field theories. Renormalization is discussed in most texts on QFT, see also the very pedagogical article "A hint of renormalization" by Delamotte [93] for a discussion of renormalization. Recently perturbative renormalization in QFT has been given a clear and rigorous mathematical interpretation by Connes and Kreimer [94–96]. This mathematical formulation of renormalization utilises the underlying Hopf algebraic structure of Feynman graphs.

Renormalization is concerned with taking care to express observable quantities in terms of the measured physical parameters, i.e., the dressed or renormalised quantities and not their bare counterparts. This process of renormalization rendered the higher order corrections of QED finite, allowing QED to be used to make predictions of incredible accuracy. However, the story does not end there. From very simple arguments by Dyson [97], based on the analyticity of the expansion parameter (coupling e or fine structure α_e) and the stability of the vacuum; this series has a zero radius of convergence. Dyson's argument was not a definite proof of the lack of convergence, but is indicative that something may be amiss. One may then ask, Why does QED work so well? It has been suggested and generally regarded that the perturbation expansion is really only asymptotic and not convergent [98–100]. The agreement between theory and experiment is due to the smallness of the coupling.

Lack of convergence of the perturbation series does not mean we need to abandon the theory. The asymptotic nature of the perturbation series means that in calculating up to higher orders we can only expect to improve the approximation up to a certain order for a fixed value of the coupling, beyond which the error between the perturbation series and the exact value will grow. This is also expected for other quantum field theories, such as QCD. The order in the expansion to which the perturbation series reflects a good approximation depends on the numerical value of the coupling and in both QED and QCD the couplings run. It was shown by Gross, Wilczek and Politzer in Ref. [101, 102] that QCD and a larger class of theories called non-Abelian Yang Mills theories are asymptotically free, meaning that the coupling becomes small at high energy or equivalently at short distances. QED on the other hand is not asymptotically free, its coupling increases with increasing energy. As a consequence of renormalization, the couplings and masses flow with energy scale and the evolution of the QED coupling given to one loop order is

$$\alpha_e(Q) = \frac{\alpha}{1 - \frac{2\alpha}{3\pi}\ln\frac{Q}{m_e}} \tag{2.2.14}$$

and for QCD it is

$$\alpha_s(Q) = \frac{6\pi}{(11N_c - 2N_{\mathrm{F}})\ln\frac{Q}{\Lambda_{\mathrm{QCD}}}} \quad , \tag{2.2.15}$$

where $\alpha = 1/137.03\ldots$, N_{F} the number of flavours for which the current quark mass is less than $|Q|$, $N_c = 3$, $\Lambda_{\mathrm{QCD}} = 200$ MeV and their evolution is depicted in Fig. 2.2.2.

In QFT, quantities like charge and mass distributions are not fixed, but rather depend upon the energy scale. From a practical point of view they depend on the wavelength or energy of the probe used to measure them. A probe with a shorter wavelength or higher energy will see deeper into the target. The running of the coupling can be understood by a simple picture. For QED, an electron feels the quantum fluctuations of the surrounding vacuum and unlike classical renormalization scenarios

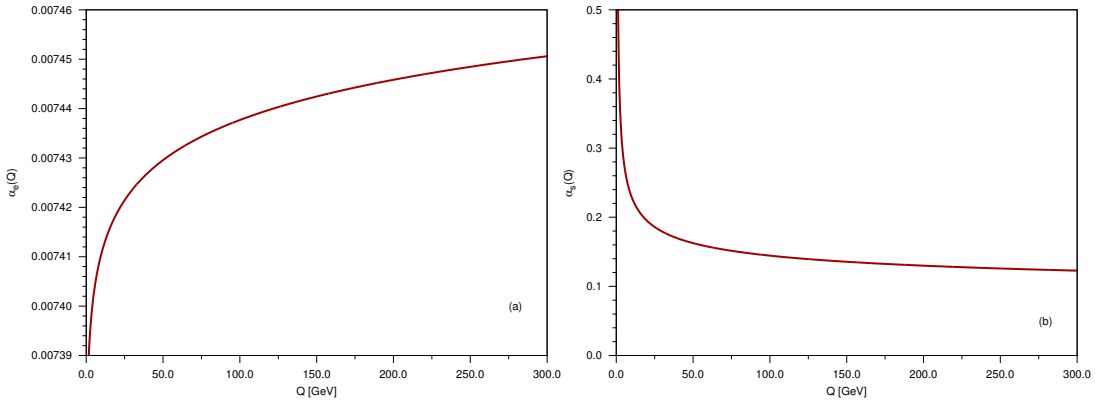

Figure 2.2.2: Running of couplings to one loop level in (a) QED and (b) QCD.

it can never be removed from its surroundings, so its bare parameters i.e. its bare charge or bare mass cannot be known. In the seething vacuum where virtual particle–anti-particle pairs and photons are popping in and out of existence the bare charge of the electron is screened from the probe. At larger distances the charge is screened more and at short distances it is screened less. The same occurs in QCD with quark–anti-quark pairs and gluons with the added important difference that the gauge group of QCD is non-Abelian. The gauge bosons of QCD carry colour charge and these gluons anti-screen the charge. This anti-screening leads to the phenomena of asymptotic freedom at high energies. As can be seen in Eq. (2.2.15) the competing contributions of the quark and gluon polarisations depend on the number of quark flavours N_{F} and the number of colours N_c.

The running of the coupling means that the region relevant for nuclear physics, cannot be described by the usual perturbation series approach and thus non-perturbative methods must be used. The only first principles approach to QCD in this non-perturbative region is Wilson's lattice gauge theory, but unfortunately it is not suitable for application to systems at finite density or equivalently finite chemical potential because of the so-called sign problem. There have been attempts to extend lattice QCD calculations to systems with finite chemical potential, but it is still not feasible for densities of interest in this thesis.

It is unknown if the coupling reaches an upper bound as it grows with separation. Presumably it could require an infinite amount of energy to remove a quark or gluon from a hadron. This is summarised by the confinement hypothesis, which states that all coloured objects are confined to colour-singlet objects and cannot be observed in isolation. The confinement hypothesis has not been proved, but to date nobody has observed individual quarks or gluons—only a large number of colour neutral bound states. Although quark structure has been inferred from deep inelastic scattering [103–107].

The baryons and mesons are the fundamental bound states in QCD. They are rather different to the ones resulting from the residual quark-gluon dynamics, leading to the formation of nuclei or the bound states of QED, like the hydrogen atom or positronium.

A key feature of these bound states is that their mass is not approximately equal to the sum of their constituents masses as is the case for nuclei and QED bound states. Most of the mass is generated dynamically by the complicated non-linear interactions of the gluons with themselves and the quarks. This feature of the quark-gluon dynamics is closely linked with the spontaneous breaking of chiral symmetry and is the reason why three light quarks with mass of a few MeV can produce a bound state with a mass ($M_N \sim 1$ GeV) greatly exceeding their sum. It is this mechanism that is responsible for the majority of the visible mass seen in our universe.

Confinement, spontaneous chiral symmetry breaking and dynamical mass generation are complicated emergent phenomena arising from the non-perturbative nature of low energy QCD. Arguments have been made that at high temperatures and/or densities deconfinement and chiral symmetry restoration may occur . It may be possible to find signals of such transitions[4] in the extreme environments of heavy ion collisions and neutrons stars.

A major focus of this thesis will be the matter in the core of neutron stars. Neutron stars are only of intermediate density on the scale of the QCD phase diagram and can be considered to be at zero temperature to good approximation. Matter of this type is not amenable to perturbative QCD nor lattice QCD calculations. This portion of the phase diagram is also not experimentally accessible, but portions of the phase diagram corresponding to nuclear physics and heavy ion experiments are, which means we are able to develop effective models constrained by experimental results in those regions. Once constrained, these models can then be used to extrapolate to the region relevant to neutron stars, allowing one to predict their properties and to make comparisons to astronomical observations.

2.2.3 Chiral Effective Field Theory

Given the difficulties faced in solving a non-perturbative quantum field theory like QCD, one could consider using these bound states as the relevant degrees of freedom to develop effective low energy theories and models of QCD. During the latter half of the previous century (1960–2000) phenomenological potentials incorporating boson exchanges; like the Bonn, Nijmegen and the Argonne AV18 potential—which included pion exchange; dominated over other approaches. These potentials are still in use today, although the last two decades has seen the emergence of effective field theories as a contender to describe the nuclear force at low energies.

Effective theories like chiral effective field theory (CEFT) [108] are simplified versions of the underlying theory which exploit a separation of scales. They employ a low energy expansion in a ratio of momentum transfer and some chiral scale (e.g. pion or kaon mass). In some sense CEFT is a return to pion theories of old, but it offers a clear connection to QCD. It is a robust alternative to phenomenological models, some of which like the very popular Argonne AV18 potential are only loosely connected to QCD and its phenomena. CEFT on the other hand is designed to describe the same low energy physics as QCD.

[4] They may not coincide.

An attractive feature possessed by CEFT is that it allows for a systematic determination of theoretical error and inclusion of many-body forces in a methodical way, which is rather difficult if not impossible in phenomenological models. This is contingent of course on the chiral expansion converging. However, at suprasaturation densities convergence may be slow. By reason of slow convergence and the necessity of relativity at high density we cannot use CEFT for the applications of interest in this thesis. For this reason in addition to the added simplicity we will rely on a relativistic phenomenological model incorporating many of the features of QCD, namely the Quark-Meson Coupling (QMC) model. Comparisons of our phenomenological model calculations of Pure Neutron Matter (PNM) with N^{3}LO CEFT will be made in Chapter 4 at low density where the convergence of the chiral expansion should be sufficiently fast and relativistic effects should be small.

2.3 Nuclear Matter

In this thesis, we are primarily concerned with calculating the equation of state (EoS) for strongly interacting matter at finite density. In particular, we intend to study the nuclear EoS of isospin symmetric and asymmetric nuclear matter (SNM and ANM) in a relativistic model incorporating the quark degrees of freedom of the baryons. The major application of this model which will be of interest will be to model neutron star interiors with the aim of predicting their observable properties. This is a formidable task and the simplifying assumptions of nuclear matter allow calculations to be performed readily.

Nuclear matter is a hypothetical form of strongly interacting matter. It is an idealised system with an infinite and homogeneous distribution of nucleons that are assumed not to interact electromagnetically. This is a useful first approximation to large nuclei as surface effects become less important for these and negligible in the limit of infinite radius. On the other hand neutron stars have considerably larger radii ($R \sim 10$km) than nuclei (a few fermis) and as such may provide the only natural realization of nuclear matter in our universe.

The characteristics of the strong nuclear force were discussed in Section 2.1; as a consequence of the attractive short range with repulsive core, the nuclear force saturates. This is particularly evident from the observations that the radii of nuclei $R \propto A^{-1/3}$ and the binding energy per nucleon is approximately constant at 8 MeV for increasing number of nucleons A. The density at which saturation occurs is $\rho_0 \sim 0.16$ fm^{-3}, which is deduced from the analysis electrons scattering from heavy nuclei.

The binding energy is well described using the liquid drop model by the semi-empirical Bethe–Weizsacker formula,

$$B(A,Z) = a_{\rm vol}A - a_{\rm surf}A^{2/3} - a_{\rm coul}\frac{Z(Z-1)}{A^{1/3}} - a_{\rm asym}\frac{(N-Z)^2}{A} + a_{\rm pair}\frac{\delta(A,Z)}{A^{1/2}}\ , \quad (2.3.1)$$

where Z is the atomic number, i.e., the number of protons, and N is the number of neutrons. The pairing energy is given by

$$\delta(A,Z) = \begin{cases} 1 & \text{even–even} \\ 0 & \text{odd–even} \\ -1 & \text{odd–odd} \end{cases} . \quad (2.3.2)$$

Term	Parameter Value [MeV]
Volume	$a_{\rm vol} = 15.85$
Surface	$a_{\rm surf} = 18.34$
Coulomb	$a_{\rm coul} = 0.71$
Symmetry	$a_{asym} = 23.21$
Pairing	$a_{\rm pair} = 12.0$

Table 2.3.1: Typical parameter set for the Bethe-Weizacker formula [109]

A typical parameter set for the Bethe–Weizacker formula is given in Table 2.3.1. These values are obtained by fitting to a large data set of nuclei.

The energy per nucleon E is related to the binding energy per nucleon by $B/A = -E$ and in the large A (thermodynamic) limit reduces to

$$E \simeq a_{\rm vol} + a_{asym}\beta^2 \quad , \tag{2.3.3}$$

where

$$\beta = \frac{(N-Z)}{A} \quad \longrightarrow \quad \frac{\rho_n - \rho_p}{\rho} \quad . \tag{2.3.4}$$

For equal numbers of neutrons and protons, known as symmetric nuclear matter (SNM), it is just the volume term. The volume term corresponds to the energy of the bulk volume of the nuclear system—it is identified with the binding energy per nucleon in symmetric nuclear matter.

Light stable nuclei consist of an approximately equal number of protons and neutrons, so experimental observations of nuclei can be used to infer the properties of SNM and vice versa, the SNM EoS can be used to predict the bulk properties of nuclei. For nuclear matter, its characterizing feature is its EoS. This is the relationship between thermodynamic state variables, such as energy per particle and the baryonic density, pressure and temperature. In this thesis, we will only be interested in nuclear matter in the zero temperature limit, because the temperature $k_{\rm B}T$ ($k_{\rm B}$ is the Boltzmann constant) of the particles is generally very much less than their Fermi energy E_F, even in neutron stars.

The nuclear EoS can be calculated if you know the nuclear force or have a model representing its key attributes. There are many nuclear models in the literature from which we can calculate the EoS. They range from non-relativistic Skyrme and Gogny models to relativistic meson exchange models like quantum hadrodynamics (QHD) and the quark-meson coupling (QMC) model. The latter are well suited to investigating hadrons in medium as relativistic effects become important with increasing density. These relativistic models will be discussed in sections 2.5 and 2.6, respectively.

At the saturation density, properties of finite nuclei or a small set of properties in SNM can be used to constrain the main parameters of a model, the coupling constants in the case of the QHD and QMC models. Common properties that are usually taken to constrain models are the minimum of binding energy $\mathcal{E}_0$, the symmetry energy S_0 and the compression modulus or incompressibility, K_0, at the saturation density. Other parameter sets for these models can also be obtained by fitting to properties of finite

nuclei. Using a given parameter set, the SNM EoS can then be calculated and also extrapolated to obtain the EoS of ANM. No matter the fitting procedure, the model should predict realistic values for both nuclear matter and the properties of finite nuclei.

In this work, when we calculate energy per baryon $E = \epsilon_{\rm HAD}/\rho$ or the hadronic energy density, $\epsilon_{\rm HAD}$, we will always take into account the rest mass energy of the baryons, so that the binding energy of nuclear matter (or binding energy per nucleon in the limit $A \to \infty$) is

$$\mathcal{E} = \frac{1}{\rho}\left(\epsilon_{\rm HAD} - \sum_B M_B \rho_B\right) \ , \tag{2.3.5}$$

where the binding energy at saturation density, ρ_0, is denoted $\mathcal{E}_0 \equiv \mathcal{E}(\rho_0)$ and known to be approximately -16 MeV [110, 111].

The second term in Eq. 2.3.3 is the asymmetry term and its coefficient is equal to the symmetry energy S at equilibrium. The symmetry energy is defined as

$$S(\rho) \ = \ \frac{1}{2}\frac{\partial^2 E}{\partial \beta^2}\bigg|_{\beta=0} \ , \tag{2.3.6}$$

where the isospin asymmetry parameter β is defined by Eq. (2.3.4) and $a_{\rm asym} \equiv S_0 \equiv S(\rho_0)$. It corresponds to a contribution to the energy which is isospin dependent and as such, crucial for asymmetric systems like heavy nuclei, nuclei far from the line of stability and the matter found in astrophysical systems (i.e supernovae and neutron stars). The symmetry energy acts as a kind of restoring force providing a source of repulsion for neutrons and attraction for protons in neutron rich matter. At saturation density and just below it is reasonably well constrained and is known to be approximately 32.5 MeV [110, 111] at equilibrium in SNM. It's density dependence above saturation on the other hand is rather uncertain and if one ignores issues related to phase transitions and deconfinement it is the leading ambiguity in the nuclear EoS. Understanding the isospin dependence of the in-medium strong force is crucial for nuclear physics and astrophysics. In the recent article by Horowitz *et al* [112] an overview of the current experimental and theoretical status of the symmetry energy is presented with suggestions for finding a way forward.

Pressure is related to the energy per particle by

$$P(\rho) = \rho^2 \frac{\partial E}{\partial \rho} \ , \tag{2.3.7}$$

where in SNM at saturation the pressure, $P_0 \equiv P(\rho_0) = 0$, since the first derivative of the energy per baryon vanishes because it is minimised at this point. If the symmetry energy has a strong density dependence it will contribute significantly to the pressure in asymmetric matter influencing the structure of nuclei, particularly neutron skins in heavy nuclei as well as the radii of neutron stars [113, 114].

A measure of the curvature of the energy density with respect to density about the minimum is given by the incompressibility or compression modulus. In terms of the pressure it is

$$K(\rho) = 9\frac{\partial P(\rho)}{\partial \rho} = 18\frac{P}{\rho} + 9\rho^2 \frac{\partial^2 E}{\partial \rho^2} \tag{2.3.8}$$

and its value at saturation simplifies to

$$K_0 = K(\rho_0) = 9\rho_0^2 \frac{\partial^2 E}{\partial \rho^2}\bigg|_{\rho=\rho_0} \quad . \tag{2.3.9}$$

This quantity is one of the major constraints on nuclear models and its value at saturation has been under debate for several decades. A recent examination of experimental data estimates it to lie in the range 250 MeV–315 MeV [115]. A larger curvature naively implies more pressure at higher density leading to predictions of larger maximum neutron star masses. This assumes that no change in the behaviour of the EoS occurs at higher density and the high density behaviour is entirely determined at saturation.

In finite nuclei, surface and Coulomb effects—which are absent by definition in nuclear matter—contribute to the incompressibility. It is commonly assumed that a leptodermous expansion of the incompressibility of a finite nucleus $K_{\rm A}$ of a nucleus A is valid [116–118]; such an expression takes the form

$$K_{\rm A}(A,\beta) = K_{\rm vol} + K_{\rm surf}A^{-1/3} + K_{\rm curv}A^{-2/3} + K_{\rm coul}A^{-4/3} + K_\tau \beta^2 \tag{2.3.10}$$

where

$$K_\tau = K_{\tau,v} + K_{\tau,s}A^{-1/3} \quad . \tag{2.3.11}$$

The coefficients $K_{\rm vol}$, $K_{\rm surf}$, $K_{\rm coul}$ and K_τ have analogous physical meanings to the coefficients in the Bethe–Weizsacker formula. The isospin contribution to the incompressibility, K_τ, is further broken up into a volume $K_{\tau,v}$ and surface $K_{\tau,s}$ contribution. In calculations the surface contribution is more complicated to evaluate and usually neglected. The $K_{\rm curv}$ is the curvature term. The volume component is identified with the incompressibility of SNM at saturation. These coefficients can be extracted by fitting to empirical data from giant resonances.

Other higher order derivatives of the energy per particle with respect to either density or the asymmetry parameter can be calculated to further determine the density and isospin dependence of the EoS. The higher order derivatives can be compared with values extracted from empirical data to further evaluate and constrain models. The next higher derivative with respect to ρ of the energy per particle i.e the third derivative, is known as the skewness and is given by

$$Q(\rho) \;=\; 27\rho^3 \frac{\partial^3 E}{\partial \rho^3} \quad . \tag{2.3.12}$$

Its value at equilibrium is denoted Q_0 and is not very well determined by experiment.

The chosen normalizations of the higher order derivatives of the energy per particle and symmetry energy along with their connection to the EoS can be more easily understood as follows. The energy per nucleon is a function of density ρ, isospin asymmetry parameter β, and the temperature T. As stated above we are only interested in the zero temperature limit such that

$$E = E(\rho,\beta,T) \xrightarrow[T\to 0]{} E(\rho,\beta) \quad , \tag{2.3.13}$$

which, if assumed to be a well behaved function of both variables, can be expanded as a Taylor series in either variable. For SNM ($\beta = \frac{\rho_n - \rho_p}{\rho} = 0$) it can be expanded about the saturation density as a function of density as follows:

$$\begin{aligned} E(\rho) &\equiv E(\rho, \beta = 0) \\ &= E(\rho_0) + \left.\frac{\partial E}{\partial \rho}\right|_{\rho=\rho_0} (\rho - \rho_0) \\ &\quad + \left.\frac{1}{2!}\frac{\partial^2 E}{\partial \rho^2}\right|_{\rho=\rho_0} (\rho - \rho_0)^2 + \left.\frac{1}{3!}\frac{\partial^3 E}{\partial \rho^3}\right|_{\rho=\rho_0} (\rho - \rho_0)^3 + \dots \end{aligned} \tag{2.3.14}$$

Note that the second term on the RHS of Eq. (2.3.14) vanishes as the energy per particle is minimised at the saturation density by definition. Eq. (2.3.14) can be rewritten in terms of the incompressibility and skewness at saturation using Eq. (2.3.8) and Eq. (2.3.12) as

$$E(\rho) = E(\rho_0) + \frac{K(\rho_0)}{2!}\chi^2 + \frac{Q(\rho_0)}{3!}\chi^3 + \dots \tag{2.3.15}$$

where $\chi = \frac{\rho - \rho_0}{3\rho_0}$. One sees immediately from Eq. (2.3.15) that around 3–4 ρ_0, densities relevant to neutron stars and heavy ion collisions, that the skewness coefficient $Q_0 \equiv Q(\rho_0)$ can potentially give a non-negligible contribution to the EoS, albeit for SNM.

Determination of the isospin dependence of the nuclear EoS is of far-reaching importance in nuclear physics. Important for understanding large and exotic nuclei, core collapse supernovae and neutron stars. In neutron stars the symmetry energy influences particle content, phase transitions and stability against gravitational collapse.

Neutron stars are isospin asymmetric systems and as a first approximation can be modelled by pure neutron matter (PNM), albeit this is an excited state and susceptible to weak decay—to reach beta equilibrium. In contrast to SNM, neither PNM nor Neutron Star Matter (NSM) are bound by the strong interaction, although the latter is gravitationally bound.

Likewise for ANM, we can make an expansion in terms of the asymmetry parameter β. To the same order we have

$$\begin{aligned} E(\rho, \beta) &= E(\rho, \beta = 0) + \left.\frac{\partial E}{\partial \beta}\right|_{\beta=0} \beta + \left.\frac{1}{2!}\frac{\partial^2 E}{\partial \beta^2}\right|_{\beta=0} \beta^2 + \left.\frac{1}{3!}\frac{\partial^3 E}{\partial \beta^3}\right|_{\beta=0} \beta^3 + \dots \\ &= E(\rho) + \left.\frac{1}{2!}\frac{\partial^2 E}{\partial \beta^2}\right|_{\beta=0} \beta^2 \quad + \quad \dots \quad . \end{aligned} \tag{2.3.16}$$

Only even powers of β survive due to the assumption of isospin symmetry of the nuclear force and so to third order in the asymmetry parameter β we have

$$E(\rho, \beta) \simeq E(\rho) + S(\rho)\beta^2 + \mathcal{O}(\beta^4) \quad . \tag{2.3.17}$$

It is also informative to expand the symmetry energy as a Taylor series as a function of density, to second order it is

$$S(\rho) \equiv \frac{1}{2!}\frac{\partial^2 E}{\partial \beta^2}\bigg|_{\beta=0} \simeq S(\rho_0) + L(\rho_0)\chi + \frac{K_{\rm sym}(\rho_0)}{2!}\chi^2 + \mathcal{O}(\chi^3) \quad . \tag{2.3.18}$$

The second and third terms on the RHS are imaginatively called the slope and curvature of the symmetry energy. The former is explicity,

$$L(\rho) = 3\rho\frac{\partial S(\rho)}{\partial \rho} \quad , \tag{2.3.19}$$

while the latter is given by,

$$K_{\rm sym}(\rho) = 9\rho^2\frac{\partial^2 S(\rho)}{\partial \rho^2} \quad . \tag{2.3.20}$$

The values of the slope and curvature at saturation are also denoted with a subscript or superscript zero, i.e. L_0, $K^0_{\rm sym}$. Their values at saturation determine, respectively, the first and second order density dependence of the symmetry energy and are not very well determined by either theory or experiment.

Utilizing the above expansion one may write the volume component of the isospin incompressibility at saturation in terms of the above higher order derivatives, taking the form

$$K^0_{\tau,v} = K^0_{\rm sym} - 6L_0 - \frac{Q_0}{K_0}L_0 \ . \tag{2.3.21}$$

One sees that the incompressibility is influenced by the higher order derivatives of the symmetry energy.

The above properties are generally not measured directly, but are extracted from empirical data using various models. Despite being extracted in a model dependent way, all realistic models of nuclear matter should be able to reproduce these quantities correctly. A summary of experimental and theoretical knowledge of these quantities is discussed next in Section 2.4.

2.4 Experimental and Theoretical Knowledge of the Nuclear EoS

Here we provide a very brief overview of the experimental and theoretical knowledge of the EoS. Through theoretical calculations quite a few physical observables have been identified that are potentially sensitive enough to bulk nuclear matter properties to constrain the EoS. The bulk properties of the nuclear EoS can be constrained empirically from various nuclear structure experiments and heavy ion collisions. From the nuclear structure experiments we can only hope to learn about the behaviour of the EoS at saturation density and below, whereas heavy ion collisions provide us with the opportunity to probe the EoS not only at normal nuclear matter densities, but also suprasaturation densities. We will discuss only the most promising observables related

to the incompressibility and the symmetry energy. Further constraints on the high density behaviour of the EoS come from astronomical observations of neutron stars. These will be discussed in Ch. 3.

The size of nuclei and the distribution of nucleons within them are among the most basic nuclear structure properties. Only the distributions of protons in nuclei are well known from experiment. These are well reproduced by theory, whereas a large variation of predictions exist for the neutron distribution and hence the corresponding root mean square (rms) radius and neutron skin thickness in neutron rich nuclei. The structure of finite nuclei is intimately connected to the bulk nuclear EoS. In Ref. [119], Brown pointed out by using a set of 18 Skyrme models, that the PNM EoS is not well constrained and each model can be characterised by the density slope of the energy per neutron at $\rho_n = 0.1$ fm^{-3}. Moreover, he found a strong linear correlation between the neutron skin thickness in heavy nuclei and the slope of the PNM EoS. This neutron skin thickness is defined as

$$\Delta R = \langle r_n^2 \rangle^{1/2} - \langle r_p^2 \rangle^{1/2} \tag{2.4.1}$$

where $\langle r_n^2 \rangle^{1/2}$ and $\langle r_p^2 \rangle^{1/2}$ are the rms radii of neutrons and protons respectively. Subsequent investigations involving other Skyrme [120] and also relativistic mean field [120–122] models found the same correlation. It was also found using realistic potentials in a Brueckner–Hartree–Fock approach [123]. The density slope of the energy per neutron is intrinsically related to the density dependence of the symmetry energy by Eq. (2.3.18) and the pressure by Eq. (2.3.7). This explicitly demonstrates that there is a large theoretical uncertainty in the density dependence of the symmetry energy in phenomenological models. Microscopic or realistic models [124] tend to agree significantly better with each other, especially at low density, but significant variation is still present at high density. All of the above predict a linear increase in the neutron skin ΔR with the slope L_0, which is not surprising since the pressure in PNM increases with L_0 and therefore neutrons are pushed out further, increasing the the neutron rms radius and hence the neutron skin thickness. As suggested originally by Brown [119] and further evidenced by later studies with a larger class of models, a measurement of a neutron skin thickness in a heavy nucleus could severely constrain the PNM EoS and hence the density dependence of the symmetry energy.

Because of the strong linear correlation, an accurate measurement of the neutron radius even for a single nucleus would be able to discriminate among models. Unfortunately only proton radii are accurately know. Their radii are determined quite precisely through unpolarised electron scattering, whereas neutron radii determinations have relied on hadronic probes. The use of hadronic probes to determine the neutron radii complicates the situation due to the uncertainty in the interaction between the probe and the nucleus.

Donnelly *et al* [125] were the first to suggest that parity violating scattering of electrons would be an accurate probe of neutrons in nuclei. Due to advances in both experiment and theory [126], there is at present a major experimental effort to use this technique to measure the neutron skin thickness of ^{208}Pb. This is known as the lead radius experiment or PREX. In this experiment the scattered electrons interact by exchanging photons (parity conserving) and Z bosons (parity violating). From the electromagnetic ($Q^n_{\rm EM} = 0$, $Q^p_{\rm EM} = 1$) and weak charges ($Q^n_{\rm W} \simeq -1$, $Q^p_W \simeq 0.08$), it is

known that the photons couple to the protons and Z bosons couple predominantly to the neutrons.

The aim of PREX is to measure the parity violating asymmetry $A_{\rm PV}$, which is the difference in cross sections of positive and negative helicity electrons. The small value of $A_{\rm PV}$ is difficult to measure. It is small because the neutrons only couple weakly to the Z bosons. It has been measured at a single momentum transfer, which can be related to the neutron skin thickness by expanding the neutron and proton form factors about $Q^2 = 0$, but unfortunately the error in the measurement is too large to be a useful constraint on the EoS. We are eagerly awaiting for the experiment to be redone more carefully. This electroweak probe offers the best hope to date for an accurate and model independent determination of the neutron skin thickness of lead. Therefore it is also a crucial constraint on the nuclear EoS through the density dependence of the symmetry energy.

Continuing on the same vein of using nuclear structure experiments to constrain the nuclear EoS, excited states of nuclei can and have provided useful additional information. Excited state information is crucial as ground state observables have not been sufficient to constrain the nuclear EoS. Numerous studies both theoretical and experimental have been carried out on excited states of nuclei in the hope of making progress. A number of observables were identified as being potentially enlightening, such as the main features of giant and pygmy resonances; their energies, widths, decay modes and the $E1$ dipole polarizability just to name a few. In this approach, the nucleus is studied by perturbing it, then its response to the perturbation is analysed. We will briefly describe giant resonances and their usefulness as it pertains to constraining the EoS of nuclear matter. For further information on giant resonances we direct the interested reader to Harakeh's monograph [127] and also Ref. [110].

The so called giant resonances which appear as prominent peaks in nuclear cross sections have played a pivotal role in understanding the EoS. These resonances have provided useful information on several key properties like the incompressibility, symmetry energy, effective (in-medium) nucleon mass and even the neutron skin in finite nuclei. By comparison with experimental data, giant resonances are interpreted as collective excitations of nuclei induced by electromagnetic or hadronic probes. That is, by photoabsorption or inelastic scattering of hadrons. This collective phenomenon arises from the superposition of many one-particle–one-hole ($1p$–$1h$) excitations from a mean field ground state. In the mean field approximation (MFA), nucleons in a nucleus only feel a self consistently generated averaged one body potential. As a first approximation the MFA describes the nucleus rather well, but it is known that the residual interaction can give rise to collective excitations and therefore this approximation is not sufficient. It does not allow for p–h excitations, so one must consider a more sophisticated approximation such as the random phase approximation (RPA). Both relativistic and non-relativistic models are able to predict giant resonances.

Giant resonances are among the most easily generated excitations of the nucleus. They are peaked at energies of 10–30 MeV with typical widths of a few MeV. There are many and they are characterised by their orbital angular momentum or multipolarity $\vec{L}$, spin $\vec{S}$ and isospin $\vec{T}$. Orbital angular momentum can take any value $L = 0, 1, 2, \ldots$ (monopole, dipole, quadrupole, ...), but the spin and isospin are constrained to either

0 (electric/isoscalar) or 1 (magnetic/isovector) due to the p–h nature of the excitation. In general, many modes are excited in a perturbed nucleus at once. Particular modes can be related to different nuclear properties and to isolate a particular mode, the probe and the observed scattering angle must be carefully chosen.

The isoscalar giant monopole resonance (ISGMR or isoscalar E0, $L = S = T = 0$), or so called breathing mode, is associated to compression and expansion of the nucleus, where neutrons and protons oscillate in phase with each other. Inelastic scattering of an alpha particle is used to excite this mode and it is enhanced about 0°. Non-relativistic and relativistic phenomenological models have been used to calculate the excitation energy E_{GMR} of this resonance, a correlation between E_{GMR} and the incompressibility has been found. This mode has been used many times over to extract the incompressibility of a finite nucleus using different models. See references [115, 116, 128–131] and references therein. The incompressibility obtained is that of a finite nucleus, which is non-trivially related to the incompressibility of nuclear matter, generally through a leptodermous expansion of the form Eq. (2.3.10), or a variation thereof.

The extraction of the incompressibility is somewhat model dependent and it is quite well known that non-relativistic models of Skyrme and Gogny type predict consistently lower values than relativistic mean field models. A recent reanalysis [115] of giant resonance data aimed at extracting the incompressibility of nuclear matter concluded that the nuclear surface plays an important role in determining its value. In this study, it was found that when the ratio $c = K_{\mathrm{surf}}/K_{\mathrm{vol}}$ is fixed to the value -1, then the generally accepted range of 240 ± 20 MeV is obtained from fits to experimental data, but the fits were significantly improved when c was allowed to deviate from this value. The best fits to the data were obtained for $-2.4 \leq c \leq -1.6$ and the corresponding incompressibility range was 250–315 MeV.

The isovector giant resonances are used to explore the isospin dependence of the nuclear interaction. In isovector modes, neutrons and protons oscillate out of phase with each other. These modes are sensitive to the symmetry energy and the neutron skin in heavy nuclei. To excite them photons are typically used as hadronic probes like protons ($T_3^{\mathrm{p}} = 1/2$) are not isospin selective. Protons will excite both $T = 0$ and $T = 1$ modes, whereas photons will only excite $T = 1$ modes.

There has been great interest in the past decade or so, both experimentally and theoretically, in the isovector giant dipole resonances (IVGDR or isovector E1, $L = 1$, $S = 0$, $T = 1$) and the low-lying electric dipole $E1$ resonances found energetically just below them in neutron rich nuclei. Giant resonances contain the majority of the strength in an excitation, but in exotic nuclei and in some stable nuclei, low-energy $E1$ modes near the nucleon separation threshold exist. The modes have been known to exist since the 70's and have been predicted in numerous models. Recently studies have been extended to examine more neutron rich and unstable nuclei. They are rather common and have been found in ^{208}Pb [132, 133]; ^{138}Ba, ^{140}Ce, and ^{144}Sm [134]; ^{130,132}Sn [135]; $^{129-132}$Sn and ^{133,134}Sb [136]; ^{136}Xe [137] and ^{68}Ni [138]. They are generally referred to as soft or pygmy dipole resonances (PDR) as their cross sections are quite small compared to the main portion of the excitation. They typically exhaust only about 1% of the energy weighted sum rule (EWSR).

Despite their long history the microscopic explanation of the low-energy electric

dipole strength is unclear. The nature of the pygmy resonances, such as its collectivity and its usefulness as a constraint on the symmetry energy is currently under debate. There has been some indication that these PDR can be interpreted as a collective excitation [139], where the neutron skin oscillates against the isospin symmetric neutron-proton core. Although not all models agree with this interpretation [140, 141].

From the interpretation of the PDR resonance as an oscillation of the neutron skin against the isospin saturated core, one would expect this to be a good observable to measure the neutron skin and also constrain the symmetry energy. In the correlation analysis of Reinhard and Nazarewicz [142, 143], the dipole polarizability, from which the PDR contributes 20–25% [144], was found to have a strong correlation with the neutron skin, whereas the strength of the PDR was found to be only weakly correlated. This is in contrast to other studies that did find a correlation, for instance the studies of Piekarewicz [144, 145] or Klimkiewicz et al [136], who found a linear relationship between the relative pygmy strength and the neutrons skin thickness. Measurements of the dipole polarizability may constitute a complementary alternative to parity violating electron scattering to determine the neutron skin thickness [144]. In addition to these, Carbone et al [146] found using a set of both non-relativistic and relativistic mean field models, a linear correlation between Thomas–Reiche–Kuhn (TRK) EWSR and the slope of the symmetry energy L_0. From the experimental data on ^{68}Ni and ^{132}Sn they extracted the value $L_0 = 64.8 \pm 15.7$ MeV and were able to infer the neutron skin thickness in ^{68}Ni, ^{132}Sn and ^{208}Pb.

Another means by which to study the nuclear EoS comes from colliding heavy ions. These experiments provide us with the only way to probe the EoS at higher densities in a laboratory setting. In these collisions high density and temperature matter is momentarily produced for approximately 10^{-23}s. Subthreshold production of kaons and flow measurements have provided constraints on the nuclear EoS [147, 148]. Interestingly, the constraints placed on the slope of the symmetry energy L_0, predict a somewhat larger value than constraints from other experiments, but with larger error bars they partially overlap. Of course there a number of hurdles to be overcome in the associated modelling of the collisions and the extraction of constraints on the EoS. For more detailed information regarding heavy ion collisions and the constraints they can place on the nuclear EoS we refer the reader to Tsang et al [87] and Li et al [149].

The symmetry energy as discussed is a crucial factor characterizing the EoS of ANM. Despite its importance and numerous studies its density dependence is still not very well understood. Nevertheless, advances in its understanding at saturation and subsaturation densities have occurred in recent years from a number of experiments, along with the identification of promising observables which are expected to constrain it further [87]. More detailed and systematic work is needed to understand the high density behaviour. Heavy ion experiments will play an prominent role in this regard, as the isospin dependence, in addition to the density dependence, of the collision can be probed by colliding nuclei with differing isospin. This will continue to be so with the commissioning of new radioactive ion beam experiments and facilities. There is a truly global effort to understand the physics involved and numerous heavy ion facilities are located world wide, such as: CSR (China), FAIR an extension of GSI (Germany), LHC at CERN (Switzerland), NSCL at MSU (United States), RHIC at BNL (United

States), RIKEN (Japan), and SPIRAL2 at GANIL (France).

These facilities enable the acceleration of unstable nuclei with increased isospin asymmetry, allowing us to probe regions of the nuclear chart away from the line of stability. This will permit us to investigate the development of EoS with increasing asymmetry and density. With this goal in mind, a number of observables have been suggested in the literature to be sensitive to the symmetry energy and its density dependence in heavy ion reactions. Several of the most sensitive are: isospin transport and diffusion, n-p spectra and flows , π^+ versus π^- production and flow.

2.5 Quantum Hadrodynamics and the Relativistic Mean Field Approximation

The purpose of this and the following section is to review the basic concepts behind the relativistic mean field approximation and its application to quantum hadrodynamics (QHD) and the quark-meson coupling (QMC) model. Emphasis will be placed on two particular parametrizations, QHD-II and NL3, and their connection to the QMC model. Quantum hadrodynamics is discussed in several textbooks and reviews, see for example Ref.[58, 110, 111, 150–152].

Historically, non-relativistic approaches were widely used to describe nuclear matter and finite nuclei. This was partly because of being experimentally limited in the early days of nuclear physics to low energies and nuclei close to the line of stability. Even with the development of modern experimental techniques, allowing us to probe higher energies and more exotic nuclei, non-relativistic models are still in use. The reason for this lies in their simplicity and rather accurate description of empirical data. Two of the most notable non-relativistic mean field models are the Skyrme and the Gogny models. The former employs an instantaneous zero range contact interaction, whereas the latter incorporates a finite range. Despite their numerous successes in describing empirical observations, these models are far from being fundamental and offer little explanation for the origin of the empirically proved existence of nuclear saturation or the spin-orbit force.

Two important points to be aware of are: (i) in these non-relativistic models the spin-orbit interaction is included in a rather ad hoc manner and (ii) the smallness of the binding energy of nucleons is used for the justification of the non-relativistic approach. A deeper understanding of these phenomena can be achieved by consideration of effective relativistic interactions mediated by meson exchange. Of particular importance is the inclusion of relativity which most importantly in the context of nuclear systems maintains the distinction between a scalar potential and the temporal component of a 4-vector potential. This in contrast to other systems where relativity becomes important because of kinematics. A relativistic treatment is also necessary for correctly treating the compact stellar objects known generically as neutron stars. It is important for the preservation of causality at high density.

Non-linear self-interactions of a scalar field were suggested by Schiff [153, 154] as early as 1951 as a possible mechanism for saturation. This idea was further developed by Johnson and Teller [155] who demonstrated that a moving nucleon immersed in

a classical potential, whose quanta are neutral scalar mesons, could account for several nuclear properties. The subsequent investigation of Duerr [156] reformulated their idea in a relativistically invariant way. He considered a number of Lorentz structures, but argued that only a scalar interaction and the temporal component of a vector field could lead to a velocity dependent potential that transformed as a scalar in the non-relativistic limit. In addition to other nuclear properties, it was found that this interaction produced a strong spin-orbit interaction comparable in strength used phenomenologically in shell model calculations.

These works paved the way for Walecka's 1974 paper [157], in which he formulated the nuclear interaction as a relativistic quantum field theory. His model has been applied to nuclear matter, finite nuclei and neutron stars [150]. The effective Lagrangian used in his original work included only nucleons and two mesons. This model and its variants have become known as quantum hadrodynamics (QHD) as all of its degrees of freedom are hadrons. In the original version of QHD introduced by Walecka, which we will denote (QHD-I), the baryons interact via the exchange of a scalar-isoscalar meson and a vector-isoscalar meson, now commonly denoted σ and ω respectively. These mesons couple directly to nucleons and are responsible for the intermediate range attraction and the short distance repulsion, respectively.

In the past, non-relativistic models were justified on the basis that the binding energy of nucleons in a nucleus is small; with their binding energy being only a fraction of the free nucleon mass and thus relativistic corrections were thought to be small too. But in a relativistic meson exchange model saturation comes naturally from a cancellation of a large attractive scalar potential produced by σ exchange with a large repulsive vector potential from the ω exchange. Both of these potentials are of the order of the nucleon's mass and it is their sum that is small. Clearly, a relativistic treatment must be pursued if this is the correct origin of saturation. The spin-orbit force also arises naturally in this framework, with the contributions from the σ and ω adding constructively to produce a strong spin-orbit interaction. The existence of these large scalar and vector potentials in nuclei is now generally accepted as empirical fact. Moreover, as a consequence of its relativistic formulation, causality is preserved in dense matter from the outset. This is in contrast to non-relativistic models which can violate causality at large densities.

QHD was shown to be a renormalisable meson theory, characterised by the meson masses and their couplings to the nucleons. Despite being renormalizable, a perturbative expansion is not possible as the coupling parameters are not small. Typical loop expansions are not convergent as higher order corrections are significant [158]. As it stands today, it is considered as an effective phenomenological model as the couplings are adjusted to reproduce properties of finite nuclei and nuclear matter at equilibrium and not the free NN scattering data like the Bonn, Nijmegen or Paris boson exchange potentials. In Ref. [159], Glendenning made a comparison between the renormalizable and effective mean field versions of QHD. He demonstrated that with or without that the vacuum polarization the EoS varies insignificantly if the model parameters are constrained to the saturation properties. This is very pleasing due to the complications with higher order corrections and in practice the model is generally applied using either

the relativistic mean field (RMF) approximation (also known as the Hartree approximation) or an extension thereof, for instance exchange (Fock) terms or random phase approximation (RPA).

Pions are the lightest mesons and as such are paramount to the description of the nuclear interaction, particularly in the long range. For this reason, the pion should also be included explicitly in QHD, but to lowest order (Hartree approximation) in which quantum fluctuations are neglected, the pion does not contribute because of its negative parity. The meson resonances, on the other hand, can contribute and are generally treated as point like mesons with no width. The physical σ meson, despite its troubling history, is generally identified with the correlated (s-wave) two pion exchange and the ω with three-pion exchange. In QHD, these mesons should not strictly be construed as the physical mesons one finds in experiment, instead they should be considered as fields with the same quantum numbers. Meson masses are set to their experimental values, while their couplings to the nucleons are treated as free parameters constrained to nuclear observables. For example, the ω meson is meant to describe the repulsive vector-isoscalar part of the interaction. This repulsive ω exchange can be viewed as being made up of the physical ω exchange and the repulsion generated from quark exchange at very short distances.

Modern incarnations of QHD are among the leading phenomenological nuclear structure models. They are capable of quantitatively describing many ground and excited state properties of nuclei as well as the bulk properties of nuclear matter. There still remains considerable uncertainty in the QHD formulation of the nuclear interaction, particularly in the isovector sector. During the intervening years numerous extensions of this model have occurred to improve the quantitative description of nuclear properties. The original version QHD-I is the simplest version of all the variants and is the basis for all descendant variations as it has been found that the σ and ω exchange are by far the most important. Variations of QHD have supplemented QHD-I with extra meson degrees of freedom, baryons containing strange quarks i.e hyperons, meson self-couplings and additional couplings between mesons. Different data sets have also been used for constraining coupling constants including both bulk nuclear matter and finite nuclei properties.

Among the most crucial extensions of QHD is the enhancement of the isovector sector, which occurred shortly after the conception of the model, where the model was extended to include a third meson, the vector-isovector ρ meson. This meson is needed to distinguish between neutrons and protons and hence improve the description of asymmetric matter. At the mean field level, the ρ meson is important for the EoS of ANM, but has no effect in SNM. We will simply refer to this version of QHD as QHD-II.

The effective Lagrangian density used in QHD-II is given by a combination of nucleon and meson components

$$\mathcal{L} = \mathcal{L}_{\mathrm{N}} + \mathcal{L}_{\mathrm{m}} \quad , \tag{2.5.1}$$

where the baryon Lagrangian density is expressed as

$$\mathcal{L}_{\mathrm{N}} = \bar{\Psi}_{\mathrm{N}} \left(i\gamma_\mu \partial^\mu - M_{\mathrm{N}} + g_\sigma \sigma - g_\omega \gamma^\mu \omega_\mu - \frac{g_\rho}{2} \gamma^\mu \boldsymbol{\tau} \cdot \boldsymbol{\rho}_\mu \right) \Psi_{\mathrm{N}} \ , \tag{2.5.2}$$

where $\boldsymbol{\tau}$ is the vector of isospin Pauli matrices and the Ψ_N denotes the nucleon isodoublet spinor expressed explicitly as

$$\Psi_{\rm N} = \begin{pmatrix} \psi_{\rm p} \\ \psi_{\rm n} \end{pmatrix} \quad . \tag{2.5.3}$$

The meson Lagrangian density is

$$\begin{aligned} \mathcal{L}_{\rm m} &= \frac{1}{2}(\partial_\mu\sigma\partial^\mu\sigma - m_\sigma^2\sigma^2) - \frac{1}{4}\Omega_{\mu\nu}\Omega^{\mu\nu} + \frac{1}{2}m_\omega^2\omega_\mu\omega^\mu \\ &\quad -\frac{1}{4}\boldsymbol{R}_{\mu\nu}\cdot\boldsymbol{R}^{\mu\nu} + \frac{1}{2}m_\rho^2\boldsymbol{\rho}_\mu\cdot\boldsymbol{\rho}^\mu \ , \end{aligned} \tag{2.5.4}$$

for which the anti-symmetric vector meson field strength tensors are

$$\Omega_{\mu\nu} = \partial_\mu\omega_\nu - \partial_\nu\omega_\mu \qquad \text{and} \qquad \boldsymbol{R}_{\mu\nu} = \partial_\mu\boldsymbol{\rho}_\nu - \partial_\nu\boldsymbol{\rho}_\mu \quad . \tag{2.5.5}$$

Note that there is no photon vector field, A_μ, as nuclear matter does not include the electromagnetic interaction. In calculations of finite nuclei this interaction is included.

From this Lagrangian, Eq. (2.5.1), we obtain through Hamilton's principle of stationary action

$$\delta S = \delta\int dt\int d^3x\mathcal{L}(\vec{x},t) = 0 \quad , \tag{2.5.6}$$

the Euler-Lagrange equations

$$\frac{\partial\mathcal{L}}{\partial\phi_\alpha} - \partial_\mu\frac{\partial\mathcal{L}}{\partial(\partial_\mu\phi_\alpha)} = 0, \tag{2.5.7}$$

where ϕ_α is any of the above mentioned fields. This leads naturally to a coupled system of non-linear partial differential equations for the quantum fields. Nucleons being spin-1/2 fermions are described by a Dirac equation of the form,

$$\left(i\gamma^\mu\partial_\mu - g_\omega\gamma^\mu\omega_\mu - \frac{g_\rho}{2}\gamma^\mu\boldsymbol{\tau}\cdot\boldsymbol{\rho}_\mu - M_{\rm N} + g_\sigma\sigma\right)\Psi_{\rm N} = 0 \ . \tag{2.5.8}$$

As for the mesons, the scalar-isoscalar σ meson is described by a Klein-Gordon equation,

$$(\partial_\mu\partial^\mu + m_\sigma^2)\sigma = g_\sigma\bar{\Psi}_{\rm N}\Psi_{\rm N} \quad , \tag{2.5.9}$$

together with the ω and ρ vector mesons, which are given by the following Proca equations,

$$\partial_\mu\Omega^{\mu\nu} + m_\omega^2\omega^\nu = g_\omega\bar{\Psi}_{\rm N}\gamma^\nu\Psi_{\rm N} \ , \tag{2.5.10}$$

$$\partial_\mu\boldsymbol{R}^{\mu\nu} + m_\rho^2\boldsymbol{\rho}^\nu = \frac{g_\rho}{2}\bar{\Psi}_{\rm N}\boldsymbol{\tau}\gamma^\nu\Psi_{\rm N} \ , \tag{2.5.11}$$

the system is complete. This is a difficult system of equations to solve and to make the problem tractable approximations are applied. Static, no sea and mean field approximations are typically used. The static approximation refers to neglecting time dependence and no sea refers to ignoring the Dirac sea of negative energy states.

In the mean field approximation the meson field operators are replaced by their ground state expectation values. Thus their fields are essentially treated classically. The ground state is assumed to be of definite spin and parity, 0^+. As we are considering infinite uniform (homogeneous) nuclear matter in the above approximations, we have translational and rotational invariance and thus the space-like components of the meson fields vanish allowing us to write:

$$\begin{aligned} \sigma &\rightarrow \langle \Psi_{\text{g.s.}} | \sigma | \Psi_{\text{g.s.}} \rangle \equiv \langle \sigma \rangle \equiv \bar{\sigma} \ , && (2.5.12) \\ \omega_\mu &\rightarrow \langle \Psi_{\text{g.s.}} | \omega_\mu | \Psi_{\text{g.s.}} \rangle \equiv \langle \omega_\mu \rangle = \langle \delta_{\mu 0} \omega_\mu \rangle \equiv \bar{\omega} \ , && (2.5.13) \\ \boldsymbol{\rho}_\mu &\rightarrow \langle \Psi_{\text{g.s.}} | \boldsymbol{\rho}_\mu | \Psi_{\text{g.s.}} \rangle \equiv \langle \boldsymbol{\rho}_\mu \rangle = \langle \delta_{\mu 0} \delta_{a3} \rho_{\mu a} \rangle \equiv \bar{\rho} \ , && (2.5.14) \end{aligned}$$

where a refers to the isospin index. The nucleon fields remain operators and are the sources for the meson fields. They must therefore be evaluated by acting on the ground state. In the equations of motion for the meson fields Eqs. (2.5.9–2.5.11) the baryon operators are replaced by their normal ordered ground state expectation values:

$$\begin{aligned} \bar{\Psi}_{\text{N}} \Psi_{\text{N}} &\rightarrow \langle \Psi_{\text{g.s.}} | : \bar{\Psi}_{\text{N}} \Psi_{\text{N}} : | \Psi_{\text{g.s.}} \rangle \equiv \langle \bar{\Psi}_{\text{N}} \Psi_{\text{N}} \rangle \quad , && (2.5.15) \\ \bar{\Psi}_{\text{N}} \gamma^\mu \Psi_{\text{N}} &\rightarrow \langle \Psi_{\text{g.s.}} | : \bar{\Psi}_{\text{N}} \gamma^0 \Psi_{\text{N}} : | \Psi_{\text{g.s.}} \rangle \equiv \langle \Psi^\dagger_{\text{N}} \Psi_{\text{N}} \rangle \quad , && (2.5.16) \\ \bar{\Psi}_{\text{N}} \boldsymbol{\tau} \gamma^\mu \Psi_{\text{N}} &\rightarrow \langle \Psi_{\text{g.s.}} | : \bar{\Psi}_{\text{N}} \tau_3 \gamma^0 \Psi_{\text{N}} : | \Psi_{\text{g.s.}} \rangle \equiv \langle \Psi^\dagger_{\text{N}} \tau_3 \Psi_{\text{N}} \rangle \quad . && (2.5.17) \end{aligned}$$

The crux of the mean field approximation is that in the many-body system the nucleons are thought of as moving independently in a one-body potential which is generated self-consistently by their interaction amongst themselves. The one-body potential originates from the meson fields. This approximation is increasingly more reliable with increasing baryonic density and therefore appropriate to the nuclear matter in neutron stars.

This is usually called the Hartree or relativistic mean-field (RMF) approximation. In this lowest order approximation the quantum fluctuations of the meson fields are ignored and the pion does not contribute because of parity considerations. Of the ρ mesons, only the neutral ρ contributes and is non-zero only in ANM. After applying these approximations the meson equations of motion Eqs. (2.5.9–2.5.11) become

$$\begin{aligned} m_\sigma^2 \bar{\sigma} &= g_\sigma \langle \bar{\Psi}_{\text{N}} \Psi_{\text{N}} \rangle = g_\sigma \left(\rho^{\text{s}}_{\text{p}} + \rho^{\text{s}}_{\text{n}} \right) = g_\sigma \rho^{\text{s}} \quad , && (2.5.18) \\ m_\omega^2 \bar{\omega} &= g_\omega \langle \Psi^\dagger_{\text{N}} \Psi_{\text{N}} \rangle = g_\omega \left(\rho^{\text{v}}_{\text{p}} + \rho^{\text{v}}_{\text{n}} \right) = g_\omega \rho^{\text{v}} \quad , && (2.5.19) \\ m_\rho^2 \bar{\rho} &= \frac{g_\rho}{2} \langle \Psi^\dagger_{\text{N}} \tau_3 \Psi_{\text{N}} \rangle = \frac{g_\rho}{2} \left(\rho^{\text{v}}_{\text{p}} - \rho^{\text{v}}_{\text{n}} \right) = \frac{g_\rho}{2} \rho^{\text{v}}_3 \quad . && (2.5.20) \end{aligned}$$

In Eqs. (2.5.18–2.5.20), ρ^{s}, ρ^{v} and ρ^{v}_3 represent the total scalar, vector and isovector baryon number densities, where ρ^{s}_i and ρ^{v}_i are the individual nucleon contributions, $(i \in \{p, n\})$, which are given by

$$\rho^{\text{s}} = \sum_{i \in \{p,n\}} \rho^{\text{s}}_i = \frac{(2J_{\text{N}} + 1)}{(2\pi)^3} \sum_{i \in \{p,n\}} \int_{|\vec{p}| \leq p_{F,i}} d^3p \ \frac{M^*_{\text{N}}}{\sqrt{\vec{p}^{\,2} + M^{*\,2}_{\text{N}}}} \qquad (2.5.21)$$

and

$$\rho^{\text{v}} = \sum_{i \in \{p,n\}} \rho^{\text{v}}_i = \frac{(2J_{\text{N}} + 1)}{(2\pi)^3} \sum_{i \in \{p,n\}} \int_{|\vec{p}| \leq p_{F,i}} d^3p \quad . \qquad (2.5.22)$$

In Eq. (2.5.21) and Eq. (2.5.22), $p_{\mathrm{F,i}}$ denotes the Fermi momentum of nucleon type i. These integrals are evaluated by making use of spherical symmetry. Our notation is such that,

$$\int\limits_{|\vec{p}|\leq p_{F,i}} d^3p \quad (\text{Integrand}) \quad = \quad \int_0^{\mathrm{pF,i}} \mathrm{dk\ k^2 4\pi} \quad (\text{Integrand}) \quad . \tag{2.5.23}$$

After performing the above approximations the Dirac equation for the nucleons also becomes simplified,

$$\left(i\gamma^\mu\partial_\mu - g_\omega\gamma^0\bar{\omega} - \frac{g_\rho}{2}\gamma^0\tau_3\bar{\rho} - M_{\mathrm{N}}^*\right)\Psi_{\mathrm{N}} = 0 \ , \tag{2.5.24}$$

where we have defined the effective nucleon mass, $M_{\mathrm{N}}^* = M_{\mathrm{N}} - g_\sigma\bar{\sigma}$. The effective mass M_{N}^* is significantly smaller than its bare value.

To summarise, the RMF or Hartree approximation results in a semi-classical theory of nucleons immersed in the averaged or classical meson fields. This is the lowest order approximation which neglects quantum fluctuations. The extension beyond the lowest order is not unique and can be derived in number of different but essentially equivalent ways. In Chapter 4 we will use the same method as used in Refs. [160–163], but it can also been achieved by reformulating QHD in terms Dyson's equation for nucleons [150].

To calculate the EoS of nuclear matter we will need to construct the energy momentum tensor from the effective Lagrangian Eq. (2.5.1), which can be defined as

$$T_{\mu\nu} = -g_{\mu\nu}\mathcal{L} + \frac{\partial\phi_\alpha}{\partial x^\nu}\frac{\partial\mathcal{L}}{\partial(\partial\phi_\alpha/\partial x_\mu)} \tag{2.5.25}$$

where ϕ_α denotes each physical field, i.e., both nucleons and mesons.

Under the assumption that the infinite and homogeneous nuclear matter can be treated as a perfect fluid the energy momentum tensor takes the form

$$T_{\mu\nu} = (\mathcal{E} + P)u_\mu u_\nu - P g_{\mu\nu} \quad , \tag{2.5.26}$$

where $\mathcal{E}$ and P are the total energy density and pressure. The four vector u_μ is the four-velocity of the perfect nuclear fluid. In the local rest frame of the fluid the four-velocity is $u_\mu = (1, 0, 0, 0)$ and the energy-momentum tensor simplifies to

$$T_{\mu\nu} = \begin{pmatrix} \mathcal{E} & 0 & 0 & 0 \\ 0 & P & 0 & 0 \\ 0 & 0 & P & 0 \\ 0 & 0 & 0 & P \end{pmatrix} \quad . \tag{2.5.27}$$

From the QHD Lagrangian, one can derive the total ground state energy density $\mathcal{E}$, which is given by the normal ordered ground state expectation value of the 00 component of the energy momentum tensor, i.e $\mathcal{E} = \langle T_{00}\rangle$. Following the usual methods [110, 111] one arrives at

$$\mathcal{E} = \frac{2J_N + 1}{(2\pi)^3}\sum_{i\in\{p,n\}}\int\limits_{|\vec{p}|\leq p_{F,i}} d^3p\ \sqrt{\vec{p}^{\,2} + M_N^{*\,2}} + \frac{1}{2}m_\sigma^2\bar{\sigma}^2 + \frac{1}{2}m_\omega^2\bar{\omega}^2 + \frac{1}{2}m_\rho^2\bar{\rho}^2 \quad , \tag{2.5.28}$$

for the total ground state energy density and

$$P = \frac{1}{3}\frac{(2J_N+1)}{(2\pi)^3}\sum_{i\in\{p,n\}}\int_{|\vec{p}|\leq p_{F,i}} d^3p\ \frac{\vec{p}^{\,2}}{\sqrt{\vec{p}^{\,2}+M_N^{*2}}} - \frac{1}{2}m_\sigma^2\bar{\sigma}^2 + \frac{1}{2}m_\omega^2\bar{\omega}^2 + \frac{1}{2}m_\rho^2\bar{\rho}^2 \quad (2.5.29)$$

for its pressure. In the ground state at zero temperature, the total baryonic vector number density ρ^{v} with the energy density $\mathcal{E}$ and pressure P given in Eq. (2.5.28) and Eq. (2.5.29) comprise the complete set of thermodynamic variables needed to describe the QHD nuclear matter EoS. This is a thermodynamically consistent approximation and the mean field equations of motion can be obtained, by minimizing the total energy density with respect to the physical fields and likewise the pressure can be obtained through Eq. (2.3.7).

The binding energy, saturation density and symmetry energy at saturation are quite well understood. In particular, the symmetry energy at saturation is generally considered to be within a few MeV of 32.5 MeV. This makes these observables useful in constraining our coupling constants, whereas the density dependence of the symmetry energy, its slope L_0, the incompressibility K_0 and the remaining nuclear matter properties are considerably more uncertain experimentally. The parameter sets of QHD-II and NL3 are given in Table 2.5.1 and 2.5.2.

In SNM, the QHD-I and QHD-II parametrizations are equivalent as the ρ mesons do not contribute. These parametrizations unfortunately produce a SNM EoS which is too stiff, by which we mean that the incompressibility is too large. An EoS is generally said to be stiffer than another EoS if greater pressure is produced for a given energy density. To overcome this failing of the most basic parameters sets it was first proposed by Boguta and Bodmer [164] to incorporate non-linear self-interactions of the scalar field, incorporating both cubic and quartic terms. The two extra couplings provide additional flexibility in the EoS to fit two more observables traditionally the incompressibility K_0 and the effective nucleon mass M_{N}^* at equilibrium [111]. The scalar potential in linear QHD models (QHD-I, QHD-II) is simply of the form

$$U_s(\sigma) = \frac{1}{2}m_\sigma^2\sigma^2 \quad , \quad (2.5.30)$$

which becomes

$$U_s(\sigma) = \frac{1}{2}m_\sigma^2\sigma^2 + \frac{\kappa}{3!}(g_\sigma\sigma)^3 + \frac{\lambda}{4!}(g_\sigma\sigma)^4 \quad (2.5.31)$$

upon inclusion of scalar self-interactions. Generally, this non-linearity in the scalar field is interpreted as being related to a density dependence of the scalar coupling. It can also be interpreted as arising from nucleon substructure and many-body forces. There are many other parameter sets in the literature, obtained, for example by fitting different data or incorporating additional non-linear self-interactions [165–167], density dependent couplings [168] and meson-meson interactions [169].

Parameter Set	g_σ^2	g_ω^2	g_ρ^2	κ	λ
QHD-II [150]	109.626	190.431	65.226	-	-
NL3 [167]	104.3871	165.5854	79.6000	3.8599	-0.01591

Table 2.5.1: Two typical QHD parameter sets. Coupling constants are dimensionless except for κ which is given in MeV. The parameter sets are given using the convention that the scalar field is positive. See the above references for the details of the fitting procedure.

Parameter Set	$M_{\rm N}$	m_σ	m_ω	m_ρ	K_0
QHD-II [150]	939	520	783	770	545
NL3 [167]	939	508.194	783.501	763.0	271.76

Table 2.5.2: Masses and incompressibility for the two typical QHD parameter sets given in Table 2.5.1. The masses and incompressibility are given in MeV.

2.6 The Quark-Meson Coupling Model

Employing baryons and mesons as the relevant degrees of freedom has provided a fruitful description of many nuclear properties. Important examples of this include the description of deuteron properties by pion exchange and realistic potentials like those from Bonn and Nijmegen that describe the NN scattering data with a high level of accuracy. But hadrons have been known to have structure in the form of quarks and gluons for decades. The usefulness of the quark model in describing the hadronic spectrum combined with the successful description of experimental data by QCD in the perturbative regime leaves little room for any other interpretation than that QCD is the correct theory of strong interactions. The question then naturally arises, are quarks and gluons relevant to the description of nuclear systems or are the effective hadron degrees of freedom are all that are needed? At normal nuclear densities this is a difficult question to answer, but theoretical studies of the EMC effect suggest that they may be important, see for example Ref. [170].

As the density increases the nucleons will begin to overlap and hence the underlying structure is likely to play an increasingly important role. It has been theorised that, at some high density and/or temperature, a phase transition may occur where hadronic matter may deconfine. Whether or not the densities in the interior of neutron stars are great enough to achieve such a phase transition is uncertain. This is one of the questions we will address using relativistic quark level models in Ch. 7.

The previous sections concentrated on introducing a formulation of QHD for nuclear matter. It is a model by which point like nucleons interact by exchanging point like mesons. All structure of the hadrons is completely neglected in this model. We would like to move beyond the simplification of structureless hadrons and investigate the properties of nuclear matter and neutron stars in a model treating baryons as a cluster of three quarks. With this goal in mind, we introduce in this section a relativistic quark level model known as the QMC model. This model is closely connected to QHD, but

incorporates hadron structure by modelling nucleons as MIT bags with mesons being exchanged between quarks in different bags.

The MIT bag model originated in the 60's with Bogolioubov [171] and was later improved upon by the MIT group [172, 173]. Bag models are phenomenological, allowing us in a simple way to impose the physical observation that quarks are confined within colour-singlet hadrons and never seen in isolation. A rigid boundary condition is implemented confining the quarks, also making the restriction that only those bound quarks should exist inside the bag cavity and that different bags should not overlap. This negates the main supposition of the model that mesons couple directly to the quarks and also its application to dense matter. In the strict definition of the bag model these bags should not overlap, but this statement is really too restrictive and the bag model picture should be interpreted as a simplified picture of the complicated confinement mechanism [161]. This is the point of view taken and why we believe that the model may be valid within the density ranges to be considered in this thesis. For a more detailed explanation of the bag model we refer the reader to [174–176], where this model is thoroughly discussed.

Through the inclusion of internal structure the model offers natural explanations from the quark level for origin of nuclear saturation and of the non-linear scalar interaction, which is phenomenologically needed to provide a quantitative description of nuclear properties, particularly for the incompressibility. Moreover, it provides a connection between hadron structure and many-body forces in non-relativistic Skyrme models. It is a phenomenological model which has had success in predicting the properties of both nuclear matter and finite nuclei. In particular, the binding energies of Λ-hypernuclei are well reproduced and Σ-hypernuclei are predicted to be unbound in qualitative agreement with experiment. The salient feature of the QMC model is that it incorporates quark substructure into the baryons by modelling them as bags and coupling the exchanged mesons directly to the quarks as opposed to the baryons, which is the case in QHD. The model was introduced using the bag model, but it can be implemented more generally by changing the model for hadronic structure. The quark mean-field (QMF) model [177–180] shares essentially the same features as the QMC model.

The QMC model first appeared in Ref. [181], where Guichon suggested a new kind of saturation mechanism for nuclear matter originating from the quark level. The nucleons were taken to be MIT bags containing three massless quarks which were coupled directly to the exchanged mesons modifying their motion. The model supplemented the usual MIT bag Lagrangian with the simplest local couplings of the σ and ω mesons to the confined quarks. That is, the couplings were taken to be $g^q_\sigma \bar{q} q \sigma$ and $g^q_\omega \bar{q} q \omega$, where q is the SU(2) isodoublet of light quarks. It was later improved and generalised to finite nuclei by Guichon, Rodinov and Thomas [182]. The model was treated in the mean field approximation as is the case with most subsequent papers using the QMC model. More recent versions of the QMC model go beyond this approximation by including Fock terms [183] or considering a fluctuation term which also amounts to a Fock term [161].

In the QMC model the coupling of the quarks to the mesons produces the mean fields which in turn modify the equations of motion of the quarks. As described in

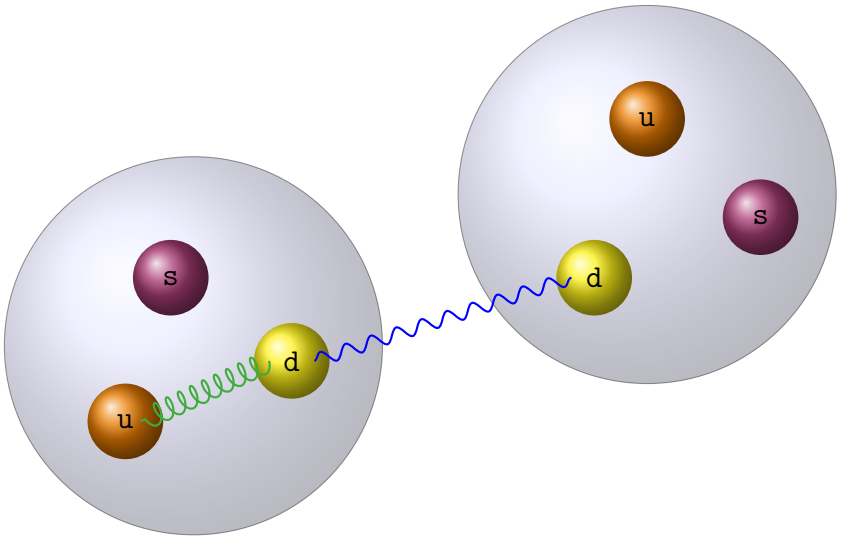

Figure 2.6.1: Schematic picture of the QMC Model.

Ref. [181], the vector mean field $\bar{\omega}$ is linear in density whereas the scalar mean field $\bar{\sigma}$ is dependent on a source term. The response of the quark wave function ultimately results in a decrease of the source term meaning that $\bar{\sigma}$ does not increase as fast as $\bar{\omega}$ as the density increases. That is, the quark structure introduces an effect that opposes the scalar field. Eventually the repulsive ω exchange is larger than that of the attractive σ exchange resulting in the saturation of nuclear matter.

Opposition to the applied scalar field is the only way in which the internal structure affects nuclear matter. By performing an explicit QMC model calculation directly solving the bag model equations one is able to produce a parametrization for the in-medium mass of a baryon. Given in terms of the nucleon coupling $g_{\sigma N}$ and the applied scalar field it takes the form,

$$M_{\mathrm{B}}^{*} = M_{\mathrm{B}} - w_{\sigma B} g_{\sigma N} \bar{\sigma} + \frac{d}{2} \tilde{w}_{\sigma B} (g_{\sigma N} \bar{\sigma})^{2} \quad , \tag{2.6.1}$$

where the weightings $w_{\sigma B}$ and $\tilde{w}_{\sigma B}$ simply allow the use of a unique coupling to nucleons. The parameter d, which is obtained from the fit, is called the scalar polarizability in analogy with electric polarizability. One can therefore replace the explicit description of the internal structure of the baryons by constructing an effective Lagrangian on the hadronic level and proceed to solve the relativistic mean field equations in a standard way [150]. This is done by reformulating the QMC Lagrangian density by redefining the scalar field σ in terms of a new scalar field $\phi = \phi(\sigma)$, such that the nuclear mass depends linearly on ϕ and the resultant QHD equivalent Lagrangian is supplemented by non-linear self-interactions of the new scalar ϕ field [184, 185]. In this manner, the non-linear dependence on the scalar field can be considered as the originating from the internal structure of the baryon. In QHD models, the non-linear scalar potentials can differ considerably for large values of the scalar field. Whereas in the QMC model it has been shown using several models for the nucleon, it has the same general behaviour regardless of the confinement mechanism.

The quark level couplings are in one to one correspondence to the hadronic couplings, thus once the couplings are fixed at the quark level, the hadronic couplings follow for free and vice versa. These couplings are determined by fitting the saturation properties of symmetric nuclear matter. Only the scalar coupling is density dependent and that dependence is calculated self-consistently through the parametrization of the in-medium effective mass obtained through the bag equations. The quadratic dependence of the effective mass induced by the internal structure of the nucleon presents itself in the equation of motion for the scalar field,

$$\bar{\sigma} = -\frac{1}{m_\sigma^2}\frac{(2J_\mathrm{N}+1)}{(2\pi)^3}\sum_{i\in\{p,n\}}\int_{|\vec{p}|\leq p_{F,i}} d^3p\ \frac{M_\mathrm{N}^*}{\sqrt{\vec{p}^{\,2}+M_\mathrm{N}^{*\,2}}}\frac{\partial M_\mathrm{N}^*}{\partial\bar{\sigma}} \tag{2.6.2}$$

$$= \frac{1}{m_\sigma^2}\frac{(2J_\mathrm{N}+1)}{(2\pi)^3}\sum_{i\in\{p,n\}} g_{\sigma N}C_\mathrm{N}(\bar{\sigma})\int_{|\vec{p}|\leq p_{F,i}} d^3p\ \frac{M_\mathrm{N}^*}{\sqrt{\vec{p}^{\,2}+M_\mathrm{N}^{*\,2}}} \quad , \tag{2.6.3}$$

where

$$-\frac{\partial M_\mathrm{N}^*}{\partial\bar{\sigma}} = g_{\sigma N}C_\mathrm{N}(\bar{\sigma}) = g_{\sigma N} - d g_{\sigma N}^2\bar{\sigma} \quad . \tag{2.6.4}$$

The internal structure of the nucleon modifies the self-consistent equation to be solved, in turn changing the density dependence of the in-medium mass. The quadratic dependence of the in-medium mass on the scalar field means that the QMC model can avoid the unfortunate prediction of negative masses at high density that occur in simple QHD parametrizations [185].

In Ref. [186], Guichon and Thomas derived a Skyrme type effective force with two-, three- and four-body forces from the QMC model. This was later improved upon by Guichon *et al* [160] by removing the need to expand about $\bar{\sigma} = 0$. A connection between the many-body interactions in Skyrme functionals and nucleon structure was emphasised. The scalar polarizability, d, was shown to be the key ingredient, with the many-body terms shown to be proportional to powers of d and thus a consequence of nucleon structure.

Many modifications and extensions of the original QMC model have been developed. The review article by Saito *et al* [187] gives a complete and critical evaluation of the QMC model up to 2007. Since this comprehensive review, the effect on the binding of hypernuclei by inclusion of one-gluon exchange (between quarks in the same bag) is a particularly interesting new development. This inclusion has the effect of changing the density dependence of the effective baryon mass and most importantly lifting the degeneracy seen in the baryon octet between the Λ and Σ hyperons. Encouragingly, the results of Ref. [188] which self-consistently incorporates the effect of the scalar field on this hyperfine interaction predicted Λ-hypernuclei to be bound and Σ-hypernuclei unbound in qualitative agreement with experiment. This is the version of the bag model we will be using for modelling the baryons and the quadratic mass parametrization obtained in Ref. [188] is included in the appendix for easy reference.

3

General Relativity and the Astrophysics of Neutron Stars

This chapter aims to introduce neutron stars, their general relativistic structure and the important role they play in constraining the nuclear equation of state. There exists a vast literature on neutron stars, a few of the most useful textbook references are [111, 189–191], see also the recent reviews [192–194].

Neutron stars have a long history, first proposed by Baade and Zwicky [195] in 1934 to be the end product of a supernova and observed by Hewish and Bell in 1967 [196]. They are quite extreme and complex objects, where all four known forces play a role. Their densities (1–10ρ_0) are far greater than what we are capable of maintaining in a laboratory. Heavy ion collisions are able to momentarily achieve high densities, but pale in comparison to neutron stars. They are the densest forms of matter this side of an event horizon and an ideal place to test phenomenological nuclear physics models in an extreme environment.

Astronomical observations provide us with information on these fascinating objects. Typical observables consist of mass, radius, photon red-shift, temperature, cooling rate, angular velocity, glitches, and their moment of inertia. These can be observed or inferred and then compared to a calculated value within a chosen model. In this thesis, we will only be interested in their masses and radii, as these two properties can place severe constraints on the high density behaviour of the EoS of neutron star matter (NSM). Unfortunately, only masses are well known empirically. Measurements of radii suffer a number of technical problems, but are generally regarded to be $\sim$10 km, see for example Refs. [197–201].

As discussed in Sec. 2.4 the measurement of the neutron skin thickness (ΔR) of a heavy nucleus, like ^{208}Pb, could constrain the EoS of nuclear matter. It would impose a constraint on its behaviour at or below the saturation density, particularly the slope of the symmetry energy. In Refs. [113, 114], it was pointed out that combining

such a measurement with the complementary observation of a neutron star radius ($R_{\rm NS}$) could together impose a significant constraint on the EoS, as radii of neutron stars are mostly sensitive to the EoS at high density. They showed, using a RMF model supplemented with non-linear couplings between isoscalar and isovector mesons, that there was a correlation between ΔR and $R_{\rm NS}$. The non-linear meson couplings allowed the manipulation of the density dependence of the symmetry energy, so by adjusting these couplings they were able to vary ΔR. Obtaining EoSs under this variation of couplings, the standard equations of hydrostatic equilibrium (i.e. the TOV equations, see later) were integrated revealing that larger ΔR corresponded to larger $R_{\rm NS}$. For example they conjectured, based on this finding, that if a larger ΔR were to be measured in an experiment, such as PREX, and the radius of a neutron star could be accurately determined to be small, this could indicate a phase transition to some other form of matter, as smaller radii generally correspond to softer EoS at high density.

Historically, masses of neutron stars have been found to be $M_{\rm NS} \sim 1.4\ M_\odot$, but recently there has been observations of not one, but two, large mass neutron stars with $M_{\rm NS} \sim 2.0\ M_\odot$ [202, 203]. These observations used different techniques with similarly small errors, allowing confidence in the existence of large mass neutron stars. The observation of such high mass neutron stars poses a difficult problem for theory, as the inclusion of additional degrees of freedom beyond nucleons and leptons will result in softening[1] of the EoS, leading to the prediction of lower mass stars. The softening occurs because, the Fermi momenta of the particles is distributed over more Fermi seas. However, there is no known mechanism to inhibit the appearance of exotic forms of matter, such as hyperons, if they become energetically favourable, and there lies the problem—reconciling realistic models, which include all energetically possible particles, with observation.

All neutron stars that have been observed do in fact rotate—some incredibly fast—with periods of rotation $P \sim 1.6$ ms–4.6 s. Their periods do increase very slowly, but by and large they make very good clocks. The inclusion of rotation is important, because as the star rotates space-time is warped differently. The shape of a rotating star deviates from having spherical symmetry. It becomes fatter and flatter about its axis of rotation, again affecting space-time[2]. In this thesis, we will be content with the simplified non-rotating model of neutron stars. It is of course possible to consider such rotating compact stars. However, the solutions to Einstein's equation for a rotating neutron star, of arbitrary angular velocity are considerably more complicated, because of the added dependence of the metric on the angular velocity of the star. Slowly rotating neutron stars were studied by Hartle in the 60's [204, 205], where he performed a second order expansion in angular velocity of the Einstein equation for a rotating star. More modern calculations are able to model rapidly rotating neutron stars, their merger with other compact objects and their gravitational wave emissions [206–210]. These offer another way to constrain the EoS through numerical modelling of gravitational wave forms, which can be compared with future observations using gravitational wave detectors.

[1] less pressure for a given energy density

[2] One must also consider frame dragging

Neutron stars have strong magnetic fields and non-zero temperatures, but these aspects will not be considered. Temperature effects are generally small for old and hence cold neutron stars, because the temperature, $k_{\rm B}T$, of the star is very much less than the Fermi energy of the particles making up the star. Although, for a newly minted neutron star, a proto-neutron star, temperature can be important. The effects of magnetic fields on neutron stars are usually ignored as a first approximation, but if the magnetic field is large enough it can affect its EoS and other properties, see for example Refs. [211–217].

3.1 Hydrostatic Equilibrium

Observationally stars are quite stable. They are the result of a balance of forces, an outward pressure force and the contracting gravitational force. During the main sequence of a star the pressure comes predominantly from the thermonuclear reactions (p–p chain and CNO cycle) within the star, i.e. from fusion of hydrogen, helium and so on. Only the more massive stars produce heavier elements like neon, magnesium, silicon, all the way up the nuclear chart until it reaches the most stable nucleus, iron—which has the greatest binding energy per nucleon. Once iron is produced, stellar nucleosynthesis stops, as there are no more exothermic nuclear reactions that can occur to generate additional pressure. Eventually the fuel (the lighter elements) becomes depleted and the outward pressure can no longer prevent the gravitational collapse of the star. The star begins to contract and depending on the initial mass of the star, typically one of three final states can be obtained: a white dwarf, a neutron star or even a black hole. White dwarfs and neutron stars are held up by degeneracy pressure, whereas black holes are a victory for gravity. The masses of these stellar corpses are summarised in Fig. (3.1.1).

For lower mass compact stars the balance of forces, hydrostatic equilibrium, can be described quite adequately using Newtonian physics. The equations of structure for such stars are given by the following coupled differential equations:

$$\frac{dP}{dr} = -\frac{GM(r)\rho(r)}{r^2} = -\frac{GM(r)\epsilon(r)}{(rc)^2} \quad , \tag{3.1.1}$$

$$\frac{dM}{dr} = 4\pi r^2\rho(r) = 4\pi r^2\frac{\epsilon(r)}{c^2} \quad , \tag{3.1.2}$$

where $M(r)$ is the total mass inside radius r. Note that in the second equality there has a been a departure from completely Newtonian physics to a relativistic regime in relating the mass density to the energy density. To solve these equations we need to express the energy density in terms of the pressure. That is, we need an EoS but which model should be used to derive it? In white dwarf stars, the pressure balancing the gravitational force comes from the Fermi pressure of electrons [111, 189–191]. A non-interacting Fermi gas of electrons would be the simplest of such models that could give us an equation of state that includes the quantum effect of the Pauli principle giving rise to the pressure in the white dwarf.

The Newtonian structure equations, Eq. (3.1.1) and Eq. (3.1.2), are only suitable if the mass of the star under consideration is not massive enough to significantly warp

White Dwarf:

$M_{\rm WD} < 1.4 M_\odot$, Progenitor $M \leq 7.0 M_\odot$

Neutron Star:

$1.4 M_\odot \leq M_{\rm NS} \leq 3.0 M_\odot$, Progenitor $M \sim 8$–$20 M_\odot$

Black Hole:

$M_{\rm BH} > 3.0 M_\odot$

Figure 3.1.1: Summary of typical estimates for the masses of main sequence star corpses and their progenitors [218].

space-time. General relativistic effects become important when the (compactness) ratio

$$\frac{GM}{c^2 R}$$

becomes non-negligible. For neutron stars it is necessary to include effects due to general relativity. When general relativistic effects become important the first differential equation describing the pressure gradient within the star becomes modified. We will only be interested in the simplified model, where neutron stars are modelled as static, spherically symmetric, and non-rotating; as considered by [219, 220]. The line element associated with this static and spherically symmetric mass in space-time is

$$ds^2 = e^{\lambda(r)} dr^2 + r^2 (d\theta^2 + \sin^2\theta d\phi^2) - e^{\mu(r)} dt^2 \quad . \tag{3.1.3}$$

This line element (Eq. (3.1.3)), which matches to the Schwarzchild solution on the surface of the star, describes the space-time outside of the star as well as the internal structure. From the line element, Eq. (3.1.3), and the energy-momentum tensor of a perfect fluid, one can obtain the generalisation of Eq. (3.1.1) through Einstein's equation. The pressure gradient is modified by general relativistic corrections, such that

$$\frac{dP}{dr} = -\frac{G}{(cr)^2} \frac{(\epsilon(r) + P(r)) \left(M(r) + 4\pi r^3 \frac{P(r)}{c^2} \right)}{(1 - \frac{2GM(r)}{c^2 r})} \tag{3.1.4}$$

$$= -\frac{G\epsilon(r) M(r)}{(cr)^2} (1 + \frac{P(r)}{\epsilon(r)})(1 + \frac{4\pi r^3 P(r)}{M(r) c^2})(1 - \frac{2GM(r)}{c^2 r})^{-1} \quad , \tag{3.1.5}$$

whereas the second equation (Eq. (3.1.2)) remains unaltered. As can be seen in the second equality, the terms that modify the pressure gradient are all positive definite, so gravity considered in the framework of general relativity has a stronger pull than in the Newtonian setting. This equation was first derived by Tolman [219] and independently by Oppenheimer and Volkoff [220]. Today the general relativistic equations

of hydrostatic equilibrium (Eq. (3.1.5) and Eq. (3.1.2)) are simply called the TOV equations.

The TOV equations can be supplemented with a third differential equation, which can be integrated to obtain the total number of baryons, A, inside the star. To summarise, the three TOV equations are

$$\frac{dM}{dr} = 4\pi r^2 \epsilon(r) \,, \tag{3.1.6}$$

$$\frac{dP}{dr} = -(\epsilon + P(r))\frac{(M(r) + 4\pi r^3 P(r))}{r^2(1 - 2M(r)/r)} \,, \tag{3.1.7}$$

$$\frac{dA}{dr} = \frac{4\pi r^2 \rho}{\sqrt{1 - 2M(r)/r}} \,. \tag{3.1.8}$$

In Eqs. (3.1.6–3.1.8) we use units in which $G = c = 1$. The difference between the total gravitational mass and baryonic mass within a radius R is defined by $M(R) - A(R)M_N$.

To integrate the TOV equations we express the pressure and energy density in terms of the density, so we have a closed system of equations. Through this EoS, the microscopic physics involved in the strong interaction impacts upon the properties of the neutron star. We can then integrate out from the centre of the star to its surface, imposing the following initial conditions: $M(r = 0) = 0$ and $P(r = 0) = P_0$. The pressure at the centre of the star, P_0, is specified by a chosen central density and the surface is identified with zero pressure. The radius at which the pressure vanishes defines the radius $R_{\rm NS}$ and mass $M_{\rm NS} = M(R_{\rm NS})$ of the neutron star. In solving these equations for a given model, one obtains a set of masses and radii parametrised by the core density. In particular, a limit is placed on the maximum mass of stable neutron stars. A realistic model should be able to predict a mass–radius relationship compatible with astronomical observations.

3.2 The Neutron Star EoS

To integrate the TOV equations, we need a model to calculate the EoS. Many models are available in the literature, but which one should be used? There have been many models developed to calculate the EoS, ranging from degenerate Fermi gases and other simple parametrisations to quite complex models. Ideally, we would like to derive it directly from QCD. This unfortunately does not seem feasible at the moment without some new insight. Instead, we can try them all and filter them on general properties. Any reliable model should be able to describe more than just one class of observables. It should be based on sound theoretical principles and encapsulate all the necessary physics, such that it is able describe a large class of different observables well. Neutron stars are interesting in their own right, but are particularly useful in placing new constraints on nuclear models through the high density behaviour of the nuclear EoS. Observations of these compact stellar objects provide stringent constraints allowing certain models to be ruled out. A few key factors to consider in filtering models are: relativity, particle content, astrophysical observables, bulk properties of nuclear matter, finite nuclei and hypernuclei observables.

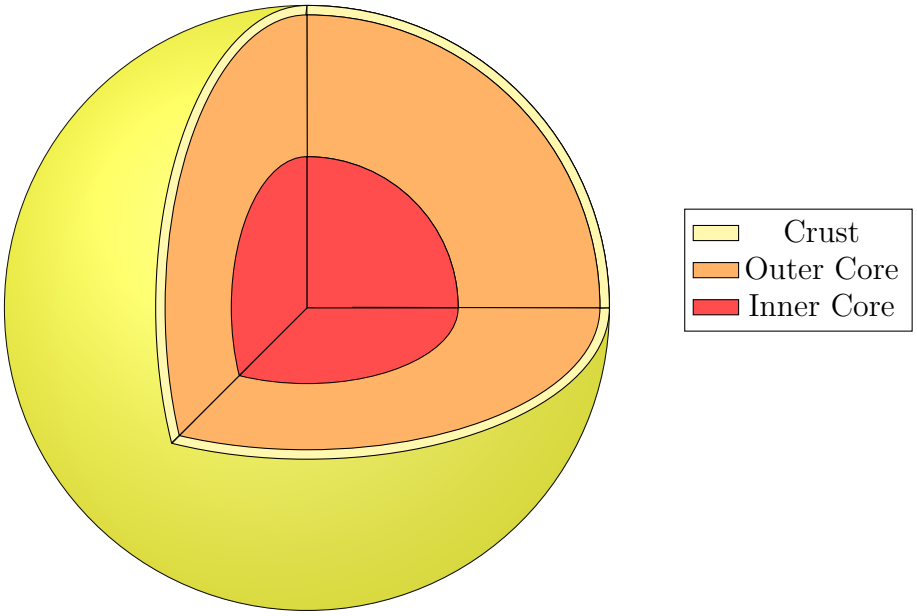

Figure 3.2.1: Schematic cross section of a neutron star, see for example Refs. [111, 189, 191]. Crust: nuclei, electrons and neutrons. Outer core: Nuclear liquid consisting of neutrons, protons, electrons and muons. Inner core: Content uncertain, commonly thought that hyperons, Bose condensates or quark matter could exist.

The first numerical calculation was done by Oppenheimer and Volkoff. They performed the calculation with a simple EoS, assuming the matter inside the neutron star to be an ideal gas of free neutrons. They found a maximum mass $M_{\rm NS} = 0.7\ M_\odot$ and a corresponding radius $R_{\rm NS} = 9.6$ km with a central density of $\rho_c = 5 \times 10^{15}{\rm gcm}^{-3}$. It was smaller than the maximum mass of supernova cores, thus it could not be the end product of supernovae collapse as suggested by Baade and Zwicky [195]. For quite sometime afterwards, neutron stars were mostly ignored. A crucial ingredient had been ignored, the strong interaction—the strong interaction is very strong! In 1959, Cameron [221] showed using a Skyrme model that nuclear forces significantly stiffen the EoS, predicting the limiting neutron star to have a mass of $M_{\rm NS} \sim 2.0\ M_\odot$, which is very much greater than the non-interacting ideal gas of neutrons and therefore it can be formed in a supernova. These early calculations are rather simple and not very realistic. Relativity is ignored, nor does it include the different types of particles which could appear through weak interactions.

Relativity is important for several reasons, which have been mentioned previously. It is a fundamental symmetry, which is important in describing nuclear systems and neutron stars, but most importantly for preserving causality[3] in dense matter. We need not work with a model in curved space-time. Special relativity is perfectly adequate for calculating the EoS, even in the core of neutron stars, where the stars themselves curve space-time. The use of the flat metric is valid, as the variation in the metric over the average distance of baryons is incredibly small ($\leq 10^{-19}$) [111]. This variation is so small that even the variation over a distance stretching across an extremely large number

[3]prevents superluminal speed of sound in matter

baryons is negligible, so we can safely work with a flat metric and the assumption of infinite matter is also reasonable [111].

The composition of the neutron star core beyond nucleons and leptons is uncertain, although it is generally thought that at higher densities cold neutron stars will reach generalised β-equilibrium with respect to all possible reactions. Fig. 3.2.1 shows a schematic cross section of a neutron star. The particle content of the inner core is rather uncertain and several hypotheses exist for its contents, such as Bose condensates, hyperons and quark matter. In this thesis we will only consider the possibility of hyperons and strange quark matter. It has been conjectured that strange quark matter is stable and is the true ground state of matter, being even more tightly bound than iron [222, 223]. Hyperonic matter will be investigated in Ch. 5 and quark matter in Ch. 6 and 7.

For matter in generalised beta equilibrium, only two quantities are conserved. They are the total charge, which is zero in neutron stars and the total baryon number. Strangeness and lepton number are not conserved quantities in neutron stars. To determine the chemical composition one solves a system of equations [111], between chemical potentials for the number densities of the particles. These equations will be derived in Ch. 5 for hyperonic matter.

Determination of chemical composition is important, so for clarity, we will expand on this further. The only possible constituents of dense matter in thermodynamic and beta equilibrium are the particles which cannot decay or escape from the star. Photons and neutrinos are assumed to be completely radiated away from old and hence cold neutron stars—therefore lepton number is not conserved. In free space, the only stable particles are the proton and electron. The neutron is unstable and can decay in minutes. For finite nuclei, neutrons and protons are conditionally stable. They decay only if the the energetically allowed final states are not already occupied. In infinite nuclear matter, which is the approximation with which we will be working, protons and neutrons are once again conditionally stable due to the Pauli exclusion principle. It is necessary to also include electrons and muons to maintain charge neutrality. Hyperons, can also appear, because of the short time scale of the weak interaction 10^{-9} s.

The new particles beyond the basic three (neutron, proton and electron) can occur through weak and strong interactions. The weak nuclear force in neutron stars behaves as a kind of regulator allowing one species of particle to change into another so that the energy of the entire system remains at a minimum. For example, as the chemical potential of the electrons increases the Fermi levels are filled and when μ_e reaches and exceeds 105 MeV it becomes more favourable to create a muon than an electron.

The muon is a new degree of freedom which contributes more to the energy density than to the pressure. Resulting in a slight softening of the EoS. The next lightest negatively charged particles that could appear by the same argument are π^- and K^-. These pions and anti-kaons are bosons and when considering cold neutron stars these mesons should macroscopically condense to a single state, forming a Bose condensate. The possibility of pion, kaon and anti-kaon condensation has been suggested and studied by many [224–237]. There have been conflicting results from various models about, at what density and even if these condensates are predicted at all. The π^- mesons are now generally thought not to occur, because of repulsive in-medium interactions resulting

in a larger in-medium mass inhibiting their production. The attractive nature of the $\bar{K}N$ interaction, which has been supported by experiments on kaonic atoms, suggests that the anti-kaon mass will decrease in-medium. So even though pions are far lighter in vacuum than anti-kaons, this does not necessarily hold in dense matter. Anti-kaons are further complicated, because of the shallow versus deep problem regarding their optical potential, see for example Refs. [238, 239]. For these reasons meson condensates will not be considered in this thesis, instead we will restrict our attention to the baryon octet and transitions to quark matter.

Hyperons must be considered, based on the time scales of the weak interactions (10^{-9} secs) and because, as the density increases, so do the chemical potentials of the nucleons. Eventually it will become energetically favourable to turn nucleons at the top of the Fermi sea into hyperons. They are generally expected to occur at $2-3\rho_0$, irrespective of the model used to describe the baryon-baryon interaction. Although the dominant hyperon and the order in which they appear does depend significantly on the model used, most models including hyperons predict the appearance of either Λ or Σ^- first.

To constrain the in-medium nucleon-hyperon (NY) and hyperon-hyperon (YY) interactions, data is needed. There is very limited to no NY and YY scattering data, with most information on the in-medium hyperon interactions coming from hypernuclear experiments. Systematic searches and studies have been performed, but hypernuclear experiments have been mostly restricted to Λ-hypernuclei. As for Σ-hypernuclei, only one very light Σ–hypernucleus has been found experimentally. The absence of medium to heavy Σ-hypernuclei indicates that phenomenologically the Σ–A interaction is repulsive. The fraction of Σ hyperons should therefore be reduced in dense matter. This is not the case for Λ-hypernuclei, whereas for Ξ-hypernuclei we are awaiting results from JPARC. Information on Ξ-hypernuclei will be most useful in shedding light on their interaction with the nuclear medium. They may also indicate which hyperon is likely to be dominant in dense matter. It is generally thought that the Λ hyperon will be the most dominant, but the mass differences $(M_\Lambda - M_N) \sim 170$ MeV and $(M_\Xi - M_N) \sim 380$ MeV, suggest that for matter in β-equilibrium we could have Ξ^- and Λ competing for dominance depending on their internal structure and its modification through interaction with the surrounding medium. This is possible since $\mu_{\Xi^-} = \mu_n + \mu_e$, where $\mu_e \sim 200$ MeV[4] [240].

It should be noted that the widely used phenomenological potentials, such as AV18 or Nijmegen potentials, require the use of a large number of parameters. These parameters are fitted to NN scattering data and to the properties of light nuclei—to be able to describe the three-body force. Due to the lack of information on hyperon interactions this method is not feasible. Thus it would be highly desirable to develop a different approach. The QMC model is a relativistic quark level model that utilises a minimal set of parameters, the couplings of the quarks to the mesons, which are adjusted to nuclear matter saturation properties. The introduction of hyperons in the model introduces no new parameters. Moreover, the prediction of unbound Σ-hypernuclei has been explained very naturally within the QMC model to be a result of one-gluon exchange.

The softening of the EoS associated with the appearance of hyperons, leads to the

[4]Neutrinos neglected.

prediction of a smaller maximum mass of the star. This has led to many models incorporating hyperons being ruled out due to the recent neutron star observations of Demorest *et al* [202]($1.97 \pm 0.04\ M_\odot$) and of Antoniadis *et al* [203] ($2.01 \pm 0.04\ M_\odot$). Since there is no known mechanism to prevent the appearance of hyperons if they are energetically favourable, one should always include them and concentrate on developing more sophisticated models consistent with both terrestrial experiments and astronomical observations. A QMC model incorporating hyperon degrees of freedom predicted a limiting neutron star mass of $1.98\ M_\odot$ [161], three years before the high mass observation of Demorest *et al* [202]. The use of simplified Fock terms were an important factor in achieving the large mass prediction with hyperons.

Heavier mesons such as the hidden strangeness vector meson $\phi(1020)$ have been considered in other works Ref. [241–243] which have found that they can produce extra vector repulsion delaying the onset of hyperons. Just as QHD can be supplemented with these additional heavier mesons, so can the QMC model. The inclusion of these mesons will mean the strange quark will no longer be just a spectator in the baryon-baryon interactions, as these mesons will couple directly to the strange quark. The additional vector repulsion between hyperons supplied by the ϕ-meson will shift their appearance to higher density in the QMC model as well, reducing the softening of the EoS. This is another possible mechanism to reconcile hyperon degrees of freedom with high mass neutron star observations.

In Ch. 4 and 5, we investigate the effect of including the full structure of the Fock terms, as it is the treatment of the lightest mesons that is the most important, and the inclusion of heavier mesons would necessarily be more model dependent. For this reason, in this thesis we have restricted ourselves to just σ, ω, ρ and π mesons and instead focussed on improving the model by incorporating more sophisticated Fock terms incorporating the tensor interaction of the vector mesons.

4

Hartree-Fock QMC Applied to Nuclear Matter

In this chapter we study the properties of nuclear matter using the QMC model in the Hartree-Fock approximation. Portions of the material presented in this chapter are adapted from Whittenbury *et al* [244]. We will endeavour to explain more clearly the equations stated very succinctly in Ref. [244] and the approximations used therein. All our parameters are fixed at saturation density in Symmetric (N=Z) Nuclear Matter (SNM). Properties at and around saturation density are considered first in SNM, then in Pure Neutron Matter (PNM). In Ch. 5 we extrapolate the model to investigate high density matter in Generalised Beta-Equilibrium (GBEM), which is relevant to neutron stars.

We extend the QMC model by performing a Hartree–Fock calculation including the full vertex structure for the vector mesons. This extension only alters the exchange contribution, including not only the Dirac vector term, as was done in [161], but also the Pauli tensor term. These terms were already included within the QMC model by Krein *et al.* [183] for symmetric nuclear matter and more recently by [245]. We generalise the work of Krein *et al.* by evaluating the full exchange terms for all octet baryons and adding them, as additional contributions, to the energy density. A consequence of this increased level of sophistication is that, if we insist on using the hyperon couplings predicted in the simple QMC model, with no coupling to the strange quarks, the Λ hyperon is no longer bound.

The present line of research compliments the work of Ref. [245], which also considered the tensor interaction in a variation of the QMC model, by investigating an extended set of nuclear matter properties with comparisons to heavy-ion collision data and other theoretical models. The present version of the QMC model differs from [245] as we use couplings as derived within the model and treat contact terms differently.

As is very well known from RMF [150, 246] and QMC [183] Hartree-Fock calculations the scalar $\Sigma^{\rm s}(k)$ and temporal vector $\Sigma^0(k)$ self-energy components are essentially independent of momentum and the spatial vector component is very small. For these reasons we make the assumption that the self-consistency can be treated approximately as in [161] and as in [183] , where the latter included a Fock correction to the scalar field. To state this more precisely we neglect the small spatial vector component of the baryon self-energy such that $\vec{k}^* = \vec{k} + \vec{k}\Sigma^v(k) \simeq \vec{k}$ and the remaining components are treated as momentum independent. This approximate self-energy,

$$\Sigma(k) = \Sigma^{\rm s}(k) - \gamma^0\Sigma^0(k) + \vec{\gamma}\cdot\vec{k}\Sigma^{\rm v}(k) \simeq \Sigma^{\rm s} - \gamma^0\Sigma^0 \tag{4.0.1}$$

has a form identical to the usual mean-field (Hartree) result and the Fock corrections to these components can be included by requiring thermodynamic consistency, which amounts to minimising the total energy density with respect to the meson fields. This results in a small correction to the scalar field.

In our calculation the Fock terms are included, as in Ref. [161], as additional contributions to the energy density. We wish go beyond this to include effects of the Pauli term, form factors and modifications to the scalar mean field coming from the exchange terms as in Ref. [183], where they considered only nucleons in symmetric matter.

In this chapter we derive the equation of state of symmetric and asymmetric nuclear matter from the QMC model using the Hartree–Fock approximation. We present numerical results for an extensive set of nuclear matter properties including incompressibility, symmetry energy and higher order derivatives of the EoS as defined in Ch. 2. We also evaluate the hyperon optical potentials at saturation density in SNM. We then conclude this chapter with a discussion and comparison with experimental constraints.

4.1 The Hartree-Fock QMC

On the surface the QMC model appears to be very similar to the commonly used Relativistic Mean Field (RMF) model. In fact, it is very closely related but fundamentally different. The underlying difference is that the baryons are modelled as MIT bags immersed in self-consistently generated mean fields and it also provides a different explanation for the origin of saturation in nuclear matter coming from the quark level. In the point-like RMF models the mesons couple to the baryons and the saturation of nuclear matter comes about self-consistently from the balance of large scalar and vector potentials. In the QMC model this also occurs, but the mesons are coupled directly to the quarks. This interaction between the quarks and the mesons self-consistently modifies the mass of the quarks and shifts their energy, leading to in-medium modification of the baryons through the non-linear bag equations. From this quark level coupling of the mesons, the saturation of nuclear matter is now dependent on the self-consistency condition between the quarks and the mesons. In the QMC model [181], the quark mass is modified by this scalar field, altering the quark scalar density and ultimately producing a different explanation for the saturation of nuclear matter . The in-medium changes of the baryon masses are calculated through the bag equations and

then parametrised as functions of the scalar field as

$$M_B^* = M_B - w_{\sigma B} g_{\sigma N} \bar{\sigma} + \frac{d}{2} \tilde{w}_{\sigma B} \left(g_{\sigma N} \bar{\sigma} \right)^2 \ , \tag{4.1.1}$$

(where the weightings $w_{\sigma B}$ and $\tilde{w}_{\sigma B}$ simply allow the use of a unique coupling to nucleons). Using this parametrisation and a corresponding density dependent coupling, we can solve for the equation of state in the same standard way as the Walecka model [150], that is at the hadronic level. In this way the sub-structure of the baryons is entirely contained in the mass parametrisation. We use the parametrisation given in Ref. [188], which includes the effects of one gluon exchange. For convenience, this parametrisation is included in Appendix A.1.

There are a number of motivations for going beyond the mean field approximation and performing a Hartree-Fock calculation. Most importantly, in the mean field approximation the pion does not contribute at all because of its parity. On the other hand, the corresponding Fock term has been show in previous versions of the QMC model to reduce the incompressibility [161]. Also, isovector mesons do not contribute at the Hartree level in isospin symmetric systems. Moreover, from earlier discussions in Ch. 2, we know there is a significant tensor component to the nuclear force, but in the mean field approximation of spin saturated nuclear matter its effect is not included. These shortcomings of the mean field approximation could affect our ability to model nuclear matter realistically. In particular, from experiment the ρN vector coupling is known to be small. If this small value for the ρN coupling were used in mean field calculations, rather than using the phenomenologically adjusted value, the calculated value of the symmetry energy would be significantly lower than the experimental value. As the tensor interaction is ignored altogether, we are neglecting the experimental fact that the ρN tensor interaction is rather strong, $f_{\rho N} \sim 3.7 g_{\rho N}$, which could contribute significantly to the symmetry energy.

4.2 The Lagrangian Density

The interaction between the pions and nucleons, or more generally with the spin-1/2 baryon octet under consideration here, is generally treated as either a pseudo-scalar or pseudo-vector coupling governed by

$$\mathcal{L}_{\pi N}^{\text{p.s.}} = g_{\pi NN}^{\text{p.s.}} \bar{\Psi}_{\text{N}} i \gamma_5 \boldsymbol{\tau} \cdot \Psi_{\text{N}} \boldsymbol{\pi} \quad \text{or} \quad \mathcal{L}_{\pi N}^{\text{p.v.}} = g_{\text{A}} \bar{\Psi}_{\text{N}} \gamma_\mu \gamma_5 \boldsymbol{\tau} \cdot \Psi_{\text{N}} \partial^\mu \boldsymbol{\pi} \quad , \tag{4.2.1}$$

respectively. These different forms of the pion nucleon coupling lead to the same one pion exchange potential in the non-relativistic limit if their couplings are related by the Goldberger-Treiman relation

$$g_{\text{A}} = \frac{f_\pi g_{\pi NN}^{\text{p.s.}}}{M_{\text{N}}} \quad . \tag{4.2.2}$$

These different descriptions of the πN interaction behave differently in-medium, with the pseudo-scalar interaction predicting unrealistically large self-energy corrections. For this reason the pseudo-vector coupling is generally used when modelling nuclear matter and finite nuclei [110, 150, 247–250].

Alternatively, one can derive an effective leading order pion baryon interaction using chiral perturbation theory, where one starts with the most general Lagrangian that is consistent with the relevant symmetries and has the smallest number of derivatives. This effective πN Lagrangian is given by [251]

$$\mathcal{L}^{(1)}_{\pi N} = \bar{\Psi}_{\rm N}\left(i\not{D} - M_{\rm N} + \frac{g_{\rm A}}{2}\gamma^\mu\gamma_5 u_\mu\right)\Psi_{\rm N} \quad , \tag{4.2.3}$$

which to lowest order gives[1] rise to the following effective pion-nucleon interaction Lagrangian [251]

$$\mathcal{L}_{\pi N} = -\frac{g_{\rm A}}{2f_\pi}\bar{\Psi}_{\rm N}\gamma_\mu\gamma_5\boldsymbol{\tau}\cdot\Psi_{\rm N}\partial^\mu\boldsymbol{\pi} = i\frac{g_{\rm A}}{2f_\pi}\bar{\Psi}_{\rm N}\not{k}\gamma_5\boldsymbol{\tau}\cdot\Psi_{\rm N}\boldsymbol{\pi} \quad . \tag{4.2.4}$$

It is important to note that there is a change of sign between Eq. (4.2.4) and the conventionally used pseudo-vector coupling in Eq. (4.2.1) [251], which is used in typical Hartree-Fock RMF calculations [110]. Although, in the approximation we are using the change in the sign will not alter the pionic contribution to the energy density, as $\epsilon_\pi \sim \gamma^\mu\gamma^5\gamma^\mu\gamma^5 = \gamma^5\gamma^\mu\gamma^5\gamma^\mu$.

Generalisation to the whole baryon octet is straightforward and the hyperon couplings are simply related to the nucleon pseudo-vector coupling by $SU(3)$ flavour symmetry. The pion-baryon interaction in this thesis is assumed to be described by an SU(3) invariant Lagrangian with the mixing parameter $\alpha = 2/5$ [161] from which the hyperon-pion coupling constants can be given in terms of the pion nucleon coupling, $g^{\rm p.v.}_{\pi BB'} = g^{\rm p.v.}_{\pi NN}\chi_{BB'} = \dfrac{g_A}{2f_\pi}\chi_{BB'}$ [161, 162, 252].

In our calculations of nuclear matter we consider only the spin-1/2 octet baryons. These baryons interact via the exchange of mesons which couple directly to the quarks. The exchanged mesons included are the scalar-isoscalar (σ), vector-isoscalar (ω), vector-isovector (ρ), and pseudo-vector-isovector (π) bosons. These mesons only couple with the light quarks by the phenomenological OZI rule. We include the full vertex structure for the vector mesons, that is, we include both the Dirac and Pauli terms.

The QMC Lagrangian density used in this work is given by a combination of baryon and meson components

$$\mathcal{L} = \sum_B \mathcal{L}_B + \sum_m \mathcal{L}_m \ , \tag{4.2.5}$$

for the octet of baryons $B \in \{N, \Lambda, \Sigma, \Xi\}$ and selected mesons $m \in \{\sigma, \omega, \rho, \pi\}$ with the individual Lagrangian densities

$$\begin{aligned}\mathcal{L}_B &= \bar{\Psi}_B\left(i\gamma_\mu\partial^\mu - M_B + g_{\sigma B}(\sigma)\sigma - g_{\omega B}\gamma^\mu\omega_\mu - \frac{f_{\omega B}}{2M_{\rm N}}\sigma^{\mu\nu}\partial_\mu\omega_\nu\right. \\ &\quad \left. - g_{\rho B}\gamma^\mu\boldsymbol{t}\cdot\boldsymbol{\rho}_\mu - \frac{f_{\rho B}}{2M_{\rm N}}\sigma^{\mu\nu}\boldsymbol{t}\cdot\partial_\mu\boldsymbol{\rho}_\nu - \frac{g_{\rm A}}{2f_\pi}\chi_{BB}\gamma^\mu\gamma^5\boldsymbol{\tau}\cdot\partial_\mu\boldsymbol{\pi}\right)\Psi_B \ ,\end{aligned} \tag{4.2.6}$$

$$\sum_m \mathcal{L}_m = \frac{1}{2}(\partial_\mu\sigma\partial^\mu\sigma - m_\sigma^2\sigma^2) - \frac{1}{4}\Omega_{\mu\nu}\Omega^{\mu\nu} + \frac{1}{2}m_\omega^2\omega_\mu\omega^\mu$$

[1] Here $u_\mu = i\left(u^\dagger\partial_\mu u - u\partial_\mu u^\dagger\right)$ and $u = \exp\left(\dfrac{i\boldsymbol{\tau}\cdot\boldsymbol{\pi}}{2f_\pi}\right) \simeq 1 + i\dfrac{\boldsymbol{\tau}\cdot\boldsymbol{\pi}}{2f_\pi} + \ldots$.

$$-\frac{1}{4}\boldsymbol{R}_{\mu\nu}\cdot\boldsymbol{R}^{\mu\nu}+\frac{1}{2}m_\rho^2\boldsymbol{\rho}_\mu\cdot\boldsymbol{\rho}^\mu+\frac{1}{2}(\partial_\mu\boldsymbol{\pi}\cdot\partial^\mu\boldsymbol{\pi}-m_\pi^2\boldsymbol{\pi}\cdot\boldsymbol{\pi})\ , \quad (4.2.7)$$

for which the vector meson field strength tensors are $\Omega_{\mu\nu}=\partial_\mu\omega_\nu-\partial_\nu\omega_\mu$ and $\boldsymbol{R}_{\mu\nu}=\partial_\mu\boldsymbol{\rho}_\nu-\partial_\nu\boldsymbol{\rho}_\mu$. For the baryon masses we take the average over the isospin multiplet of their experimental values, whereas for the mesons we simply use the experimental values. We also include a $\pi\Lambda\Sigma$ pseudo-vector interaction, as in Ref. [161], which is not shown in the above Lagrangian (Eq. (4.2.6)). As this term is only relevant when both Λ- and Σ-hyperons are present, it has essentially no effect on our results. This is because Σ-hyperons are not energetically favoured. The isospin baryon multiplets are

$$\Psi_{\rm N}=\begin{pmatrix}\psi_{\rm p}\\ \psi_{\rm n}\end{pmatrix}\ ,\quad \Psi_\Lambda=\begin{pmatrix}\psi_\Lambda\end{pmatrix}\ ,\quad \Psi_\Sigma=\begin{pmatrix}\psi_{\Sigma^+}\\ \psi_{\Sigma^0}\\ \psi_{\Sigma^-}\end{pmatrix}\ ,\quad \Psi_\Xi=\begin{pmatrix}\psi_{\Xi^0}\\ \psi_{\Xi^-}\end{pmatrix}\ . \quad (4.2.8)$$

Note that there is no photon vector field, A_μ, as nuclear matter does not include the electromagnetic interaction. In calculations of finite nuclei this interaction is included.

4.3 Equations of Motion and the MFA

From the Lagrangian given in Eq. 4.2.5 we obtain through the Euler-Lagrange equations,

$$\frac{\partial\mathcal{L}}{\partial\phi}-\partial_\mu\frac{\partial\mathcal{L}}{\partial(\partial_\mu\phi)}=0, \quad (4.3.1)$$

where ϕ is any of the above mentioned fields, a system of coupled non-linear partial differential equations for the quantum fields,

$$(\partial_\mu\partial^\mu+m_\sigma^2)\sigma = \sum_B-\left(\frac{\partial}{\partial\sigma}M_B^*\right)\bar\Psi_B\Psi_B\ , \quad (4.3.2)$$

$$\partial_\mu\Omega^{\mu\nu}+m_\omega^2\omega^\nu = \sum_B\left\{g_{\omega B}\bar\Psi_{\rm B}\gamma^\nu\Psi_{\rm B}-\frac{f_{\omega B}}{2M_{\rm N}}\partial_\mu\left(\bar\Psi_{\rm B}\sigma^{\mu\nu}\Psi_{\rm B}\right)\right\}\ , \quad (4.3.3)$$

$$\partial_\mu\boldsymbol{R}^{\mu\nu}+m_\rho^2\boldsymbol{\rho}^{\,\nu} = \sum_B\left\{g_{\rho B}\bar\Psi_{\rm B}\boldsymbol{t}\gamma^\nu\Psi_{\rm B}-\frac{f_{\rho B}}{2M_{\rm N}}\partial_\mu\left(\bar\Psi_{\rm B}\boldsymbol{t}\sigma^{\mu\nu}\Psi_{\rm B}\right)\right\}\ , \quad (4.3.4)$$

$$(\partial_\mu\partial^\mu+m_\pi^2)\boldsymbol{\pi} = \sum_B\frac{g_{\rm A}}{2f_\pi}\chi_{BB}\partial^\mu\left(\bar\Psi_B\gamma_\mu\gamma_5\boldsymbol{\tau}\Psi_B\right)\ , \quad (4.3.5)$$

along with a Dirac equation for the baryon spinors

$$\begin{aligned}(i\gamma^\mu\partial_\mu &- g_{\omega B}\gamma^\mu\omega_\mu-\frac{f_{\omega B}}{2M_{\rm N}}\sigma^{\mu\nu}\partial_\mu\omega_\nu \\ &- g_{\rho B}\gamma^\mu\boldsymbol{t}\cdot\boldsymbol{\rho}_\mu-\frac{f_{\rho B}}{2M_{\rm N}}\sigma^{\mu\nu}\boldsymbol{t}\cdot\partial_\mu\boldsymbol{\rho}_\nu \\ &- \frac{g_{\rm A}}{2f_\pi}\chi_{BB}\gamma^\mu\gamma^5\boldsymbol{\tau}\cdot\partial_\mu\boldsymbol{\pi}\ -M_B+g_{\sigma B}(\sigma)\sigma\Big)\Psi_B=0\ .\end{aligned} \quad (4.3.6)$$

This is a difficult system of equations to solve and to make the problem tractable approximations are applied. Static, no sea and mean field approximations are typically

used. The static approximation means that there is no time dependence included and no sea refers to ignoring the Dirac sea of negative energy states. In the mean field approximation the meson field operators are replaced by their expectation values, and as such their fields are essentially treated classically. The idea is that the many body system of baryons is thought of as sitting in an average or mean nuclear field generated by themselves, which in turn modifies them and this is how they interact. In mean field theories the self consistent determination of this nuclear mean field is key.

The mesons σ, ω, ρ and π need not be precisely the mesons you find in experiment, they are simply meant to represent the scalar, vector-isoscalar, vector-isovector and pseudo-vector-isovector channels of interaction between the baryons. Of these, the first three generate a mean field in which the baryons reside. It is worth commenting that this approximation is increasingly more reliable with increasing baryonic density and therefore appropriate to the matter in neutron stars.

As we are considering infinite uniform (homogeneous) nuclear matter in the above approximations, we have translational and rotational invariance and therefore space-like components of the meson fields vanish allowing us to write:

$$\sigma \rightarrow \langle\sigma\rangle \equiv \bar{\sigma} \ , \tag{4.3.7}$$

$$\omega_\mu \rightarrow \langle\omega_\mu\rangle = \langle\delta_{\mu 0}\omega_\mu\rangle \equiv \bar{\omega} \ , \tag{4.3.8}$$

$$\boldsymbol{\rho}_\mu \rightarrow \langle\boldsymbol{\rho}_\mu\rangle = \langle\delta_{\mu 0}\delta_{a3}\rho_{\mu a}\rangle \equiv \bar{\rho} \ , \tag{4.3.9}$$

$$\boldsymbol{\pi} \rightarrow \langle\boldsymbol{\pi}\rangle \equiv \bar{\pi} = 0 \ , \tag{4.3.10}$$

where a refers to the isospin index. The baryon fields remain operators acting as sources for the meson fields. In the equations of motion, the currents are replaced by their normal ordered ground state expectation values. This is usually called the Hartree mean-field approximation. In this approximation the pion does not contribute because of parity considerations. After applying the static and Hartree mean field approximation, the equations of motion (Eqs. (4.3.2–4.3.5)) become

$$m_\sigma^2\bar{\sigma} = \sum_B -\left(\frac{\partial}{\partial\bar{\sigma}}M_B^*\right)\left\langle\bar{\Psi}_B\Psi_B\right\rangle \ , \tag{4.3.11}$$

$$m_\omega^2\bar{\omega} = \sum_B g_{\omega B}\left\langle\Psi_B^\dagger\Psi_B\right\rangle \text{ and} \tag{4.3.12}$$

$$m_\rho^2\bar{\rho} = \sum_B g_\rho\left\langle\Psi_B^\dagger t_{3B}\Psi_B\right\rangle \tag{4.3.13}$$

for the mesons. The Dirac equation for the baryons also becomes simplified.

4.4 The Hamiltonian Density

To calculate the EoS of nuclear matter we will need the Hamiltonian density, which is related to the Lagrangian density through the following Legendre transformation:

$$\mathcal{H} = \sum_{j=B,\alpha}\Pi_j\partial_0\phi_j - \mathcal{L} \quad , \tag{4.4.1}$$

where the conjugate momentum for particle field j is

$$\Pi_j(x) = \frac{\partial \mathcal{L}}{\partial(\partial\phi_j/\partial t)} \quad . \tag{4.4.2}$$

Specifically for each particle

$$\begin{aligned}
\Pi_{\mathrm{B}}(x) &= i\Psi^\dagger_{\mathrm{B}}(x) \quad , && (4.4.3)\\
\Pi_\sigma(x) &= \partial^0\sigma(x) \quad , && (4.4.4)\\
\Pi^\nu_\omega(x) &= \Omega^{\nu 0} + \sum_{\mathrm{B}} \frac{f_{\omega B}}{2M_{\mathrm{N}}}\bar{\Psi}_{\mathrm{B}}\sigma^{\nu 0}\Psi_{\mathrm{B}} \quad , && (4.4.5)\\
\boldsymbol{\Pi}^\nu_\rho(x) &= \boldsymbol{R}^{\nu 0} + \sum_{\mathrm{B}} \frac{f_{\rho B}}{2M_{\mathrm{N}}}\bar{\Psi}_{\mathrm{B}}\boldsymbol{t}\sigma^{\nu 0}\Psi_{\mathrm{B}} \quad , && (4.4.6)\\
\boldsymbol{\Pi}_\pi(x) &= \partial^0\boldsymbol{\pi}(x) - \sum_B \left(\frac{g_{\mathrm{A}}}{2f_\pi}\right)\chi_{BB}\bar{\Psi}_{\mathrm{B}}\gamma^0\gamma^5\boldsymbol{\tau}\Psi_{\mathrm{B}} \quad . && (4.4.7)
\end{aligned}$$

From the Hamilton density the total energy density is given by

$$\epsilon_{\mathrm{total}} = \frac{\left\langle \Psi_{\mathrm{g.s.}}\right| \int d^3r \ :\mathcal{H}: \ \left|\Psi_{\mathrm{g.s.}}\right\rangle}{V} \ , \tag{4.4.8}$$

where $|\Psi_{\mathrm{g.s.}}\rangle$ is the ground state.

From Eq. (4.4.1), the full Hamiltonian density, can be shown to be

$$\begin{aligned}
\mathcal{H} \ = \ & \sum_{B\in\{N,\Lambda,\Sigma,\Xi\}} \bar{\Psi}_{\mathrm{B}}\Big[-i\vec{\gamma}\cdot\vec{\nabla} + M_{\mathrm{B}} - g_{\sigma B}(\sigma)\sigma - \frac{g_{\mathrm{A}}}{2f_\pi}\chi_{BB}\gamma_5\boldsymbol{\tau}\cdot(\vec{\gamma}\cdot\vec{\nabla})\boldsymbol{\pi} \qquad (4.4.9)\\
& + g_{\omega B}\gamma_\mu\omega^\mu - \frac{f_{\omega B}}{2M_{\mathrm{N}}}\sigma_{\mu i}\partial^i\omega^\mu + g_{\rho B}\gamma_\mu\boldsymbol{t}\cdot\boldsymbol{\rho}^{\ \mu} - \frac{f_{\rho B}}{2M_{\mathrm{N}}}\sigma_{\mu i}\boldsymbol{t}\cdot\partial^i\boldsymbol{\rho}^{\ \mu}\Big]\Psi_{\mathrm{B}}\\
& + \frac{1}{2}\dot{\sigma}^2 + \frac{1}{2}\vec{\nabla}\sigma\cdot\vec{\nabla}\sigma + \frac{1}{2}m_\sigma^2\sigma^2 + \Omega_{\mu 0}\dot{\omega}^\mu + \frac{1}{4}\Omega_{\mu\nu}\Omega^{\mu\nu} - \frac{1}{2}m_\omega^2\omega_\mu\omega^\mu\\
& + \boldsymbol{R}_{\mu 0}\cdot\dot{\boldsymbol{\rho}}^\mu + \frac{1}{4}\boldsymbol{R}_{\mu\nu}\cdot\boldsymbol{R}^{\mu\nu} - \frac{1}{2}m_\rho^2\boldsymbol{\rho}_\mu\cdot\boldsymbol{\rho}^{\ \mu} + \frac{1}{2}\dot{\boldsymbol{\pi}}\cdot\dot{\boldsymbol{\pi}} + \frac{1}{2}\vec{\nabla}\boldsymbol{\pi}\cdot\vec{\nabla}\boldsymbol{\pi} + \frac{1}{2}m_\pi^2\boldsymbol{\pi}\cdot\boldsymbol{\pi} \quad .
\end{aligned}$$

We apply the static approximation to the Hamiltonian density (Eq. (4.4.9)) meaning that the meson fields are treated as time independent and hence time derivatives of their fields do not contribute. Specifically for the ω-meson, this means

$$\begin{aligned}
\Omega_{\mu 0}\dot{\omega}^\mu \ + \ & \frac{1}{4}\Omega_{\mu\nu}\Omega^{\mu\nu} - \frac{1}{2}m_\omega^2\omega_\mu\omega^\mu\\
= \ & (\partial_\mu\omega_0 - \partial_0\omega_\mu)\dot{\omega}^\mu - \frac{1}{2}m_\omega^2\omega_\mu\omega^\mu + \frac{1}{4}(\partial_\mu\omega_\nu - \partial_\nu\omega_\mu)(\partial^\mu\omega^\nu - \partial^\nu\omega^\mu)\\
= \ & (\partial_\mu\omega_0 - \partial_0\omega_\mu)\dot{\omega}^\mu - \frac{1}{2}m_\omega^2\omega_\mu\omega^\mu + \frac{1}{2}\left((\partial_\mu\omega_\nu)^2 - (\partial\cdot\omega)^2\right)\\
\xrightarrow{\text{Static Approx.}} \ & -\frac{1}{2}\left[\vec{\nabla}\omega_\mu\cdot\vec{\nabla}\omega^\mu + (\vec{\nabla}\cdot\vec{\omega})^2 + m_\omega^2\omega_\mu\omega^\mu\right] \quad . \qquad (4.4.10)
\end{aligned}$$

The Hamiltonian density in the static approximation then becomes

$$\begin{aligned}
\mathcal{H} \ = \ & \sum_{B\in\{N,\Lambda,\Sigma,\Xi\}} \bar{\Psi}_{\mathrm{B}}\Big[-i\vec{\gamma}\cdot\vec{\nabla} + M_{\mathrm{B}} - g_{\sigma B}(\sigma)\sigma - \frac{g_{\mathrm{A}}}{2f_\pi}\chi_{BB}\gamma_5\boldsymbol{\tau}\cdot(\vec{\gamma}\cdot\vec{\nabla})\boldsymbol{\pi} \qquad (4.4.11)
\end{aligned}$$

$$+g_{\omega B}\gamma_\mu\omega^\mu - \frac{f_{\omega B}}{2M_{\rm N}}\sigma_{\mu i}\partial^i\omega^\mu + g_{\rho B}\gamma_\mu \boldsymbol{t}\cdot\boldsymbol{\rho}^{\ \mu} - \frac{f_{\rho B}}{2M_{\rm N}}\sigma_{\mu i}\boldsymbol{t}\cdot\partial^i\boldsymbol{\rho}^{\ \mu}\Big]\Psi_{\rm B}$$
$$+\frac{1}{2}\vec{\nabla}\sigma\cdot\vec{\nabla}\sigma + \frac{1}{2}m_\sigma^2\sigma^2 - \frac{1}{2}\left[\vec{\nabla}\omega_\mu\cdot\vec{\nabla}\omega^\mu + (\vec{\nabla}\cdot\vec{\omega})^2 + m_\omega^2\omega_\mu\omega^\mu\right]$$
$$-\frac{1}{2}\left[\vec{\nabla}\boldsymbol{\rho}_\mu\cdot\vec{\nabla}\boldsymbol{\rho}^\mu + (\vec{\nabla}\cdot\vec{\boldsymbol{\rho}})^2 + m_\rho^2\boldsymbol{\rho}_\mu\cdot\boldsymbol{\rho}^\mu\right] + \frac{1}{2}\vec{\nabla}\boldsymbol{\pi}\cdot\vec{\nabla}\boldsymbol{\pi} + \frac{1}{2}m_\pi^2\boldsymbol{\pi}\cdot\boldsymbol{\pi} \quad .$$

This can be decomposed into its baryon and meson components as

$$H = \int d^3r \left\{ \mathcal{K} + \sum_{m\in\{\sigma,\omega,\rho,\pi\}} \mathcal{H}_m \right\} \quad , \tag{4.4.12}$$

where

$$\mathcal{K} = \sum_B \bar{\Psi}_{\rm B}\left[-i\vec{\gamma}\cdot\vec{\nabla} + M_{\rm B} - g_{\sigma B}(\sigma)\sigma\right]\Psi_B \quad , \tag{4.4.13}$$

$$\mathcal{H}_\sigma = \frac{1}{2}\vec{\nabla}\sigma\cdot\vec{\nabla}\sigma + \frac{1}{2}m_\sigma^2\sigma^2 \quad , \tag{4.4.14}$$

$$\mathcal{H}_\omega = \sum_B \bar{\Psi}_{\rm B}\left[g_{\omega B}\gamma_\mu\omega^\mu - \frac{f_{\omega B}}{2M_{\rm N}}\sigma_{\mu i}\partial^i\omega^\mu\right]\Psi_{\rm B} \tag{4.4.15}$$
$$-\frac{1}{2}\left[\vec{\nabla}\omega_\mu\cdot\vec{\nabla}\omega^\mu + (\vec{\nabla}\cdot\vec{\omega})^2 + m_\omega^2\omega_\mu\omega^\mu\right] \quad ,$$

$$\mathcal{H}_\rho = \sum_B \bar{\Psi}_{\rm B}\left[g_{\rho B}\gamma_\mu\boldsymbol{t}\cdot\boldsymbol{\rho}^{\ \mu} - \frac{f_{\rho B}}{2M_{\rm N}}\sigma_{\mu i}\boldsymbol{t}\cdot\partial^i\boldsymbol{\rho}^{\ \mu}\right]\Psi_{\rm B} \tag{4.4.16}$$
$$-\frac{1}{2}\left[\vec{\nabla}\boldsymbol{\rho}_\mu\cdot\vec{\nabla}\boldsymbol{\rho}^\mu + (\vec{\nabla}\cdot\vec{\boldsymbol{\rho}})^2 + m_\rho^2\boldsymbol{\rho}_\mu\cdot\boldsymbol{\rho}^\mu\right] \quad ,$$

$$\mathcal{H}_\pi = -\sum_B \bar{\Psi}_{\rm B}\left[\frac{g_{\rm A}}{2f_\pi}\chi_{BB}\gamma_5\boldsymbol{\tau}\cdot(\vec{\gamma}\cdot\vec{\nabla})\boldsymbol{\pi}\right]\Psi_{\rm B} + \frac{1}{2}\vec{\nabla}\boldsymbol{\pi}\cdot\vec{\nabla}\boldsymbol{\pi} + \frac{1}{2}m_\pi^2\boldsymbol{\pi}\cdot\boldsymbol{\pi}\,. \tag{4.4.17}$$

4.5 Hartree-Fock Approximation

To solve the equations of motion for the mesons the standard methods of Green's function theory are used [253]. Specifically for the σ meson, one first defines the propagator $\tilde{\Delta}_\sigma$, such that

$$(\partial^2 + m_\sigma^2)\tilde{\Delta}_\sigma(x-y) = -\delta^{(4)}(x-y) \quad . \tag{4.5.1}$$

Following the usual procedure one finds the following solution to the homogeneous Klein-Gordon differential operator in energy-momentum space,

$$\tilde{\Delta}_\sigma(k) = \frac{1}{k^2 - m_\sigma^2 + i\epsilon} \quad , \tag{4.5.2}$$

where the extra Feynman $i\epsilon$ term is put in by hand to avoid the poles on the real axis. In the static approximation this becomes

$$\tilde{\Delta}_\sigma(k) \xrightarrow{\text{Static Approx.}} \Delta_\sigma^{\rm static}(\vec{k}) = \frac{-1}{\vec{k}^2 + m_\sigma^2} \quad , \tag{4.5.3}$$

which is related to the Yukawa propagator by $\Delta_\sigma(\vec{k}) = -\Delta_\sigma^{\rm static}(\vec{k})$. Using the Yukawa propagator the inhomogeneous Klein-Gordon equation can be solved order by order.

To perform the Hartree-Fock approximation we follow Refs. [160–163] by considering each meson field to be decomposed into two parts, a mean field part $\langle\phi\rangle$ and a fluctuation part $\delta\phi$, such that $\phi = \langle\phi\rangle + \delta\phi$ and solve the equations of motion order by order. The fluctuation terms are to be considered small with respect to the mean field contribution, the exception to this being the π and ρ meson fluctuations. In this fashion, the σ meson equation of motion is decomposed according to

$$\left(-\vec{\nabla}^2 + m_\sigma^2\right)(\bar{\sigma} + \delta\sigma) = -\frac{\partial\mathcal{K}}{\partial\sigma} = -\frac{\partial\mathcal{K}}{\partial\sigma}(\bar{\sigma}) - \delta\sigma\frac{\partial^2\mathcal{K}}{\partial\sigma^2}(\bar{\sigma}) - \ldots \quad , \tag{4.5.4}$$

where

$$-\frac{\partial\mathcal{K}}{\partial\sigma} = \sum_B\left(-\frac{\partial M_B^*}{\partial\sigma}\bar{\Psi}_B\Psi_B\right) \tag{4.5.5}$$

and

$$-\frac{\partial^2\mathcal{K}}{\partial\sigma^2} = \sum_B\left(-\frac{\partial^2 M_B^*}{\partial\sigma^2}\bar{\Psi}_B\Psi_B\right) \quad . \tag{4.5.6}$$

Eq. (4.5.6) would be zero in a point-like model of hadrons and is only non-zero due to the quadratic dependence of the baryon masses on the scalar field—see for example the mass parametrisation given Eq. (4.1.1), obtained in Ref. [188] from the QMC model using a bag model including self-consistent one-gluon exchange. The following shorthand notation is introduced:

$$\frac{\partial\mathcal{K}}{\partial\bar{\sigma}} \equiv \frac{\partial\mathcal{K}}{\partial\sigma}(\bar{\sigma}) \quad , \quad \frac{\partial^2\mathcal{K}}{\partial\bar{\sigma}^2} \equiv \frac{\partial^2\mathcal{K}}{\partial\sigma^2}(\bar{\sigma}) \quad , \quad \ldots \quad . \tag{4.5.7}$$

Expanding Eqs. (4.5.5–4.5.6) about their expectation values we have

$$\frac{\partial\mathcal{K}}{\partial\bar{\sigma}} = \left\langle\frac{\partial\mathcal{K}}{\partial\bar{\sigma}}\right\rangle + \delta\left[\frac{\partial\mathcal{K}}{\partial\bar{\sigma}}\right] = \left\langle\frac{\partial\mathcal{K}}{\partial\bar{\sigma}}\right\rangle + \left(\frac{\partial\mathcal{K}}{\partial\bar{\sigma}} - \left\langle\frac{\partial\mathcal{K}}{\partial\bar{\sigma}}\right\rangle\right) \tag{4.5.8}$$

and

$$\frac{\partial^2\mathcal{K}}{\partial\bar{\sigma}^2} = \left\langle\frac{\partial^2\mathcal{K}}{\partial\bar{\sigma}^2}\right\rangle + \delta\left[\frac{\partial^2\mathcal{K}}{\partial\bar{\sigma}^2}\right] = \left\langle\frac{\partial^2\mathcal{K}}{\partial\bar{\sigma}^2}\right\rangle + \left(\frac{\partial^2\mathcal{K}}{\partial\bar{\sigma}^2} - \left\langle\frac{\partial^2\mathcal{K}}{\partial\bar{\sigma}^2}\right\rangle\right) \quad . \tag{4.5.9}$$

We are assuming that all the fluctuation terms

$$\delta\sigma \quad , \quad \delta\left[\frac{\partial\mathcal{K}}{\partial\bar{\sigma}}\right] \quad , \quad \delta\left[\frac{\partial^2\mathcal{K}}{\partial\bar{\sigma}^2}\right] \quad , \quad \ldots \tag{4.5.10}$$

are small. We now proceed to solve the σ meson equation of motion order by order. At the mean field or Hartree level we obtain

$$\left(-\vec{\nabla}^2 + m_\sigma^2\right)\bar{\sigma} = -\left\langle\frac{\partial\mathcal{K}}{\partial\bar{\sigma}}\right\rangle = \sum_B\left(-\frac{\partial M_B^*}{\partial\bar{\sigma}}\left\langle\bar{\Psi}_B\Psi_B\right\rangle\right) \tag{4.5.11}$$

and at the Fock level

$$\left(-\vec{\nabla}^2 + m_\sigma^2\right)\delta\sigma = -\left(\frac{\partial\mathcal{K}}{\partial\bar{\sigma}} - \left\langle\frac{\partial\mathcal{K}}{\partial\bar{\sigma}}\right\rangle\right) - \delta\sigma\left[\left\langle\frac{\partial^2\mathcal{K}}{\partial\bar{\sigma}^2}\right\rangle + \left(\frac{\partial^2\mathcal{K}}{\partial\bar{\sigma}^2} - \left\langle\frac{\partial^2\mathcal{K}}{\partial\bar{\sigma}^2}\right\rangle\right)\right] \tag{4.5.12}$$

$$= -\frac{\partial\mathcal{K}}{\partial\bar{\sigma}} + \left\langle\frac{\partial\mathcal{K}}{\partial\bar{\sigma}}\right\rangle - \delta\sigma\frac{\partial^2\mathcal{K}}{\partial\bar{\sigma}^2} \quad , \tag{4.5.13}$$

where to this order $(\delta\sigma)$

$$\frac{\partial^2\mathcal{K}}{\partial\bar{\sigma}^2} \longrightarrow \left\langle\frac{\partial^2\mathcal{K}}{\partial\bar{\sigma}^2}\right\rangle \quad . \tag{4.5.14}$$

The fluctuation equation of motion becomes

$$\left(-\vec{\nabla}^2 + m_\sigma^2\right)\delta\sigma = -\frac{\partial\mathcal{K}}{\partial\bar{\sigma}} + \left\langle\frac{\partial\mathcal{K}}{\partial\bar{\sigma}}\right\rangle - \delta\sigma\left\langle\frac{\partial^2\mathcal{K}}{\partial\bar{\sigma}^2}\right\rangle \quad . \tag{4.5.15}$$

Eq. (4.5.15) can be re-expressed in terms of an in-medium σ-meson mass and the fluctuation of the scalar baryon current as

$$\left(-\vec{\nabla}^2 + m_\sigma^{*\,2}\right)\delta\sigma = \sum_B -\frac{\partial M_B^*}{\partial\bar{\sigma}}\left(\bar{\Psi}_B\Psi_B - \left\langle\bar{\Psi}_B\Psi_B\right\rangle\right) \quad , \tag{4.5.16}$$

where

$$m_\sigma^{*\,2} = m_\sigma^2 + \left\langle\frac{\partial^2\mathcal{K}}{\partial\bar{\sigma}^2}\right\rangle = m_\sigma^2 + \sum_B\frac{\partial^2 M_B^*}{\partial\bar{\sigma}^2}\left\langle\bar{\Psi}_B\Psi_B\right\rangle \quad . \tag{4.5.17}$$

This in-medium σ meson mass is only relevant to the fluctuating part and does not appear in the mean field portion of the σ meson's equation of motion. This in-medium modification due to the baryons internal structure was included in Ref. [160–162], but we will not include it here. We are neglecting this in-medium modification as we are approximating the Fock terms in the static approximation, omitting all other meson retardation effects and implementing a crude method of subtracting the contact terms that arise in the Fock terms. For these reasons it is reasonable to disregard it and use the free σ meson mass in the Fock term, thereby treating it in the same manner as the other mesons.

The expectation value of the σ field is given by

$$\bar{\sigma} = -\frac{1}{m_\sigma^2}\left\langle\frac{\partial\mathcal{K}}{\partial\bar{\sigma}}\right\rangle = -\frac{1}{m_\sigma^2}\sum_B\frac{\partial M_B^*}{\partial\bar{\sigma}}\left\langle\bar{\Psi}_B\Psi_B\right\rangle \quad , \tag{4.5.18}$$

which is then determined numerically. Krein *et al.* also considered an additional correction involving the mean scalar field from the Fock terms. This can be done by considering the energy density as a functional and requiring it to be thermodynamically consistent, meaning that the total energy density, ϵ, is minimised with respect to $\bar{\sigma}$ such that,

$$\bar{\sigma} = -\frac{1}{m_\sigma^2}\frac{\partial\epsilon}{\partial\bar{\sigma}} \quad . \tag{4.5.19}$$

This amounts to Eq. (4.5.18) plus an additional term because of the dependence of the Fock contribution to the energy density on $\bar{\sigma}$.

The fluctuation of the σ field can now be written in terms of the σ meson's Green function as

$$\begin{aligned}
\delta\sigma(\vec{r}) &= \int d^3r'\ \Delta_\sigma(\vec{r}-\vec{r}\,')\left(-\frac{\partial\mathcal{K}}{\partial\bar{\sigma}}+\left\langle\frac{\partial\mathcal{K}}{\partial\bar{\sigma}}\right\rangle\right)(\vec{r}\,') && (4.5.20)\\
&= \sum_B\int d^3r'\ \Delta_\sigma(\vec{r}-\vec{r}\,')\left[-\frac{\partial M_B^*}{\partial\bar{\sigma}}\left(\bar{\Psi}_B\Psi_B-\left\langle\bar{\Psi}_B\Psi_B\right\rangle\right)(\vec{r}\,')\right] && (4.5.21)\\
&= \sum_B\int d^3r'\frac{d^3q}{(2\pi)^3}\ e^{i\vec{q}\cdot(\vec{r}-\vec{r}\,')}\Delta_\sigma(\vec{q})\left[-\frac{\partial M_B^*}{\partial\bar{\sigma}}\left(\bar{\Psi}_B\Psi_B-\left\langle\bar{\Psi}_B\Psi_B\right\rangle\right)(\vec{r}\,')\right]\quad . && (4.5.22)
\end{aligned}$$

To obtain the Fock contribution, we have approached the problem in the same manner as Refs. [160–163] by considering the meson fields decomposed into a mean field part and a fluctuating part. As can be seen in Eq.(4.5.16) and (4.5.22), this is related to a similar decomposition of the baryon currents, where they are composed of a mean field part and a fluctuation part. We introduce the following notation:

$$\begin{aligned}
\bar{\Psi}_B\tilde{\Gamma}_{\alpha B}\Psi_B &= \left\langle\bar{\Psi}_B\tilde{\Gamma}_{\alpha B}\Psi_B\right\rangle+(\bar{\Psi}_B\tilde{\Gamma}_{\alpha B}\Psi_B-\left\langle\bar{\Psi}_B\tilde{\Gamma}_{\alpha B}\Psi_B\right\rangle) && (4.5.23)\\
&= \left\langle\bar{\Psi}_B\tilde{\Gamma}_{\alpha B}\Psi_B\right\rangle+\delta(\bar{\Psi}_B\tilde{\Gamma}_{\alpha B}\Psi_B)\quad , && (4.5.24)
\end{aligned}$$

where $\tilde{\Gamma}_{\alpha B}$ denotes one of the interaction currents associated with the mesons appearing in the Lagrangian (Eq. (4.2.6)).

The solution of the vector meson equations of motion follow in the same manner, but with an added complication. In four dimensional space-time a spin-1 massive vector field has four components, but only $2s+1=3$ independent spin components—two transverse and one longitudinal polarisation states. We need to impose a constraint to remove the extra component. It follows naturally from the equation of motion.

For the vector fields a Lorentz gauge-like condition naturally follows from the equations of motion (Eqs. (4.3.3–4.3.4)) by taking a partial derivative. It is not actually a gauge condition, as the Proca equation is not gauge invariant, but rather a consistency condition. In the case of the ω meson, that is

$$\partial_\nu\partial_\mu\Omega^{\mu\nu}+m_\omega^2\partial_\nu\omega^\nu=\sum_B\left[g_{\omega B}\partial_\nu\left(\bar{\Psi}_{\mathrm{B}}\gamma^\nu\Psi_{\mathrm{B}}\right)-\frac{f_{\omega B}}{2M_{\mathrm{N}}}\partial_\nu\partial_\mu\left(\bar{\Psi}_{\mathrm{B}}\sigma^{\mu\nu}\Psi_{\mathrm{B}}\right)\right]\quad , \quad (4.5.25)$$

where the first term on the l.h.s. and the second term on the r.h.s. are zero because a symmetric tensor is fully contracted with an anti-symmetric tensor. The first term on the r.h.s. is also zero as it expresses the four-divergence of the baryonic current, which is conserved. This coupling of the ω meson to the conserved baryonic current allows the further simplification of the Hamiltonian density given in Eq. (4.4.12) by

$$\partial_\mu\omega^\mu=0\xrightarrow{\text{Static Approx.}}\vec{\nabla}\cdot\vec{\omega}=0\quad . \quad (4.5.26)$$

Moreover, the Lorentz structure of the corresponding equations of motion is simplified from Proca equations to Klein-Gordon equations, where each component of the vector fields separately satisfies a Klein-Gordon equation.

$$\begin{aligned}
\partial_\mu \Omega^{\mu\nu} + m_\omega^2 \omega^\nu &= \partial_\mu(\partial^\mu\omega^\nu - \partial^\nu\omega^\mu) + m_\omega^2\omega^\nu && (4.5.27)\\
&= \partial^2\omega^\nu - \partial^\nu(\partial\cdot\omega) + m_\omega^2\omega^\nu && (4.5.28)\\
&\xrightarrow{\text{Static Approx.}} -\nabla^2\omega^\nu + \delta_i^\nu\partial^i(\vec{\nabla}\cdot\vec{\omega}) + m_\omega^2\omega^\nu && (4.5.29)\\
&\overset{\text{Lorentz Cond.}}{=} (-\nabla^2 + m_\omega^2)\omega^\nu \quad . && (4.5.30)
\end{aligned}$$

This can similarly be done for the the ρ meson.

It is possible to combine the 4 Klein-Gordon equations and the Lorentz condition into a single equation using a projection operator,

$$\tilde{P}^{\mu\nu}_{\omega,\rho} \equiv \sum_{s=1}^{3} \epsilon^\mu_{\omega,\rho}(\vec{k},s)\epsilon^\nu_{\omega,\rho}(\vec{k},s) = -g^{\mu\nu} + \frac{k^\mu k^\nu}{m^2_{\omega,\rho}} \quad , \tag{4.5.31}$$

which corresponds to a sum over polarisation states of the particle. The Lorentz condition then becomes a condition on the polarisation tensor ϵ^μ. Moreover, the momentum dependence of the propagator is independent of the spin structure and takes the same form as Eq. (4.5.2). In the static limit the vector meson propagator is

$$\tilde{\Delta}^{\mu\nu}_{\omega,\rho}(k) = \tilde{P}^{\mu\nu}_{\omega,\rho}\tilde{\Delta}_{\omega,\rho}(k) \xrightarrow{\text{Static Approx.}} -P^{\mu\nu}_{\omega,\rho}\Delta_{\omega,\rho}(\vec{k}) \quad . \tag{4.5.32}$$

Where in Eq. (4.5.32) we denote the static limit of the projection operator by $P^{\mu\nu}_{\omega,\rho}$, which has the following components:

$$P^{00}_{\omega,\rho} = -1 \quad , \quad P^{0i}_{\omega,\rho} = P^{i0}_{\omega,\rho} = 0 \quad , \quad P^{ij}_{\omega,\rho} = \delta^{ij} + \frac{k^i k^j}{m^2_{\omega,\rho}} \quad . \tag{4.5.33}$$

Fourier transforming to obtain the projection operator in position space one makes use of $k_\mu \to i\partial_\mu$.

Using the following notation for source of the ω-B interaction in configuration space (Eq. 4.3.3):

$$\tilde{\Gamma}^\mu_{\omega B} = g_{\omega B}\gamma^\mu - \frac{f_{\omega B}}{2M_{\mathrm{N}}}\partial_i\sigma^{i\mu} \quad , \tag{4.5.34}$$

the separation of the ω meson equation of motion follows in the same manner as for the σ meson. Only the temporal component of the vector mesons survive at the mean field level because of spatial isotropy. This also implies the tensor contribution vanishes at this order, such that

$$\begin{aligned}
(-\nabla^2 + m_\omega^2)\bar{\omega} &\equiv (-\nabla^2 + m_\omega^2)\omega^0 && (4.5.35)\\
&= \sum_B -(P_\omega)^0{}_0 \left\langle \bar{\Psi}_B \tilde{\Gamma}^0_{\omega B}\Psi_B \right\rangle \\
&= \sum_B \left[-(P_\omega)^0{}_0 g_{\omega B}\left\langle \bar{\Psi}_{\mathrm{B}}\gamma^0\Psi_{\mathrm{B}}\right\rangle + (P_\omega)^0{}_0\frac{f_{\omega B}}{2M_{\mathrm{N}}}\partial_i\left\langle\bar{\Psi}_{\mathrm{B}}\sigma^{i0}\Psi_{\mathrm{B}}\right\rangle\right]
\end{aligned}$$

$$= \sum_B g_{\omega B} \left\langle \Psi_{\rm B}^\dagger \Psi_{\rm B} \right\rangle \quad .$$

The mean ω meson field is then

$$\bar{\omega} = \frac{1}{m_\omega^2} \sum_B g_{\omega B} \left\langle \Psi_{\rm B}^\dagger \Psi_{\rm B} \right\rangle \quad . \tag{4.5.36}$$

The fluctuation part of the ω meson equation of motion is given by

$$(-\nabla^2 + m_\omega^2)\delta\omega^\mu = \sum_B -(P_\omega)^\mu{}_\nu \left(\bar{\Psi}_B \tilde{\Gamma}^\nu_{\omega B} \Psi_B - \left\langle \bar{\Psi}_B \tilde{\Gamma}^\nu_{\omega B} \Psi_B \right\rangle \right) \quad . \tag{4.5.37}$$

The second part of the projection operator can be ignored from here on because when it is contracted with $\bar{\Psi}_B \tilde{\Gamma}^\nu_{\omega B} \Psi_B$ the outcome is zero. This follows as a result of the continuity equation and the full contraction of a symmetric tensor with an anti-symmetric tensor. Eq. (4.5.37) can then be written as

$$(-\nabla^2 + m_\omega^2)\delta\omega^\mu = \sum_B g^\mu{}_\nu \left(\bar{\Psi}_B \tilde{\Gamma}^\nu_{\omega B} \Psi_B - \left\langle \bar{\Psi}_B \tilde{\Gamma}^\nu_{\omega B} \Psi_B \right\rangle \right) \tag{4.5.38}$$

$$= \sum_B \delta \left(\bar{\Psi}_B \tilde{\Gamma}^\mu_{\omega B} \Psi_B \right) \quad . \tag{4.5.39}$$

Using standard Green's function methods again, the fluctuation of the ω meson field is

$$\delta\omega^\mu(\vec{r}) = \sum_B \int d^3r' \; \frac{d^3q}{(2\pi)^3} e^{i\vec{q}\cdot(\vec{r}-\vec{r}')} \Delta_\omega(\vec{q}) \; \delta(\bar{\Psi}_B \tilde{\Gamma}^\mu_{\omega B} \Psi_B)(\vec{r}') \tag{4.5.40}$$

The analogous equations for the remaining mesons follow in same manner. Here we summarise the equations of motion for all mesons decomposed into mean field and fluctuation components

$$\left(-\vec{\nabla}^2 + m_\sigma^2 \right) \bar{\sigma} = \sum_B \left(-\frac{\partial M_B^*}{\partial \bar{\sigma}} \left\langle \bar{\Psi}_B \Psi_B \right\rangle \right) \quad , \tag{4.5.41}$$

$$(-\nabla^2 + m_\omega^2)\bar{\omega} = \sum_B g_{\omega B} \left\langle \Psi_{\rm B}^\dagger \Psi_{\rm B} \right\rangle \quad , \tag{4.5.42}$$

$$(-\nabla^2 + m_\rho^2)\bar{\rho} = \sum_B g_{\rho B} \left\langle \Psi_{\rm B}^\dagger t_{3B} \Psi_{\rm B} \right\rangle \tag{4.5.43}$$

$$\tag{4.5.44}$$

and

$$\left(-\vec{\nabla}^2 + m_\sigma^2 \right) \delta\sigma = \sum_B -\frac{\partial M_B^*}{\partial \bar{\sigma}} \left(\bar{\Psi}_B \Psi_B - \left\langle \bar{\Psi}_B \Psi_B \right\rangle \right) = \sum_B \delta \left(\bar{\Psi}_B \tilde{\Gamma}_{\sigma B} \Psi_B \right) \; , \tag{4.5.45}$$

$$(-\nabla^2 + m_\omega^2)\delta\omega^\mu = \sum_B \delta \left(\bar{\Psi}_B \tilde{\Gamma}^\mu_{\omega B} \Psi_B \right) \quad , \tag{4.5.46}$$

$$(-\nabla^2 + m_\rho^2)\delta\boldsymbol{\rho}^\mu = \sum_B \delta\left(\bar{\Psi}_B \tilde{\boldsymbol{\Gamma}}^\mu_{\rho B}\Psi_B\right) \quad , \tag{4.5.47}$$

$$(-\nabla^2 + m_\pi^2)\delta\boldsymbol{\pi} = \sum_B \delta\left(\bar{\Psi}_B \tilde{\boldsymbol{\Gamma}}_{\pi B}\Psi_B\right) \quad . \tag{4.5.48}$$

In Eqs. (4.5.45–4.5.48), the meson-baryon interaction sources are written in terms of the appropriate Lorentz and isospin structures , $\tilde{\Gamma}_{\alpha B}$, in configuration space.

All meson mean fields and fluctuations can be calculated by using the same methods as used above for the σ and ω mesons. The expressions for the meson mean fields are:

$$\bar{\sigma} = -\frac{1}{m_\sigma^2}\sum_B \frac{\partial M_B^*}{\partial\bar{\sigma}}\left\langle\bar{\Psi}_B\Psi_B\right\rangle \ , \tag{4.5.49}$$

$$\bar{\omega} = \frac{1}{m_\omega^2}\sum_B g_{\omega B}\left\langle\Psi_{\rm B}^\dagger\Psi_{\rm B}\right\rangle \ , \tag{4.5.50}$$

$$\bar{\rho} = \frac{1}{m_\rho^2}\sum_B g_{\rho B}\left\langle\Psi_{\rm B}^\dagger t_{3B}\Psi_{\rm B}\right\rangle \ , \tag{4.5.51}$$

$$\bar{\pi} = 0 \quad . \tag{4.5.52}$$

The expression for each meson field fluctuation can be condensed to

$$\delta\phi(\vec{r}) = \sum_B \int d^3r' \ \Delta_\phi(\vec{r}-\vec{r}')\delta(\bar{\Psi}_{\rm B}\tilde{\Gamma}_{\phi B}\Psi_{\rm B})(\vec{r}') \quad , \tag{4.5.53}$$

where Δ_ϕ is the Yukawa propagator for the meson $\phi \in \{\sigma,\omega,\rho,\pi\}$ determined by

$$(-\nabla^2 + m_\phi^2)\Delta_\phi(\vec{r}-\vec{r}') = +\delta^{(3)}(\vec{r}-\vec{r}') \quad . \tag{4.5.54}$$

The decomposition of the meson fields also occurs in the Hamiltonian. The Hamiltonian describing the free σ meson is expanded as

$$H_\sigma = \frac{1}{2}\int d^3r \ \left[\vec{\nabla}\sigma\cdot\vec{\nabla}\sigma + m_\sigma^2\sigma^2\right] \tag{4.5.55}$$

$$= \frac{1}{2}\int d^3r \ \left[\vec{\nabla}(\bar{\sigma}+\delta\sigma)\cdot\vec{\nabla}(\bar{\sigma}+\delta\sigma) + m_\sigma^2(\bar{\sigma}+\delta\sigma)^2\right] \tag{4.5.56}$$

$$= \frac{1}{2}\int d^3r \ \Big[\vec{\nabla}\bar{\sigma}\cdot\vec{\nabla}\bar{\sigma} + m_\sigma^2\bar{\sigma}^2 + \vec{\nabla}\delta\sigma\cdot\vec{\nabla}\delta\sigma + m_\sigma^2\delta\sigma^2 + 2\vec{\nabla}\bar{\sigma}\cdot\vec{\nabla}\delta\sigma + 2m_\sigma^2\bar{\sigma}\delta\sigma\Big] \ . \tag{4.5.57}$$

Using integration by parts we obtain

$$H_\sigma = \int d^3r \ \Big[\frac{1}{2}\bar{\sigma}(-\nabla^2 + \frac{1}{2}m_\sigma^2)\bar{\sigma} + \frac{1}{2}\delta\sigma(-\nabla^2 + \frac{1}{2}m_\sigma^2)\delta\sigma + \delta\sigma(-\nabla^2 + m_\sigma^2)\bar{\sigma}\Big] \ , \tag{4.5.58}$$

where we have neglected surface terms, as surface terms do not contribute in infinite matter. Analogous expressions can be obtained for the remaining terms. Expanding

$\mathcal{K}$ about the mean fields and combing it with Eq. (4.5.58) we see that to second order in the scalar fluctuation

$$\int d^3r\ [\mathcal{K}+\mathcal{H}_\sigma] = \int d^3r\ \Big[\ \mathcal{K}(\bar\sigma)+\delta\sigma\frac{\partial\mathcal{K}}{\partial\bar\sigma}+\frac{1}{2}\delta\sigma^2\frac{\partial^2\mathcal{K}}{\partial\bar\sigma^2} + \frac{1}{2}\bar\sigma(-\nabla^2+\frac{1}{2}m_\sigma^2)\bar\sigma\ +\ \frac{1}{2}\delta\sigma(-\nabla^2+\frac{1}{2}m_\sigma^2)\delta\sigma + \delta\sigma(-\nabla^2+m_\sigma^2)\bar\sigma\Big]\ . \tag{4.5.59}$$

Using Eq. (4.5.14), (4.5.41) and (4.5.45) this amounts to

$$\int d^3r\ [\mathcal{K}+\mathcal{H}_\sigma] = \int d^3r\left[\mathcal{K}(\bar\sigma)+\frac{1}{2}\delta\sigma\left(\frac{\partial\mathcal{K}}{\partial\bar\sigma}-\left\langle\frac{\partial\mathcal{K}}{\partial\bar\sigma}\right\rangle\right)+\frac{1}{2}m_\sigma^2\bar\sigma^2\right] \tag{4.5.60}$$

$$= \int d^3r\left[\sum_B\bar\Psi_{\rm B}\left[-i\vec\gamma\cdot\vec\nabla+M_{\rm B}-g_{\sigma B}(\bar\sigma)\bar\sigma\right]\Psi_B + \frac{1}{2}\sum_B\frac{\partial M_{\rm B}^*}{\partial\bar\sigma}\delta\sigma(\vec r)\delta\left(\bar\Psi_{\rm B}\Psi_{\rm B}\right)(\vec r)+\frac{1}{2}m_\sigma^2\bar\sigma^2\right]\ . \tag{4.5.61}$$

The first term in the last line is the σ meson's Fock term contribution to the energy and is further evaluated using Eq. (4.5.53), such that

$$\frac{1}{2}\sum_B\int d^3r\frac{\partial M_{\rm B}^*}{\partial\bar\sigma}\delta\sigma(\vec r)\delta\left(\bar\Psi_{\rm B}\Psi_{\rm B}\right)(\vec r) = -\frac{1}{2}\sum_{B,B'}\frac{\partial M_{\rm B}^*}{\partial\bar\sigma}\frac{\partial M_{\rm B'}^*}{\partial\bar\sigma}\int d^3rd^3r'\ \Delta_\sigma(\vec r-\vec r\,')\delta\left(\bar\Psi_{\rm B'}\Psi_{\rm B'}\right)(\vec r\,')\delta\left(\bar\Psi_{\rm B}\Psi_{\rm B}\right)(\vec r)\ . \tag{4.5.62}$$

In the Lagrangian under investigation, Eq. (4.2.6), in the Fock terms isoscalar mesons are only exchanged between like baryons. Isovector mesons are exchanged between different baryons, but only between baryons from the same isospin multiplet. With this in mind, Eq. (4.5.62) simplifies to

$$\frac{1}{2}\sum_B\int d^3r\frac{\partial M_{\rm B}^*}{\partial\bar\sigma}\delta\sigma(\vec r)\delta\left(\bar\Psi_{\rm B}\Psi_{\rm B}\right)(\vec r) = -\frac{1}{2}\sum_i\left(\frac{\partial M_{\rm i}^*}{\partial\bar\sigma}\right)^2\int d^3rd^3r'\ \Delta_\sigma(\vec r-\vec r\,')\delta\left(\bar\psi_i\psi_i\right)(\vec r\,')\delta\left(\bar\psi_i\psi_i\right)(\vec r)\ . \tag{4.5.63}$$

To proceed further, we must first explain how the in-medium Dirac equation for the baryons is solved in the Hartree-Fock approximation. This is presented in Sec. 4.6 and we provide a detailed evaluation of Eq. (4.5.63) in Sec. 4.7. In the process of doing this, we Fourier transform to momentum space, where the energy density of nuclear matter is more easily evaluated.

4.6 The In-medium Dirac Equation

The in-medium Dirac equation, for a baryon i in nuclear matter, can be written as

$$\left(\not{p} - M_i - \Sigma_i(p)\right) u_i(p,s) = 0 \quad , \tag{4.6.1}$$

where $\Sigma_i(p)$ is the self-energy of the baryon. The self-energy takes into account the self-consistent generation of the nuclear mean fields. From parity conservation and translational, rotational and time reversal invariance, the self-energy can be decomposed into three scalar functions in the nuclear matter rest frame. Written in terms of these functions it is expressed as [150]

$$\Sigma_i(p) = \Sigma_i^{\mathrm{s}}(p) + \gamma^0 \Sigma_i^0(p) + \vec{\gamma}\cdot\vec{p}\,\Sigma_i^{\mathrm{v}}(p) \quad . \tag{4.6.2}$$

The exact decomposition given in Eq. (4.6.2) can vary among different works, where other definitions of the scalar functions are used. The functions $\Sigma_i^{\mathrm{s}}(k)$, $\Sigma_i^0(k)$ and $\Sigma_i^{\mathrm{v}}(k)$ are the scalar, temporal vector and spatial vector components of the self-energy and can be obtained by taking appropriate traces of Eq. (4.6.2), see App. A.2. In general, the self-energy of a particle can be complex, but throughout this thesis we make the assumption that the self-energies of the baryons are entirely real. This is usually referred to as the quasi-particle approximation and is common in calculations of this type.

If we introduce the following effective quantities

$$M_i^*(p) = M_i + \Sigma_i^{\mathrm{s}}(p) \quad , \tag{4.6.3}$$

$$E_i^*(p) = E_i(p) + \Sigma_i^0(p) = \sqrt{\vec{p}^{\,*\,2} + M_i^{*\,2}} \quad , \tag{4.6.4}$$

$$\vec{p}^{\,*} = \vec{p}\,(1 + \Sigma_i^{\mathrm{v}}(p)) \quad , \tag{4.6.5}$$

the Dirac equation can be written as

$$\left(\not{p}^{\,*} - M_i^*\right) u_i(p,s) = 0 \quad , \tag{4.6.6}$$

which is formally equivalent to the Dirac equation in vacuum. Therefore, as in vacuum, the positive energy solution to Eq. (4.6.6) is

$$u_i(p,s) = \sqrt{\frac{M_{\mathrm{i}}^* + E_{\mathrm{i}}^*}{2E_i^*}} \begin{pmatrix} 1 \\ \dfrac{\vec{\sigma}\cdot\vec{p}^{\,*}}{M_i^* + E_i^*} \end{pmatrix} \chi_s \quad , \tag{4.6.7}$$

where χ_s are Pauli spinors and we have used the normalisation convention

$$u_i^\dagger(p,s) u_i(p,s) = 1 \tag{4.6.8}$$

for the spinor. This normalization differs from the usual convention used in introductory texts on QFT (c.f. Refs. [253, 254]) as it is more useful for studying nuclear matter [150]. The isospin baryon multiplets are

$$u_{\mathrm{N}} = \begin{pmatrix} u_{\mathrm{p}} \\ u_{\mathrm{n}} \end{pmatrix} \quad , \quad u_\Lambda = \begin{pmatrix} u_\Lambda \end{pmatrix} \quad , \quad u_\Sigma = \begin{pmatrix} u_{\Sigma^+} \\ u_{\Sigma^0} \\ u_{\Sigma^-} \end{pmatrix} \quad , \quad u_\Xi = \begin{pmatrix} u_{\Xi^0} \\ u_{\Xi^-} \end{pmatrix} \quad . \tag{4.6.9}$$

From fully self-consistent calculations performed using QHD [150, 246] and QMC [183] models, it is known that the scalar and temporal vector self-energy components are approximately momentum independent and the spatial vector component is very small. Therefore, we proceed by carrying out the self-consistency approximately, as in Eq. (4.0.1). The self-energy then has a form identical to the usual mean-field (Hartree) result and the Fock corrections to these components can be included by requiring thermodynamical consistency, which amounts to minimising the total energy density with respect to the meson fields. This results in a small correction to the scalar field. Moreover, we have $u_i(p,s) = u_i(\vec{p},s)$ and $E_i^*(p) = E_i^*(\vec{p}) = \sqrt{\vec{p}^2 + M_i^{*2}}$.

In this approximation, the effective mass is only dependent on the mean scalar field. As we are working with the QMC model, the baryons are modelled as MIT bags immersed in this scalar field. By solving the non-linear bag equations, the effective mass can then be parametrised as a function of the the scalar coupling and mean scalar field. The scalar self-energy component is then $\Sigma_i^{\rm s}(\bar{\sigma}) = M_i^*(\bar{\sigma}) - M_i$, where we use the parametrisation of the effective mass, including self-consistent one-gluon exchange, obtained in Ref. [188]. For convenience, the baryon effective mass parametrisations for the spin-1/2 octet are given in App. A.1.

The no sea approximation is used, i.e., the negative energy states of the baryons are ignored. Therefore, the in-medium propagators for baryons propagating on-shell in the nuclear matter rest frame is given entirely by the Dirac portion of the baryon propagator [150]

$$G^i_{\alpha\beta}(p) = \frac{i\pi}{E_i^*(p)}(\not{p}^* + M_i^*)_{\alpha\beta}\delta(p^0 - E(p))\Theta(p_{F,i} - |\vec{p}|) \quad . \tag{4.6.10}$$

With the above approximations and definitions, the Fock contribution can be evaluated. In Sec. 4.7, we present the detailed evaluation of the σ meson contribution to the energy density.

4.7 Detailed Evaluation of σ Meson Fock Term

What we actually want is the energy density, which is defined by Eq. (4.4.8). To evaluate the σ meson contribution to the energy density (see Eq. (4.5.63), we need to evaluate the following ground state expectation value

$$\begin{aligned}
&\left\langle \delta\left(\bar{\psi}_i\psi_i\right)(\vec{r}\,')\delta\left(\bar{\psi}_i\psi_i\right)(\vec{r})\right\rangle \\
&\qquad = \left\langle \left(\bar{\psi}_i\psi_i - \left\langle\bar{\psi}_i\psi_i\right\rangle\right)(\vec{r}\,')\left(\bar{\psi}_i\psi_i - \left\langle\bar{\psi}_i\psi_i\right\rangle\right)(\vec{r})\right\rangle \qquad (4.7.1)\\
&\qquad = \left\langle\bar{\psi}_i(\vec{r}\,')\psi_i(\vec{r}\,')\bar{\psi}_i(\vec{r})\psi_i(\vec{r})\right\rangle - \left\langle\bar{\psi}_i(\vec{r}\,')\psi_i(\vec{r}\,')\right\rangle\left\langle\bar{\psi}_i(\vec{r})\psi_i(\vec{r})\right\rangle \quad .
\end{aligned}$$

To simplify further we transform the field operators to the Heisenberg representation. Specifically for the first term in the last line we find

$$\begin{aligned}
A &\equiv \left\langle\bar{\psi}_i(\vec{r}')\psi_i(\vec{r}')\bar{\psi}_i(\vec{r})\psi_i(\vec{r})\right\rangle \qquad (4.7.2)\\
&= \left\langle e^{iHt_1}\bar{\psi}_i(\vec{r}')e^{-iHt_1}e^{iHt_1}\psi_i(\vec{r}')e^{-iHt_1}e^{iHt_1}\bar{\psi}_i(\vec{r})e^{-iHt_1}e^{iHt_1}\psi_i(\vec{r})e^{-iHt_1}\right\rangle \qquad (4.7.3)
\end{aligned}$$

$$= \left\langle \bar{\psi}_i(\vec{r}',t_1)\psi_i(\vec{r}',t_1)\bar{\psi}_i(\vec{r},t_1)\psi_i(\vec{r},t_1)\right\rangle \tag{4.7.4}$$

$$= \lim_{t_1'\to t_1} \left\langle \bar{\psi}_i(\vec{r}',t_1')\psi_i(\vec{r}',t_1')\bar{\psi}_i(\vec{r},t_1)\psi_i(\vec{r},t_1)\right\rangle \tag{4.7.5}$$

$$= \lim_{\substack{t_1'\to t_1\\ t_1'>t_1}} \left\langle \mathrm{T}\left[\bar{\psi}_i(\vec{r},t_1)\psi_i(\vec{r},t_1)\bar{\psi}_i(\vec{r}',t_1')\psi_i(\vec{r}',t_1')\right]\right\rangle \quad . \tag{4.7.6}$$

Using Wick's theorem to simplify further, only fully contracted terms survive

$$A = \lim_{\substack{t_1'\to t_1\\ t_1'>t_1}} \bar{\psi}_i(\vec{r},t_1)\psi_i(\vec{r},t_1)\bar{\psi}_i(\vec{r}',t_1')\psi_i(\vec{r}',t_1') + \bar{\psi}_i(\vec{r},t_1)\psi_i(\vec{r},t_1)\bar{\psi}_i(\vec{r}',t_1')\psi_i(\vec{r}',t_1) \tag{4.7.7}$$

$$= \lim_{t_1'\to t_1^+} \mathrm{Tr}\left[iG^i(\vec{r},t_1;\vec{r},t_1)iG^i(\vec{r}',t_1';\vec{r}',t_1')\right] - \mathrm{Tr}\left[iG^i(\vec{r}',t_1';\vec{r},t_1)iG^i(\vec{r},t_1;\vec{r}',t_1')\right] \tag{4.7.8}$$

$$= \lim_{t_1'\to t_1^+} \mathrm{Tr}\left[iG^i(x;x)iG^i(x';x')\right] - \mathrm{Tr}\left[iG^i(x';x)iG^i(x;x')\right] \quad . \tag{4.7.9}$$

The first term in Eq. (4.7.9) cancels the second term in Eq. (4.7.2). We evaluate the second term by using the momentum space representation of the baryon's in-medium Greens function (Eq. (4.6.10),

$$\lim_{t_1'\to t_1^+} -\mathrm{Tr}\left[iG^i(x';x)iG^i(x;x')\right] \tag{4.7.10}$$

$$= \lim_{t_1'\to t_1^+} -i\int \frac{d^4p}{(2\pi)^4} G^i_{\alpha\beta}(p)e^{-ip\cdot(x'-x)} i\int \frac{d^4p'}{(2\pi)^4} G^i_{\beta\alpha}(p')e^{-ip'\cdot(x-x')} \tag{4.7.11}$$

$$= \int \frac{d^4p}{(2\pi)^4}\frac{d^4p'}{(2\pi)^4} G^i_{\alpha\beta}(p)G^i_{\beta\alpha}(p')e^{i(\vec{p}-\vec{p}')\cdot(\vec{r}'-\vec{r})} \tag{4.7.12}$$

$$= \int \frac{d^4p}{(2\pi)^4}\frac{d^4p'}{(2\pi)^4} \left(\not{p}^* + M_i^*\right)_{\alpha\beta} \frac{i\pi}{E_i^*(p)}\delta(p_0 - E_i(p))\Theta(p_{F,i} - |\vec{p}|) \times \left(\not{p}'^* + M_i^*\right)_{\beta\alpha} \frac{i\pi}{E_i^*(p')}\delta(p_0' - E_i(p'))\Theta(p_{F,i}' - |\vec{p}'|)e^{+i(\vec{p}-\vec{p}')\cdot(\vec{r}'-\vec{r})} \quad . \tag{4.7.13}$$

Performing the p_0 and p_0' integrals we obtain

$$\lim_{t_1'\to t_1^+} -\mathrm{Tr}\left[iG^i(x';x)iG^i(x;x')\right] \tag{4.7.14}$$

$$= -\int \frac{d^3p}{(2\pi)^3}\frac{d^3p'}{(2\pi)^3} \frac{\mathrm{Tr}\left[\left(\not{p}^* + M_i^*\right)\left(\not{p}'^* + M_i^*\right)\right]}{4E_i^*(p)E_i^*(p')} \times e^{+i(\vec{p}-\vec{p}')\cdot(\vec{r}'-\vec{r})}\Theta(p_{F,i} - |\vec{p}|)\Theta(p_{F,i}' - |\vec{p}'|)\,. \tag{4.7.15}$$

Using Eq. (4.7.15) and (4.5.63), the σ mesons Fock contribution to the energy density is

$$\epsilon_\sigma^{\mathrm{F}} = -\frac{1}{V}\frac{1}{2}\sum_i \left(\frac{\partial M_i^*}{\partial\bar{\sigma}}\right)^2 \int d^3r \int d^3r' \int \frac{d^3q}{(2\pi)^3}\,\Delta_\sigma(\vec{q})e^{-i\vec{q}\cdot(\vec{r}'-\vec{r})}$$

$$\left[- \int\limits_{|\vec{p}| \leq\ p_{F,i}} \frac{d^3p}{(2\pi)^3} \int\limits_{|\vec{p}'| \leq\ p'_{F,i}} \frac{d^3p'}{(2\pi)^3} \frac{\mathrm{Tr}\left[\left(\not{p}^* + M_i^*\right)\left(\not{p}'^* + M_i^*\right)\right]}{4E_i^*(p)E_i^*(p')} e^{+i(\vec{p}-\vec{p}')\cdot(\vec{r}'-\vec{r})} \right] \quad . \tag{4.7.16}$$

Making use of the exponential representation of the Dirac delta function,

$$(2\pi)^3\delta^{(3)}(\vec{p}-\vec{p}') = \int d^3r e^{-i(\vec{p}-\vec{p}')\cdot\vec{r}} \quad , \tag{4.7.17}$$

to perform the d^3r and d^3r' integrals we obtain,

$$\begin{aligned} \epsilon_\sigma^{\mathrm{F}} &= \frac{1}{2V}\sum_i \left(\frac{\partial M_i^*}{\partial\bar{\sigma}}\right)^2 \int \frac{d^3q}{(2\pi)^3} \int\limits_{|\vec{p}|\leq p_{F,i}} \frac{d^3p}{(2\pi)^3} \int\limits_{|\vec{p}'|\leq p'_{F,i}} \frac{d^3p'}{(2\pi)^3} \\ &\quad \times \Delta_\sigma(\vec{q}) \frac{\mathrm{Tr}\left[\left(\not{p}^* + M_i^*\right)\left(\not{p}'^* + M_i^*\right)\right]}{4E_i^*(p)E_i^*(p')} \\ &\quad \times (2\pi)^3\delta^{(3)}(\vec{p}-\vec{p}'-\vec{q})\ (2\pi)^3\delta^{(3)}(-\vec{p}+\vec{p}'+\vec{q}) \quad . \end{aligned} \tag{4.7.18}$$

Now performing the d^3q integral and using $V = (2\pi)^3\delta^{(3)}(0)$ from Eq. (4.7.17), we finally obtain

$$\epsilon_\sigma^{\mathrm{F}} = \frac{1}{2}\sum_i \left(\frac{\partial M_i^*}{\partial\bar{\sigma}}\right)^2 \int\limits_{|\vec{p}|\leq p_{F,i}} \frac{d^3p}{(2\pi)^3} \int\limits_{|\vec{p}'|\leq p'_{F,i}} \frac{d^3p'}{(2\pi)^3} \Delta_\sigma(\vec{q}) \frac{\mathrm{Tr}\left[\left(\not{p}^* + M_i^*\right)\left(\not{p}'^* + M_i^*\right)\right]}{4E_i^*(p)E_i^*(p')} \quad , \tag{4.7.19}$$

where the trace is evaluated by the usual methods [253] to be

$$\mathrm{Tr}\left[\left(\not{p}^* + M_i^*\right)\left(\not{p}'^* + M_i^*\right)\right] = 4(E_i^*(p)E_i^*(p') - \vec{p}\cdot\vec{p}' + {M_i^*}^2) \quad . \tag{4.7.20}$$

As can be seen in Eq. (4.7.19), there is an additional scalar dependence in this Fock term, which appears after explicit evaluation. A correction to the mean scalar field can easily be included numerically. This is a small contribution and it is included in the scenarios labelled "Fock $\delta\sigma$". This will be discussed further later. The other mesons also have an additional scalar dependence and their expressions are straightforwardly obtained in the same manner.

4.8 Final Expressions for the Fock Terms

Before giving the expressions for the remaining mesons we consider a naive amplification of the tensor interaction and introduce form factors.

We introduce a crude method to amplify the effect of the tensor interaction,

$$\frac{f_{\eta B}}{2M_{\mathrm{N}}} \longrightarrow \frac{f_{\eta B}}{2M_{\mathrm{N}}^*} \quad , \tag{4.8.1}$$

neglecting any additional corrections to $\delta\sigma$ and ultimately the σ-meson Fock energy density that may ensue. We also introduce form factors, because of the extended nature of the baryons, by

$$g_{\alpha B} \longrightarrow g_{\alpha B} F^{\alpha}(k^2) \quad . \tag{4.8.2}$$

The σ, ω, ρ and π form factors are all taken to have the dipole form $F(k^2) \simeq F(\vec{k}^2)$ with the same cut-off Λ. We explore values of the cut-off mass in the range 0.9 – 1.3 GeV. Clearly, these form factors are only of concern for the Fock terms as these allow for a finite momentum transfer, whereas Hartree contributions do not. We make specific note of the two terms which contribute to the vector meson vertices, a vector 'Dirac' term and a tensor 'Pauli' term.

Taking into account these modifications, the Fock level contributions to the energy density can be expressed as in Ref. [244]. These terms involve the meson baryon vertices which are expressed as

$$\Gamma_{\sigma B} = g_{\sigma B} C_B(\bar{\sigma}) F^{\sigma}(k^2)\mathbf{1} = -\frac{\partial M_B^*}{\partial \bar{\sigma}} F^{\sigma}(k^2)\mathbf{1} \ , \tag{4.8.3}$$

$$\mathbf{\Gamma}_{\eta B} = \epsilon_{\eta}^{\mu}\mathbf{\Gamma}_{\mu\eta B} = \epsilon_{\eta}^{\mu}\left[g_{\eta B}\gamma_{\mu}F_1^{\eta}(k^2) + \frac{i f_{\eta B}\sigma_{\mu\nu}}{2M_B^*}k^{\nu}F_2^{\eta}(k^2)\right]\boldsymbol{t} \ ; \quad \eta \in \{\omega, \rho\} \ , \tag{4.8.4}$$

$$\mathbf{\Gamma}_{\pi B} = i\frac{g_A}{2f_{\pi}}F^{\pi}(k^2)\gamma^{\mu}k_{\mu}\gamma_5\boldsymbol{\tau} \ , \tag{4.8.5}$$

with the isospin matrix $\boldsymbol{t}$ only applicable to isovector mesons. For nucleons and cascade particles $\boldsymbol{t} = \dfrac{\boldsymbol{\tau}}{2}$. For the ρ meson the flavour dependence is contained completely in the isospin matrix, such that $g_{\rho B} = g_{\rho N} = g_{\rho}$.

Note that we have written the vector meson, $\Gamma_{\eta B}$, with an effective baryon mass, $M_{\rm B}^*$ in the denominator of Eq. (4.8.4). The expressions are worked out using this form. To obtain the standard form of the equations, without this amplification, the ratios of tensor to vector couplings $\kappa_{(\omega,\rho)}^{B} = f_{B(\omega,\rho)}/g_{B(\omega,\rho)}$ given in Table 4.9.1 are rescaled using the free proton mass

$$\kappa_{(\omega,\rho)}^{B} \rightarrow \kappa_{(\omega,\rho)}^{B} \times \frac{M_B^*}{M_p} \ . \tag{4.8.6}$$

Equation (4.8.6) is used in all variants of the model ("scenarios"), considered in this work except where a result is labeled "Eff. Proton Mass", where it is rescaled using the effective proton mass instead. The reason for this choice is that the derivation of the QMC model is based on an order by order expansion in the effect of the scalar field. Using the effective mass of the proton in the Pauli term coupling assumes that the scalar field does not appear in some other way at the level of momentum dependent couplings. A systematic expansion would ensure that all effects are included consistently to a given order. In the absence of such a derivation it would be natural to write the couplings in terms of the free baryon mass as is done in Ref. [245, 255] and not include just one effect of the scalar field at this order.

Within the QMC model, the hadronic energy density $\epsilon_{hadronic}$ is the sum of the of

the baryonic energy density in nuclear matter which is

$$\epsilon_B = \frac{2}{(2\pi)^3} \sum_B \int_{|\vec{p}|\leq p_F} d^3p \, \sqrt{\vec{p}^2 + M_B^{*\,2}} \,, \tag{4.8.7}$$

and the mesonic energy density $\epsilon_{\sigma\omega\rho\pi}$. This can be divided into two parts, the Hartree $\epsilon_H = \epsilon_B + \epsilon^H_{\sigma\omega\rho}$ and the Fock $\epsilon_F = \epsilon^F_{\sigma\omega\rho} + \epsilon_\pi$ contribution. The total mesonic energy density is given by $\epsilon_{\sigma\omega\rho\pi} = \epsilon^H_{\sigma\omega\rho} + \epsilon_F$, where the Hartree and Fock components of the mesonic energy density are given respectively by

$$\epsilon^H_{\sigma\omega\rho} = \sum_{\alpha\in\{\sigma,\omega,\rho\}} \frac{1}{2} m_\alpha^2 \bar{\alpha}^2 \tag{4.8.8}$$

where $\bar{\alpha}$ refers to the mean field value of meson α and

$$\epsilon_F = \frac{1}{(2\pi)^6} \sum_{m\in\{\sigma,\omega,\rho,\pi\}} \sum_{BB'} C^m_{BB'} \int_{|\vec{p}|\leq p_F} \int_{|\vec{p}'|\leq p_{F'}} d^3p d^3p' \; \Xi^\alpha_{BB'} \,, \tag{4.8.9}$$

where $C^\sigma_{BB'} = C^\omega_{BB'} = \delta_{BB'}$. $C^\rho_{BB'}$ and $C^\pi_{BB'}$, which arise from symmetry considerations, are given in Ref. [161] and $\Xi^\alpha_{BB'}$, is explained below. The meson mean fields are given by applying the mean field approximation to the above system of equations, this is a minimisation of the energy density, leading to the self-consistency equations. Including exchange terms to the meson energy density gives an additional term from the minimisation to the scalar mean field which is evaluated numerically. This additional self-consistency significantly increases computation time and only makes a small change in our results. For this reason we include only one full calculation demonstrating its correction to the σ mean field. For the mean scalar field ($\bar{\sigma}$) at a given density it is self-consistently expressed as

$$\begin{aligned} \bar{\sigma} &= -\frac{1}{m_\sigma^2}\frac{\partial \epsilon_B}{\partial \bar{\sigma}} - \frac{1}{m_\sigma^2}\frac{\partial \epsilon_F}{\partial \bar{\sigma}} \\ &= -\frac{2}{m_\sigma^2 (2\pi)^3} \sum_B \int_{|\vec{p}|\leq p_F} d^3p \, \frac{M_B^*}{\sqrt{\vec{p}^2 + M_B^{*\,2}}} \frac{\partial M_B^*}{\partial \bar{\sigma}} - \frac{1}{m_\sigma^2}\frac{\partial \epsilon_F}{\partial \bar{\sigma}} \quad , \end{aligned} \tag{4.8.10}$$

where ϵ_b, ϵ_F are the baryon and Fock contributions to the energy density. The vector meson mean fields are given by

$$\bar{\omega} = \sum_i \frac{g_{\omega i}}{m_\omega^2} \rho_i^{\rm v} \quad , \tag{4.8.11}$$

$$\bar{\rho} = \sum_i \frac{g_{\rho i}}{m_\rho^2} t_{3i} \rho_i^{\rm v} \quad . \tag{4.8.12}$$

The total baryonic vector and scalar densities are given by

$$\rho^s = \sum_i \rho_i^s = \frac{2}{(2\pi)^3} \sum_i \int_{|\vec{p}|\leq p_{F,i}} d^3p \, \frac{M_i^*}{\sqrt{\vec{p}^2 + M_i^{*\,2}}} \tag{4.8.13}$$

and

$$\rho^v = \sum_i \rho_i^v = \frac{2}{(2\pi)^3} \sum_i \int_{|\vec{p}| \le p_{F,i}} d^3p \quad . \tag{4.8.14}$$

In Eq.(4.8.13) and Eq.(4.8.14), $p_{\rm F,i}$ denotes the Fermi momentum of a baryon of type i. These integrals are evaluated by making use of spherical symmetry.

For ϵ^F, the integrand has the form

$$\Xi^m_{BB'} = \frac{1}{2} \sum_{s,s'} |\bar{u}_{B'}(p',s') \Gamma_{mB} u_B(p,s)|^2 \Delta_m(\vec{k}) \ , \tag{4.8.15}$$

where $\Delta_m(\vec{k})$ is the Yukawa propagator for meson m with momentum $\vec{k} = \vec{p} - \vec{p'}$ and u_B are the baryon spinors. The integrands take the following form for $B = B'$

$$\Xi^\sigma_B = \frac{1}{2} \frac{\left(g_{\sigma B} C_B(\bar{\sigma}) F^\sigma(\vec{k}^2) \right)^2}{E^*(\vec{p}\,')E^*(\vec{p})} \left\{ M_B^{*2} + E^*(\vec{p}\,')E^*(\vec{p}) - \vec{p}\,' \cdot \vec{p} \right\} \Delta_\sigma(\vec{k}) \, . \tag{4.8.16}$$

Here for the vector meson integrands we denote $\eta = \omega, \rho$

$$\Xi^{\eta V}_B = -\frac{\left(g_{\eta B} F_1^\eta(\vec{k}^2) \right)^2}{E^*(\vec{p}\,')E^*(\vec{p})} \left\{ 2M_B^{*2} - E^*(\vec{p}\,')E^*(\vec{p}) + \vec{p}\,' \cdot \vec{p} \right\} \Delta_\eta(\vec{k}) \tag{4.8.17}$$

$$\Xi^{\eta VT}_B = (g_{\eta B})^2 \kappa_{\eta B} F_1^\eta(\vec{k}^2) F_2^\eta(\vec{k}^2) . \left\{ \frac{-3M_B^{*2} + 3E^*(\vec{p}\,')E^*(\vec{p})) - 3\vec{p}\,' \cdot \vec{p}}{E^*(\vec{p}\,')E^*(\vec{p})} \right\} \Delta_\eta(\vec{k}) \tag{4.8.18}$$

$$\Xi^{\eta T}_B = -\frac{\left(g_{\eta B} \kappa_{\eta B} F_2^\eta(\vec{k}^2) \right)^2}{E^*(\vec{p}\,')E^*(\vec{p})} . \cdot \left\{ \frac{(5M_B^{*2} - E^*(\vec{p}\,')E^*(\vec{p}) + \vec{p}\,' \cdot \vec{p})}{4M_B^{*2}} . (M_B^{*2} - E^*(\vec{p}\,')E^*(\vec{p}) + \vec{p}\,' \cdot \vec{p}) \right\} \Delta_\eta(\vec{k}) \tag{4.8.19}$$

and for the pion

$$\Xi^\pi_B = -\frac{2M_B^{*2} (\frac{g_A}{2f_\pi} F_\pi(\vec{k}^2))^2}{E^*(\vec{p})E^*(\vec{p}\,')} \left\{ M_B^{*2} - E^*(\vec{p})E^*(\vec{p}\,') + \vec{p}\,' \cdot \vec{p} \right\} \Delta_\pi(\vec{k}). \tag{4.8.20}$$

where $E^*(\vec{p}) = \sqrt{\vec{p}^2 + M_B^{*2}}$. In the above integrands we expand the terms in the braces multiplied by the propagator to isolate the momentum independent pieces and multiply these contact terms by the variable ξ which we use to investigate the consequences of contact subtraction. We emphasise here the importance of subtraction of the momentum independent piece, which when transformed to configuration space corresponds to a delta function. In this manner our subtraction is implemented by the variable ξ,

such that $\delta(\vec{r}) \mapsto \xi \times \delta(\vec{r})$. The removal of the contact terms is a common procedure due to the fact that these contact terms represent very short range, effectively zero range correlations between the baryons, which is not consistent in this model which treats the baryons as clusters of quarks and not as point-like objects. Moreover, it is also required because of the suppression of the relative wave function at short distance originating from the repulsive hard core. We give this explicitly for the Vector-Vector piece of the vector mesons

$$\begin{aligned}
\frac{2M_B^{*2} - E^*(\vec{p}\,')E^*(\vec{p}) + \vec{p'} \cdot \vec{p}}{\vec{k^2} + m_\eta^2} &= \frac{2M_B^{*2} - p' \cdot p}{\vec{k^2} + m_\eta^2} \\
&\simeq \frac{M_B^{*2} - \frac{\vec{k}^2}{2}}{\vec{k^2} + m_\eta^2} \\
&= \frac{M_B^{*2}}{\vec{k}^2 + m_\eta^2} - \frac{1}{2}\frac{\vec{k}^2}{\vec{k}^2 + m_\eta^2} \\
&= \frac{M_B^{*2} + \frac{m_\eta^2}{2}}{\vec{k}^2 + m_\eta^2} - \frac{1}{2}\xi
\end{aligned} \tag{4.8.21}$$

the remaining subtractions follow in the same manner, see Appendix A.

4.9 Model Parameters

The expression for total energy density is dependent on just the three main adjustable coupling constants, which control the coupling of the mesons to the two lightest quarks, g_σ^q, g_ω^q, and g_ρ^q for $q = u, d$ ($g_\alpha^s = 0$ for all mesons α). In addition, one has the meson masses, the value of the cut-off parameter Λ appearing in the dipole form factors needed to evaluate the Fock terms and finally the bag radius of the free nucleon. The σ, ω, and ρ couplings to the quarks are constrained to reproduce the standard empirical properties of symmetric (N=Z) nuclear matter; the saturation density $\rho_0 = 0.16$ fm^{-3}, the binding energy per nucleon at saturation of $\mathcal{E}(\rho = \rho_0) = -15.865$ MeV as well as the asymmetry energy coefficient $a_{\rm asym} \equiv S_0 \equiv S(\rho_0) = 32.5$ MeV [161] (see also Ch. 2, Secs. 2.3–2.6).

The ω, ρ and π meson masses are set to their experimental values. The ambiguity in defining the mass of the σ after quantising the classical equations of motion was explained in detail in Ref. [182]. Here it is set to the value that gave the best agreement with experiment for the binding energies of finite nuclei in a previous QMC model calculation [160], which was 700 MeV. This is a common value taken for the σ meson mass which is generally considered in RMF models to be in the range 400–800 MeV.

The form factor cut-off mass, Λ, controls the strength of the Fock terms Eqs. (4.8.3 - 4.8.5). We considered a range of values; 0.9 GeV $\leq \Lambda \leq$ 2.0 GeV, with the preferred value, as we shall see, being 0.9 GeV. For simplicity we have used the same cut-off for all mesons. Since the pion mass is much lower than that of the other mesons, we have confirmed that using a lower cut-off for the pion does not significantly influence the results. This is not surprising as Fock terms are expected to be more significant at higher density where we have found that the pion does not contribute greatly.

Relation	Magnetic Moments [n.m.]	$\kappa^B_{(IS,IV)} =: \kappa^B_{(\omega,\rho)}$
$\mu_p = 1 + \frac{1}{2}(\kappa^N_{IS} + \kappa^N_{IV})$ $\mu_n = \frac{1}{2}(\kappa^N_{IS} - \kappa^N_{IV})$	$\mu_n = -1.913$ $\mu_p = 2.793$	$\kappa^N_{IS} = -0.12$ $\kappa^N_{IV} = 3.706$
$\mu_\Lambda = \kappa^\Lambda_{IS}$	$\mu_\Lambda = -0.61$	$\kappa^\Lambda_{IS} = -0.61$
$\mu_{\Sigma^+} = 1 + (\kappa^\Sigma_{IS} + \kappa^\Sigma_{IV})$ $\mu_{\Sigma^-} = -1 + (\kappa^\Sigma_{IS} - \kappa^\Sigma_{IV})$	$\mu_{\Sigma^-} = -1.16$ $\mu_{\Sigma^+} = 2.458$	$\kappa^\Sigma_{IS} = 0.649$ $\kappa^\Sigma_{IV} = 0.809$
$\mu_{\Xi^0} = \frac{1}{2}(\kappa^\Xi_{IS} + \kappa^\Xi_{IV})$ $\mu_{\Xi^-} = -1 + \frac{1}{2}(\kappa^\Xi_{IS} - \kappa^\Xi_{IV})$	$\mu_{\Xi^-} = -0.65$ $\mu_{\Xi^0} = -1.25$	$\kappa^\Xi_{IS} = -0.9$ $\kappa^\Xi_{IV} = -1.5993$

Table 4.9.1: Relations between baryon magnetic moments and anomalous isoscalar and isovector magnetic moments $\kappa^B_{(IS,IV)} =: \kappa^B_{(\omega,\rho)} = f_{B(\omega,\rho)}/g_{B(\omega,\rho)}$ using experimental magnetic moments [256].

All the other coupling constants in the expression for the total energy density are *calculated* within the QMC model or determined from symmetry considerations without further need for adjustable parameters. The one exception is $g_{\sigma B}(\bar{\sigma})$, which shows a weak dependence on the free nucleon radius $R_N^{\rm free}$. We checked that changes of order 20% in $R_N^{\rm free}$, consistent with nucleon properties, have no significant effect on the properties of nuclear matter and chose $R_N^{\rm free} = 1.0$ fm.

The baryon-meson coupling constants $g_{\sigma N}(0)$, $g_{\omega B}$, and $g_{\rho B}$ (or equivalently the three quark-meson coupling constants) are determined by fitting the saturation properties of symmetric nuclear matter. Only $g_{\sigma B}$ is density dependent and that dependence is calculated self-consistently according to

$$\frac{\partial}{\partial\bar{\sigma}}\left[g_{\sigma B}(\bar{\sigma})\bar{\sigma}\right] = g_{\sigma B}(0)\, C_B(\bar{\sigma}) = -\frac{\partial M_B^*}{\partial\bar{\sigma}} \equiv -\frac{\partial M_B^*(\bar{\sigma}, g_{\sigma N}, R_N^{\rm free})}{\partial\bar{\sigma}}\ , \tag{4.9.1}$$

where M_B^* is calculated in the QMC model using the MIT bag with one gluon exchange for the baryon structure. The couplings $g_{\omega B}$ and $g_{\rho B}$ are expressed in terms of the quark

level couplings as:

$$g_{\omega B} = n^B_{u,d} g^q_\omega \ ; \ g_{\rho B} = g_{\rho N} = g^q_\rho \ , \tag{4.9.2}$$

where $n^B_{u,d}$ is the number of light quarks in baryon B.

At densities $\sim 2-3\ \rho_0$ one expects, simply because the Fermi level of the neutrons rises rapidly, that for matter in beta-equilibrium hyperons must be considered. There is very little experimental data on the N–Y and Y–Y interactions, which makes the traditional approach through phenomenological pair-wise interactions very difficult. There is certainly no hope of determining the relevant three-body forces which are expected to be critical at high density. One of the attractive features of the QMC model is that it predicts all of these forces in terms of the underlying quark-meson couplings, the scalar meson mass and the particular quark model chosen (the MIT bag here). Furthermore, the density dependence of the scalar couplings to each baryon is also determined by the bag model mass parametrisation. The inclusion of this density dependent, in-medium interaction is equivalent in a density independent framework to including the appropriate three-body force between all baryons.

Remarkably, in the absence of the Pauli Fock terms, the model predicted realistic Λ binding energies and, at the same time realistic Σ repulsion in matter [188]. As we show later in Sec. 5.2, the additional repulsion associated with the Fock term, is not adequately compensated and the agreement is lost. In this work we assess the magnitude of the needed change by artificially modifying the σ–couplings for the hyperons to match the empirical observations. This procedure will serve as a guidance in the future development of the model.

It is well known that the coupling of the ρ meson to a particular baryon has a relatively large Pauli, or tensor, coupling (i.e. $f_{\rho B}$ in Eq. (4.8.4)). The value used varies from one model of the nuclear force to another. In the QMC model the prediction of the tensor coupling at zero momentum transfer is unambiguous—it is exactly the anomalous, iso-vector magnetic moment of the baryon in the MIT bag model. Similarly, the tensor coupling of the ω, which in the case of the nucleon is much smaller than for the ρ, is determined by the isoscalar magnetic moment. Since the MIT bag model reproduces the experimental values of the magnetic moments quite well, the tensor coupling required within the QMC model is equivalent to using vector meson dominance [257] and in practice we use values for the magnetic moments from the Particle Data Group [256]. Finally and purely as an exercise aimed at exploring the model dependence, we consider two different choices for the ratios of tensor to vector coupling constants $f_{\alpha B}/g_{\alpha B}$; with $\alpha \in \{\rho, \omega\}$. Whereas, as we explained, in the standard QMC calculation we take $f_{\rho N}/g_{\rho N} = 3.70$, we also explore the consequences of arbitrarily setting $f_{\rho N}/g_{\rho N} = 5.68$ in the 'Increased $f_{\rho N}/g_{\rho N}$' scenario. In this scenario we arbitrarily take the ratios of tensor to vector couplings of all baryons from the Nijmegen potentials (Table VII of Ref. [258]).

The only other parameters in the QMC model are those entering the bag model. We refer the reader to Ref. [188] where those parameters were obtained. None of them have been adjusted to any property of nuclear matter, although all calculations involving the QMC model at present rely on the MIT bag model with one gluon exchange and could be in principle improved upon by using a more sophisticated model of quark confinement. Nonetheless, with this simple quark-based model, remarkable agreement

with a broad range of experimental data has been obtained [187].

Having established the QMC model parameters, in the following section we calculate properties of symmetric nuclear matter (SNM) and pure neutron matter (PNM). In chapter 5, we calculate matter in beta-equilibrium (BEM) which consists of nucleons and leptons, and also matter in generalised beta-equilibrium (GBEM) containing the full baryon octet and leptons. Using the derived EoS, we calculate the properties of cold neutron stars and make a comparison with up-to-date experimental and observational data. We also examine the robustness of those results on the limited number of parameters entering the model.

4.10 Nuclear Matter Properties

In Sec. 4.9, the QMC model parameters were discussed and it was explained that a minimal set of saturation properties of symmetric nuclear matter is used to constrain them. Specifically, the the saturation density, the binding energy per particle and the symmetry energy at saturation, were used to fix the three quark-meson coupling constants. None of those properties is actually an *empirical* quantity, since they are not measured directly but extracted from experiments or observations in a model dependent way. However, there is a general consensus that all meaningful theories of nuclear matter should reproduce these quantities correctly. Moreover, other properties of both symmetric and pure neutron matter, derived from derivatives of the energy per particle with respect to particle number density or asymmetry parameter, together with their density dependence, can be compared to empirical data to further test the theories. These include the pressure, incompressibility (compression modulus), the slope of the symmetry energy and other higher order derivatives. These are defined in Ch. 2, Sec. 2.3. In Sec. 2.4, a brief review of the experimental knowledge concerning the EoS was given. However, there is no rigorous constraint available for the skewness coefficient except for the results of Farine *et al.* [259]. They obtained a model dependent value $K' = 700 \pm 500$ MeV from an analysis of the nuclear breathing mode, using a selection of Skyrme forces.

Values of an extended set of nuclear matter properties have been obtained using the QMC model developed in this chapter and presented in Table 4.13.1. The particular values at saturation density, ρ_0, are indicated with a subscript zero (e.g., K_0, Q_0 etc.). In symmetric nuclear matter, $\rho_\mathrm{n} = \rho_\mathrm{p} = 1/2\ \rho$, the values of these properties at saturation density can be compared to experiment.

The long range one pion exchange does not contribute in the Hartree approximation as it is coupled via a pseudo-vector current. The inclusion of the exchange terms allows the observables of nuclear matter to be affected by the pion. Most notably we find that in concordance with Ref [161] the pion reduces the incompressibility. Conversely, increasing the strength of the Fock terms as a whole has the net effect of increasing the value of incompressibility of nuclear matter.

In PNM, $\rho_\mathrm{n} = \rho$ and $\rho_\mathrm{p} = 0$. Although PNM does not exist in nature, it is seen as a first approximation to matter in the outer core of neutron stars at densities higher than ρ_0. The density dependence of the energy per particle of PNM is poorly known, except for the fact that PNM does not bind—i.e. the energy per particle is positive at

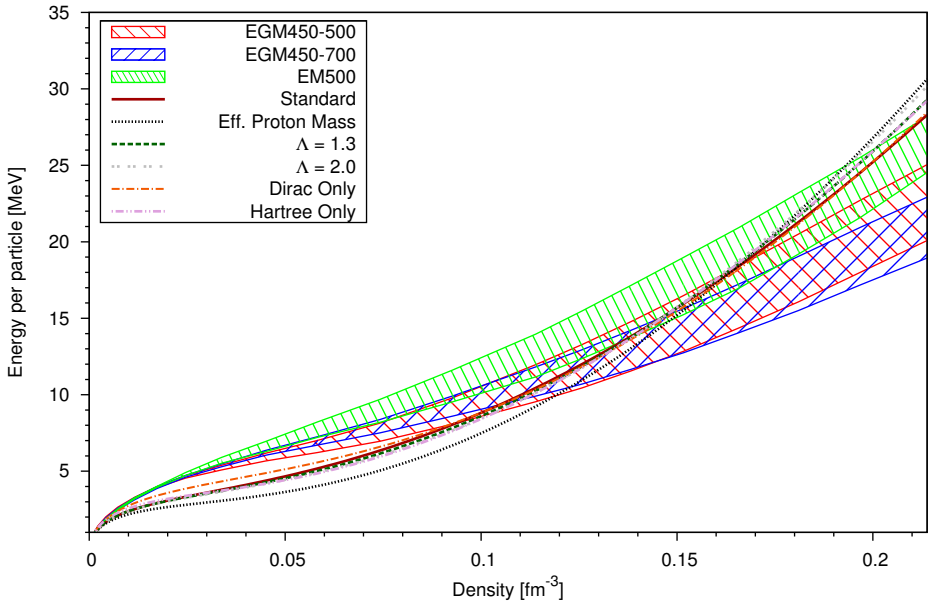

Figure 4.10.1: Pure neutron matter energy per particle as a function of density as obtained in the present work, in comparison with complete CEFT at N^{3}LO order – for more details of the latter, see Ref. [260].

all densities.

Very recently, Tews *et al.* [260] presented the first complete N^{3}LO calculation of the PNM energy, and Hebeler and Furnstahl [261] investigated the energy per particle in PNM at sub-saturation densities using two- and three-nucleon CEFT interactions that were consistently evolved within the framework of the similarity renormalization group. We compare their results with the QMC predictions in Fig. 4.10.1. Clearly the QMC prediction for the density dependence of the energy per particle in PNM is very similar to that of Tews *et al.* [260] at sub-saturation density, with a somewhat steeper increase at densities above saturation.

An interesting connection has been made between the pressure in the PNM neutron skin in heavy nuclei and the radius and crust thickness of a cold neutron star [114]. Thus a microscopic theoretical calculation of the PNM pressure became of interest, in particular at sub-saturation densities. Tsang *et al.* (see Fig. 4 and related references in Ref. [87]) collected several recent calculations of the PNM pressure as a function of particle number density. We show in Fig. 4.10.2 a selection of the models; Bruckner-Hartree-Fock (BHF) with Av18 two-body potential [262], Quantum Monte Carlo (QuMoCa) with Av8' two-body potential [263] and CEFT [264]. The main uncertainty in these calculations is the strength of three-body forces, which clearly make a significant contribution to the total pressure in these models (compare the left and right panels of Fig. 4.10.2, with the QMC result shown in the right panel). The QMC model, which naturally includes three-body forces without additional parameters (see Sec. 2.6), indicates a somewhat faster growth of pressure with increasing density than the other three-body interactions.

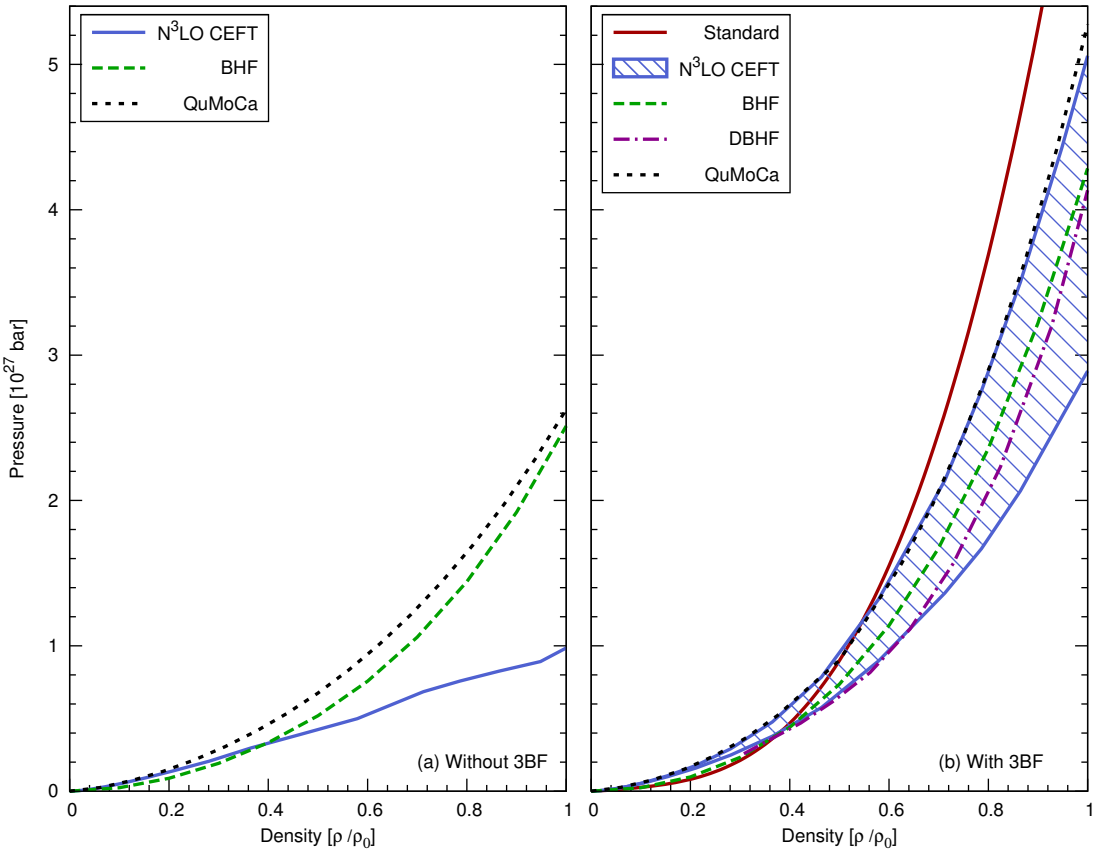

Figure 4.10.2: Density dependence of pressure in PNM as predicted in BHF, DBHF, QuMoCa and CEFT with and without three-body forces. (a) Without three-body forces. (b) With three-body forces. The QMC model prediction is shown in (b). For more details see the text and ref. [87].

Limits for the pressure-density relationship in SNM and PNM in the density region $2 - 5\ \rho_0$ have been inferred from a comparison of experimental data on matter flow in energetic heavy ion collisions and predictions of a dynamical transport theory by Danielewicz *et al.* (see Ref. [265] and references therein). The matter created in the collision, lasting $\sim 10^{-23}$s at an incident kinetic energy per nucleon varying from about 0.15 to 10 GeV per nucleon, was modelled as consisting of stable and excited nucleons (Δ and N*) as well as pions. The basic constraints on this matter are charge symmetry and strangeness conservation (although in this case the strangeness is zero). This is in contrast to matter in cold neutron stars, constrained by charge neutrality and generalised beta-equilibrium, where strangeness will not be conserved.

The transport theory was extrapolated to cold symmetric and pure neutron matter, with the latter augmented by empirical symmetry pressure [265]. We show in Fig. 4.10.3 the pressure versus density for SNM and PNM, as predicted in different scenarios for the QMC model in this work. The standard QMC model is consistent with the suggested constraints but at the upper end of the range determined in [265].

We now give details of how the optical potentials of hyperons embedded in symmetric nuclear matter are calculated. We refrain from discussing these results until Section 5.1 as these potentials are intimately connected to the particle content of matter in generalised beta equilibrium and are therefore more naturally discussed there. In many works optical potentials for the hyperons in symmetric nuclear matter are evaluated and used to constrain hyperon coupling constants. In the QMC model these couplings are derived within the model. We make the following approximation to evaluate the optical potentials in symmetric nuclear matter at saturation density. For each hyperon a small number density is chosen, so that we can evaluate the corresponding chemical potential numerically via Eq. (5.1.17). A small density means that this chemical potential is approximately the energy of a zero momentum hyperon embedded in symmetric nucleon only matter. We can then calculate the optical potentials by $U_i(\rho_0) = \mu_i - M_i$. These values are tabulated in Table 4.13.1 for the Λ, Σ^- and Ξ^- hyperons.

4.11 Asymmetric Nuclear Matter

Our knowledge of asymmetric nuclear matter is incomplete, mainly because of our rudimentary understanding of the symmetry energy, $\mathcal{S}$, and particularly its density dependence. It is related to the isospin dependence of the nuclear force and is an important property of highly asymmetric systems, such as heavy nuclei and the nuclear matter found in neutron stars. It is defined in Eq. (2.3.6) and is equal to the asymmetry coefficient in the Bethe–Weisacker mass formula in the limit A $\to \infty$ [111].

The definition of $\mathcal{S}(\rho)$ in Eq. (2.3.6) is related but not identical to the commonly used approximation as the difference between the binding energy per baryon in PNM and SNM

$$S(\rho) = \mathcal{E}(\rho, \beta = 1) - \mathcal{E}(\rho, \beta = 0) \ , \tag{4.11.1}$$

where the binding energy per baryon, $\mathcal{E}$, is defined in Eq. (2.3.5). This difference approximation is valid under two assumptions: (i) E$(\rho, \beta = 0)$ is a minimum energy of the matter at a given density ρ and thus in the expansion of E(ρ, β) about this value with respect to β the leading non-zero term is the second derivative term and (ii) all the other derivatives in the expansion are negligible [266]. In this work we consider Eq. (4.11.1) only to examine the validity of this approximation and to observe the impact of the Fock terms, specifically the tensor contribution, upon the symmetry energy.

As shown in Sec. 2.3, the symmetry energy can be expanded in a power series about its value at saturation, $\mathcal{S}_0$. The first three coefficients in this expansion are $\mathcal{S}_0$, its slope L_0, and its curvature $K_{\rm sym}$. These values are also presented in Table 4.13.1 for each of the model variations.

The search for constraints on the symmetry energy and its slope, L_0, has received considerable attention during the last decade. Recently Tsang *et al.* [87] evaluated constraints from a wide range of experiments. However, as again the symmetry energy is not measured directly but extracted from experimental data in a model dependent way, only limits on the symmetry energy can be established. One of the outcomes of the evaluation was a confirmation of a previously observed correlation between the value of $\mathcal{S}_0$ and its derivative L_0 at saturation density. Taking this correlation into

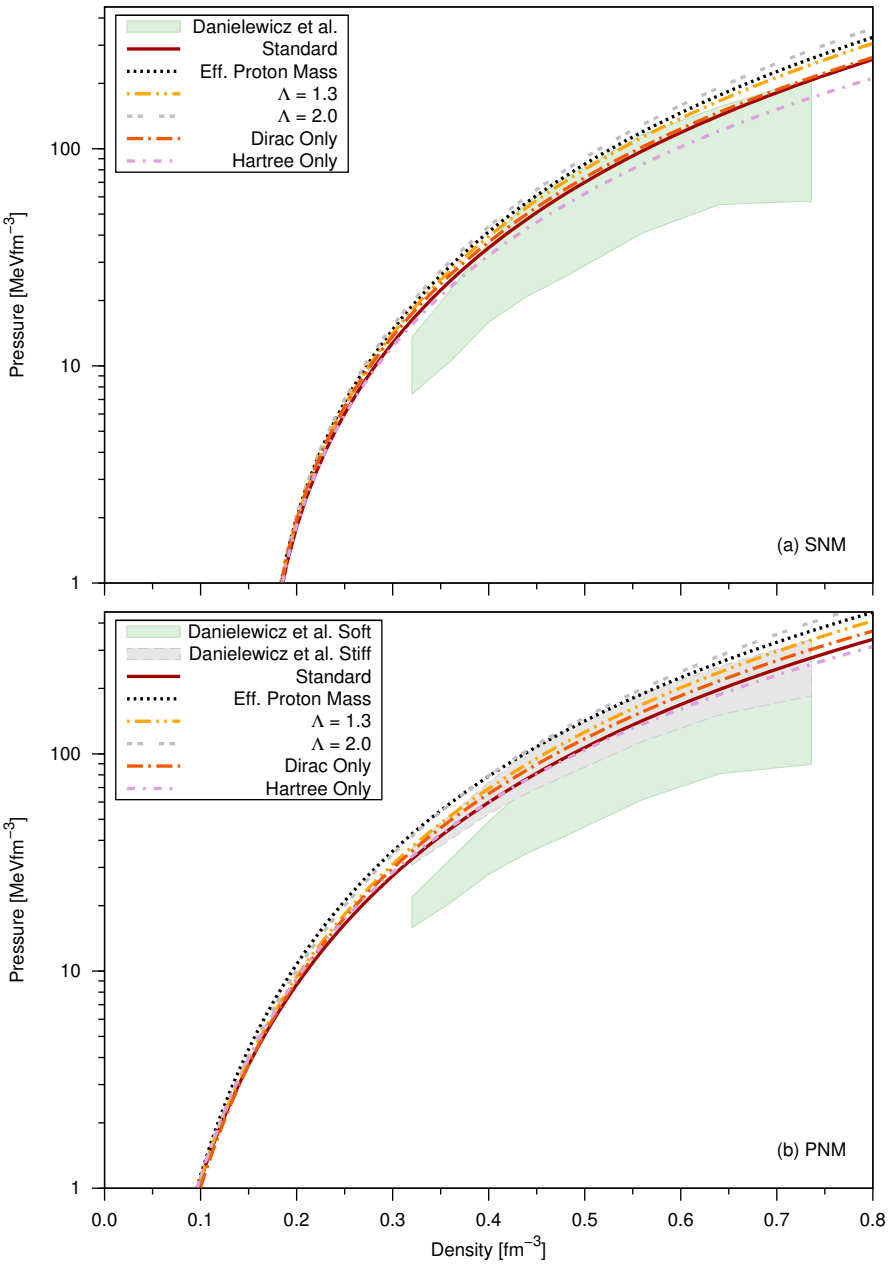

Figure 4.10.3: (a) Pressure in SNM as a function of density as predicted in QMC model. The shaded area is taken from Ref. [265]. (b) Pressure in PNM as a function of density as predicted in the QMC model. The upper and lower shaded areas correspond to two different estimates of the contribution of the symmetry pressure to the total pressure. For more detail see Ref. [265]

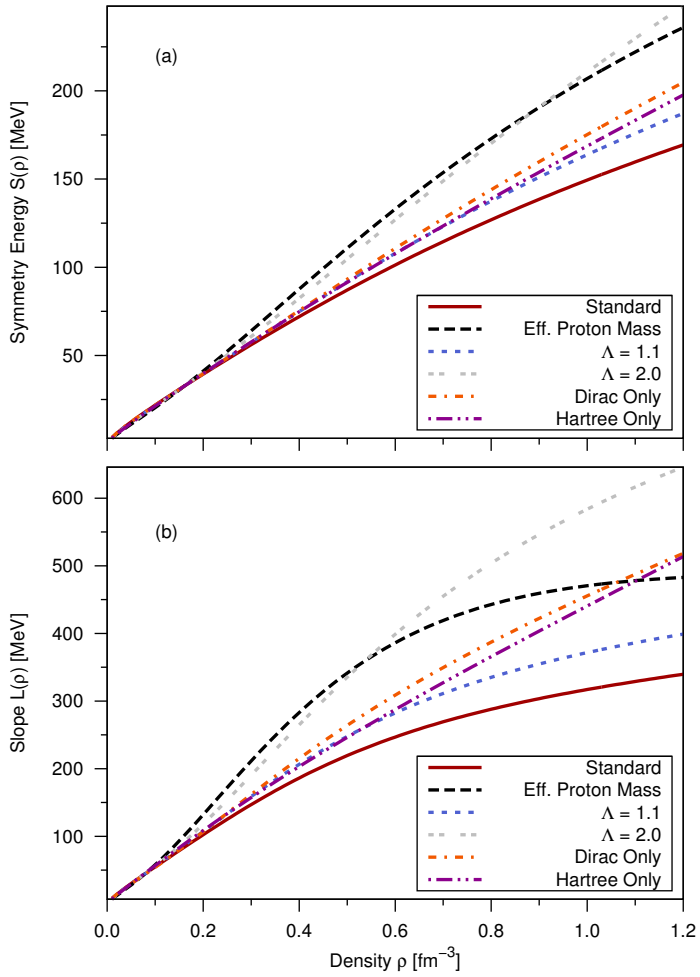

Figure 4.11.1: (a) Symmetry energy, $\mathcal{S}$, as a function of baryon number density, as calculated in this work. (b) Slope L of the symmetry energy, as a function of baryon number density $L(\rho) = 3\rho\left(\frac{\partial \mathcal{S}}{\partial \rho}\right)$.

account, the constraint centered on $(\mathcal{S}_0, L_0) \sim (32.5, 70)$ MeV, with the uncertainty in $\mathcal{S}_0$ allowing values $30 < \mathcal{S}_0 < 35$ MeV and related values of L_0 in the range of $35 < L_0 < 115$ MeV (see Fig. 2 in Ref. [87] for more details).

While theoretical predictions of $\mathcal{S}_0$ are also more or less confined to the range 30 to 35 MeV, the calculated values of L_0, corresponding to the range of $\mathcal{S}_0$, vary widely. For example, the QuMoCa and CEFT models predict very similar low values of L_0, between $\sim$ 30 - 50 MeV [87]. The best performing Skyrme forces, selected in Ref. [267], produce values of L_0 clustered around 50 MeV. On the other hand, relativistic mean field models show a much larger spread. The models which satisfied most of the constraints on the properties of nuclear matter, studied by Dutra *et al.* [268], predicted L_0 in the range $\sim$ 50 – 70 MeV. However, frequently used relativistic mean field model parametrisations, e.g. NL3, NL-SH, NLC, TM1 and TM2 predict L_0 values of order $\sim$ 110 – 120 MeV [269]. Chen *et al.* [270] found a linear the correlation between K_{sym}

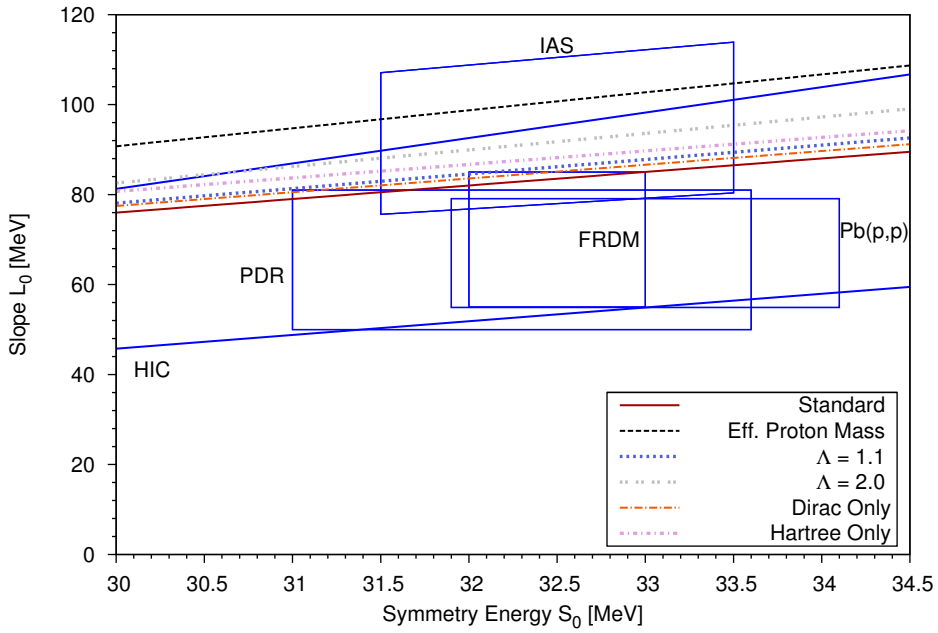

Figure 4.11.2: The correlation between the slope and magnitude of the symmetry energy $\mathcal{S}_0$. Constraints on the slope L_0 and the symmetry energy S_0 at saturation density from different experiments are overlaid. The experimental methods are labelled next to the boxes with the estimated uncertainties. See Ref. [87] for more details.

and L_0 for a specific selection of equations of state. For a range of positive values of L_0 between about 30 - 120 MeV K_{sym} is between $\sim$ -200 and 100 MeV.

In the QMC model the isospin dependent part of the interaction is mostly controlled by the exchange of the ρ meson. For this reason, here and in other works (e.g. [111]) the symmetry energy at saturation $\mathcal{S}_0 = 32.5$ MeV is used to fix the ρ meson coupling constant. The QMC result for L_0 is 84 MeV (see Table 4.13.1), which is within the broader limits found by Tsang *et al.* [87], although outside their preferred range.

We show the density dependence of the symmetry energy $\mathcal{S}$ and its slope, L, in Fig. 4.11.1 and the correlation between $\mathcal{S}_0$ and L_0 in Fig. 4.11.2. It can be seen that the linear relationship between $\mathcal{S}_0$ and L_0, observed in QuMoCa calculations [263] and CEFT models [87] is also predicted in this work, although at higher values of L_0 and a somewhat different incline. When the approximate expression is used to evaluate the symmetry energy the linear relationship between $\mathcal{S}_0$ and L_0 is shifted to values which are at most only a few MeV lower.

As explained in Sec. 2.4, the incompressibility of a finite nucleus can be studied by examining the breathing modes of heavy nuclei (i.e. the isoscalar giant monopole resonances) [115, 127]. The energy of these modes are related to incompressibility of a finite nucleus, which can be expanded in powers of the mass number, A, see Eq. (2.3.10). The isospin dependent coefficient in this expansion offers another way to study the symmetry energy. It can be broken up into a surface and volume component [116–118], of which the latter can be calculated in nuclear matter. It can be shown to be related to the slope and curvature of the symmetry energy and is given by Eq. (2.3.21).

In Ref. [115], Stone *et al.* analysed all currently available GMR data in nuclei with 56 $<$ A $<$ 208 and found a limit -700 $\leq K_{\tau,v} \leq$ -372 MeV. The QMC result is $K_{\tau,v}$ = -431 MeV, which lies well within the experimental limits.

4.12 Sensitivity to Parameter Variation

Our calculations for the Hartree–Fock QMC model follow similar lines to Refs. [160, 161, 183] in that in each case an approximation is made for the Fock terms. More specifically, in our calculation of the Fock terms we omit energy transfer in the meson propagator (meson retardation effects). We also omit the modification of momenta because of the vector component of the self energy, which has been shown to be small in Refs. [183] and [245]. We include the tensor interaction in the Fock terms, with a common form factor, which has a dipole form. The lowest mass, Λ, for that cut-off, which should be larger than the masses of the mesons included, is 0.9 GeV. This is taken as our standard or baseline scenario value for 2 reasons:

(i) The incompressibility K_0 rises as Λ is increased. In the range Λ = 0.9 – 2.0 GeV, for the scenarios considered K_0 remains within the range 250 $\leq K_0 \leq$ 315MeV, which was the constraint derived in [115].

(ii) Increasing the form factor cut-off Λ, effectively increases the strength of the Fock terms, for which the ω and ρ mesons contribute a significant attraction once contact subtraction has been performed. To obtain the saturation properties of SNM, one must compensate for this additional attraction, resulting in a larger vector coupling. If the vector couplings of the hyperons are simply related to the vector couplings of the nucleons by Eq. (4.9.1), the results for the hyperon optical potentials at saturation density in SNM are not consistent with the values extracted from hypernuclear experiments largely because of the change in the ratio of the scalar to vector couplings.

We demonstrate the effect of changing the value of Λ between 0.9 – 1.3 GeV in the subsequent scenarios (lines 2 - 5) in Table 4.13.1 which differ from the standard one only by the value of Λ. We observe a minor increase in K_0 and L_0 which both remain within the empirically expected range.

However, once the full Fock terms are included, the results for the standard scenario, even with variable Λ, are not consistent with values of the phenomenological hyperon optical potentials extracted from experiments. This is because of a change in the ratio of the scalar to vector coupling, leaving the Λ hyperon effectively unbound. The additional attraction generated by the Fock terms, especially the ρ tensor contribution, has altered the coupling constants such that the ω coupling is larger. In the extreme scenario "$\Lambda = 2.0$, $g_{\sigma Y} \times 1.9$" discussed in Sec. 5.1, we meet the constraints of phenomenological hyperon optical potentials.

In the scenarios "Eff. Proton Mass", "Eff. Proton Mass, $\Lambda = 1.1$" and "Eff. Proton Mass + $\delta\sigma$" (lines 11–13 of Table 4.13.1) the ratio of tensor to vector coupling is rescaled using the effective proton mass in Eq. (4.8.6) as opposed to the free proton mass. This is a simplified way to introduce a scalar dependence into the Pauli term coupling. This

substitution effectively increases the strength of the Pauli term due to the reduction of the proton mass. It causes a significant increase in K_0 as Λ takes on larger values. Indeed, as we see in Table 4.13.1, K_0 rises above 311 MeV for Λ greater than 1.1 GeV. Similar observations apply for the slope of the symmetry energy at saturation density, L_0.

The contribution to the mean scalar field arising from the Fock terms is incorporated in the cases denoted "Fock $\delta\bar{\sigma}$" and "Eff. Proton Mass + $\delta\sigma$". It has practically no effect on the properties of nuclear matter for our standard scenario, but when applied to the "Eff. Proton Mass" scenario there is a noticeable effect. For example, it decreases the incompressibility by 12 MeV and increases the slope of the symmetry energy by 8 MeV. This is obviously because of the extra scalar dependence naively introduced in the tensor coupling.

The tensor couplings used in this work, arising from the underlying MIT bag model, are consistent with Vector Meson Dominance (VDM) and hence our tensor couplings are calculated from the experimental magnetic moments. Purely as a test of the effect of a variation in those couplings we arbitrarily took the ratios of tensor to vector couplings of all baryons from the Nijmegen potentials (Table VII of Ref. [258]), where there is a larger value of $f_{\rho N}/g_{\rho N} = 5.7$. These were also used by Miyatsu *et al.* [245, 255]. This variation, denoted "Increased $f_{\rho N}/g_{\rho N}$", produces very similar values for the nuclear matter properties.

In scenarios "Dirac only" and "Hartree only" we show results of the QMC calculation with the same parameters as the standard set but leaving out the Pauli part of the Fock term and the full Fock term, respectively. These results are particularly useful for understanding of the role of individual terms in the QMC Lagrangian.

The last four scenarios in Table 4.13.1 document the effect of changes in the value of the free nucleon radius and the evaluation of the symmetry energy from the difference formula Eq. (4.11.1) "App." and from the second derivative the the energy per particle "$S_0 = 30.0$". All of which have very little effect on the properties of nuclear matter.

4.13 Summary

We started this chapter by introducing the QMC hadronic Lagrangian. We then proceeded to the derive the equations of motion, Hamilitonian density and finally the EoS of nuclear matter in the Hartree-Fock approximation. These were derived by applying the method used Refs. [160–162]. The properties of symmetric nuclear matter (SNM) and pure neutron matter (PNM) were investigated and the phenomenological hyperon optical potentials were calculated. Comparisons of our numerical results with empirical data, CEFT and other models were also presented.

The results for a comprehensive set of nuclear matter properties, including K_0, L_0, K_{sym}, Q_0 and $K_{\tau,v}$ have been studied in detail. The model prediction for the incompressibility lies within the range extracted from experimental data for most model variations considered. While the incompressibility is increased by this addition in some cases and tends to lie at the mid to top end of the acceptable range, it serves as a useful constraint on the additional mass parameter, Λ, associated with the form factor that

appears at the meson-baryon vertices (the latter only being needed when the Fock terms are computed). The modest variation of the nuclear matter observables with this parameter (which must lie above the masses of the exchanged mesons included in the theory) is illustrated in Table 4.13.1. Increasing Λ beyond 0.9 GeV raises the incompressibility and in the case denoted "Eff. Proton Mass, $\Lambda = 1.1$ GeV" it is close to the limit $K_0 < 315$ MeV.

The symmetry energy and its slope are noticeably influenced by the Fock terms, specifically curvature is introduced into these quantities through the tensor interaction, as can be seen in Fig. 4.11.1. At saturation density we find in all cases that the isospin incompressibility is within accepted constraint limits and while the slope of the symmetry energy is on the larger side, it does lie within the broad limits reported by Tsang *et al.* [87].

It is interesting to note that there is a satisfying level of consistency between theoretical predictions of N^3LO chiral effective field theory and the QMC model results studied here for densities of PNM up to and around nuclear matter density. Above saturation density a slightly higher energy per particle as a function of density is found here. It is also found that the natural incorporation of many body forces in the QMC model tends to produce a somewhat stiffer PNM EoS above saturation density than other models including 3-body forces.

In Ch. 5, we apply the Hartree-Fock QMC model developed in this chapter to matter in generalised beta equilibrium and investigate the static properties of cold neutron stars.

Model/ Scenario	$g_{\sigma N}$	$g_{\omega N}$	g_{ρ}	K_0 [MeV]	L_0 [MeV]	K_{sym} [MeV]	Q_0 [MeV]	$K_{\tau,v}$ [MeV]	U_Λ [MeV]	U_{Σ^-} [MeV]	U_{Ξ^-} [MeV]
Standard	8.97	9.38	4.96	273	84	-23	-305	-431	3	26	5
$\Lambda = 1.0$	9.07	9.73	5.05	278	85	-15	-282	-439	10	32	8
$\Lambda = 1.1$	9.16	10.06	5.16	283	86	-8	-261	-446	16	39	11
$\Lambda = 1.2$	9.24	10.37	5.28	286	87	-2	-241	-451	23	46	15
$\Lambda = 1.3$	9.31	10.67	5.40	289	88	4	-224	-456	29	53	18
$\Lambda = 1.1$, $g_{\sigma Y} \times 1.3$	9.16	10.06	5.16	283	86	-8	-261	-446	-15	14	-4
$\Lambda = 1.3$, $g_{\sigma Y} \times 1.3$	9.31	10.67	5.40	289	88	4	-224	-456	-3	28	3
$\Lambda = 2.0$, $g_{\sigma Y} \times 1.9$	9.69	12.27	6.16	302	92	31	-137	-478	-29	20	-7
Increased $f_{\rho N}/g_{\rho N}$	8.70	9.27	3.86	267	81	-34	-321	-424	6	27	6
Fock $\delta\sigma$	9.01	9.44	4.97	273	84	-21	-296	-432	4	26	5
Eff. Proton Mass	10.40	11.0	4.55	297	101	64	-190	-476	11	41	10
Eff. Proton Mass, $\Lambda = 1.1$	11.08	12.31	4.85	311	111	126	-87	-509	34	67	22
Eff. Proton mass + $\delta\sigma$	10.89	11.55	4.53	285	109	132	-232	-432	17	49	13
Dirac Only	10.10	9.22	7.84	294	85	0	-299	-424	-23	4	-8
Hartree Only	10.25	7.95	8.40	283	88	-17	-455	-405	-49	-23	-21
$R = 0.8$	9.30	9.85	4.98	277	85	-15	-269	-443	6	25	5
App. $S_0 = 32.5$	9.05	9.38	4.86	275	82	-27	-303	-429	2	24	4
App. $S_0 = 30.0$	9.31	9.35	4.50	280	74	-24	-298	-391	-4	19	1
$S_0 = 30.0$	9.24	9.36	4.61	278	76	-20	-299	-394	-2	21	2

Table 4.13.1: Couplings, nuclear matter properties and selected hyperon optical potentials determined for our standard case (for which $\Lambda = 0.9$ GeV, and $R_N^{\rm free} = 1.0$ fm) and the effect of subsequent variations in which differences from the standard parameter set are indicated in column 1. The tabulated quantities at saturation are the slope and curvature of the symmetry energy, L_0 and K_{sym}, the incompressibility K_0, skewness coefficient Q_0 and the volume component of isospin incompressibility $K_{\tau,v}$, respectively.

5

Hartree–Fock QMC Applied to Neutron Stars

In this chapter we study cold, asymmetric nuclear matter (ANM) which is expected to exist in the outer core of cold neutron stars. We supplement the QMC model developed in Ch. 4 with non-interacting leptons to study matter in both beta-equilibrium and generalised beta-equilibrium (allowing for hyperons as well as nucleons). Some portions of the material presented in this chapter are adapted from Whittenbury *et al* [244].

5.1 Generalised Beta Equilibrium Matter and Neutron Stars

As the density of hadronic matter increases beyond saturation density nuclei dissolve to form an interacting system of nucleons and leptons. If this system survives longer than the time scale of weak interactions, $\tau \approx 10^{-10}$ s, it reaches equilibrium with respect to beta decay $n \rightarrow p + e^- + \tilde{\nu}$ and its inverse . As these particles are fermions they obey the Fermi-Dirac distribution law and the Pauli exclusion principle. In the zero temperature limit, this distribution becomes a step function. The Fermi sea of each particle species has each level occupied by $2S + 1 = 2$ particles, one spin up and the other spin down. The single particle states with energy less than the corresponding chemical potential will be filled and those above will be left unoccupied. The level which separates the occupied and unoccupied regions is called the Fermi level and has energy equal to the chemical potential, the energy needed to add one more particle of this type to the system. Fourier transforming to momentum space these occupied states lie inside a sphere of radius $p_{\rm F}$, where $p_{\rm F}$ is the Fermi momentum. Increasing the density of a particle increases its chemical potential. When the total baryonic density reaches about $2 - 3$ ρ_0 and because baryons obey the Pauli exclusion principle, it becomes

energetically more favourable to create a slow and more massive hyperon, rather than another energetic nucleon. A generalised beta equilibrium (GBEM) develops with respect to all reactions involving either weak or strong interactions, that leads to the lowest energy state. Only two quantities are conserved in GBEM—the total charge (zero in stars) and total baryon number. Strangeness is conserved only on the time scale of strong interaction, $\tau \approx 10^{-24}$s, and lepton number is conserved only on the time-scale of tens of seconds, because of the diffusion of neutrinos out of the star [111].

In neutron stars the leptons, e^- and μ^- must be included in addition to the hadrons. Non-interacting leptons are described by the following Lagrangian density

$$\mathcal{L}_{\rm Lept} = \sum_{\ell} \mathcal{L}_{\ell} \quad , \tag{5.1.1}$$

where $\mathcal{L}_{\ell} = \bar{\Psi}_{\ell}(i\gamma_{\mu}\partial^{\mu} - m_{\ell})\Psi_{\ell}$ and $\ell \in \left\{e^-, \mu^-\right\}$. Tau leptons are not considered as they are too massive to be found in neutron stars. As we are considering old neutron stars, neutrinos are assumed to have radiated out of the star, so they can also be neglected. For the lepton masses we use their experimental values [256]. The corresponding lepton energy density and number density are given by the usual formulas for a degenerate Fermi gas [111]

$$\epsilon_l = \frac{2}{(2\pi)^3} \int\limits_{|\vec{k}| \le k_F^{\ell}} d^3k \, \sqrt{\vec{k}^{\,2} + m_{\ell}^2}, \quad \rho_{\ell} = \frac{(k_F^{\ell})^3}{3\pi^2} \quad . \tag{5.1.2}$$

The total energy density of the GBEM is then given by the sum of the hadron and lepton energy densities, $\epsilon_{\rm total} = \epsilon_{\rm hadronic} + \epsilon_{\ell}$. Similarly the total pressure is the sum of the hadron and lepton pressures and can be calculated as

$$P_{\rm total} = \rho^2 \frac{\partial}{\partial \rho}\left(\frac{\epsilon_{\rm total}}{\rho}\right) = \sum_{i,\ell} \mu_i \rho_i - \epsilon_{\rm total} \quad . \tag{5.1.3}$$

To describe GBEM, we need determine the lowest energy state under the two constraints of baryon number conservation,

$$\sum_i \rho_i^{\rm v} = \rho \tag{5.1.4}$$

and charge neutrality,

$$\sum_i Q_i \rho_i^{\rm v} - \sum_{\ell} \rho_{\ell} = 0 \quad , \tag{5.1.5}$$

we use the standard method of Lagrange multipliers. The equilibrium configuration of the system is then determined variationally by,

$$\delta\left[\epsilon_{\rm aux}\right] \equiv \delta\left[\epsilon_{\rm total}\left[\{\rho_i^{\rm v}\}, \{\rho_{\ell}\}\right] + \lambda\left(\sum_i \rho_i^{\rm v} - \rho\right) + \nu\left(\sum_i Q_i \rho_i^{\rm v} - \sum_{\ell} \rho_{\ell}\right)\right] = 0 \quad , \tag{5.1.6}$$

where $\epsilon_{\rm aux}$ is an auxiliary energy density function introduced to implement the two constraints. From the equilibrium condition, Eq. (5.1.6), we obtain the following system of equations:

$$\frac{\partial \epsilon_{\rm aux}}{\partial \rho_i^{\rm v}} = \frac{\partial \epsilon_{\rm total}}{\partial \rho_i^{\rm v}} + \lambda + \nu Q_i = 0 \quad , \tag{5.1.7}$$

$$\frac{\partial \epsilon_{\rm aux}}{\partial \rho_\ell} = \frac{\partial \epsilon_{\rm total}}{\partial \rho_\ell} - \nu = 0 \quad . \tag{5.1.8}$$

In this system of equations, it is possible to eliminate the Lagrange multipliers and re-express each equation in terms of the chemical potentials of the participating particles. It can be shown that there are as many independent chemical potentials as the number of conserved quantities. The two independent chemical potentials are typically taken to be the neutron and electron chemical potentials. Chemical potentials of all the other species in GBEM are then expressed via a relation

$$\mu_i = B_i \mu_n - Q_i \mu_e \, , \tag{5.1.9}$$

where the baryon number, B_i, is 0 or 1 and the charge number, Q_i, is 0 or ± 1. The system of equations therefore reduces to essentially three equations, depending on the charge of the particle. For negatively charged, neutral and positively charged baryons present in the system, we have

$$\mu_- = \mu_{\rm n} + \mu_{\rm e} \quad , \tag{5.1.10}$$

$$\mu_0 = \mu_{\rm n} \quad , \tag{5.1.11}$$

$$\mu_+ = \mu_{\rm n} - \mu_{\rm e} \quad , \tag{5.1.12}$$

respectively.

In equilibrium, some of the particle densities may be zero and therefore the equation generated by their independent variation is no-longer included in the system of equations to be solved. In particular, if the neutron star becomes deleptonised at some density, i.e leptons disappear, we run into a problem in using Eqs. (5.1.10–5.1.12) as it does not make sense to use the the electron chemical potential when they are not present. To handle this possibility and consistently implement the two constraints we need to solve the full system of equations including the Lagrange multipliers. We solve the following system of equations

$$0 = \mu_i + B_i \lambda + \nu Q_i \ , \tag{5.1.13}$$

$$0 = \mu_\ell - \nu \ , \tag{5.1.14}$$

$$0 = \sum_i B_i \rho_i^{\rm v} - \rho \ , \tag{5.1.15}$$

$$0 = \sum_i B_i \rho_i^{\rm v} Q_i + \sum_\ell \rho_\ell Q_\ell \ , \tag{5.1.16}$$

to obtain the number densities for each particle ($i \in \{n, p, \Lambda, \Sigma^-, \Sigma^0, \Sigma^+, \Xi^-, \Xi^0\}$ and $\ell \in \{e^-, \mu^-\}$), $\rho_i^{\rm v}$, as well as the Lagrange multipliers (λ, ν). At Hartree–Fock level,

the following formulas to numerically evaluate the chemical potentials, must be used to ensure we encapsulate the Fock contribution to the energy densities correctly

$$\mu_i = \frac{\partial \epsilon_{\rm total}}{\partial \rho_i^{\rm v}} \ , \quad \mu_\ell = \frac{\partial \epsilon_\ell}{\partial \rho_\ell} = \sqrt{k^2 + m_\ell^2} \, . \tag{5.1.17}$$

The number of equations that must actually be solved from Eqs. (5.1.13–5.1.14) at any particular density varies, depending on how many of these particles are energetically possible. To determine which equations must be included and those that can be dropped from the system, we need a test for each particular particle to find out if it is energetically favourable. To do this we need to first evaluate the chemical potential for each particle. We do this numerically using a simple finite difference formula for the derivative. When the particle is not already present in the system, we use a small number density, a threshold number density, to evaluate the chemical potential. This is done to allow us to determine when the corresponding equation for the particle is added to the system of equations. The equations that are included are those which have a sign change in their corresponding equation (Eqs. (5.1.13–5.1.16)). This also allows us to easily visualise why, or why not, a particle may appear, since this corresponds to the energy needed to create the minimum threshold number density of that particle species at that density. As the total baryonic density is incremented, this is checked for each particle that is not already present in the system. If the species fraction of a particle already present in the system drops below a small cut-off value then the equation is removed from the system.

The EoS of GBEM is not valid in the outer regions (crust) of the star, where nuclei and nuclear processes become dominant. Following the customary procedure, we introduce a smooth transition between our EoS in GBEM and the standard low density EoS of Baym, Pethick and Sutherland (BPS) [271] at low density ($\rho \sim 10^{-2}$ fm^{-3}).

In order to calculate neutron star properties, such as the total gravitational mass, $M(R)$, and the baryon number, $A(R)$, within the stellar radius R, we solve the TOV equations [219, 220, 272] for hydrostatic equilibrium of spherically symmetric (non-rotating) matter (see Ch. 3). Using the EoS calculated here, these differential equations (Eqs. 3.1.6–3.1.8) are integrated using a Runge-Kutta-Cash-Karp algorithm.

5.2 Numerical Results and Discussions

In Fig. 5.1.1 we show the EoS of GBEM with various parameter variations. The kinks in pressure appear at hyperon thresholds. A comparison between calculations for either Hartree alone, Hartree – Fock with only the Dirac piece of the coupling to vector mesons, or the full model highlights the importance of the Fock terms at high density. As compared to the EoS of matter in which the hyperons are not included above their natural thresholds and nucleons are assumed to be the only baryons up to densities $\sim$ 5–6 ρ_0, the pressure in GBEM increases with density more slowly. It is challenging to produce reasonable scenarios where the empirical constraints are met and the pressure still increases fast enough to support high mass, cold neutron stars, as will be discussed below.

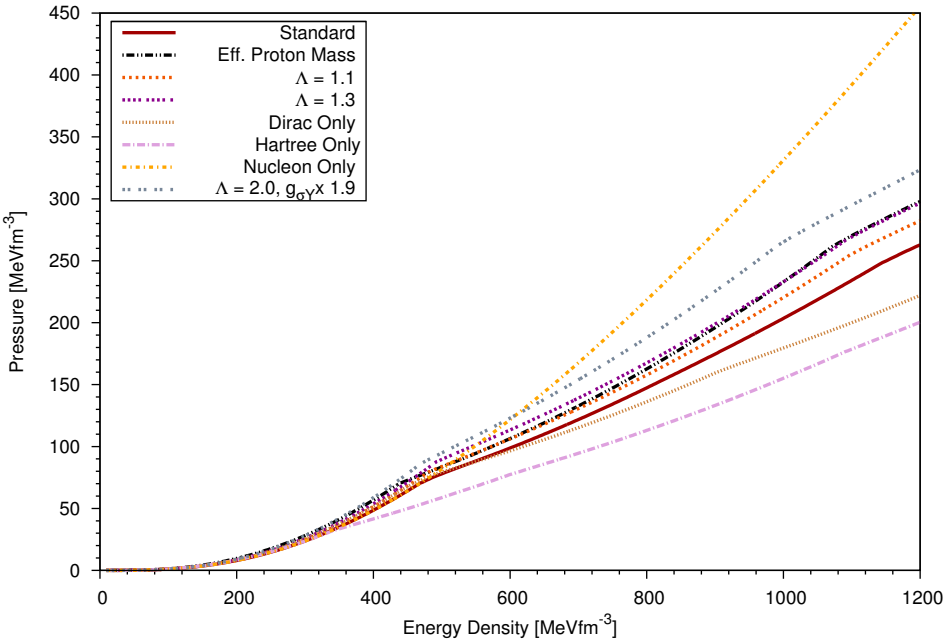

Figure 5.1.1: GBEM equation of state. Kinks occur at significant hyperon threshold densities. The divergences between the "Hartree Only" QMC parametrisation and the Hartree–Fock scenarios highlights the importance of Fock terms at high density. The "Nucleon only" BEM EoS is added for a comparison.

In Fig. 5.1.3 the particle content of GBEM matter and corresponding Fock energy contributions is displayed for three scenarios, "Standard", "Eff. Proton Mass" and "$\Lambda = 2.0$, $g_{\sigma Y} \times 1.9$". We observe that, in all scenarios, at low density we have predominantly neutrons, which are then isotopically enriched by the creation of protons. To maintain charge conservation, electrons appear at the same density. As density increases, the electron chemical potential rises and at ~ 0.14 fm^{-3} it reaches the muon's mass, making it energetically favourable to create muons. At higher densities, non-conservation of strangeness leads to the creation of hyperons from nucleons. In the "Standard" scenario, the first hyperon to appear is Σ^-, at 0.46fm^{-3}, followed by Ξ^- at 0.47fm^{-3}. The Σ^- is quickly replaced by the Ξ^-, which is then followed by the appearance of Λ at 0.74fm^{-3} and then Ξ^0 at 0.97fm^{-3}. Since the latter is above the maximum density reached in any of our realistic model variations it is largely irrelevant. We show in Fig. 5.1.2 that the Λ chemical potential approaches and meets the neutron chemical potential, meaning that it is energetically favourable for it to appear. On the other hand, for the Σ^- we see that at low density it is more favourable than the Ξ^-, while beyond ~ 0.4 fm^{-3} this is no longer so.

The static neutron star properties obtained from solving the TOV equations, Eqs. (3.1.6–3.1.8), is presented in Table 5.3.1 for each variation of the QMC model investigated in Ch. 4. Table 5.3.1 also includes the value of incompressibility, slope of the symmetry energy and the hyperon optical potentials evaluated at ρ_0 in SNM for easy comparison. The relationship between stellar mass and radius is shown in Fig. 5.2.1.

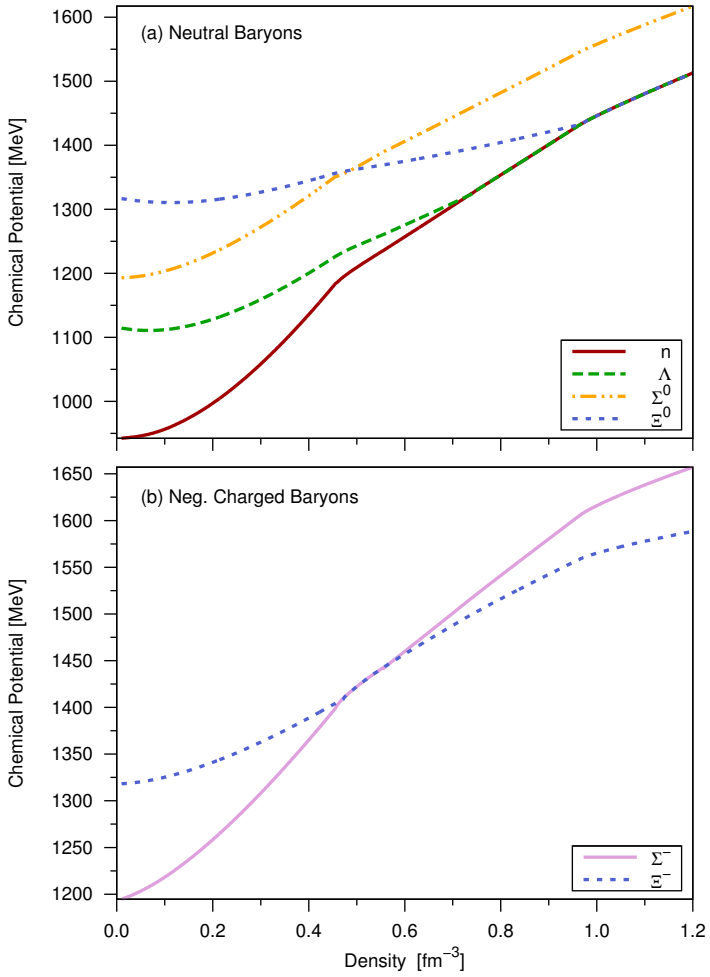

Figure 5.1.2: (a) Neutral baryon chemical potentials as a function of baryon number density for the standard scenario. (b) Negative charge baryon chemical potentials as a function of baryon number density for the standard scenario.

Varying the value of the cut-off Λ between 0.9 –1.3 GeV, effectively increasing the strength of the Fock terms, we observe an increase in the maximum mass of the neutron star by $\sim 8\%$. Recall from Ch. 4, Sec. 4.12, this increase in the cut-off also corresponds to small increases in both K_0 and L_0, but they still remain within empirical limits.

However, once the full Fock terms are included, the results of the standard scenario, even with the variable Λ, are not consistent with the values of the phenomenological hyperon optical potentials extracted from experiments. As the saturation of nuclear matter is a delicate balance between attraction and repulsion generated by the mesons, the ω coupling has increased in response to the additional attraction produced by the Fock terms, especially the ρ-tensor contribution. This change in the ratio of the scalar to vector coupling, leaves the Λ hyperon effectively unbound. This effect of an increase in the vector coupling is illustrated by the larger maximum neutron star masses, which also correspond to poor results for the hyperon optical potentials.

In the work of Miyatsu *et al.* the scalar couplings from the QMC model were not used. Instead they rescaled the scalar coupling of each hyperon to obtain an

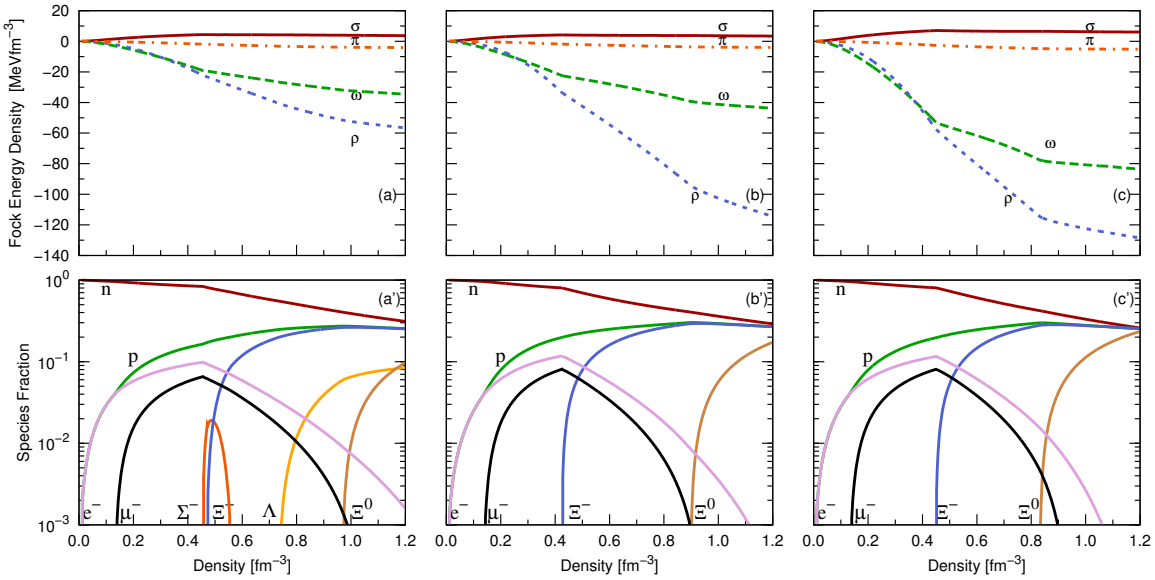

Figure 5.1.3: (Top) Fock energy density contributions and (bottom) species fraction as a function of baryon number density in GBEM, for the "Standard" (a,a'), "Eff. Proton Mass" (b,b') and the "$\Lambda = 2.0$, $g_{\sigma Y} \times 1.9$ (c,c') scenarios. The corresponding EoSs are shown in Fig. 5.1.1

acceptable optical potential. We consider the possibility of rescaling the scalar coupling reasonable, as the bag model used is a very simple model of the baryons in which only the light quarks participate in the interaction. An amplification of only the hyperon scalar couplings of 30% is considered in "$\Lambda = (1.1, 1.3)$, $g_{\sigma Y} \times 1.3$". This improves the predictions of the optical potentials, binds the Λ hyperon and maintains a repulsive potential for the Σ^- hyperon. In doing this the optical potentials are closer to the values extracted from experimental studies of hypernuclei, but the EoS of β-equilibriated matter is softer, Λ and Σ^- both appear. The increased attraction for the hyperons only has a minor effect on the maximum mass of the neutron star. In this scenario we increase the form factor cut-off and hence the strength of the Fock terms forcing the vector coupling to become larger and then rescale the hyperon scalar coupling. In this very phenomenological scenario, we meet both the constraints of phenomenological hyperon optical potentials and high mass neutron star observations.

In the scenario "Eff. Proton Mass" the ratio of tensor to vector coupling is rescaled using the effective proton mass in Eq. (4.8.6) as opposed to the free proton mass. This is a naive way to introduce a scalar dependence into the Pauli term coupling. This substitution effectively increases the strength of the Pauli term due to the reduction of the proton mass. The increased attraction produced leads to an increase in the ω coupling. The change in strength of the tensor coupling has a significant impact on the composition. Because of the increased ω coupling, the maximum mass of the neutron star is significantly increased, but the hyperon optical potentials remain at variance with expected values. This particle content is different from our standard scenario and most other models, which generally find that either the Λ or Σ^- appears first.

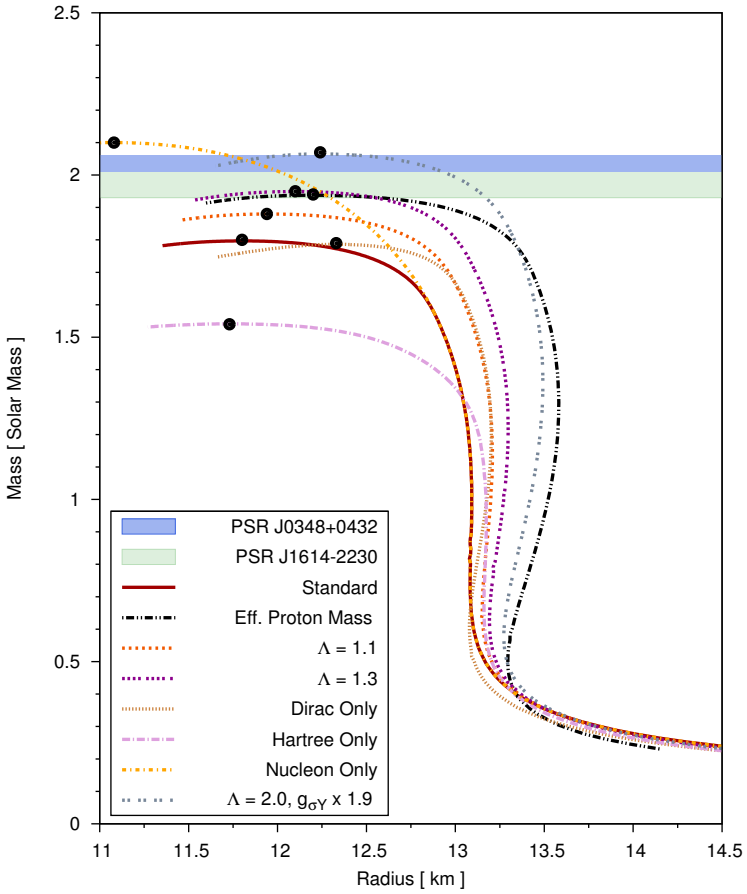

Figure 5.2.1: Gravitational Mass versus radius relationship for various scenarios described in the text. The black dots represent maximum mass stars and the coloured bars represent observed pulsar constraints.

The increased strength of the tensor contribution, and hence attraction, has increased the vector coupling and as a consequence the Λ is not bound at saturation density in symmetric nuclear matter. This combined with the attraction from the Fock terms for the Ξ's makes them more energetically favourable than Λ or the Σ^-.

Considering the extreme scenario "$\Lambda = 2.0$, $g_{\sigma Y} \times 1.9$", even though the Λ feels a significant attraction at saturation density, it appears that it cannot compete with the attraction generated by the Fock terms at high density, specifically the tensor part for the Ξ. The contributions of the Fock energies is more significant and the composition is similar to "Eff. Proton Mass".

The contribution to the mean scalar field arising from the Fock terms is incorporated in the cases denoted "Fock $\delta\bar{\sigma}$" and "Eff. Proton Mass + $\delta\sigma$". When applied to neutron star properties it negligibly increases the maximum mass in our baseline scenario and increases it by a few percent when a scalar dependence is introduced into the Pauli term, to just below $2M_\odot$.

Purely as a test of the effect of a variation in the tensor couplings we consider the scenario "Increased $f_{\rho N}/g_{\rho N}$", where we arbitrarily take the ratios of tensor to vector couplings of all baryons from the Nijmegen potentials (Table VII of Ref. [258]). In

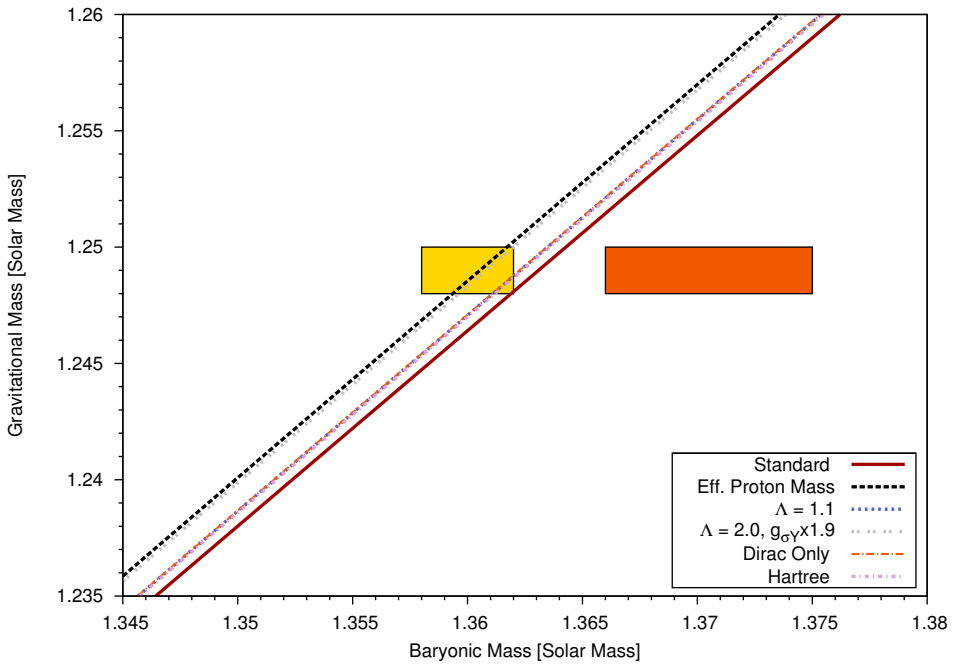

Figure 5.2.2: Gravitational mass versus baryonic mass. The boxes are constraints from simulations (Yellow) by Kitaura *et al.* [273] and (Orange) by Podsiadlowski *et al.* [274], which are explained in the text.

this scenario a larger value of $f_{\rho N}/g_{\rho N} = 5.7$ is used. These couplings were also used by Miyatsu *et al.* [245, 255]. This variation, denoted "Increased $f_{\rho N}/g_{\rho N}$", produced an EoS for GBEM which was practically indistinguishable from our standard result

In scenarios "Dirac only, Hartree only and Nucleon only' we show results of the QMC calculation with the same parameters as the standard set but leaving out the Pauli part of the Fock term, the full Fock term and the hyperons, respectively. These results are particularly useful for understanding of the role of individual terms in the QMC Lagrangian.

At the Hartree level the "hyperfine" interaction from one gluon exchange makes the Λ more energetically favourable than the Σ^-, providing a source of attraction for the former and repulsion for the latter. This has been shown at the Hartree level in the QMC model to suppress the appearance of Σ^- hyperons in GBEM matter [275]. This can also be considered a qualitative explanation for the absence of medium to heavy Σ hypernuclei [188].

The last four scenarios in Table 5.3.1 document the effect of changes in the value of the free nucleon radius and the evaluation of the symmetry energy from the difference formula Eq. (4.11.1) "App.' and from the second derivative the the energy per particle "$S_0 = 30.0$'. Neither effect changes significantly the properties of GBEM matter and neutron stars.

We find that the predicted maximum masses for several of the scenarios, lie very close to the constraints set by Demorest *et al.* [202] of a (1.97 ± 0.04) $M_\odot$ pulsar, as well as the new constraint set by PSR J0348+0432 with a mass of 2.03 ± 0.03 $M_\odot$ [203]. In

each of the scenarios presented here, the radii of the maximum stellar mass solutions are somewhat large, but because of the current difficulties in reliably measuring radii we do not consider this a problem. They are somewhat larger than those extracted from recent observations of Type I X-ray bursters (see e.g. Refs. [197, 276]). Extraction of radii from observation is rather complicated and there are still many questions to be addressed. For example, Steiner *et al.* [197] analyzed observations of six low mass X-ray binaries (emitting X-rays regularly) and their statistical analysis yielded R in the range 10–12 km for masses around $1.6M_{\odot}$. However, the uncertainty in the relation between the extracted photospheric radius and the actual radius of the star remains large. The results of Guillot *et al.*, namely $R = 9.1^{+1.3}_{-1.5}$ km (90%-confidence), are based on observations of five quiescent low mass X-ray binaries (which emit X-rays only occasionally) under the assumption that the radius is constant for a wide range of masses.

Whilst the observations Refs. [202, 203] provide constraints on high mass neutron stars, the observation of the double pulsar J0737-3039 and its interpretation [274] offers a constraint on the neutron star EoS in a region of central densities $\sim 2-3\ \rho_0$. The constraint concerns the ratio between the gravitational and baryonic mass of the star. The gravitational mass of pulsar B is measured very precisely to be $M_{\rm g} = 1.249 \pm 0.001 M_{\odot}$ and the baryonic mass depends on the mode of its creation, which can be modelled. If pulsar B was formed from a white dwarf with an O-Ne-Mg core in an electron capture supernova, with negligible loss of baryonic mass during the collapse, the newly born pulsar should have the same baryonic mass as the progenitor star. Podsiadlowski *et al.* [274] estimated the baryonic mass of the pulsar B to be between 1.366 and 1.375 $M_{\odot}$. Another simulation of the same process, by Kitaura *et al.* [273], gave a value for the baryonic mass of $1.360 \pm 0.002\ M_{\odot}$. We show in Fig. 5.2.2 the QMC result, which supports the model of Kitaura *et al.*, accepting some small loss of baryonic mass during the birth of pulsar B.

5.2.1 Comparison with Other Models

The Hartree – Fock calculation in Ref. [277] differs considerably from that presented here, as well as from that in Refs. [245, 255, 278, 279]. The first and major difference is that the tensor interaction of the baryons was ignored there, whereas in Refs. [245, 255, 278, 279] and in our work it is found to have a very significant effect. A second difference between Ref. [277], our work, and Refs. [245, 255, 278, 279] is that in their preferred QMC scenario (QMC-HF3) they artificially adjust a parameter, C, which is related to the scalar polarisability, to obtain a lower value for the incompressibility. This represents a dramatic change in the model.

The masses of the baryons in the QMC model are determined by the bag equations and the scalar coupling is calculated directly from the density dependence of the baryon mass in-medium. Thus, changing C, or equivalently the scalar polarisability, changes the mass and the density dependent coupling in a manner which is inconsistent with the traditional form of the QMC model [187]. In this manner the many body interaction is also being changed through the density dependent scalar coupling. Their QMC-HF3 variation gives an incompressibility of $K = 285$ MeV and a very low prediction for the

maximum mass of neutron stars, $M = 1.66\ M_\odot$. In our Dirac-only variation we find a slightly larger value for the incompressibility, $K = 294$ MeV with a maximum stellar mass of $M = 1.79\ M_\odot$. Other variations were considered in Ref. [277] where they do not modify C: one where they calculate fully relativistic Fock terms, and another where they make a non-relativistic approximation to the Fock terms. These variations both produce maximum masses of neutron stars of $M = 1.97\ M_\odot$.

References [245, 255, 278, 279] carry out a relativistic calculation in which they treat the Fock and Hartree terms on the same level. More precisely they calculate self-energy contributions arising from both terms and these self energies modify the baryon mass, momentum and energy. They include the tensor interaction, subtract contact terms, and consider two variations of the bag model. In their first paper [245] they used much larger values for the tensor couplings without form factors. In the later paper [278] they include the effect of form factors, ignoring effects of meson retardation (as we do) but with a lower cut-off mass, i.e. $\Lambda = 0.84$ GeV. The latter had the effect of keeping the incompressibility from being too large. Their conclusions are very similar to our own, in that they find that the tensor terms provide a source of attraction and that overall the Fock terms enhance the maximum neutron star mass.

The maximum stellar masses in their first paper [245] are larger than those in their second paper [278], almost certainly because the inclusion of the form factor decreases the effect of the Fock term at high density. They consider two variations of the QMC model: one with, and one without the pion contribution in the bag (CQMC) which tends to give a slightly stiffer EoS, because of its effect on the baryon masses. For QMC they obtain $M = 1.86\ M_\odot$, $R = 11.2$ km, and for CQMC $M = 1.93\ M_\odot$, $R = 11.5$ km for the maximum stellar mass solutions. Despite the differences in how we handle the Fock terms and their use of larger tensor couplings and more phenomenological hyperon couplings, we are led to the same conclusion about the importance of the tensor contribution. We also find a very similar particle content in scenarios where the Fock terms are quite strong, such as the "Eff. Proton Mass" and "$\Lambda = 2.0$, $g_{\sigma Y} \times 1.9$" scenarios, where the Ξ^- is the first hyperon to appear.

5.3 Summary

In this chapter, we began by supplementing the QMC model developed in Ch. 4 with non-interacting Fermi gases of electrons and muons. It was then explained how the lowest energy state of matter relevant to neutron stars is determined using the method of Lagrange multipliers. A system of equations relating the chemical potentials and number densities of relevant particles was derived. These equations were solved numerically for the EoS of GBEM, which was then used as input to integrate the TOV equations.

Even at densities above three times nuclear matter density, the nucleon Fock terms are found to contribute significantly to the EoS and the corresponding attraction is what is responsible for the increased pressure and larger maximum stellar masses in several scenarios. This can be seen in Fig. 5.2.1, where there is a clear transition from a Hartree QMC calculation to a Hartree–Fock calculation with no tensor interaction (Dirac-only; no Pauli term), to our "Eff. Proton Mass" calculation (Dirac and

Pauli (with scalar dependence) terms). In these three variations, as well as those with increasing form factor mass, Λ, the maximum stellar mass increases because of the increased vector coupling and pressure coming from the Fock terms. This increased pressure arises mainly from the ρ meson contribution. As we can readily see in Table 5.3.1 and Fig. 5.2.1, the value of Λ cannot be varied far in the "Eff. Proton Mass" calculations. Indeed, in that case, the incompressibility is already as high as it can be. The maximum neutron star mass, for our "Standard" scenario is approximately the same as the "Dirac Only" scenario because of the change in composition, where in the latter the appearance of Σ^- is avoided and only the Λ and Ξ^- appear followed by the Ξ^0. Even with the brief appearance of an additional hyperon in our baseline scenario, the value of $M_{\rm max}$ is still slightly larger because of the tensor interaction. We see that the maximum neutron star mass, for the case of nuclear matter in beta-equilibrium where hyperons must appear, lies in the range 1.80 to $2.07 M_\odot$.

The EoS and the maximum masses of the corresponding neutron stars are insensitive to the choice of the larger ρ tensor couplings used, for example, by Miyatsu *et al.* [245]. Similarly, modest variations in the radius of the free nucleon have only very minor effects on these quantities. Finally, we note that the correction ($\delta\bar{\sigma}$) to the scalar mean field arising from the Fock terms has a negligible effect on the incompressibility in our baseline scenario. On inclusion of a naive scalar dependence into the Pauli term the incompressibility decreases by 12 MeV, yet other observables remain largely unaltered by this addition.

This, plus the dependence of the incompressibility and maximum mass on Λ , leads us to conclude that the Hartree-Fock model used here with σ, ω, ρ and π mesons can only reproduce nuclear matter properties, phenomenological hypernuclear optical potentials and massive neutron star observations if there is significant rescaling of the hyperon coupling constants. Allowing for the rescaling of hyperon couplings we conclude that the maximum mass allowed in the model lies in the range $1.8 - 2.1 M_\odot$.

It is the treatment of the lightest mesons that is the most important, and the inclusion of heavier mesons would necessarily be more model dependent. For this reason, in this work we have restricted ourselves to just σ, ω, ρ and π mesons. The model could be extended to include mesons containing strange quarks, of which the next lightest mesons are $K(495)$ and $K^*(895)$. These mesons will induce mixing in the baryon octet, possibly changing the composition of matter in generalised beta-equilibrium. Heavier mesons such as the hidden strangeness vector meson $\phi(1020)$ have been considered in other works Ref. [241, 242], which have found that they can produce extra vector repulsion delaying the onset of hyperons. This extra repulsion is solely for baryons with non-zero strangeness and in this model, this exchange will allow the strange quark to participate in the interaction rather than being just a spectator. It should be noted that with every new meson that is included more parameters must be introduced into the model.

Purely for comparison purposes, we also include a nucleon-only scenario, in which hyperons are artificially excluded. In this case the EoS is increasingly stiffer at densities above 0.4 fm^{-3}, leading to a large maximum stellar mass of 2.10 $M_\odot$, consistent with many other nucleon-only models.

We stress that the QMC model does not predict a significant abundance of Σ hyperons at any density where the model can be considered realistic and they are completely absent in model variations compatible with large neutron star mass observations. This is in contrast to a number of other relativistic models which do predict the Σ threshold to occur, even prior to that of the Λ [280, 281]. We note that Schaffner-Bielich [280] considered a phenomenological modification of the Σ potential with additional repulsion, which significantly raised its threshold density. In the case of the QMC model the physical explanation of the absence of Σ-hyperons is very natural, with the mean scalar field enhancing the repulsive hyperfine force for the in-medium Σ (recall that the hyperfine splitting, which arises from one-gluon-exchange, determines the free Σ–Λ mass splitting in the MIT bag model).

It is worth remarking that upon inclusion of the tensor coupling, the proton fraction increases more rapidly as a function of total baryon density. This is likely to increase the probability of the direct URCA cooling process in proto-neutron stars. As a further consequence, the maximum electron chemical potential is increased in this case, which may well influence the production of π^- and $\bar{K}$ condensates. Changes to the Λ threshold (it occurs at higher density with lower maximum species fraction) reduce the possibility of H-dibaryon production as constrained by beta-equilibrium of the chemical potentials.

For the matter considered in this chapter we have taken the view that hadrons remain the relevant degrees of freedom. Transitions to quark matter have been studied by many authors, see Refs.[282–284] for recent accounts. Such a transition may indeed be possible in the interior of neutron stars. We will investigate quark matter using the NJL model in Ch. 6 and the possibility of such a transition in Ch. 7.

In summary, taking into account the full tensor structure of the vector-meson-baryon couplings in a Hartree–Fock treatment of the QMC model results in increased pressure at high density – largely because of the ρN tensor coupling – while maintaining reasonable values of the incompressibility at saturation density. The conceptual separation between the incompressibility at saturation density and the slope of the symmetry energy or 'stiffness' at higher densities is critical. It is the latter that leads to neutron stars with maximum masses ranging from 1.8 $M_\odot$ to 2.1 $M_\odot$, even when allowance is made for the appearance of hyperons. This suggests that hyperons are very likely to play a vital role as constituents of neutron stars with central densities above three times nuclear matter density.

Model/ Scenario	K_0 [MeV]	L_0 [MeV]	U_Λ [MeV]	U_{Σ^-} [MeV]	U_{Ξ^-} [MeV]	$M_{\max}$ [$M_\odot$]	R [km]	$\rho_c^{\max}$ [ρ_0]
Standard	273	84	3	26	5	1.80	11.80	5.88
$\Lambda = 1.0$	278	85	10	32	8	1.84	11.86	5.82
$\Lambda = 1.1$	283	86	16	39	11	1.88	11.94	5.70
$\Lambda = 1.2$	286	87	23	46	15	1.92	12.03	5.60
$\Lambda = 1.3$	289	88	29	53	18	1.95	12.10	5.52
$\Lambda = 1.1$, $g_{\sigma Y} \times 1.3$	283	86	-15	14	-4	1.84	11.91	5.78
$\Lambda = 1.3$, $g_{\sigma Y} \times 1.3$	289	88	-3	28	3	1.92	12.01	5.66
$\Lambda = 2.0$, $g_{\sigma Y} \times 1.9$	302	92	-29	20	-7	2.07	12.24	5.38
Increased $f_{\rho N}/g_{\rho N}$	267	81	6	27	6	1.77	11.61	6.14
Fock $\delta\sigma$	273	84	4	26	5	1.81	11.82	5.86
Eff. Proton Mass	297	101	11	41	10	1.94	12.20	5.48
Eff. Proton Mass, $\Lambda = 1.1$	311	111	34	67	22	2.07	12.57	5.08
Eff. Proton mass + $\delta\sigma$	285	109	17	49	13	1.99	12.22	5.46
Dirac Only	294	85	-23	4	-8	1.79	12.33	5.22
Hartree Only	283	88	-49	-23	-21	1.54	11.73	6.04
Nucleon Only	273	84	3	26	5	2.10	11.08	6.46
$R = 0.8$	277	85	6	25	5	1.83	11.88	5.80
App. $S_0 = 32.5$	275	82	2	24	4	1.80	11.82	5.82
App. $S_0 = 30.0$	280	74	-4	19	1	1.81	11.82	5.76
$S_0 = 30.0$	278	76	-2	21	2	1.81	11.81	5.80

Table 5.3.1: Selected nuclear matter properties, hyperon optical potentials and neutron star properties determined for our standard case (for which $\Lambda = 0.9$ GeV, and $R_N^{\text{free}} = 1.0$ fm) and the effect of subsequent variations in which differences from the standard parameter set are indicated in column 1. The tabulated quantities at saturation are the incompressibility K_0, the slope of the symmetry energy, L_0, and hyperon optical potentials, respectively. Tabulated neutron star quantities are the stellar radius, maximum stellar mass and corresponding central density (units $\rho_0 = 0.16$ fm^{-3}).

6

Quark Matter in the Nambu–Jona-Lasinio Model

In this chapter, we introduce the three flavour Nambu–Jona-Lasinio (NJL) model and use it to study quark matter. The quark matter model presented here will then be used to investigate hybrid stars in Ch. 7.

6.1 A Brief Introduction to the NJL Model

The NJL model is an effective model of the strong interaction named after Nambu and Jona-Lasinio who introduced it in 1961 [285, 286]. The original model was formulated in terms of nucleons as a local effective interaction inspired by the BCS theory of superconductivity [287, 288]. In analogy to the energy gap of a superconductor, the mass of the nucleon is generated by the Cooper pairing of a nucleon and anti-nucleon, thereby dynamically breaking chiral symmetry. This is its greatest selling point, its ability to model the breaking of chiral symmetry dynamically by spontaneously generating the nucleon mass. At this time quarks were yet to be discovered, so the model was formulated at the hadronic level. Later it was redeveloped in terms of quarks to model low and intermediate energy QCD. It has since been used for numerous applications from parton distribution functions [289] to quark matter in compact stars (see for example Refs. [282, 283, 290–305]). A number of reviews are available on the NJL model and its applications [306–311].

As an effective model of QCD it introduces simplifications to make calculations tractable. The NJL model assumes that gluons are only important over very small length scales and can be safely integrated out forming the local (contact) four Fermi interaction between quarks, see Fig.(6.1.1). There are many NJL–type models available and their Lagrangians take the general form

$$\mathcal{L}_{\rm NJL} = \bar{\psi}(i\partial\!\!\!/ - \hat{m})\psi + \mathcal{L}_{\rm int} \tag{6.1.1}$$

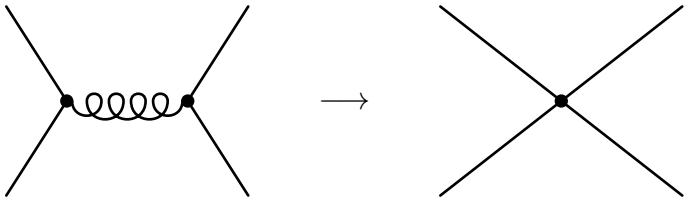

(6.1.4)

Figure 6.1.1: Gluons are integrated out, leading to an effective four–point quark interaction in the NJL model.

where ψ is a multi-component quark spinor and $\bar{\psi}$ is its adjoint, $\hat{m}$ is a current quark mass matrix and the interaction part of the Lagrangian can have the general form[1]

$$\mathcal{L}_{\text{int}} = \sum_{\alpha} G_{\alpha}(\bar{\psi}\mathcal{O}_{\alpha}\psi)^2 \quad . \tag{6.1.2}$$

A general interaction vertex, $\mathcal{O}_{\alpha}$, can be decomposed into the three separate spaces of Dirac (spin), colour and flavour, which can be expressed mathematically as the tensor product of the vertex structure in each space

$$\mathcal{O}_{\alpha} = \mathcal{O}_{\alpha}^{\text{Dirac}} \otimes \mathcal{O}_{\alpha}^{\text{Colour}} \otimes \mathcal{O}_{\alpha}^{\text{Flavour}} \quad . \tag{6.1.3}$$

Upon integrating out gluons the local colour symmetry of QCD is reduced to a global symmetry and confinement is lost. Moreover, from simple dimensional analysis of the interaction Lagrangian one can see that the dimension of the couplings is $[G_{\alpha}] = (\text{Mass})^{-2}$ and therefore NJL models are not renormalizable. Lack of confinement and renormalizability are the two major drawbacks of the model.

Unrenormalizable theories are still useful and information can be obtained through the process of regularization, whereby a cut-off is introduced setting the scale of the model. There are many regularization schemes in common use, ranging from the simple non-covariant three momentum cut-off to covariant schemes such as the four-momentum cut-off, Pauli-Villars, dimensional and Schwinger's proper time regularization [307, 310]. In this thesis we will make use of the latter with comparisons to the more common and simpler three momentum cut-off regularization. Of course, one would hope that the final results will be scheme independent, but in an unrenormalizable model this may not be true. In the absence of a physically preferred regularization scheme one should make a comparison between schemes and choose the scheme which best preserves the relevant symmetries and physics. Each of the schemes have their advantages and disadvantages, see Ref. [307, 310] for details.

The NJL model possesses the ability to describe the spontaneous breaking of chiral symmetry. It is well known that the spontaneous breaking of a symmetry is intimately connected to the appearance of bosons through Goldstone's theorem. In a purely fermionic model, like the NJL model, these bosons must be bound states. The lack of a confinement mechanism in the NJL model is a real drawback, although it has been argued in the literature [314] that the introduction of an infra-red cut off in the

[1] Multiquark interactions have also been developed, see for example Ref. [312, 313].

the proper time regularization scheme can simulate confinement. By imposing a low energy cut-off, one crudely enforces one of the key features of confinement—no non-physical decays to free quarks occur. This additional cut-off has been seen to have important consequences for the saturation of nuclear matter and preventing what is called the chiral collapse [315]. In the absence of a genuine confinement mechanism all is not lost. Bosons can be interpreted as a quark and anti-quark propagating together for some time producing a resonance and then decaying. The poles in the quark–anti-quark scattering matrix can then be used to identify their masses. One common procedure for modelling mesons in the NJL model solves the Bethe-Salpeter equation for the scattering T-matrix in the random phase approximation (RPA). They can also be introduced as auxiliary fields using the exact transformations developed by Stratonovich [316] and Hubbard [317] in the path integral formalism.

Quarks are generally treated at the mean field level, while to consider mesons we must work at a level which includes the mean field solution plus higher order quantum corrections (generally RPA in the BSE approach). The mean field approximation is essentially a semi-classical approximation and for particles not already present in the classical action (i.e. hadrons) it is difficult to see their origin. In the models mentioned earlier, the QMC and Walecka models, the mean field approach is sufficient since the mesons and baryons both have fields present in the Lagrangian, but with the NJL model only quarks are present. For this reason, it is more difficult. Hadrons can be understood as poles in the four and six point Green's functions of the quarks, respectively for mesons and baryons. As indicated above, in this way they can be studied using the BSE for mesons [306–311], or the Faddeev equation for baryons [318–320], within some approximation scheme. Hadronic masses are then determined by the position of the poles in the corresponding T-matrices and their hadron-quark couplings by the expansion of these scattering matrices about the poles.

Despite these descriptions of hadrons in the NJL model, it is still non-confining in the sense that hadronic bound states do not remain confined clusters of quarks and anti-quarks. They transition to virtual resonant states which can dissociate into free (unbounded not necessarily non-interacting) quarks when the hadronic masses are greater than the threshold for the continuum of states of free quarks, which occurs as a result of partial chiral restoration. This shortcoming of the NJL model will not be an issue when modelling quark matter at high density, where the quarks will be considered to be de-confined.

The formation of bound states is a purely non-perturbative phenomenon and cannot be understood by the usual perturbative approach used in high energy particle physics, where a series expansion is performed in powers of the coupling constant. We require a different calculational approach that allows us to obtain this non-perturbative information. Here is an example where the path integral formalism really shines. The basic formalism and results of the path integral approach is summarised in the appendices. It accentuates the connection between the quantum and classical worlds. Combing this formalism with techniques developed in the analysis of integrals the transition from quantum to classical can be studied and furthermore non-perturbative information can

be obtained. We understand the composite nature of mesons from QCD and experiment. Using this knowledge we can introduce auxiliary fields with the correct quantum numbers through Hubbard-Stratononvich transformations, essentially furnishing us with a way to understand mesons as collective and composite objects through these new fields.

Typically, one starts with the NJL generating functional then does one or more Hubbard-Stratonovich transformations by introducing new auxillary fields through a slick decomposition of unity using a Gaussian integral. This replaces the quartic quark interactions with a Gaussian fermion integral and a linear Yukawa coupling between the fermion and auxiliary fields. After which a stationary phase analysis of the path integral is performed, where the leading term, evaluated at the actions stationary point, corresponds to the mean field result and the corrections about this stationary point are related to meson fluctuations. This method provides us with the necessary non-perturbative information.

In this way the NJL model is capable of reasonably describing the meson spectrum and low energy hadron phenomenology. In particular it satisfies several results from current algebra, such as the Gell-Mann–Oaks–Renner and Goldberger–Treiman relations [306, 307], preserving the key features of chiral symmetry.

6.2 A Simple and Less Intuitive Explanation of the Mean Field Approximation

Even with models of QCD, calculations cannot in general be performed exactly—one must resort to approximations. In this section we introduce the mean field approximation in a very simple, but somewhat less intuitive way, which glosses over certain subtleties. Here we use the operator formalism, but in Sec. 6.4 we will explain how it can be better understood and formalised more generally in the path integral formulation of QFT. In this formalism it arises as a saddle point approximation to a generating functional and one is also afforded a way to go beyond the mean field approximation in a well defined way. Earlier in the introduction we introduced the mean field approximation to the Walecka and QMC models. A similar procedure follows for the NJL model with the exception that the model does not yet contain bosons in its Lagrangian, so the fundamental fermions must be paired, bosonizing the model.

The mean field approximation can be introduced simply by writing the fermionic bilinears as a bosonic mean field plus a small fluctuation term

$$\bar{\psi}\mathcal{O}_i\psi = \langle\bar{\psi}\mathcal{O}_i\psi\rangle + \delta(\bar{\psi}\mathcal{O}_i\psi) \quad , \tag{6.2.1}$$

where our notation is

$$\langle\ldots\rangle \equiv \langle\Psi_{\text{g.s.}}| : \ldots : |\Psi_{\text{g.s.}}\rangle \tag{6.2.2}$$

and $|\Psi_{\text{g.s.}}\rangle$ is the ground state. Using Eq. (6.2.1) the quartic interaction terms in $\mathcal{L}_{\text{int}}$ can be written as

$$(\bar{\psi}\mathcal{O}_i\psi)^2 = \langle\bar{\psi}\mathcal{O}_i\psi\rangle^2 + 2\langle\bar{\psi}\mathcal{O}_i\psi\rangle\delta(\bar{\psi}\mathcal{O}_i\psi) + (\delta(\bar{\psi}\mathcal{O}_i\psi))^2 \quad . \tag{6.2.3}$$

Neglecting squared fluctuation terms and using Eq. (6.2.1) for $\delta(\bar{\psi}\mathcal{O}_i\psi)$ this simplifies to

$$(\bar{\psi}\mathcal{O}_i\psi)^2 = \langle\bar{\psi}\mathcal{O}_i\psi\rangle^2 + 2\langle\bar{\psi}\mathcal{O}_i\psi\rangle(\bar{\psi}\mathcal{O}_i\psi - \langle\bar{\psi}\mathcal{O}_i\psi\rangle) \quad (6.2.4)$$

$$= 2\bar{\psi}\mathcal{O}_i\psi\langle\bar{\psi}\mathcal{O}_i\psi\rangle - \langle\bar{\psi}\mathcal{O}_i\psi\rangle^2 \quad . \quad (6.2.5)$$

The pairing in Eq. (6.2.1) is said to be in the the direct channel.

In a local quartic interaction there are 3 possible ways to pair the fields. They can be paired in the so called direct, exchange and Cooper channels. These three channels are related to each other by Fierz transformations, see App. B.3. Thus if one was to perform the mean field approximation by pairing in the direct channel starting from one NJL Lagrangian which will give rise to one set of bosons, one could Fierz transform to an equivalent Lagrangian obtaining a different set of bosons leading to a completely different low energy approximation to QCD. In the next section we will develop an NJL Lagrangian which is inspired by perturbative QCD leading to a Fierz invariant Lagrangian from which we can perform the mean field approximation by pairing only in the direct channel, side-stepping the need to calculate exchange terms explicitly.

6.3 A Fierz Invariant NJL Lagrangian Derived from the Colour Current Interaction

In perturbative QCD one gluon exchange is important and it should therefore be a good starting point for developing our NJL interaction Lagrangian. It is also important for the "hyperfine" spitting of the Λ and Σ hyperons in the bag model. Approximately, one gluon exchange can be described by the conserved current

$$J^a_\mu = \bar{\psi}\gamma_\mu t^a\psi \quad , \quad (6.3.1)$$

referred to as the colour current. In Eq. (6.3.1) we use t_a to label the Gell-Mann matrices of colour space, whereas later we use λ_b to label them in flavour space. Note that the colour current interaction vertex actually has the structure of

$$\mathcal{O}_{\text{Col. Cur.}} = \gamma_\mu \otimes t^a \otimes 1_F \quad . \quad (6.3.2)$$

This interaction vertex leads to the following current–current interaction

$$\mathcal{L}^{\text{Col. Cur.}}_{\text{int}} = -G_c \sum_{a=1}^{N_c^2-1} J^a_\mu \, J^\mu_a \quad (6.3.3)$$

$$= -G_c \sum_{a=1}^{N_c^2-1} \bar{\psi}_{\alpha,i,p}\psi_{\beta,j,q}\bar{\psi}_{\gamma,k,r}\psi_{\delta,l,s} \times [(\gamma_\mu)_{\alpha\beta}(\gamma^\mu)_{\gamma\delta} \otimes (t_a)_{ij}(t^a)_{kl} \otimes (I)_{pq}(I)_{rs}] \quad . \quad (6.3.4)$$

The order of labels on spinors in Eq. (6.3.4) is the same as in vertex structure i.e Dirac, colour, and then flavour. Greek letters for Dirac indices (μ, α, β, γ, δ) and Latin

indices for symmetry group indices (a, i, j, k and l for colour and b, p, q, r, and s for flavour). For example the matrix γ_μ, written explicitly with matrix indices is $(\gamma_\mu)_{\alpha\beta}$. Using Eq. (B.3.1) and Eq. (B.3.2) to Fierz transform the colour current interaction Lagrangian to the exchanged $q\bar{q}$–channel and adding it to the original Lagrangian we obtain

$$\mathcal{L}_{\rm int}^{\rm Col.\,Cur.} + \mathcal{F}_{\rm Ex.}(\mathcal{L}_{\rm int}^{\rm Col.\,Cur.}) = \mathcal{L}_{\rm int}^{\rm Col.\,Singlet} + \mathcal{L}_{\rm int}^{\rm Col.\,Octet} \quad , \tag{6.3.5}$$

where

$$\mathcal{L}_{\rm int}^{\rm Col.\,Singlet} = \frac{8}{9}G_{\rm c}\sum_{b=0}^{N_{\rm F}^2-1}\left[(\bar{\psi}\lambda_b\psi)^2 + (\bar{\psi}i\gamma_5\lambda_b\psi)^2 - \frac{1}{2}(\bar{\psi}\gamma_\mu\lambda_b\psi)^2 - \frac{1}{2}(\bar{\psi}\gamma_\mu\gamma_5\lambda_b\psi)^2\right] \tag{6.3.6}$$

is the portion of the Lagrangian containing the colour–singlet terms and

$$\mathcal{L}_{\rm int}^{\rm Col.\,Octet} = -\frac{1}{6}\sum_{a=1}^{N_{\rm C}^2-1}\sum_{b=0}^{N_{\rm F}^2-1}\left[(\bar{\psi}t_a\lambda_b\psi)^2 + (\bar{\psi}i\gamma_5 t_a\lambda_b\psi)^2 - \frac{1}{2}(\bar{\psi}\gamma_\mu t_a\lambda_b\psi)^2 - \frac{1}{2}(\bar{\psi}\gamma_\mu\gamma_5 t_a\lambda_b\psi)^2\right] \tag{6.3.7}$$

is the remainder containing the colour–octet terms. We assume that the quark matter in a neutron star is locally in a colour neutral state, so that all matrix elements of colour octet operators will be zero. Moreover, we will only have the so called chiral and vector condensates, because of the assumption of charge conjugation and parity invariance of the charge neutral ground state, which means that the matrix elements of the pseudo–scalar and axial–vector operators are also zero. Even though the pseudo-scalar terms do not contribute they are still necessary for the chiral symmetry of the Lagrangian. In the mean field approximation the contribution of a pair of chiral partners is rotationally invariant under chiral transformations, allowing us to essentially ignore the pseudo-scalar contributions. Without loss of generality we can assume that they do not contribute.

To be clear the Lagrangian density we will be investigating is

$$\begin{aligned}\mathcal{L}_{\rm NJL} = \bar{\psi}(i\partial\!\!\!/ - \hat{m}_0)\psi + G_{\rm S}\sum_{b=0}^{N_{\rm F}^2-1}\left[\left(\bar{\psi}\lambda_b\psi\right)^2 + \left(\bar{\psi}i\gamma_5\lambda_b\psi\right)^2\right] \\ -G_{\rm V}\sum_{b=0}^{N_{\rm F}^2-1}\left[\left(\bar{\psi}\gamma_\mu\lambda_b\psi\right)^2 + \left(\bar{\psi}\gamma_\mu\gamma_5\lambda_b\psi\right)^2\right] \quad ,\end{aligned} \tag{6.3.8}$$

where $\hat{m}_0$ =diag(m_u, m_d, m_s). It is the same as the colour-singlet Lagrangian in Eq. (6.3.6) with redefined couplings

$$G_{\rm S} = \frac{8}{9}G_c \qquad \text{and} \qquad G_{\rm V} = \frac{G_{\rm S}}{2} \quad . \tag{6.3.9}$$

Applying the simple mean field approximation to the Lagrangian density (Eq. (6.3.8)) in all channels, we can obtain the mean field Lagrangian. With the mean field Lagrangian, the effective (thermodynamic) potential can then be obtained by using it in

the NJL generating functional and following the usual procedure. This procedure is discussed in Sec. 6.4, where we will develop a better understanding of the mean field approximation.

6.4 A Better Explanation of the Mean Field Approximation Using the Path Integral Formalism

The simple mean field procedure, as described in Sec. 6.2, can be formalised using path integral quantisation. This is done by introducing bosonic auxiliary fields, applying Hubbard–Stratonovich transformations and performing a stationary phase analysis of the generating functional.

In this and the following sections we will first use Hubbard–Stratonovich transformations to bosonise the NJL model given by the Lagrangian in Eq. (6.3.8). After this, a stationary phase analysis will be performed in the $\hbar \to 0$ limit, where we will approximate the effective action to leading order and consider constant bosonic field configurations resulting in the mean field effective potential. The obtained expressions will be divergent requiring regularization, which will be implemented using Schwinger's proper time method [321]. Similar procedures for other regularization schemes can be found in the literature [307, 310]. Including next-to-leading-order corrections will lead to meson corrections to the effective potential, which will not be considered. Meson phenomenology, i.e their propagators, decay constants and so on will follow simply using this approach and is equivalent to solving the BSE in the RPA.

The ambiguity discussed in the simple form of the mean field approximation still exists and is connected to the way in which these fields are introduced. The quartic contact interaction of the fermion fields allows for 3 different possibilities to pair them, which are generally referred to as the direct, exchange and Cooper channels. The exchange channel is related to Fock contributions and the Cooper channel is related to diquarks and superconducting phases of quark matter.

Performing Fierz transformations on the interaction terms in the quark–anti-quark and quark–quark channels and adding these to the original Lagrangian allows one to obtain a new Lagrangian from which one can perform the pairing in the mean field approximation only in the direct channel, obtaining these extra contributions with no extra work. For this purpose, in Sec. 6.3 we developed an NJL Lagrangian based on the colour current interaction which is Fierz invariant in the quark–anti-quark channel. As we are not interested in superconducting quark matter in this thesis we did not make the Lagrangian Fierz invariant in the quark–quark channel, the so called Cooper channel. Thus, the Lagrangian, Eq. (6.3.8), is only suitable for modelling non-superconducting quark matter. We have chosen to refrain from studying the superconducting phases of quark matter. These phases have been studied extensively using the NJL model (see for example Refs. [290–292, 294]) and are likely to be important for very high density quark matter. Inner regions of neutron stars may exhibit some or all of these phases, but as a first step we want to develop a non-superconducting NJL model to be used to investigate phase transitions from Hartree–Fock QMC to NJL quark matter in neutron

stars.

The generating functional for the NJL model is

$$Z_{\rm NJL}[\eta,\bar{\eta}] = \int \mathcal{D}\psi\mathcal{D}\bar{\psi}\exp\left(i\int d^4x\left[\mathcal{L}_{\rm NJL}+\bar{\eta}(x)\psi(x)+\bar{\psi}(x)\eta(x)\right]\right) \quad , \qquad (6.4.1)$$

where η, $\bar{\eta}$ are fermionic sources and $\mathcal{L}_{\rm NJL}$ is given by Eq. (6.3.8).

The auxiliary fields are used to remove the quartic fermion interactions. They are introduced into the path integral by writing unity in a crafty way. This decomposition of unity is an exact transformation named after Hubbard and Stratonovich, it is also referred to as bosonization. Specifically for the scalar and pseudo-scalar channels, we introduce the auxiliary fields S_a and P_a using

$$\begin{aligned}\mathbf{1} &= \mathcal{N}^{'}\exp\left\{-i\int d^4x\; G_{\rm S}\left[(\bar{\psi}\lambda_a\psi)^2+(\bar{\psi}i\gamma_5\lambda_a\psi)^2\right]\right\}\\ &\quad\times\int\mathcal{D}S_a\mathcal{D}P_a\;\exp\left\{i\int d^4x\left[-\left(\frac{S_a^2+P_a^2}{4G_{\rm S}}\right)+S_a(\bar{\psi}\lambda_a\psi)+P_a(\bar{\psi}i\gamma_5\lambda_a\psi)\right]\right\} \quad .\end{aligned} \qquad (6.4.2)$$

There are differences in the signs in the Lagrangian for the vector and axial vector interactions as compared to the scalar and pseudo-scalar interactions. Although, with care a similar decomposition of unity can still be performed [310]. For the vector and axial-vector channels we introduce V_a^μ and A_a^μ by

$$\begin{aligned}\mathbf{1} &= \mathcal{N}^{''}\exp\left\{+i\int d^4x\; G_{\rm V}\left[(\bar{\psi}\gamma^\mu\lambda_a\psi)^2+(\bar{\psi}\gamma_5\gamma^\mu\lambda_a\psi)^2\right]\right\}\\ &\quad\times\int\mathcal{D}V_a^\mu\mathcal{D}A_a^\mu\;\exp\left\{i\int d^4x\left[+\left(\frac{V_a^2+A_a^2}{4G_{\rm V}}\right)-V_a^\mu(\bar{\psi}\gamma_\mu\lambda_a\psi)-A_a^\mu(\bar{\psi}\gamma_\mu\gamma_5\lambda_a\psi)\right]\right\} \quad ,\end{aligned} \qquad (6.4.3)$$

These transformations are exact and an arbitrary number of them can be performed. They allow quartic fermion interactions to be replaced by a quadratic bosonic interaction and a Yukawa coupling between the auxiliary field and the fermions. These transformations are purely a mathematical trick and must be motivated by physical arguments as the resulting mean field model results will differ even though the transformations are exact. The way in which these transformations should be introduced is by requiring that they represent the effective low energy collective modes of the physical theory, which in our case are the mesons of QCD. Using a Fierz invariant Lagrangian we can unambiguously introduce these auxiliary fields in the path integral of the generating functional using Eq. (6.4.2) and (6.4.3). As the Lagrangian is Fierz invariant we do not have to worry about mesons disappearing if we re-express the Lagrangian in an equivalent Fierz transformed Lagrangian.

Making use of Eq. (6.4.2) and (6.4.3), the NJL generating functional takes the form

$$Z_{\rm NJL}[\eta,\bar{\eta}] \;=\; \mathcal{N}^{'''}\int\mathcal{D}\bar{\psi}\mathcal{D}\psi\mathcal{D}S_a\mathcal{D}P_a\mathcal{D}V_a^\mu\mathcal{D}A_a^\mu$$

$$\times \exp\left(i \int d^4x \ \left[\mathcal{L}_{\rm HS} + \bar{\eta}(x)\psi(x) + \bar{\psi}(x)\eta(x)\right]\right) \quad . \tag{6.4.4}$$

where $\mathcal{N}''' = \mathcal{N}'\mathcal{N}''$ and the semi-bosonised Lagrangian is

$$\mathcal{L}_{\rm HS} = \bar{\psi} S^{-1} \psi - \frac{S_a^2 + P_a^2}{4G_{\rm S}} + \frac{V_a^2 + A_a^2}{4G_{\rm V}} \quad . \tag{6.4.5}$$

The full inverse fermion propagator given in terms of the bare inverse propagator as

$$\begin{aligned} S^{-1} &= S_0^{-1} + S_a\lambda_a + P_a i\gamma_5\lambda_a - V_a^\mu \gamma_\mu \lambda_a - A_a^\mu \gamma_\mu\gamma_5\lambda_a & (6.4.6)\\ &= i\partial\!\!\!/ - \hat{m} + S_a\lambda_a + P_a i\gamma_5\lambda_a - V_a^\mu \gamma_\mu \lambda_a - A_a^\mu \gamma_\mu\gamma_5\lambda_a \quad . & (6.4.7) \end{aligned}$$

This defines a semi-bosonised NJL action

$$I_{\rm HS}[\psi, \bar{\psi}, S_a, P_a, V_a^\mu, A_a^\mu] = \int d^4x \ \mathcal{L}_{\rm HS} \quad . \tag{6.4.8}$$

Using this action we can infer from the Euler-Lagrange equations that each of these auxiliary fields depend upon the quark fields, such that

$$\begin{aligned} S_a &= 2G_{\rm S}\bar{\psi}\lambda_a\psi \quad , & (6.4.9)\\ P_a &= 2G_{\rm S}\bar{\psi} i\gamma_5\lambda_a\psi \quad , & (6.4.10)\\ V_a^\mu &= 2G_{\rm V}\bar{\psi}\gamma^\mu\lambda_a\psi \quad , & (6.4.11)\\ A_a^\mu &= 2G_{\rm V}\bar{\psi}\gamma^\mu\gamma_5\lambda_a\psi \quad . & (6.4.12) \end{aligned}$$

On substitution of Eqs. (6.4.9–6.4.12) into Eq. (6.4.5) we retrieve the original Lagrangian, because the bosonic auxiliary fields depend on the quark fields and are not completely independent. After performing the Hubbard–Stratonovich transformations, the fermionic path integral takes a Gaussian form and can therefore be done in the usual way. This results in a determinant of the inverse fermion propagator and the resulting generating functional is

$$\begin{aligned} Z_{\rm NJL}[\eta, \bar{\eta}] &= \mathcal{N} \int \mathcal{D}S_a \mathcal{D}P_a \mathcal{D}V_a^\mu \mathcal{D}A_a^\mu \ {\rm Det}\left(S^{-1}\right) \exp^{-\int d^4x \ \bar{\eta}(x) i S(x,x) \eta(x)} \\ &\quad \times \exp\left(i \int d^4x \ \left[-\frac{S_a^2 + P_a^2}{4G_{\rm S}} + \frac{V_a^2 + A_a^2}{4G_{\rm V}}\right]\right) \quad . \end{aligned} \tag{6.4.13}$$

In the absence of sources this takes the form

$$\begin{aligned} Z_{\rm NJL}[\eta = 0, \bar{\eta} = 0] &= \mathcal{N} \int \mathcal{D}S_a \mathcal{D}P_a \mathcal{D}V_a^\mu \mathcal{D}A_a^\mu \\ &\quad \times \exp\left({\rm Tr}\left[{\rm Log}\left(S^{-1}\right)\right] + i \int d^4x \ \left[-\frac{S_a^2 + P_a^2}{4G_{\rm S}} + \frac{V_a^2 + A_a^2}{4G_{\rm V}}\right]\right) , \end{aligned} \tag{6.4.14}$$

where the trace Tr is a trace over space-time, as well as internal spaces. From Eq. (6.4.14) we infer that the (classical) action is now

$$I_{\rm HS}[S_a, P_a, V_a^\mu, A_a^\mu] = -i{\rm Tr}\left[{\rm Log}\left(S^{-1}\right)\right] + \int d^4x \, \left[-\frac{S_a^2 + P_a^2}{4G_{\rm S}} + \frac{V_a^2 + A_a^2}{4G_{\rm V}}\right] \quad . \tag{6.4.15}$$

The remaining path integrals over bosonic fields still cannot be evaluated exactly and must be simplified further. We use a variation of Laplace's method called a stationary phase approximation [322]. When analytically continuing the above generating functional to Euclidean space the stationary phase approximation amounts to a saddle point approximation. We perform this approximation as a semi-classical approximation, that is we take $\hbar \to 0$ which appears in the denominator of the exponential[2]. To be precise, we are interested in finding the dominant asymptotic behaviour of the generating functional as $\hbar \to 0$. This is in contrast to other authors who prefer the large number of colours N_c expansion [307]. At the Hartree–Fock level they are essentially equivalent.

When using the stationary phase approximation we consider a set of stationary fields $\left\{\phi_\alpha^{(\rm c)}\right\}$. This set represents the extremum of the action and as such these constant fields must satisfy the stationary conditions

$$\left.\frac{\delta I_{\rm HS}[\{\phi_\alpha\}]}{\delta\phi_\alpha(x)}\right|_{\phi_\alpha=\phi_\alpha^{(\rm c)}} = 0 \quad , \tag{6.4.16}$$

where for convenience we denote by ϕ_α one of the auxiliary fields S_a, P_a, V_a^μ or A_a^μ. Equation (6.4.16) leads to the classical equations of motion given by the Euler-Lagrange equations, where the $\phi_\alpha^{(\rm c)}$ have the physical meaning of $\phi_\alpha^{(\rm c)} = \langle\phi_\alpha\rangle$. This physical meaning can be easily understood as a generalisation of Ehrenfest's theorem in quantum mechanics to quantum field theory, which follows from considering the the effect of a variation of an auxiliary field ϕ_α on the generating functional defined using the action $I_{\rm HS}[\{\phi_\alpha\}]$ given by Eq. (6.4.15). This generating functional is explicitly given by

$$Z_{\rm NJL}[\{J_\alpha\}] = \mathcal{N}\int\left(\prod_\alpha \mathcal{D}\phi_\alpha\right) e^{\frac{i}{\hbar}(I_{\rm HS}[\{\phi_\alpha\}]+J_\alpha\cdot\phi_\alpha)} \quad , \tag{6.4.17}$$

where we have reinstated $\hbar$ and introduced the classical source functions, J_α, one for each auxiliary field ϕ_α. In Eq. (6.4.17), we have used the notation

$$J_\alpha\cdot\phi_\alpha \equiv \sum_\alpha \int d^4x \; J_\alpha(x)\phi_\alpha(x) \quad . \tag{6.4.18}$$

As all auxiliary fields are integrated over, the variation of the generating functional is zero leading to

$$0 = \delta Z_{\rm NJL}[\{J_\alpha\}] \tag{6.4.19}$$

$$= \mathcal{N}\int\left(\prod_\alpha \mathcal{D}\phi_\alpha\right)\left(\frac{i}{\hbar}\delta\left(I_{\rm HS}[\{\phi_\alpha\}] + J_\alpha\cdot\phi_\alpha\right)\right) e^{\frac{i}{\hbar}(I_{\rm HS}[\{\phi_\alpha\}]+J_\alpha\cdot\phi_\alpha)} \tag{6.4.20}$$

[2]Previously we set $\hbar = 1$ in all equations.

$$= \frac{i\mathcal{N}}{\hbar}\int\left(\prod_\alpha \mathcal{D}\phi_\alpha\right)\left(\sum_\alpha\int d^4x\ \delta\phi_\alpha(x)\left(\frac{\delta I_{\rm HS}[\{\phi_\alpha\}]}{\delta\phi_\alpha}+J_\alpha(x)\right)\right)e^{\frac{i}{\hbar}(I_{\rm HS}[\{\phi_\alpha\}]+J_\alpha\cdot\phi_\alpha)} \quad . \tag{6.4.21}$$

This must be valid for an arbitrary variation of an auxiliary field ϕ_α, which means in the absence of sources we have [3]

$$0=\mathcal{N}\int\left(\prod_\alpha\mathcal{D}\phi_\alpha\right)\frac{\delta I_{\rm HS}[\{\phi_\alpha\}]}{\delta\phi_\alpha}e^{\frac{i}{\hbar}I_{\rm HS}[\{\phi_\alpha\}]}=\left\langle\frac{\delta I_{\rm HS}[\{\phi_\alpha\}]}{\delta\phi_\alpha}\right\rangle \quad . \tag{6.4.22}$$

From Eqs. (6.4.9–6.4.12) and Eq. (6.4.22), we have explicitly

$$\begin{aligned}
\langle S_a\rangle &= S_a^{(\rm c)}=2G_{\rm S}\langle\bar\psi\lambda_a\psi\rangle \quad , &(6.4.23)\\
\langle P_a\rangle &= P_a^{(\rm c)}=2G_{\rm S}\langle\bar\psi i\gamma_5\lambda_a\psi\rangle \quad , &(6.4.24)\\
\langle V_a^\mu\rangle &= V_a^{\mu\ (\rm c)}=2G_{\rm V}\langle\bar\psi\gamma^\mu\lambda_a\psi\rangle \quad , &(6.4.25)\\
\langle A_a^\mu\rangle &= A_a^{\mu\ (\rm c)}=2G_{\rm V}\langle\bar\psi\gamma^\mu\gamma_5\lambda_a\psi\rangle \quad . &(6.4.26)
\end{aligned}$$

It should be noted that we have more information in this semi-classical approximation than can be obtained from classical field theory, as the expansion results in a phase factor for each stationary point and there could potentially be more than one stationary point and therefore they would interfere. For simplicity we will assume that the stationary point is unique, expanding each field about this point $\phi_\alpha=\phi_\alpha^{(\rm c)}+\phi_\alpha^{(\rm q)}\sqrt{\hbar}$, where $\phi_\alpha^{(\rm q)}\sqrt{\hbar}$ is a small quantum fluctuation. This does not necessarily mean that quantum effects are small.

The action obtained above (Eq.(6.4.15)) can be expanded in a power series

$$\begin{aligned}
I_{\rm HS}\left[\{\phi_\alpha\}\right] &= I_{\rm HS}(\{\phi_\alpha^{(c)}\})+\hbar^{1/2}\sum_\alpha\int d^4x\ \phi_\alpha^{(\rm q)}(x)\frac{\delta I_{\rm HS}}{\delta\phi_\alpha(x)}\bigg|_{\phi_\alpha=\phi_\alpha^{(\rm c)}} &(6.4.27)\\
&\quad+\frac{\hbar}{2}\sum_\alpha\int d^4x\int d^4y\ \phi_\alpha^{(\rm q)}(x)\frac{\delta I_{\rm HS}}{\delta\phi_\alpha(x)\delta\phi_\alpha(y)}\bigg|_{\phi_\alpha=\phi_\alpha^{(\rm c)}}\phi_\alpha^{(\rm q)}(y)+\ldots \quad .
\end{aligned}$$

Note that the second term on the right hand side, which is linear in the fluctuation is zero by the classical equations of motion (Eq. (6.4.16)). The measure in Eq.(6.4.17) simply becomes

$$\mathcal{D}\phi_\alpha=\mathcal{D}(\phi_\alpha^{(\rm c)}+\sqrt{\hbar}\phi_\alpha^{(\rm q)})=\mathcal{D}(\sqrt{\hbar}\phi_\alpha^{(\rm q)}) \tag{6.4.28}$$

as $\phi_\alpha^{(\rm c)}$ is just a constant point in the space in all field configurations. Truncating at quadratic order in the fluctuation results in Gaussian integral and can be calculated in the usual manner yielding

$$Z_{\rm NJL}[\{J_\alpha\}] = \mathcal{N}\int\left(\prod_\alpha\mathcal{D}\phi_\alpha\right)\ e^{\frac{i}{\hbar}(I_{\rm HS}[\{\phi_\alpha\}]+J_\alpha\cdot\phi_\alpha)} \tag{6.4.29}$$

[3] Assuming that the measure is invariant under the variation, otherwise an additional term can appear. These terms can be important in the study of anomalies.

$$= \mathcal{N} e^{\frac{i}{\hbar}\left(I_{\rm HS}\left(\left\{\phi_\alpha^{(\rm c)}\right\}\right)+J_\alpha\cdot\phi_\alpha^{(\rm c)}\right)} \int \left(\prod_\alpha \mathcal{D}(\hbar^{1/2}\phi_\alpha^{(\rm q)})\right) \; e^{\frac{i}{\hbar}\left(\frac{\hbar}{2}\phi_\alpha^{(\rm q)}\cdot\frac{\delta^2 I_{\rm HS}\left(\left\{\phi_\alpha^{(\rm c)}\right\}\right)}{\delta\phi_\alpha\delta\phi_\alpha}\cdot\phi_\alpha^{(\rm q)} \; + \ldots\right)} \tag{6.4.30}$$

$$\simeq \tilde{\mathcal{N}} e^{\frac{i}{\hbar}\left(I_{\rm HS}\left(\left\{\phi_\alpha^{(\rm c)}\right\}\right)+J_\alpha\cdot\phi_\alpha^{(\rm c)}\right)} \prod_\alpha \left[\mathrm{Det}\left(\frac{\delta^2 I_{\rm HS}\left(\left\{\phi_\alpha^{(\rm c)}\right\}\right)}{\delta\phi_\alpha\delta\phi_\alpha}\right)\right]^{-1/2} \quad , \tag{6.4.31}$$

where in the second equality a summation over α is implied in the dot notation as in Eq. (6.4.18). From which we can obtain the connected generating functional up to one loop (as expansion in $\hbar$ is equivalent to an expansion in the loop number). For the bosonised NJL model omitting an irrelevant infinite constant we obtain

$$W_{\rm NJL}[\{J_\alpha\}] = -i\hbar \mathrm{Log}\left(Z_{\rm NJL}[\{J_\alpha\}]\right) \tag{6.4.32}$$

$$= \left(I_{\rm HS}(\left\{\phi_\alpha^{(\rm c)}\right\}) + J_\alpha\cdot\phi_\alpha^{(\rm c)}\right) + \frac{i\hbar}{2}\sum_\alpha \mathrm{Log}\left[\mathrm{Det}\left(\frac{\delta^2 I_{\rm HS}\left(\left\{\phi_\alpha^{(\rm c)}\right\}\right)}{\delta\phi_\alpha\delta\phi_\alpha}\right)\right] \tag{6.4.33}$$

$$= \left(I_{\rm HS}\left(\left\{\phi_\alpha^{(\rm c)}\right\}\right) + J_\alpha\cdot\phi_\alpha^{(\rm c)}\right) + \frac{i\hbar}{2}\sum_\alpha \mathrm{Tr}\left[\mathrm{Log}\left(\frac{\delta^2 I_{\rm HS}\left(\left\{\phi_\alpha^{(\rm c)}\right\}\right)}{\delta\phi_\alpha\delta\phi_\alpha}\right)\right] \quad . \tag{6.4.34}$$

It should be noted that the second term is only meaningful if the argument of the logarithm is positive definite [323]. To obtain the (quantum) effective action which is the generating functional for proper vertices (or equivalently 1PI graphs) we introduce the classical background fields

$$\varphi_\alpha = \frac{\delta W_{\rm NJL}\left[\{J_\alpha\}\right]}{\delta\phi_\alpha} \quad , \tag{6.4.35}$$

which can be shown to be $\varphi_\alpha = \phi_\alpha^{(\rm c)} + \mathcal{O}(\hbar)$. These background fields are a functional of the J_α and vice versa. Based on this we can perform a Legendre transformation on the generating functional $W_{\rm NJL}[J_\alpha]$ obtaining the effective action

$$\Gamma_{\rm NJL}\left[\{\varphi_\alpha\}\right] = W_{\rm NJL}\left[\{J_\alpha\}\right] - J_\alpha\cdot\varphi_\alpha \quad , \tag{6.4.36}$$

where the Legendre transform has removed any dependence on the source functions. This generating functional is a functional of the background fields only. The dominant asymptotic or leading order term is just the classical action in the mean field approximation (constant bosonic background fields i.e the background field to first order) given by

$$\Gamma_{\rm MF}^{\rm NJL}\left(\left\{\phi_\alpha^{(\rm c)}\right\}\right) = I_{\rm HS}\left(\left\{\phi_\alpha^{(\rm c)}\right\}\right) \quad . \tag{6.4.37}$$

To next-to-leading order or 1-loop we have

$$\Gamma_{\rm 1-loop}^{\rm NJL}\left(\left\{\phi_\alpha^{(\rm c)}]\right\}\right) = \Gamma_{\rm MF}^{\rm NJL}\left(\left\{\phi_\alpha^{(\rm c)}\right\}\right) + \frac{i\hbar}{2}\mathrm{Tr}\left[\mathrm{Log}\left(\frac{\delta^2 I_{\rm HS}\left(\left\{\phi_\alpha^{(\rm c)}\right\}\right)}{\delta\phi_\alpha\delta\phi_\alpha}\right)\right] \quad . \tag{6.4.38}$$

In deriving equations of state for quark matter we will only consider the leading or mean-field contribution to the effective potential. At this order, the (mean field) effective potential is simply

$$V_{\rm MF}^{\rm NJL}\left(\{\phi_\alpha^{(\rm c)}\}\right) = -\frac{1}{V_{\mathbb{R}^{1,3}}}\Gamma_{\rm MF}^{\rm NJL}\left(\{\phi_\alpha^{(\rm c)}\}\right) \quad . \tag{6.4.39}$$

Although this is the dominant contribution to the thermodynamic variables, it may be necessary to consider the 1-loop or higher contributions to the effective action [323].

To make connection to low energy hadron phenomenology, we need to calculate the meson propagators through performing second order functional derivatives of the mean field effective action (Eq. (6.4.37) which will in turn allow us to fit the parameters of the NJL model, namely the coupling constant and the UV cut off necessary to regularise the theory. This is not the only way to make the connection to the low energy hadron phenomenology, other authors use the Bethe-Salpeter equation, usually solved using the RPA, which is completely equivalent to the expressions obtained from the effective action approach at this leading order. These parameters will be fit in vacuum to the phenomenology of the pion, namely its mass and decay constant.

The mass of each of the background fields is obtained as the pole in the corresponding propagator. The inverse of these propagators is equal to the second order functional derivative of the effective action (restricted to MFA). In configuration space this is defined as

$$(\Delta_\varphi^{ab})^{-1}(x,y) = \left.\frac{\delta^2\Gamma_{\rm MF}^{\rm NJL}}{\delta\varphi_a(x)\delta\varphi_b(y)}\right|_{\varphi_{a,b}=\varphi_{a,b}^{(\rm c)}} \tag{6.4.40}$$

evaluated at the stationary point. As each of the quark propagators is linear in the background fields we obtain in momentum space

$$(\Delta_\varphi^{ab})^{-1}(p) = -\frac{\delta_{ab}}{2G_\alpha} + i\int\frac{d^4k}{(2\pi)^2}{\rm Tr}\left[\frac{\delta S^{-1}}{\delta\varphi_a}S(k+p)\frac{\delta S^{-1}}{\delta\varphi_b}S(k)\right] \quad , \tag{6.4.41}$$

where we have used Eq. (B.4.2) and Eq. (B.4.3) given in App. B.4 and $G_\alpha = G_{\rm S}$ or $-G_{\rm V}$ depending on the channel. The second term in Eq. (6.4.41) is usually denoted $\Pi_{\varphi_a}(p)$ and referred to as the polarisation function (bubble graph) of φ_a in analogy to QED. Note that we have omitted any additional indices, such as Lorentz indices, on the background fields and the subsequent expressions involving these fields. Of course to make the connection to the physical hadron spectrum we must change to a different flavour basis. Moreover, the mesons (η and η', ω and ϕ, K_{1A} and K_{1B}) are mixed and there are additional issues for scalar mesons. To aid the transition to the physically relevant quark flavour basis we note that

$$(\varphi)_{cd} \equiv (\lambda_a\varphi_a)_{cd} \tag{6.4.42}$$

$$\equiv \left(\sum_{a=0}^{8}\lambda_a\varphi_a\right)_{cd} \tag{6.4.43}$$

$$= \begin{pmatrix} \sqrt{\frac{2}{3}}\varphi_0 + \varphi_3 + \frac{\varphi_8}{\sqrt{3}} & \varphi_1 - i\varphi_2 & \varphi_4 - i\varphi_5 \\ \varphi_1 + i\varphi_2 & \sqrt{\frac{2}{3}}\varphi_0 - \varphi_3 + \frac{\varphi_8}{\sqrt{3}} & \varphi_6 - i\varphi_7 \\ \varphi_4 + i\varphi_5 & \varphi_6 + i\varphi_7 & \sqrt{\frac{2}{3}}\varphi_0 - 2\frac{\varphi_8}{\sqrt{3}} \end{pmatrix}_{cd} \quad (6.4.44)$$

where we have used our standard basis in flavour space $\{\lambda_0, \lambda_1, \ldots, \lambda_8\}$. To make contact with the physical hadron spectrum we change to the basis $\left\{\lambda_0, \lambda_1^{\pm}, \lambda_3, \lambda_4^{\pm}, \lambda_6^{\pm}, \lambda_8\right\}$ with

$$\lambda_1^{\pm} = \frac{\lambda_1 \pm i\lambda_2}{\sqrt{2}}, \qquad \lambda_4^{\pm} = \frac{\lambda_4 \pm i\lambda_5}{\sqrt{2}} \quad \text{and} \quad \lambda_6^{\pm} = \frac{\lambda_6 \pm \mathrm{i}\lambda_7}{\sqrt{2}} \quad . \quad (6.4.45)$$

The Gell-Mann matrices λ_3 and λ_8 form the Cartan subalgebra of $\mathfrak{su}(3)$ i.e its largest commutative subalgebra. The λ_0 matrix combined with λ_3 and λ_8 form the Cartan subalgebra of $\mathfrak{u}(3)$.

Note that there may still not be a direct correspondence between the physical mesons and the auxiliary fields in this basis. This is especially true for the scalar channel. There the experimental situation is more tenuous than for the other mesons. Most notably the $K_0^*(800)$ or κ mesons, which are commonly thought to form the lightest scalar nonet with $\sigma(600)$ and the $a_0(980)$ mesons, are still not even listed in the PDG meson listings [256]. In general, scalar mesons have quite large widths and their experimental verification is an ongoing struggle for theory and experiment [256]. Extraction of their properties are complicated by a number of effects which make it difficult to separate their signal from background noise and alternative origins such as multi-quark interactions and glueballs. The physical mesons may in fact be more complicated than simply a quark and anti-quark pairing. For example, in the case of the $f_0(600)$ or σ meson, it is usually considered to be a resonance resulting from correlated two pion exchange, although alternative descriptions exist such as a glueball [324] or even a dilaton [325–328]. These difficulties in the scalar channel are in stark contrast to the other channels where the mesons are well established.

Here we will only make the specific identification of the auxiliary fields in the pseudo-scalar channel with the corresponding physical mesons. In this sector we have

$$(P)_{cd} = \begin{pmatrix} \sqrt{\frac{2}{3}}P_0 + \varphi_3 + \frac{P_8}{\sqrt{3}} & P_1 - iP_2 & P_4 - iP_5 \\ P_1 + i\varphi_2 & \sqrt{\frac{2}{3}}P_0 - P_3 + \frac{P_8}{\sqrt{3}} & P_6 - iP_7 \\ P_4 + iP_5 & P_6 + iP_7 & \sqrt{\frac{2}{3}}P_0 - 2\frac{P_8}{\sqrt{3}} \end{pmatrix}_{cd} \quad (6.4.46)$$

$$= \begin{pmatrix} \sqrt{\frac{2}{3}}\eta_0 + \pi^0 + \frac{\eta_8}{\sqrt{3}} & \sqrt{2}\pi^+ & \sqrt{2}K^+ \\ \sqrt{2}\pi^- & \sqrt{\frac{2}{3}}\eta_0 - \pi^0 + \frac{\eta_8}{\sqrt{3}} & \sqrt{2}K^0 \\ \sqrt{2}K^- & \sqrt{2}\bar{K}^0 & \sqrt{\frac{2}{3}}\eta_0 - 2\frac{\eta_8}{\sqrt{3}} \end{pmatrix}_{cd} \quad (6.4.47)$$

The low energy phenomenology of the pion is then used to constrain the parameters of our model, which will be described in Sec. 6.5. For the remaining channels we express the auxiliary fields in terms of their quark flavour content and after applying the MFA the so-called chiral ($\rho_i^{\rm s} = \langle\bar{\psi}_i\psi_i\rangle$) and vector ($\rho_i^{\rm v} = \langle\psi_i^\dagger\psi_i\rangle$) condensates. This is the common procedure, which is quite useful and allows us to reuse some notation used earlier in our hadronic equations.

It is well known that the NJL model can describe the hadron spectrum very well but we will not need to make specific use of other mesons in the calculation of the quark matter equation of state. One caveat not yet mentioned in this regard is that their exists an unwanted $U_{\rm A}(1)$ symmetry in our Lagrangian, Eq. (6.3.8). In reality it is broken. Some authors break this symmetry explicitly on the Lagrangian level by introducing the so-called t'Hooft determinantal term, which amounts to a six quark interaction mixing flavour. This additional term alters the behaviour of the in-medium condensates and it has been demonstrated that its inclusion produces the correct mass splitting between the isoscalar-pseudo-scalar η and η' mesons. The physical η and η' mesons are mixtures of the pure η_0 and η_8 fields and are given as a superposition according to a unitary transformation such that

$$\eta = \eta_8\cos\theta - \eta_0\sin\theta \quad , \tag{6.4.48}$$

$$\eta' = \eta_8\sin\theta + \eta_0\cos\theta \quad , \tag{6.4.49}$$

where the mixing angle $\theta \simeq -11.4^\circ$ is obtained from experiment [256]. We note that there are reservations in the literature as to whether this is the correct explanation of the $U_{\rm A}(1)$ anomaly, where this symmetry is broken explicitly [329–331]. For this reason we do not include this additional term in our chosen quark matter model. Nevertheless, incorporation of this t' Hooft term provides a way to incorporate the η–η' mass splitting in the NJL model, more accurately reproducing the hadron spectrum, which is why NJL models incorporating this term have been studied extensively in the literature [306, 332]. In Sec. 6.8, we will make comparisons to NJL models used in Ref. [282] which include this additional term. The corresponding expressions for the effective potential and gap equations for these models are included in App. B.12 for easy reference.

Moreover, upon inclusion of this determinant term the vacuum is destabilised, meaning that the effective potential is no longer bounded from below [312, 313]. This is an unacceptable feature and it has been argued that higher multi-quark interactions (8-quark) can be used to stabilise the vacuum provided certain relations between the couplings hold [312, 313].

In the scalar channel the only non-zero stationary solutions or condensates are the so-called chiral condensates, which in the quark flavour basis are given by

$$S_u^{(\rm c)} \equiv \sqrt{\frac{2}{3}}S_0^{(\rm c)} + S_3^{(\rm c)} + \frac{1}{\sqrt{3}}S_8^{(\rm c)} \quad , \tag{6.4.50}$$

$$S_d^{(\rm c)} \equiv \sqrt{\frac{2}{3}}S_0^{(\rm c)} - S_3^{(\rm c)} + \frac{1}{\sqrt{3}}S_8^{(\rm c)} \quad , \tag{6.4.51}$$

$$S_s^{(\rm c)} \equiv \sqrt{\frac{2}{3}}S_0^{(\rm c)} - \frac{2}{\sqrt{3}}S_8^{(\rm c)} \quad . \tag{6.4.52}$$

Mixed flavour scalar condensates vanish because they break charge conjugation symmetry. For this reason one usually considers the restriction of flavour sums to the $\mathfrak{u}(3)$ Cartan subalgebra such that

$$\sum_{a\in\{0,3,8\}} S_a^{(\mathrm{c})}\lambda_a = 2G_{\mathrm{S}} \sum_{a\in\{0,3,8\}} \langle\bar{\psi}\lambda_a\psi\rangle\lambda_a = 4G_{\mathrm{S}} \begin{pmatrix} \langle\bar{u}u\rangle & 0 & 0 \\ 0 & \langle\bar{d}d\rangle & 0 \\ 0 & 0 & \langle\bar{s}s\rangle \end{pmatrix} \equiv 4G_{\mathrm{S}}\mathrm{diag}(\rho_u^{\mathrm{s}},\rho_d^{\mathrm{s}},\rho_s^{\mathrm{s}})\,, \tag{6.4.53}$$

where we have reused the same notation for quark scalar densities as used earlier in the hadronic equations. In the pseudo-scalar channel all condensates are zero as they break both charge conjugation and parity symmetries. Note that this can always be chosen to be the case as the scalar and pseudo-scalar auxiliary fields are chiral partners of each other allowing one to perform a chiral rotation, so that the ground state has the correct quantum numbers (i.e., preserves parity). As a result, for calculations beyond MFA the pseudo-scalar fields are such that $P_a = P_a^{(\mathrm{q})}$. For the vector channel only same flavour timelike components survive due to the spatial isotropy[4]. Specifically,

$$V_u^{0\ (\mathrm{c})} \equiv \sqrt{\frac{2}{3}}V_0^{0\ (\mathrm{c})} + V_3^{0\ (\mathrm{c})} + \frac{1}{\sqrt{3}}V_8^{0\ (\mathrm{c})} \tag{6.4.54}$$

$$V_d^{0\ (\mathrm{c})} \equiv \sqrt{\frac{2}{3}}V_0^{0\ (\mathrm{c})} - V_3^{0\ (\mathrm{c})} + \frac{1}{\sqrt{3}}V_8^{0\ (\mathrm{c})} \tag{6.4.55}$$

$$V_s^{0\ (\mathrm{c})} \equiv \sqrt{\frac{2}{3}}V_0^{0\ (\mathrm{c})} - \frac{2}{\sqrt{3}}V_8^{0\ (\mathrm{c})} \tag{6.4.56}$$

and similarly the flavour sum found in the quark propagator for the vector channel is

$$\sum_{a\in\{0,3,8\}} V_a^{0\ (\mathrm{c})}\lambda_a = 2G_{\mathrm{V}} \sum_{a\in\{0,3,8\}} \langle\bar{\psi}\gamma^0\lambda_a\psi\rangle\lambda_a \equiv 4G_{\mathrm{V}}\mathrm{diag}(\rho_u^{\mathrm{v}},\rho_d^{\mathrm{v}},\rho_s^{\mathrm{v}}) \quad . \tag{6.4.57}$$

Clearly at zero density the vector contributions vanish. In this thesis the axial-vector contributions are also neglected due to parity considerations.

The explicit expression for the effective potential V_{MF} is most easily obtained in momentum space from Eq. (6.4.39) using the identity (property # 4 in App. B.5)

$$\mathrm{Log}\left[\mathrm{Det}\left(\hat{\mathcal{O}}\right)\right] = \mathrm{Tr}\left[\mathrm{Log}\left(\hat{\mathcal{O}}\right)\right] \quad . \tag{6.4.58}$$

The final expression at zero density, which is derived in App. B.7, is given by

$$V_{\mathrm{MF}}^{\mathrm{NJL}}(M_u,M_d,M_s) = 2iN_{\mathrm{C}} \sum_{i\in\{u,d,s\}} \int \frac{d^4p}{(2\pi)^4}\mathrm{Log}(p^2-M_i^2) + 2G_{\mathrm{S}} \sum_{i\in\{u,d,s\}} (\rho_i^{\mathrm{s}})^2 \tag{6.4.59}$$

$$= 2iN_{\mathrm{C}} \sum_{i\in\{u,d,s\}} \int \frac{d^4p}{(2\pi)^4}\mathrm{Log}(p^2-M_i^2) + \sum_{i\in\{u,d,s\}} \frac{(M_i-m_i)^2}{8G_{\mathrm{S}}} \quad . \tag{6.4.60}$$

[4]homogeneous quark matter

In the process of evaluating the expression in Eq. (6.4.60) we make use of a Wick rotation to Euclidean space. The first term is the divergent vacuum contribution (quark loop term) and must be regularised. In our chosen scheme it evaluates to

$$2iN_{\rm C}\sum_{i\in\{u,d,s\}}\int\frac{d^4p}{(2\pi)^4}{\rm Log}(p^2-M_i^2) \;=\; \frac{3}{8\pi^2}\sum_{i\in\{u,d,s\}}M_i^4\Gamma(-2,\frac{M_i^2}{\Lambda_{\rm UV}^2})\,, \quad (6.4.61)$$

where $\Gamma(a,z)$ is the incomplete gamma function and $\Lambda_{\rm UV}$ is a UV cutoff. The remaining symbols we have introduced, M_i, are the effective, dynamical or constituent quark masses

$$M_i = m_i - 4G_{\rm S}\langle\bar{\psi}_i\psi_i\rangle \quad (6.4.62)$$

where m_i is the current quark mass of flavour $i\in\{u,d,s\}$. The explicit proper time regularised expression is

$$M_i = m_i + \frac{3G_{\rm S}M_i}{\pi^2}\int_{\frac{1}{\Lambda_{UV}^2}}^{\infty}d\tau\frac{1}{\tau^2}e^{-\tau M_i^2} \quad (6.4.63)$$

and its derivation is provided in App. B.8. The chiral condensates can also be calculated from the quark propagator $\rho_i^s = -i{\rm Tr}\,[S_i]$, where the inverse quark propagator in momentum space at zero density can be shown in matrix form to be simply

$$S^{-1}=\begin{pmatrix} S_u^{-1} & 0 & 0\\ 0 & S_d^{-1} & 0\\ 0 & 0 & S_s^{-1}\end{pmatrix} \qquad \text{with} \qquad S_i^{-1}(p)=(\not{p}-m_i+4G_{\rm S}\rho_i^s) \quad . \quad (6.4.64)$$

The effective quark masses, or equivalently the chiral condensates, behave as order parameters for chiral symmetry. After the analytic continuation to Euclidean space the stationary condition of Eq. (6.4.16) translates to the condition that the mean field effective (thermodynamic) potential is determined at a global minimum and must therefore satisfy

$$\frac{\partial V_{\rm MF}^{\rm NJL}}{\partial M_i}=0 \quad \text{and} \quad \frac{\partial^2 V_{\rm MF}^{\rm NJL}}{\partial M_i^2}\geq 0 \quad . \quad (6.4.65)$$

The relevant vacuum equations are now present and we are now in a position to fit the parameters of the model.

6.5 Pion Phenomenology and the Fitting of the NJL Model Parameters

Here we will discuss how pions are treated in the NJL model. To fit our parameters we require that the model reproduce the low energy phenomenology of the pion. The mass of the pion is defined by the pole in its propagator, Eq. (6.4.41). Transforming to the physical basis this condition becomes

$$\Delta_\eta^{-1}(p) = -\frac{1}{2G_{\rm S}}+i\int\frac{d^4p}{(2\pi)^4}{\rm Tr}\left[\bar{\Gamma}_\eta S(k+p)\Gamma_\eta S(k)\right]=0 \quad , \quad (6.5.1)$$

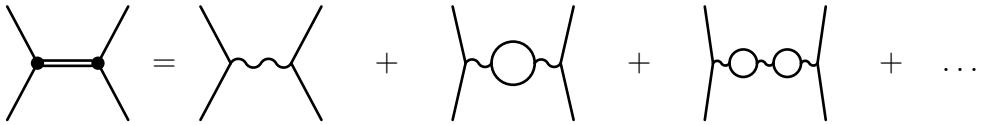

Figure 6.5.1: Bethe–Salpeter in the random phase approximation.

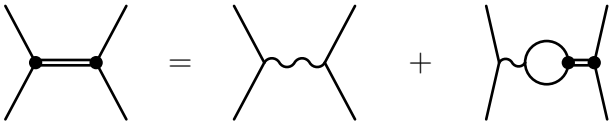

Figure 6.5.2: Bethe–Salpeter in the random phase approximation summed.

where the second term, denoted $\Pi_\eta(p)$, is the polarisation function for particle η. For pions we have the following vertex structures in flavour, Dirac and colour space

$$\begin{aligned}
\bar{\Gamma}_{\pi^0} &= \lambda_3 \otimes i\gamma_5 \otimes \mathbb{1}_{\rm C} \ , & \Gamma_{\pi^0} &= \lambda_3 \otimes i\gamma_5 \otimes \mathbb{1}_{\rm C} \ , \\
\bar{\Gamma}_{\pi^-} &= \frac{1}{\sqrt{2}}(\lambda_1 + i\lambda_2) \otimes i\gamma_5 \otimes \mathbb{1}_{\rm C} \ , & \Gamma_{\pi^-} &= \frac{1}{\sqrt{2}}(\lambda_1 - i\lambda_2) \otimes i\gamma_5 \otimes \mathbb{1}_{\rm C} \ , \\
\bar{\Gamma}_{\pi^+} &= \frac{1}{\sqrt{2}}(\lambda_1 - i\lambda_2) \otimes i\gamma_5 \otimes \mathbb{1}_{\rm C} \ , & \Gamma_{\pi^+} &= \frac{1}{\sqrt{2}}(\lambda_1 + i\lambda_2) \otimes i\gamma_5 \otimes \mathbb{1}_{\rm C} \ .
\end{aligned}$$

Vertex structures for other mesons can be found in Ref. [307].

In the isospin symmetric limit ($m_u = m_d$) combined with the fact that the flavour traces for the 3 pions all give a factor of 2 and the colour trace a factor of $N_{\rm c} = 3$, the polarisation function for all the pions reduces to

$$\Pi_\pi(k) = 6i \int \frac{d^4p}{(2\pi)^4} {\rm Tr}_{\rm D} \left[i\gamma_5 S_\ell(p + \frac{k}{2}) i\gamma_5 S_\ell(p - \frac{k}{2}) \right] \quad , \tag{6.5.2}$$

where the trace ${\rm Tr}_{\rm D}$ is over Dirac space and $S_\ell = S_u = S_d$ is the light quark propagator. Calculation of the pion polarisation graph in the proper time regularisation scheme can be found in App. B.9 and is explicitly given by

$$\frac{1}{i}\Pi_\pi(k^2) = -\frac{3i}{\pi^2} I_1(M^2) - \frac{3k^2 i}{4\pi^2} I_2(k^2, M^2) \quad , \tag{6.5.3}$$

where

$$I_1(M^2) = \int_{1/\Lambda_{UV}^2}^{\infty} d\tau \ \frac{e^{-\tau M^2}}{2\tau^2} \quad , \tag{6.5.4}$$

$$I_2(k^2, M^2) = \int_0^1 dx \int_{1/\Lambda_{UV}^2}^{\infty} d\tau \ \frac{e^{-\tau\left[k^2(x^2-x)+M^2\right]}}{\tau} \quad . \tag{6.5.5}$$

In regularising the divergent integrals (Eqs. (6.5.4-6.5.5)) the ultra-violet cut-off $\Lambda_{\rm UV}$ was introduced (see App. B.6). Equation 6.5.3 can be evaluated numerically. A similar procedure can be followed for other mesons.

An alternative and often used approach to obtaining meson masses is to solve the Bethe-Salpeter equation (BSE) [333], which is the relativistic two-body bound state equation. This approach is equivalent to the above method when restricted to the random phase approximation (RPA), which is graphically depicted in Fig. 6.5.1 and summed in Fig. 6.5.2 for mesons in the NJL model. Note that in these figures the quark–quark interaction is drawn as non-local for aesthetic reasons, but in this model it should be understood that this interaction is indeed local.

The inverse pion propagator defined in Eq. (6.5.1) is not just the free pion propagator, but it also contains a momentum dependence, which can be understood as momentum dependent coupling such that,

$$\Delta_\pi(q^2) = \frac{g^2_{\pi qq}(q^2)}{q^2 - m_\pi^2} \quad , \tag{6.5.6}$$

where m_π is the free pion mass. To obtain the on-shell pion–quark coupling constant we evaluate the coupling at the pole

$$g_{\pi qq} \equiv g_{\pi qq}(q^2 = m_\pi^2) \quad . \tag{6.5.7}$$

This is done by expanding the pion polarisation function about the pole

$$\Pi_\pi(q^2) = \Pi_\pi(m_\pi^2) + (q^2 - m_\pi^2)\frac{\partial \Pi_\pi(q^2)}{\partial q^2}\bigg|_{q^2=m_\pi^2} + \ \ldots \tag{6.5.8}$$

and substituting back into Eq. (6.5.1) yielding

$$\begin{aligned} \Delta_\pi(q^2) &= \frac{-2G_{\rm S}}{1 - 2G_{\rm S}\Pi_\pi(q^2)} & (6.5.9)\\ &= \frac{-2G_{\rm S}}{1 - 2G_{\rm S}\left(\Pi_\pi(m_\pi^2) + (q^2 - m_\pi^2)\frac{\partial \Pi_\pi(q^2)}{\partial q^2}\Big|_{q^2=m_\pi^2} + \ \ldots\right)} \quad . & (6.5.10) \end{aligned}$$

Using the pole condition $1 - 2G_{\rm S}\Pi_\pi(m_\pi^2) = 0$, we obtain

$$\Delta_\pi(q^2) = \frac{g^2_{\pi qq}}{q^2 - m_\pi^2} \quad , \tag{6.5.11}$$

where we have defined the on-shell pion–quark coupling constant as

$$g^2_{\pi qq} \equiv \left(\frac{\partial \Pi_\pi(q^2)}{\partial q^2}\bigg|_{q^2=m_\pi^2}\right)^{-1} \quad . \tag{6.5.12}$$

To calculate the pion decay constant we take as our starting point the matrix element, Eq. (2.2.11),

$$\langle 0|\bar\psi(0)\gamma^\mu\gamma_5\frac{\lambda_a}{2}\psi(0)|\pi_b\rangle = i f_\pi q^\mu \delta_{ab} \quad . \tag{6.5.13}$$

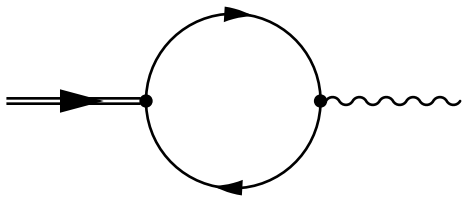

(6.5.14)

Figure 6.5.3: Graphical depiction of the matrix element associated to pion decay.

This matrix element is graphically depicted in Fig. (6.5.3). This matrix in expanded form reads

$$
\begin{aligned}
iq^\mu f_\pi \delta_{ab} &= -g_{\pi qq}\int \frac{d^4p}{(2\pi)^4}\mathrm{Tr}\left[\gamma^\mu\gamma_5\frac{\lambda_a}{2}S(p+\frac{1}{2}q)\gamma_5\lambda_b S(p-\frac{1}{2}q)\right] && (6.5.15)\\
&= -g_{\pi qq}N_{\mathrm{C}}\delta_{ab}\int \frac{d^4p}{(2\pi)^4}\mathrm{Tr}\left[\gamma^\mu\gamma_5 S_\ell(p+\frac{1}{2}q)\gamma_5 S_\ell(p-\frac{1}{2}q)\right] , && (6.5.16)
\end{aligned}
$$

where in the second line we evaluated the flavour and colour traces, $\mathrm{Tr}\frac{\lambda_a}{2}\lambda_b = \delta_{ab}$, $\mathrm{Tr}[\mathbb{1}_{\mathrm{C}}] = N_{\mathrm{C}}$ and the remaining trace is over Dirac space. The explicit expressions for the pion–quark coupling and the pion decay constant in the Schwinger proper time regularisation scheme are given in App. B.10 and B.11, respectively.

We constrain our model parameters in two ways. In parameter set PS1, we take as input the constituent quark masses $M_\ell = 400$ MeV and $M_s = 563$ MeV, the pion's mass $m_\pi = 140$ MeV and its decay constant $f_\pi = 93$ MeV. By requiring these values for M_ℓ and f_π, the UV cut-off, Λ_{UV}, is constrained to be 636.67 MeV. Then using the pole condition for the pion with m_π, M_ℓ, and Λ_{UV} the scalar coupling G_{S} is found to be 19.76 GeV^{-2}. Finally, using M_α, Λ_{UV} and G_{S} the current quark masses can be calculated from

$$
m_\alpha = M_\alpha - \frac{3G_{\mathrm{S}}M_\alpha}{\pi^2}\int_{\frac{1}{\Lambda_{UV}^2}}^{\infty} d\tau \frac{e^{-\tau M_\alpha^2}}{\tau^2} \quad , \qquad (6.5.17)
$$

where $\alpha = \ell,\, s$.

An additional cut-off, Λ_{IR} can be introduced in our regularisation procedure by including an additional regulating function $r_{\mathrm{IR}}(\tau) \equiv \Theta(\frac{1}{\Lambda_{\mathrm{IR}}^2} - \tau)$. This new cut-off is generally considered to be related to confinement as it can crudely simulate one of its key features that free quarks do not propagate [314],

$$
\frac{1}{k_{\mathrm{E}}^2 + M_i^2} = \int_{\frac{1}{\Lambda_{\mathrm{UV}}^2}}^{\frac{1}{\Lambda_{\mathrm{IR}}^2}} d\tau\; e^{-\tau(k_{\mathrm{E}}^2+M_i^2)} = \frac{e^{-(k_{\mathrm{E}}^2+M_i^2)/\Lambda_{\mathrm{UV}}^2} - e^{-(k_{\mathrm{E}}^2+M_i^2)/\Lambda_{\mathrm{IR}}^2}}{k_{\mathrm{E}}^2 + M_i^2} \quad . \qquad (6.5.18)
$$

Choosing a value $\Lambda_{\mathrm{IR}} \sim 200$ MeV results only in small variation in parameters, see Table 6.5.1 for a comparison. In quark matter, the infra-red cut-off is not relevant and is taken to be zero in all quark matter calculations.

In our first parameter set, PS1, the calculated current quark mass is ~ 10 MeV, larger than the values typically used in the three momentum regularised versions of the model. As an additional test of sensitivity of the parameters to our fitting procedure we take instead the current quark masses as input, $m_\ell = 5.5$ MeV and $m_s = 135.7$ MeV, the pion's mass $m_\pi = 140$ MeV and its decay constant $f_\pi = 93$ MeV. By following a similar procedure as above we determine the other parameters and calculate the constituent quark mass. This leads to a new and substantially different parameter set, PS2, with the constituent quark mass considerably lower. When fitting our model parameters, we are enforcing a scale in our model. With this in mind we should compare and choose the parameter set which is both consistent with hadron phenomenology (enforced through the above mentioned fitting procedures) and also favourable for modelling high density quark matter. We will compare the proper time regularised model with both parameter sets to the three momentum regularised model [282] in Sec. 6.8.

6.6 At Finite Density

At finite density we have conservation of baryon number and associated chemical potentials. To handle this in the grand canonical formalism an extra term is added to our NJL Lagrangian Eq. (6.3.8),

$$\mathcal{L}_{\rm NJL} \to \mathcal{L}_{\rm NJL} + \bar{\psi}\hat{\mu}\gamma^0\psi \tag{6.6.1}$$

where $\hat{\mu}$ is the chemical potential matrix given by $\hat{\mu}$ =diag(μ_u,μ_d,μ_s). The derivation of the effective potential follows through as in the previous section in vacuum, except with extra terms in the effective potential and gap equations for the quarks. Because of the Fermi sea of quarks and at finite density the vector interaction will contribute, the effective potential will have extra terms. This extension is straightforward and is performed in App. B.7.

The inverse quark propagator in momentum space is now of the form

$$S_i^{-1}(p) = (p_0 + \mu_i - 4G_{\rm V}\rho_i^v)\gamma^0 - \vec{p}\cdot\vec{\gamma} - m_i + 4G_{\rm S}\rho_i^s \tag{6.6.2}$$

for each flavour i. Using Eq. (6.6.2) in Eq. (6.4.39) the final expression at finite density for the effective potential which is derived in the appendices is given by

$$V_{\rm MF}(\{M_i\},\{\mu_i\}) \;=\; V_{\rm div}(\{M_i\},\{\mu_i\}) + V_{\rm fin}(\{M_i\},\{\mu_i\}) \quad , \tag{6.6.3}$$

where the first part is the divergent contribution and must be regularised. We choose to regularise using Schwinger's covariant proper time method. The divergent part is derived in App. B.7 to be

$$\begin{aligned} V_{\rm div}(\{M_i\},\{\mu_i\}) &= V_{\rm div}^{\rm vac}(\{M_i\},\{\mu_i\}) + 2G_{\rm S}\sum_{i\in\{u,d,s\}}(\rho_i^{\rm s})^2 - 2G_{\rm S}\sum_{i\in\{u,d,s\}}(\rho_{i0}^{\rm s})^2 \\ &= V_{\rm div}^{\rm vac}(\{M_i\},\{\mu_i\}) + \sum_{i\in\{u,d,s\}}\frac{(M_i-m_i)^2}{8G_{\rm S}} - \sum_{i\in\{u,d,s\}}\frac{(M_{i0}-m_i)^2}{8G_{\rm S}} \quad . \end{aligned} \tag{6.6.4}$$

Parameter set	m_ℓ [MeV]	m_s [MeV]	M_ℓ [MeV]	M_s [MeV]	Λ_{IR} [MeV]	Λ_{UV} [MeV]	G_{S} [GeV^{-2}]	G_{D} [GeV^{-5}]	$\lvert\langle\bar{\psi}_\ell\psi_\ell\rangle_0\rvert^{1/3}$ [MeV]	$\lvert\langle\bar{\psi}_s\psi_s\rangle_0\rvert^{1/3}$ [MeV]
Proper time reg.										
PS1†	17.08	279.81	400*	563*	0*	636.67	19.76	-	169.20	153.01
PS1-IR200	16.93	278.69	400*	563*	200*	638.46	19.60	-	169.69	153.64
PS1-IR225	16.67	276.55	400*	563*	225*	641.70	19.31	-	170.57	154.78
PS1-IR250	16.23	272.60	400*	563*	250*	647.57	18.82	-	172.10	156.83
PS2†	5.5*	135.7*	201.07	440.41	0*	1078.9	3.17	-	249.0	288.67
PS2-IR200	5.5*	135.7*	214.36	444.10	200*	1053.9	3.41	-	248.25	282.69
PS2-IR225	5.5*	135.7*	220.22	446.74	225*	1045.76	3.51	-	248.13	280.76
PS2-IR250	5.5*	135.7*	226.72	450.10	250*	1037.94	3.62	-	248.05	278.89
Three mom. reg.										
HK† [282, 308]	5.5	135.69	334.59	527.28	-	631.38	4.60	92.57	246.72	266.94

Table 6.5.1: We fitted all parameter sets using low energy hadron phenomenology. The proper time parameter sets used $f_\pi = 93$ MeV and $m_\pi = 140$ MeV. The three momentum regularised parameter set HK [282, 308] used $f_\pi = 93$ MeV, $m_\pi = 138$ MeV, $m_K = 495.7$ MeV, $m_{\eta'} = 957.5$ MeV and $m_\ell = 5.5$ MeV. An $(*)$ marks variables used in the fitting procedure. A dagger $(\dagger)$ indicates parameter sets used in other plots.

(6.6.5)

The first is the divergent vacuum contribution (quark loop term) and is

$$V_{\rm div}^{\rm vac}(\{M_i\},\{\mu_i\}) = 2iN_c \sum_{i\in\{u,d,s\}} \int \frac{d^4k}{(2\pi)^4}\, {\rm Log}\left[\frac{k^2-M_i^2+i\epsilon}{k^2-M_{i0}^2+i\epsilon}\right] \quad . \tag{6.6.6}$$

In App. (B.7) Eq. (6.6.6) is evaluated in our chosen scheme giving

$$V_{\rm div}^{\rm vac}(M_u,M_d,M_s) \;=\; \frac{3}{8\pi^2}\sum_{i\in\{u,d,s\}}\left[M_i^4\Gamma(-2,\frac{M_i^2}{\Lambda_{\rm UV}^2}) - M_{i0}^4\Gamma(-2,\frac{M_{i0}^2}{\Lambda_{\rm UV}^2})\right] \tag{6.6.7}$$

where $\Gamma(a,z)$ is the incomplete gamma function. In Eqs. (6.6.3-6.6.7) we have subtracted the constant vacuum contribution, these terms are labelled by subscript 0. The subtraction is performed so that the pressure ($P_{\rm MF} = -V_{\rm MF}$) at zero density is zero. From the Gibbs-Duhem relation, this also implies the energy density is also zero in vacuum. The finite contribution to the effective potential is

$$V_{\rm fin}(\{M_i\},\{\mu_i\}) \;=\; V_{\rm Fermi}(\{M_i\},\{\mu_i\}) - 2G_{\rm V}\sum_{i\in\{u,d,s\}}(\rho_i^{\rm v})^2 \tag{6.6.8}$$

$$\;=\; V_{\rm Fermi}(\{M_i\},\{\mu_i\}) - \sum_{i\in\{u,d,s\}}\frac{(\tilde{\mu}_i-\mu_i)^2}{8G_{\rm V}} \quad . \tag{6.6.9}$$

The contribution associated to the Fermi sea of quarks is

$$V_{\rm Fermi}(\{M_i\},\{\mu_i\}) \;=\; -2N_{\rm C}\sum_{i\in\{u,d,s\}}\int\frac{d^3p}{(2\pi)^3}\,\Theta(\tilde{\mu}_i-E_{p,i})(\tilde{\mu}_i-E_{p,i})\,, \tag{6.6.10}$$

where we have introduced the "reduced" chemical potential

$$\tilde{\mu}_i = \mu_i - 4G_{\rm V}\langle\psi_i^\dagger\psi_i\rangle \quad . \tag{6.6.11}$$

6.7 Flavour Independent Vector Interaction

Before discussing the numerical results for the thermodynamic properties of interest, we anticipate that the vector interaction is important (as is well known, see Ref. [295]) and that the strength and type of this interaction is crucial for a realistic description of quark matter. For this reason we introduce a "simplified" vector interaction which is flavour independent, such that

$$\mathcal{L}_{\rm v} = -g_{\rm V}(\bar{\psi}\gamma^\mu\psi)^2 \quad . \tag{6.7.1}$$

This form of vector interaction has been used in many NJL studies, particularly interesting are those that use it to produce high mass neutron stars if the coupling is large enough, see for example Refs. [282, 334].

With the vector interaction given by Eq. (6.7.1), rather than the flavour dependent interaction derived earlier (see Sec. 6.3), the reduction in the chemical potentials is different between these two interactions.

$$\tilde{\mu}_i = \begin{cases} \mu_i - 4G_{\rm V}\rho_{\rm i}^{\rm v} & \text{for flavour dependent vector interaction} \\ \mu_i - 2g_{\rm V}\rho_{\rm tot} & \text{for flavour independent vector interaction} \end{cases} . \tag{6.7.2}$$

The factor of two difference, in the reduction, between them is due to the flavour sum in the flavour dependent vector interaction. This summation is also why each of the reduced chemical potentials is only dependent on its own density. The other factor of two comes from performing the mean field approximation and our choice of normalization for the interaction Lagrangians, which is why it is present for both types of interactions.

By the same token, the effective potential will differ depending on the type of vector interaction. The vector contributions to the effective potential are

$$V_{\rm vec} = \begin{cases} -2G_{\rm V} \sum\limits_{i\in\{u,d,s\}} (\rho_{\rm i}^{\rm v})^2 & \text{for flavour dependent vector interaction} \\ -g_{\rm V}\rho_{\rm tot}^2 & \text{for flavour independent vector interaction} \end{cases} . \tag{6.7.3}$$

The latter has additional cross terms contributing to the effective potential and hence likely to increase the pressure.

Clearly, in symmetric two flavour quark matter ($\rho_{\rm u} = \rho_{\rm d}$ and $\rho_{\rm s} = 0$) these two interactions are equivalent, but differ otherwise. In asymmetric two flavour quark matter they will differ and there should be a substantial difference when strange quarks are present. In flavour symmetric three flavour quark matter ($\rho_{\rm q} \equiv \rho_{\rm u} = \rho_{\rm d} = \rho_{\rm s}$) the additional cross terms for the flavour independent interaction could give a substantial increase in pressure coming from the vector contribution as

$$V_{\rm vec} = \begin{cases} -6G_{\rm V}\rho_{\rm q}^2 & \text{for flavour dependent vector interaction} \\ -9g_{\rm V}\rho_{\rm q}^2 & \text{for flavour independent vector interaction} \end{cases} . \tag{6.7.4}$$

Of course, each of the quark chemical potentials will be reduced by the same amount, determined by the total quark density, as opposed to the flavour dependent interaction, where each quark's chemical potential is only reduced by its own density. This difference will also affect the pressure coming from both models. Consequently, the type of vector interaction could be important in the description of hybrid and quark stars, particularly when strange quarks are involved.

6.8 Numerical Results and Discussion

In this section we will present and discuss the numerical results of the NJL model parameter sets PS1, PS2 and HK. We begin with the behaviour of various quantities of interest, in particular the constituent quark mass, as a function of quark chemical potential. This is followed by the density dependence of quark masses in flavour symmetric quark matter ($\rho_{\rm u} = \rho_{\rm d} = \rho_{\rm s}$). We will then conclude with the main results of this section—the properties of quark matter in beta equilibrium with leptons. These

quark matter equations of state will then be used in Ch. 7 to study hybrid stars, where the HF-QMC equation of state developed in Ch. 5 will be used for the description of the hadronic matter.

Chiral symmetry is broken explicitly in all parameter sets considered (see Table 6.5.1) by the presence of a non-zero current quark mass but it is also broken dynamically in vacuum for sufficiently large coupling strength [306]. All parameter sets produce a constituent quark mass which is significantly larger than the current quark mass in vacuum for all flavours. The constituent quark masses, or equivalently their condensates, are the order parameters of chiral symmetry. The chirally broken phase is marked by a large constituent quark mass and its approximate restoration is expected to occur at large chemical potential for all three parameter sets.

The numerical results presented in Figure 6.8.1, show the behaviour of the constituent quark masses (a–c), reduced quark chemical potentials (d–f) and normalised densities (g–i) as a function of the quark chemical potential ($\mu = \mu_\ell = \mu_s$) for the parameter set PS1. The plots from left to right have varying vector coupling strength. In the first column the vector coupling is set to zero, and in the second and third columns they are $G_\mathrm{V} = G_\mathrm{S}/2$ and $G_\mathrm{V} = G_\mathrm{S}$, respectively. Figures 6.8.2 and 6.8.3 are the same as Fig. 6.8.1, but for the parameter sets PS2 and HK respectively.

The constituent quark masses are determined through the solution of the so-called gap equation, obtained from the minimisation of the effective potential. It must be solved carefully, as it is well known that the NJL effective potential can have multiple minima, although only the global minimum is the physically relevant solution to the gap equation. The gap equation can be solved by either using a non-linear solver to find the solution to Eq. (B.8.24) or a minimisation routine can be applied directly to the effective potential, Eq. (6.6.3). We opt for the former utilising the GNU Scientific Library (GSL) [335].

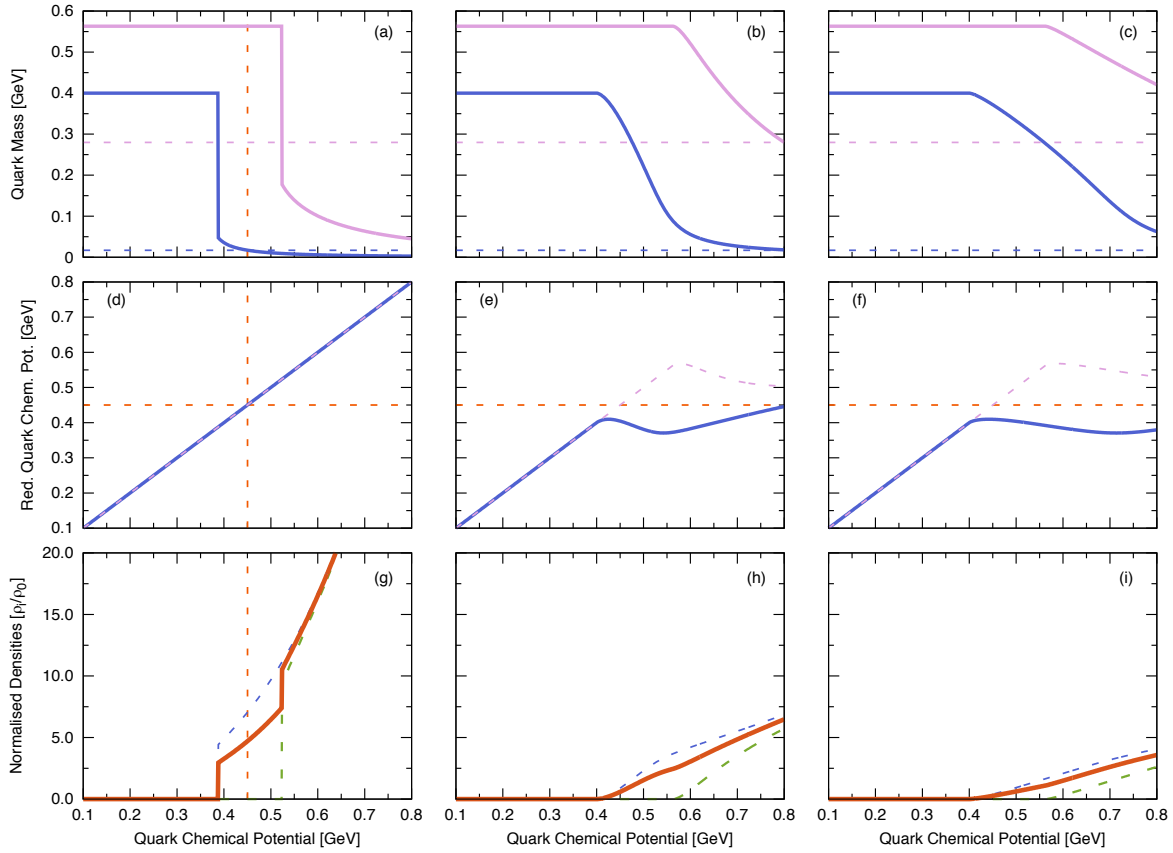

Figure 6.8.1: The behaviour of the constituent quark masses (a–c), reduced quark chemical potentials (d–f) and normalised densities (g–i) as a function of the quark chemical potential ($\mu = \mu_\ell = \mu_s$) for the parameter set PS1. The plots from left to right have varying vector coupling strength. In the first column the vector coupling is set to zero, and in the second and third columns they are $G_{\rm V} = G_{\rm S}/2$ and $G_{\rm V} = G_{\rm S}$, respectively. Specific line types are: (a–c) M_ℓ (blue solid), m_ℓ (blue dashed), M_s (pink solid), and m_s (pink dashed); (d–f) $\tilde{\mu}_\ell$ (blue solid) and $\tilde{\mu}_s$ (pink dashed); (g–i) ρ_ℓ/ρ_0 (blue dashed), ρ_s/ρ_0 (green dashed) and the total baryonic density ρ/ρ_0 (red solid), where $\rho_0 = 0.17$ fm^{-3} is the nuclear saturation density; (a,d–f,g) critical (reduced) chemical potential $\mu_{\rm crit}$ ($\tilde{\mu}_{\rm crit}$) are red dashed.

To ensure that we obtain the correct solution we solve the Eq. (B.8.24) with multiple starting points. For each solution found we evaluate the effective potential, the solution which gives the smallest value of the effective potential is chosen as the correct solution. This was implemented by two different methods. First, a few well chosen starting points were picked for the iterative procedure which should cover the entire range of solutions. In the second slightly more sophisticated approach, a random number generator was used to obtain starting values for a user defined number of starting points. The larger this number, the more confident one can be that the correct solution is found. It was found that both procedures produced equivalent and reproducible results, although to be definite all figures presented here used the latter method.

In the NJL model, which models the dynamical generation of mass breaking chiral

symmetry, it is unnatural for the constituent quark mass to be smaller than current quark mass. Obviously, this can occur when the finite density terms overwhelm the vacuum terms in the gap equation (see Eq. (B.8.24)). One would naively expect that this would not occur before the UV cut-off, which was introduced to regulate the model, effectively setting the scale of the model using relevant hadron phenomenology. This is quite plainly not the case for parameter PS1, see Fig. 6.8.1 plot (a). The constituent quark mass for light quarks very abruptly drops at $\mu \simeq 388$ MeV. Shortly after this first order transition occurs, the constituent quark mass becomes smaller than the current quark mass at $\mu \simeq 451$ MeV—which is moderately lower than the cut-off $\Lambda_{\mathrm{UV}} \simeq 637$ MeV. More seriously, however, is the behaviour of the constituent strange quark mass, which drops sharply below its current quark mass as soon as it is energetically favourable to appear at $\mu \simeq 524$ MeV—compare with the calculated strange quark density in Fig. 6.8.1 plot (g).

The behaviour of the constituent quark masses as a function of quark chemical potential for parameter set PS2 are markedly different from the behaviour for PS1, compare plot (a) in Figs. 6.8.1 and 6.8.2. The only difference in the fitting procedure between the two parameter sets is that we chose small values for the current quark masses and calculated the constituent quark masses, as opposed to choosing quite large values for the constituent quark masses and calculating the current quark masses for PS1 (see Table 6.5.1). To begin with, there is no-longer a first order transition for all flavours in the absence of vector coupling. The transition between the chirally broken phase and the symmetric phase is smooth with the constituent quark masses still going below the current quark masses at $\mu \simeq 763$ MeV for light quarks and $\mu \simeq 771$ MeV for strange quarks—once again at a chemical potential moderately lower than the cut-off $\Lambda_{\mathrm{UV}} = 1.0789$ GeV. The calculated densities in PS2 increase with increasing chemical potential as expected, however in a considerably smoother fashion than in PS1. This is clearly because of the smoother behaviour of the constituent quark masses.

Figure 6.8.3 shows the same quantities as Figs. 6.8.1 and 6.8.2 but for the three momentum regularised NJL model with t' Hooft determinantal term. This model has been used extensively in the literature [306–308, 311], and in particular, it was recently used to study hybrid stars in Ref. [282]. This variation of the NJL model is included for comparative purposes using the HK parameter set [308]. Table 6.5.1 contains the HK parameter set for convenience, but the interested reader is referred to Ref. [308] for how it was obtained. The values of the current quark masses in this parameter set were used as input for our proper time regularised parameter set PS2, so a close comparison could be performed. Current quark masses of the HK parameter set are the same as in PS2, but the constituent quark masses are considerably larger and comparable to the ones used in PS1. Moreover, the scalar coupling and UV cut-off are comparable to their counter parts in PS2 and PS1, respectively. The densities are similar to those found for the PS2 parameter set but not quite as smooth.

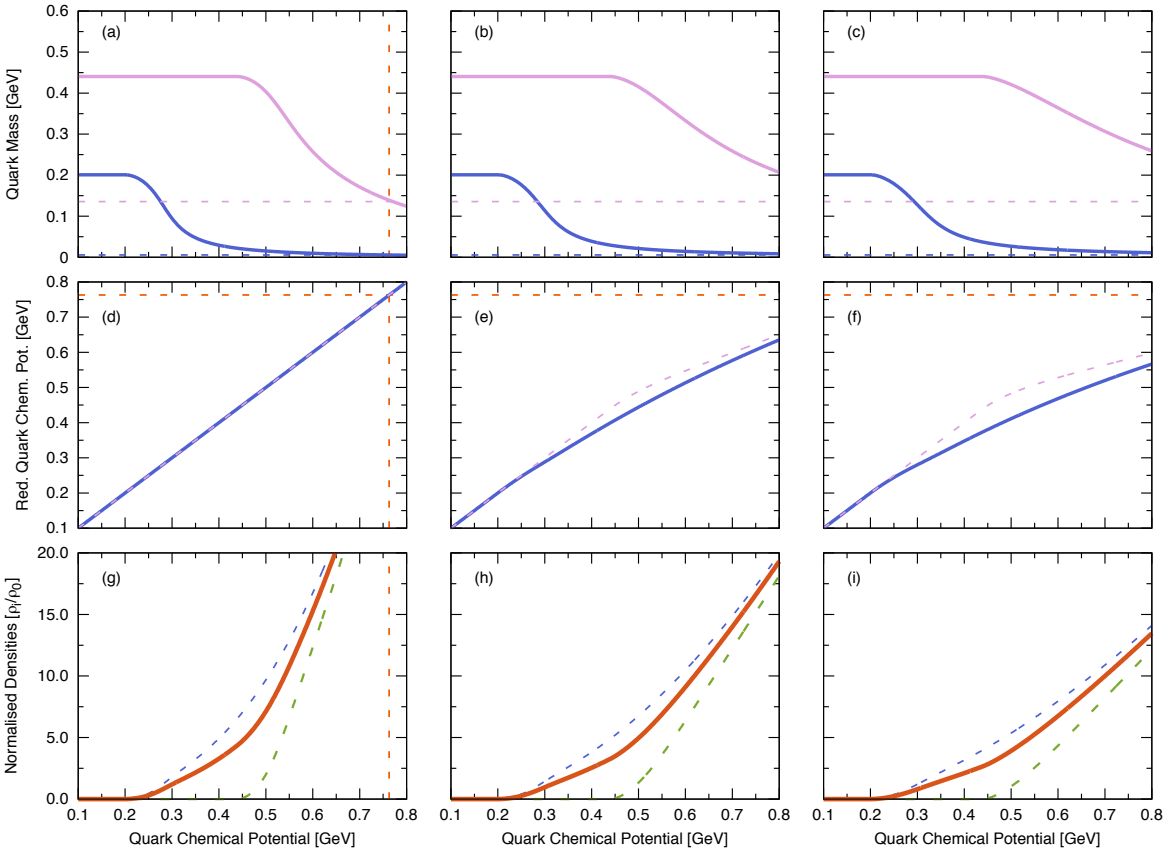

Figure 6.8.2: Same as Fig. 6.8.1 for the parameter set PS2.

The t' Hooft determinantal term has a pronounced effect on the constituent quark masses—see Fig. 6.8.3 plots (a–c). The mixing of different flavours produced by the flavour determinant means that the constituent quark masses of different flavours are inter-related. In plots (a—c) the strange quark mass drops abruptly when the light quark mass drops, before it is actually favourable to appear (see plots (g–i)), illustrating the dependence of the strange quark mass on the light quark condensates.

Of considerable interest is that, unlike in the proper time regularised models described above, the constituent quark masses of both the light and strange quarks do not go below the current quark mass until the quark chemical potential approximately reaches the UV cut-off. This is somewhat disconcerting as we could interpret this as a signal that the NJL model with our chosen regularisation scheme is breaking down and, in the case of PS1, it is occurring at only a moderate chemical potential. Albeit, in the case of PS2 it breaks down at a chemical potential greater than in the HK parameter set, but still lower than the UV cut-off. The regularisation scheme is a defining feature of the model, therefore this difference should be clearly understood. Furthermore, we will be applying the NJL model to describe hybrid stars in Ch. 7, where the inner core densities are expected to be immense. The large quark chemical potentials that are anticipated to be achieved could surpass the breaking point of the model.

To address this concern we now examine why in the proper time regularisation scheme, the constituent quark mass, M_i, goes below the current quark mass, m_i, at

moderate quark chemical potential for parameter set PS1. Also, why this does not occur until a larger chemical potential is reached for PS2 but still below the UV cut-off. Likewise, we would also like to understand why for the three momentum regularised model, using the HK parameter set, this does not occur until the chemical potential approximately reaches the cut-off. As was pointed out in appendix B of Ref. [336], this can be understood by studying the in-medium gap equation in detail. The in-medium gap equation takes the form (see App. B.8)

$$M_i = m_i + \frac{3G_{\rm S}M_i}{\pi^2}\left(\int_{\frac{1}{\Lambda_{\rm UV}^2}}^{\infty} d\tau \frac{e^{-\tau M_i^2}}{\tau^2} - 4\int_0^{\sqrt{-M_i^2+\mu_i^2}} \frac{p^2 dp}{\sqrt{p^2+M_i^2}}\right) \quad (6.8.1)$$

$$\equiv m_i + \frac{3G_{\rm S}M_i}{\pi^2}\left(I_{\rm v}(M_i) - I_{\rm Fermi}(M_i,\mu_i)\right) \quad . \quad (6.8.2)$$

When the finite density contribution is greater than the vacuum contribution, the constituent quark mass is smaller than the current quark mass. This occurs at some critical chemical potential denoted $\mu_{\rm crit}$. The value of the critical chemical potential is dependent on the regularization scheme through the vacuum contribution to the gap equation only, as the Fermi term is finite. It can be estimated by performing an expansion of vacuum and finite density terms about $M_i/\Lambda_{\rm UV} = 0$. In the proper time scheme, the pertinent integral that must be expanded needs be treated with care, because of the singular nature of this integral in the limit $M_i/\Lambda_{\rm UV} \to 0^+$. Specifically, it contains a logarithmic singularity. Because of this singularity the Taylor series expansion has a zero radius of convergence and it therefore must be treated as an asymptotic expansion rather than a Taylor expansion. We will give the details of this expansion here, deriving the result of Ref. [336].

To do the expansion for the vacuum term we first perform a change of variables such that $t = \tau M_i^2$, $d\tau = dt/M_i^2$, leading to

$$I_{\rm v}(M_i) = \int_{\frac{1}{\Lambda_{\rm UV}^2}}^{\infty} d\tau \frac{e^{-\tau M_i^2}}{\tau^2} = \int_{\frac{M_i^2}{\Lambda_{\rm UV}^2}}^{\infty} \frac{dt}{M_i^2}\frac{e^{-t}}{(t/M_i^2)^2} = M_i^2 \int_{\frac{M_i^2}{\Lambda_{\rm UV}^2}}^{\infty} dt\ \frac{e^{-t}}{t^2} \quad . \quad (6.8.3)$$

We now introduce the rescaled mass $x = (M_i/\Lambda_{\rm UV})^2$ and write the integral as

$$I_{\rm v}(M_i) = \Lambda_{\rm UV}^2 x I(x) = \Lambda_{\rm UV}^2 x \int_x^{\infty} dt\ \frac{e^{-t}}{t^2} \quad . \quad (6.8.4)$$

This integral can be put in the form

$$\Lambda_{\rm UV}^2 x I(x) = \Lambda_{\rm UV}^2 x\left[\int_x^{\infty} \frac{e^{-t}}{t^2}\, dt\right] = \Lambda_{\rm UV}^2 x\left[\frac{e^{-x}}{x} + {\rm Ei}(-x)\right] = \Lambda_{\rm UV}^2 x\left[\frac{e^{-x}}{x} - {\rm E}_1(x)\right] \quad . \quad (6.8.5)$$

The asymptotic expansion of Eq. (6.8.5) is then

$$\Lambda_{\rm UV}^2 x I(x) = \Lambda_{\rm UV}^2\left[e^{-x} - x{\rm E}_1(x)\right]$$

$$\sim \Lambda_{\rm UV}^2\left[1 - x + \ldots \quad - x\left(-\gamma + {\rm Log}|x| + \sum_{n=1}^{\infty}\frac{(-1)^{n+1}x^n}{n.n!}\right)\right] \quad \text{as} \quad x \to 0^+$$

$$\sim \quad \Lambda_{\rm UV}^2\,[1+x(\gamma-1)+\ldots] \qquad \text{as} \quad x\to 0^+ \quad . \tag{6.8.6}$$

To obtain the second line we Taylor expanded the exponential and used the methods of Ref. [322] to perform the asymptotic expansion of $\mathrm{E}_1(x)$. The symbol γ is the Euler constant and in the third line we neglected terms of order x^2.

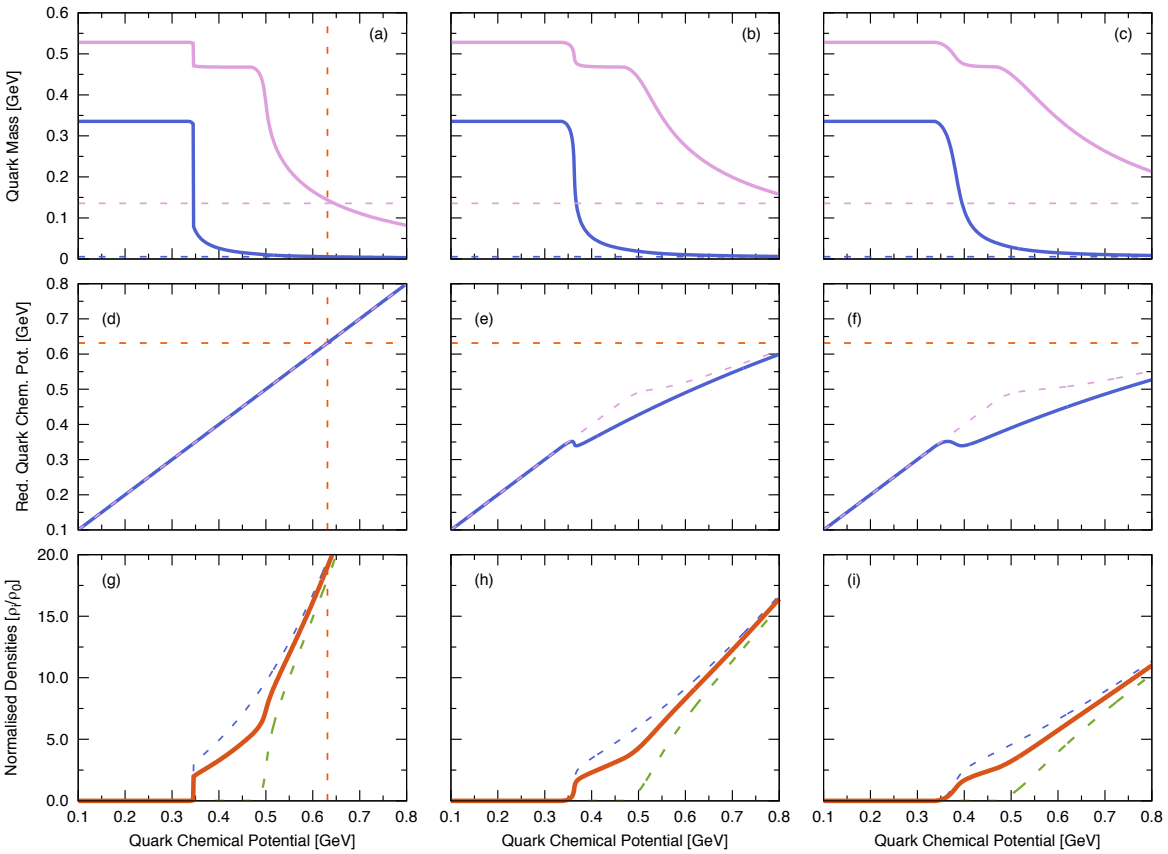

Figure 6.8.3: Same as Fig. 6.8.1 for the parameter set HK.

The expansion of the finite density contribution is straightforward and can be shown to be

$$\begin{aligned} I_{\rm Fermi}(M_i,\mu_i) &= 4\int_0^{\sqrt{-M_i^2+\mu_i^2}} \frac{p^2dp}{\sqrt{p^2+M_i^2}} \\ &= 4.\frac{1}{2}\left(\mu_i\sqrt{\mu_i^2-M_i^2}-M_i^2\mathrm{Log}\left[\frac{\mu_i+\sqrt{\mu_i^2-M_i^2}}{M_i}\right]\right) \\ &= 2\Lambda_{\rm UV}^2\left(\left(\frac{\mu_i}{\Lambda_{\rm UV}}\right)\sqrt{\left(\frac{\mu_i}{\Lambda_{\rm UV}}\right)^2-\left(\frac{M_i}{\Lambda_{\rm UV}}\right)^2}\right. \\ &\qquad \left.-\left(\frac{M_i}{\Lambda_{\rm UV}}\right)^2\mathrm{Log}\left[\frac{\left(\frac{\mu_i}{\Lambda_{\rm UV}}\right)+\sqrt{\left(\frac{\mu_i}{\Lambda_{\rm UV}}\right)^2-\left(\frac{M_i}{\Lambda_{\rm UV}}\right)^2}}{\left(\frac{M_i}{\Lambda_{\rm UV}}\right)}\right]\right) \end{aligned} \tag{6.8.7}$$

$$\simeq \; 2\Lambda_{\rm UV}^2 \left[\left(\frac{\mu_i}{\Lambda_{\rm UV}} \right)^2 - \frac{1}{2} \left(\frac{M_i}{\Lambda_{\rm UV}} \right)^2 \; + \ldots \; \right] \quad . \tag{6.8.8}$$

The critical chemical potential to lowest order is then

$$\mu_{\rm crit} \simeq \frac{\Lambda_{\rm UV}}{\sqrt{2}} \simeq \begin{cases} 450 \text{ MeV} & \text{for PS1} \\ 763 \text{ MeV} & \text{for PS2} \end{cases} \quad . \tag{6.8.9}$$

Similarly, one can show in the three momentum cut-off regularisation that $\mu_{\rm crit} \simeq \Lambda_{\rm UV}$ [336]. These critical chemical potentials are depicted in Figs. 6.8.1–6.8.3 as red dashed lines to clearly illustrate this point, where the model should be considered unreliable.

We now turn to the influence that the vector interaction has on the quark chemical potential, constituent masses and densities. The vector interaction renormalises the chemical potential, effectively increasing it. However, it is the reduced chemical potential (see Eq. (6.6.11) and Figs. 6.8.1–6.8.3 plots (d–f)) that appears, for example, in the in-medium gap equation. The critical value of the chemical potential derived above will now apply to the reduced chemical potential. It will then provide a limiting value to the reduced chemical potential, up to which we can consider the model to be reliable in the presence of the vector interaction.

The vector coupling by definition of our model is half the scalar coupling, although in practice, it can be constrained by some physical quantity such as a vector meson mass. However, we allow the coupling to vary from zero to up to being equal to the scalar coupling, in order to understand its affect on the model. On increasing the vector coupling in each of the models the transition from the chirally broken phase to the symmetric phase occurs more smoothly. In particular, in the case of parameter set PS1 it changes the transition from a first order transition to a second order transition. This is not surprising as this effect has been seen in studies of two-flavour quark matter [311] using a flavour independent vector interaction. It has also in been seen in NJL model studies of the QCD phase diagram in the T–μ plane, whereby the vector interaction shifts the critical point closer to the μ axis [337–339]. For each of the models the vector coupling defers chiral restoration to larger chemical potential. The reduction of the chemical potential from the vector interaction curtails the effect of the finite density contribution to the gap equation meaning that the constituent quark masses approach their current quark masses at greater chemical potential productively delaying the break-down of the model.

The change in the behaviour of the order parameters is intimately tied to the steady increase of the densities with chemical potential, which can be seen in Figs. 6.8.1–6.8.3 plots (g–i). The vector interaction can be seen to drastically decrease each of the densities in the parameter set PS1, while in PS2 and HK the effect is less severe. This is certainly because of the larger scalar coupling in PS1.

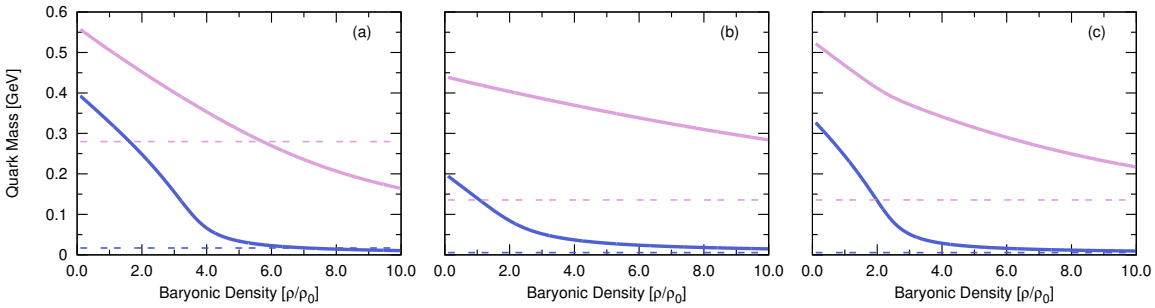

Figure 6.8.4: Quark mass versus total baryonic density for parameter sets (a) PS1, (b) PS2 and (c) HK.

For the three flavour symmetric case ($\rho_u = \rho_d = \rho_s$) shown in Fig. 6.8.4, the vector interaction does not alter the density dependence of the quark masses. In plot (a) for PS1, both the light and strange constituent quark masses go below their current mass values at approximately $\rho \simeq 6\rho_0$, precisely the density region where strange quark matter would be expected to be substantially present in neutron stars. This is, of course, a naive assumption as old neutron stars are usually considered to have reached thermal equilibrium with respect to weak and strong interactions, although at high densities they tend to approach flavour symmetric matter. Based on the above discussions, the PS1 parameter set will not likely make a reliable description of hybrid stars. In the modelling of quark matter in beta-equilibrium with leptons, we will restrict ourselves to the parameter sets PS2 and HK.

Thermal equilibrium of quarks and leptons with respect to the weak and strong interactions, under the constraints of charge and baryon number conservation, is described by the following system of equations:

$$\frac{2}{3}\rho_{\rm u}^{\rm v} - \frac{1}{3}\left(\rho_{\rm d}^{\rm v} + \rho_{\rm s}^{\rm v}\right) - \rho_{\rm e}^{\rm v} - \rho_{\mu}^{\rm v} = 0 \tag{6.8.10}$$

$$\rho - \frac{1}{3}\left(\rho_{\rm u}^{\rm v} + \rho_{\rm d}^{\rm v} + \rho_{\rm s}^{\rm v}\right) = 0 \tag{6.8.11}$$

$$\mu_{\rm d} - \mu_{\rm u} - \mu_{\rm e} = 0 \tag{6.8.12}$$

$$\mu_{\rm d} - \mu_{\rm s} = 0 \tag{6.8.13}$$

$$\mu_{\mu} - \mu_{\rm e} = 0 \quad . \tag{6.8.14}$$

The relations imposed in Eqs. (6.8.12–6.8.13) are between the thermodynamic chemical potentials and not the reduced chemical potentials. In terms of the individual quark densities ($\rho_{\rm i}^{\rm v}$), the total quark density ($\rho_{\rm tot}$) the total baryonic density (ρ) are defined as

$$\rho \equiv \frac{\rho_{\rm tot}}{3} \equiv \frac{1}{3}\sum_{i\in\{u,d,s\}} \rho_{\rm i}^{\rm v} \quad , \tag{6.8.15}$$

where the 1/3 is the baryonic charge of each quark. In the limit of zero vector coupling, the individual number densities of each quark species is related to their respective chemical potential by

$$\rho_{\rm i}^{\rm v} = \frac{(p_{\rm F}^i)^3}{\pi^2} = \frac{(-M_i^2 + \mu_i^2)^{3/2}}{\pi^2} \xrightarrow{G_{\rm V}\neq 0} \frac{(-M_i^2 + \tilde{\mu}_i^2)^{3/2}}{\pi^2} \quad , \tag{6.8.16}$$

where $p_{\rm F}^i$ is the quarks Fermi momentum. For non-zero vector coupling, the chemical potential in Eq. (6.8.16) is replaced with its reduced counterpart. As in Ch. 5, the lepton chemical potentials are once again simply $\mu_\ell = \sqrt{(p_{\rm F}^\ell)^2 + m_\ell^2}$, where $p_{\rm F}^\ell$ is the lepton's Fermi momentum. This system of five equations with five unknowns, combined with the three gap equations, is then solved to determine the particle content and thermodynamic behaviour of three flavour quark matter in beta-equilibrium with leptons.

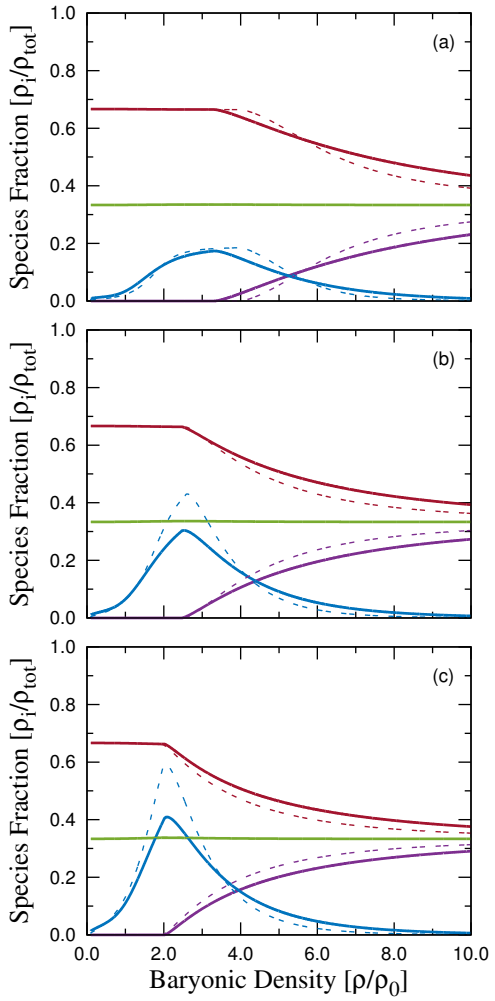

Figure 6.8.5: Beta-equilibrium quark matter for parameter set PS2 (solid) and HK (dashed). Each of the particle number densities is divided by the total quark density $\rho_{\rm tot} = \rho_d + \rho_u + \rho_s = 3\rho$. The down quark fraction is red, up green, strange purple. The electron fraction (blue) is multiplied by 100 so as to be visible on the same plot. Note that the electron fraction defined here differs by a factor of 1/3 from the figures in Ch. 5. Plot (a) zero vector coupling and non-zero flavour independent vector coupling (b) flavour dependent vector interaction with $G_{\rm V} = G_{\rm S}/2$ and (c) flavour dependent vector interaction with $G_{\rm V} = G_{\rm S}$. Here we use the saturation density $\rho_0 = 0.17$ fm^{-3}.

Figure 6.8.5 shows the species fractions as a function of total baryon density. In this

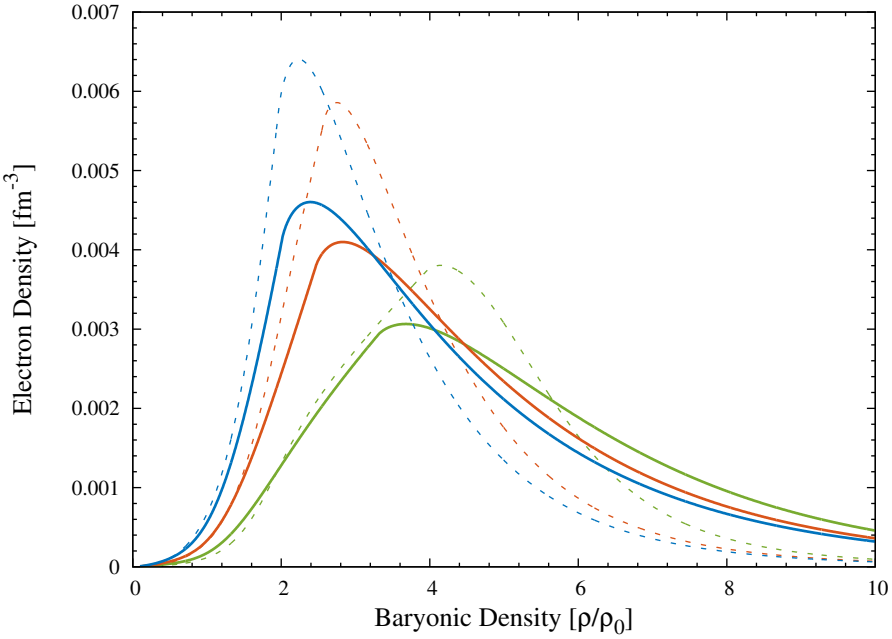

Figure 6.8.6: Electron density as a function of total baryonic density for parameter set PS2 (solid) and HK (dashed). The colours indicate the strength of the flavour dependent vector interaction, $G_{\mathrm{V}} = 0$ green, $G_{\mathrm{V}} = G_{\mathrm{S}}/2$ orange and $G_{\mathrm{V}} = G_{\mathrm{S}}$ blue.

figure, the results for both the PS2 and HK parameter sets are shown and are found to have similar particle content and behaviour. In contrast to hadronic calculations, the only leptons to appear are electrons and in a reduced number. In Fig. 6.8.5, the electron fraction was multiplied by 100 to make it clearly visible on the same plot as the quark fractions. Just how small it actually is can be seen in Fig. 6.8.6. The species fraction in the absence of a vector interaction is shown in Fig. 6.8.5 (a). Incorporating a non-zero flavour independent vector interaction leaves the number densities of the particles unchanged. Similar plots showing species fractions in the three flavour NJL model with flavour independent vector interaction can be found in Refs. [282] and [334]. The onset of strangeness occurs at a slightly lower density using the PS2 model than in the HK model. The strange quarks appear at $\rho \simeq 3.32\rho_0$ in PS2 and at $\rho \simeq 3.98\rho_0$ in HK. As expected, the appearance of strange quarks reduces the number of down quarks because of the charge neutrality constraint and the up quark fraction remains approximately constant over the density range considered. The strength of the flavour independent vector interaction does not change the species fraction as a function of density, but does have an affect on the thermodynamic variables, as will be discussed below. However, in the case of a flavour dependent vector interaction, particle densities do vary with vector coupling strength, see plot (b–c) of Fig. 6.8.5. Figure 6.8.5 (b–c) shows the onset of strangeness occurs at lower density with increasing strength of the flavour dependent vector interaction for both PS2 and HK models. With varying the vector coupling between $(0, G_{\mathrm{S}})$, the threshold density for strange quarks is in the range ~ 2–$4\rho_0$.

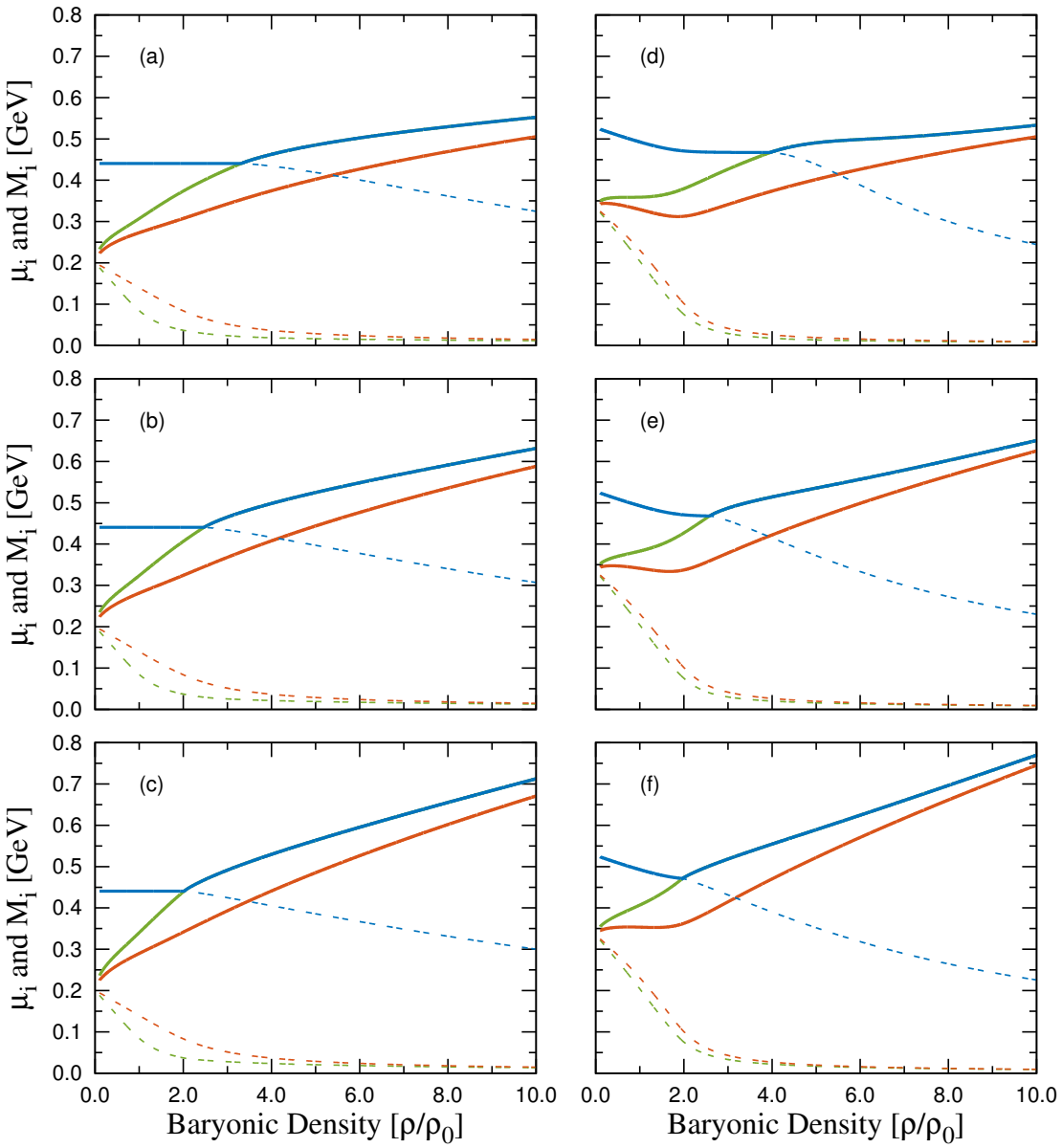

Figure 6.8.7: Chemical potentials (solid) and constituent quark masses (dashed) as a function of total baryonic density (ρ) for the flavour dependent vector interactions. The line colours for the quarks are up (orange), down (green) and strange (blue). Plots (a–c) PS2 model with $G_{\rm V} = 0, G_{\rm S}/2, G_{\rm S}$, respectively. Plots (d–f) HK model with $G_{\rm V} = 0, G_{\rm S}/2, G_{\rm S}$, respectively. Here we use the saturation density $\rho_0 = 0.17$ fm^{-3}.

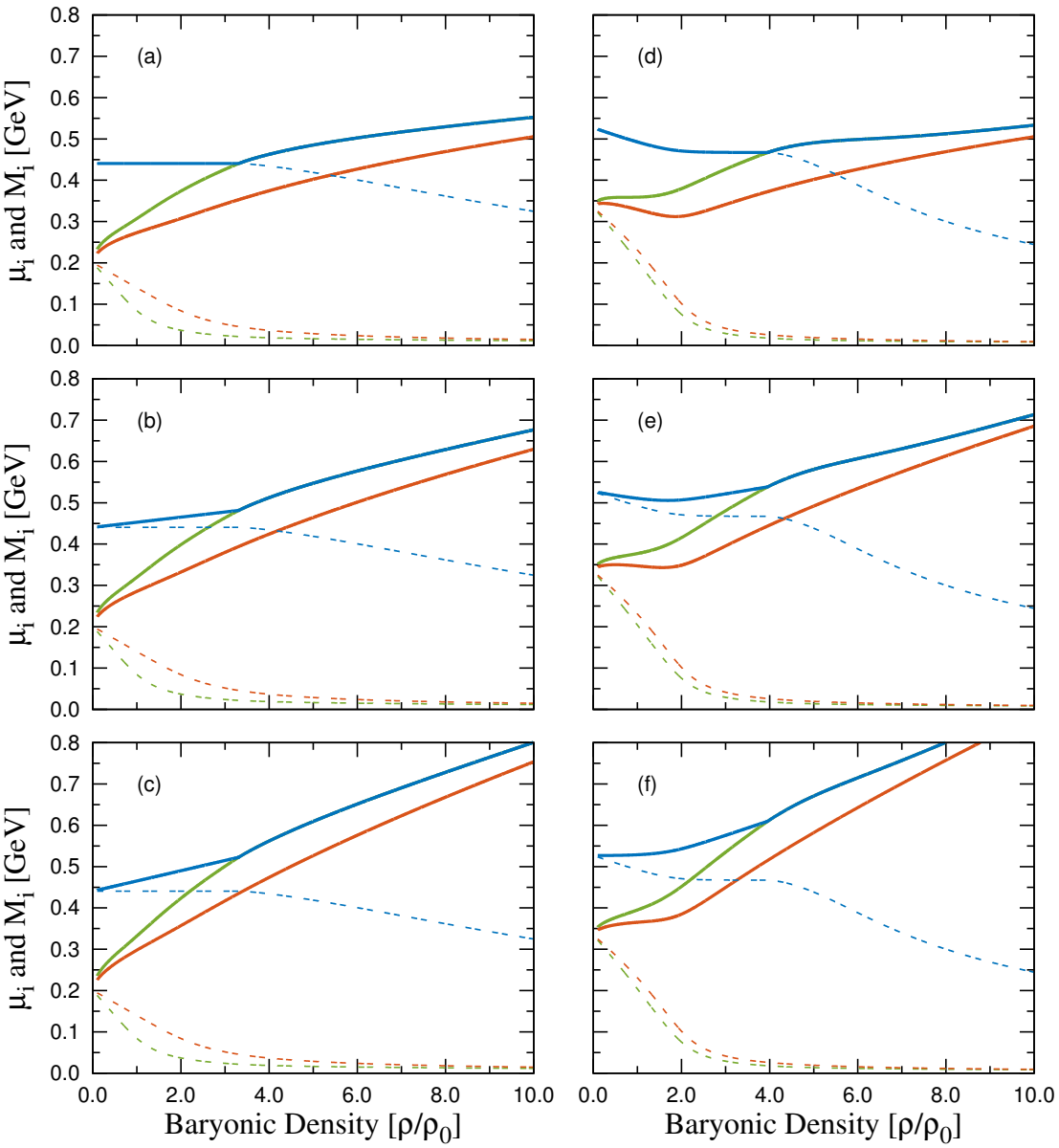

Figure 6.8.8: Same as Fig. 6.8.7, but for the flavour independent vector interaction.

Figures 6.8.7 and 6.8.8 show chemical potentials and constituent quark masses as a function of total baryonic density. Figure 6.8.7 includes a flavour dependent vector interaction, whereas Fig. 6.8.8 includes a flavour independent vector interaction. Both PS2 and HK models show similar trends with the exception that in the HK parameter set there is more curvature of the chemical potentials at low density. This is undoubtedly connected to the t' Hooft term causing the condensates to be dependent on one another. In the HK parameter set, the strange quark mass decreases as the light quark masses decrease—even when strange quarks have not yet appeared. Whereas in PS2, it remains constant until it is energetically favourable to be produced. This is because the quark condensates of each flavour are independent of each other in

PS2. From Fig. 6.8.5, we see that at low density only the light quarks are present for both parameter sets and all variations of the vector interaction considered. For models incorporating the flavour dependent vector interaction, we have $\mu_s = M_s$ at zero strange quark density, which can be seen in Fig. 6.8.7. As the baryonic density increases, the separation of the chemical potential curve from the constituent quark mass curve can be clearly seen for the strange quark. This coincides with the appearance of strange quarks. With increasing strength of the vector interaction, the down quark chemical potential increases faster with increasing density leading to an earlier onset of strange quarks—compare with Fig. 6.8.5. However, for models with the flavour independent vector interaction $\mu_s = M_s + 2g_{\mathrm{V}}(\rho_u + \rho_d)$ at zero strange quark density. Before the density threshold is reached for strange quarks, there is a separation between the strange quark's chemical potential and its constituent quark mass owing to the already present light quarks. This can be seen in Fig. 6.8.8.

Moreover, as we are working in the isospin symmetric limit i.e the current quark masses of the light quarks are equal, the only cause for a difference between the light constituent quark masses is the finite density contribution. In contrast to the usual expectation that the up quark be lighter than the down quark and thereby the neutron heavier than the proton, the down quark is found to be lighter than the up quark. This is due to the conditions of beta-equilibrium under charge and baryon number conservation. The down quark fraction is greater than the up quark fraction, as can be seen in Fig. 6.8.5 and so its effective mass is reduced more than that of the up quark. However, this difference is small and decreases with increasing density.

The reason for the differences between the flavour dependent and independent vector interactions lies in the imposed beta-equilibrium relations in Eqs. (6.8.12 -6.8.13). Writing Eq. (6.8.12) in terms of the reduced chemical potentials for the flavour independent vector interaction one finds

$$\mu_d - \mu_u - \mu_e = \tilde{\mu}_d + 2g_{\mathrm{V}} \sum_{i\in\{u,d,s\}} \rho_i - \tilde{\mu}_u - 2g_{\mathrm{V}} \sum_{i\in\{u,d,s\}} \rho_i - \mu_e = \tilde{\mu}_d - \tilde{\mu}_u - \mu_e \quad (6.8.17)$$

and for Eq. (6.8.13),

$$\mu_d - \mu_s = \tilde{\mu}_d + 2g_{\mathrm{V}} \sum_{i\in\{u,d,s\}} \rho_i - \tilde{\mu}_s - 2g_{\mathrm{V}} \sum_{i\in\{u,d,s\}} \rho_i = \tilde{\mu}_d - \tilde{\mu}_s \quad . \quad (6.8.18)$$

This equivalence of the beta-equilibrium relations between chemical potentials and reduced chemical potentials is the reason why the species fraction of particles do not change with increasing vector coupling. The particle number densities are directly related to the reduced chemical potentials via Eq. (6.8.16). This combined with the gap equation for the quark masses, which is also only dependent on the reduced chemical potential, the whole system of beta-equilibrium equations is independent of the vector coupling. However, at a given density the chemical potentials are larger with increasing vector coupling, but their increase is cancelled in the beta-equilibrium relations (Eqs. (6.8.12–6.8.13)) leaving the particle number densities and hence also the constituent quark masses invariant.

For the models including a flavour dependent vector interaction, there are extra terms which do not cancel that are proportional to the vector coupling. For Eq. (6.8.12),

$$\mu_d - \mu_u - \mu_e = \tilde{\mu}_d + 4G_{\mathrm{V}}\rho_d - \tilde{\mu}_u - 4G_{\mathrm{V}}\rho_u - \mu_e = \tilde{\mu}_d - \tilde{\mu}_u - \mu_e + 4G_{\mathrm{V}}(\rho_d - \rho_u) \quad (6.8.19)$$

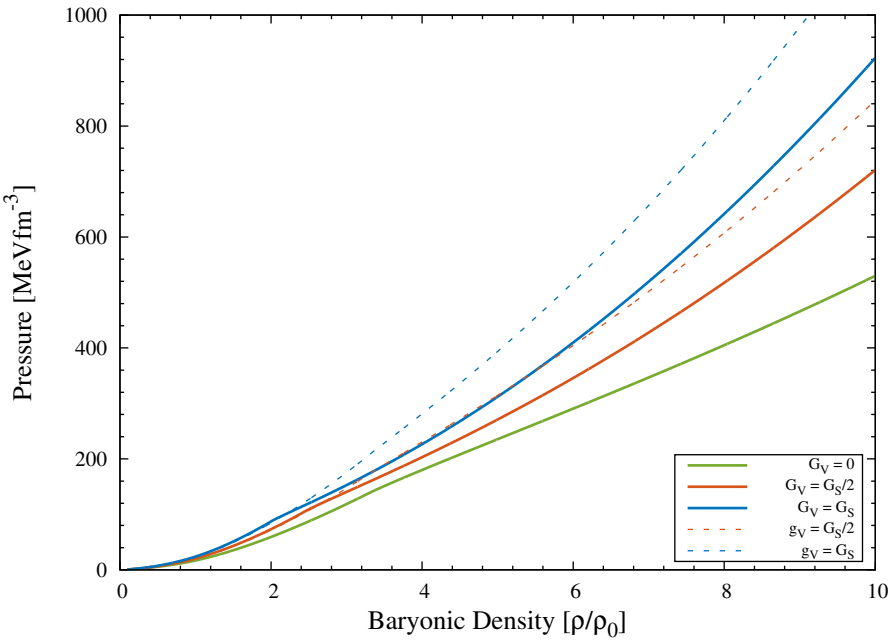

Figure 6.8.9: Pressure as a function of density for the PS2 parameter set. Results using the flavour dependent interaction G_{V} (i.e. use Eq. (6.3.8)) (solid) and flavour independent interaction g_{V} (i.e. use Eq. (6.7.1)) (dashed) for different values of the vector coupling.

and for Eq. (6.8.13),

$$\mu_d - \mu_s = \tilde{\mu}_d + 4G_{\mathrm{V}}\rho_d - \tilde{\mu}_s - 4G_{\mathrm{V}}\rho_s = \tilde{\mu}_d - \tilde{\mu}_s + 4G_{\mathrm{V}}(\rho_d - \rho_s) \quad . \tag{6.8.20}$$

The equilibrium conditions do not simplify down to relations of the same form between the reduced chemical potentials. Because there remains an explicit dependence on the vector coupling in the beta-equilibrium relations the particle number densities and hence also the constituent quark masses change.

The pressure of quark matter is calculated from the thermodynamic relation

$$P = -V_{\mathrm{total}} = -V_{\mathrm{MF}}\left(\{M_i\}, \{\mu_i\}\right) - V_l(\{\mu_l\}) \quad , \tag{6.8.21}$$

where V_l is the effective potential contribution of the non-interacting leptons. This gives the same pressure contribution as in Ch. 5. The energy density is obtained from the following formula

$$\epsilon_{\mathrm{total}} = V_{\mathrm{total}} + \sum_{i\in\{u,d,s,e,\mu\}} \mu_i \rho_i^{\mathrm{v}} \quad , \tag{6.8.22}$$

where in the second term μ_i remains the un-reduced thermodynamic chemical potential.

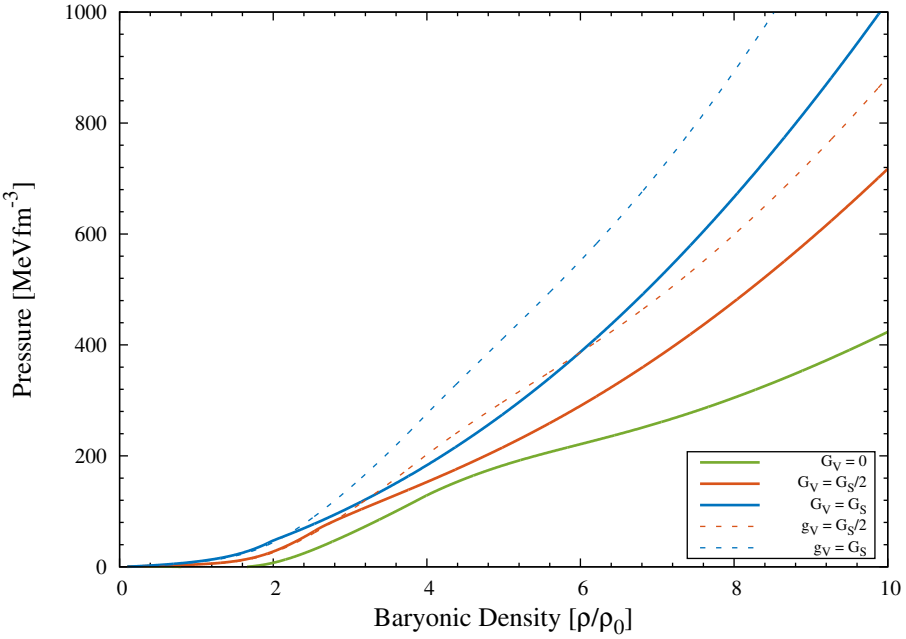

Figure 6.8.10: Same as Fig. 6.8.9, but for the parameter set HK.

Figures 6.8.9 and 6.8.10, plainly show the appreciable affect the vector interaction has on the pressure as a function of density. Overall, the behaviour of the two parameter sets with change in strength and type of vector interaction is not dissimilar. For both, there is a considerable increase in pressure upon turning on the vector coupling and then increasing further to be equal to the scalar coupling. As anticipated, the flavour independent vector interaction provides a larger increase in pressure at high density ($\rho \gtrsim 2\rho_0$) for both parameter sets. The earlier onset of the strange quark makes the models with a flavour dependent vector interaction a little softer again. However, the vector interaction still produces a stiffer EoS state on increasing the vector coupling. The onset of strangeness is apparent in both figures, but a little more prominent for the HK parameter set, where the increase in strange quark fraction increases more rapidly with density than the PS2 parameter set, softening the curve more—compare with Fig. 6.8.5. The PS2 parameter set produces a slightly stiffer EoS, particularly at low density. It also produces considerably less curvature in the pressure at low density and around the region where strange quarks appear as compared to the the HK parameter set. Figures 6.8.11 and 6.8.12 show the pressure against energy density. As would be expected, the pressure exhibits similar behaviour as a function of energy density.

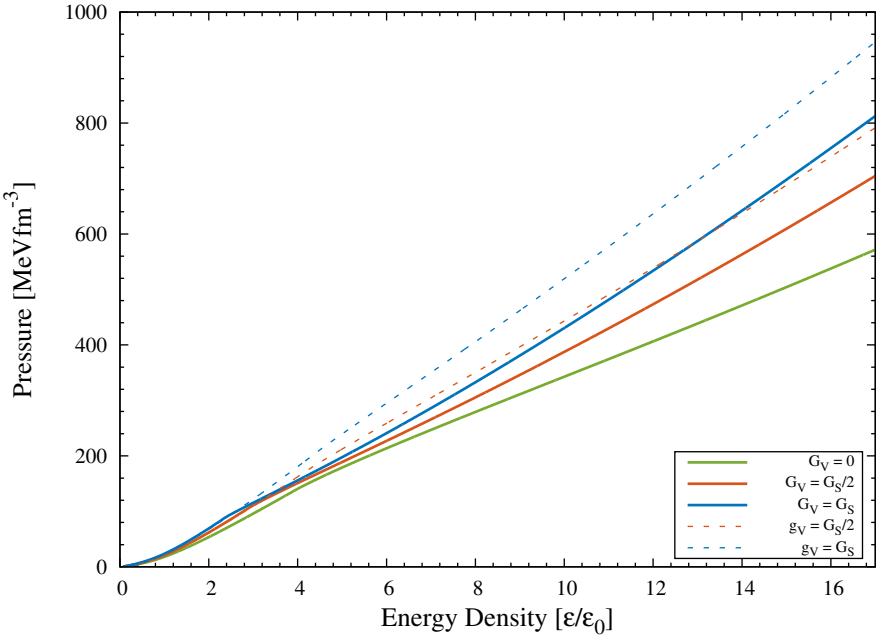

Figure 6.8.11: Pressure as a function of energy density for the PS2 parameter set. Results using the flavour dependent interaction $G_{\rm V}$ (i.e. use Eq. (6.3.8)) (solid) and flavour independent interaction $g_{\rm V}$ (i.e. use Eq. ((6.7.1)) (dashed) for different values of the vector coupling. Here we normalise the energy density with $\epsilon_0 = 140$ MeVfm^{-3}.

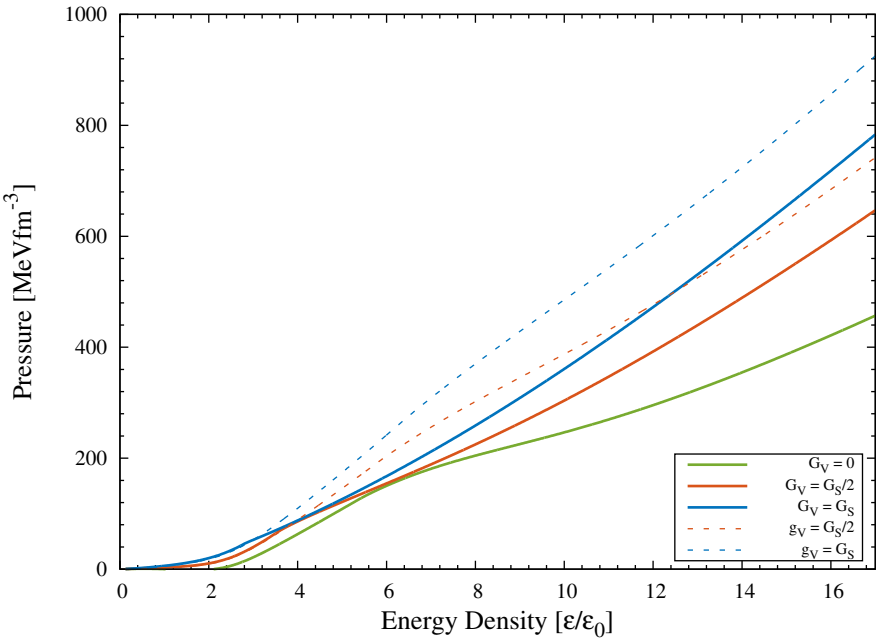

Figure 6.8.12: Same as Fig. 6.8.11, but for the parameter set HK.

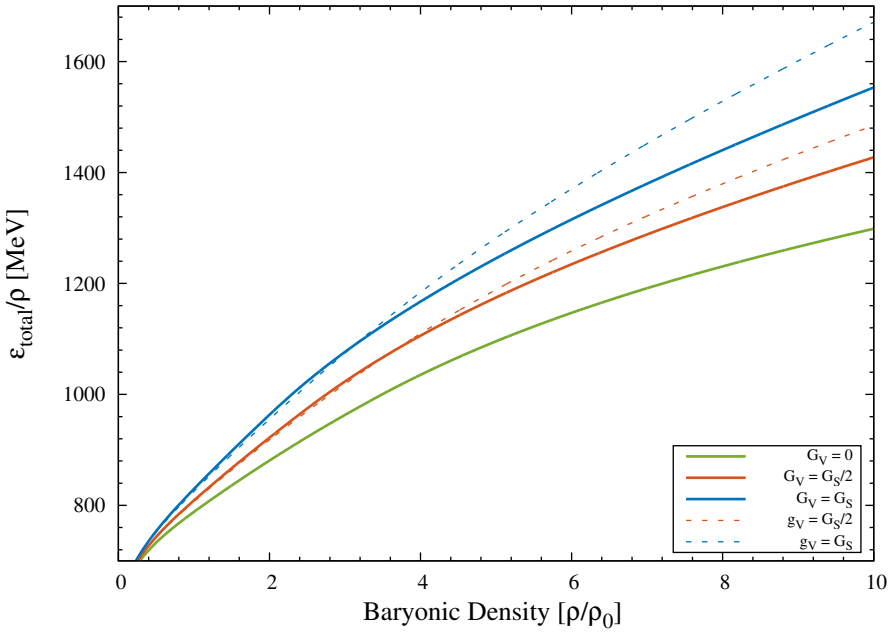

Figure 6.8.13: Average energy per particle (including leptons) as a function of total baryonic density for the PS2 parameter set. Results using the flavour dependent interaction G_V (i.e. use Eq. (6.3.8)) (solid) and flavour independent interaction g_V (i.e. use Eq. (6.7.1) (dashed) for different values of the vector coupling.

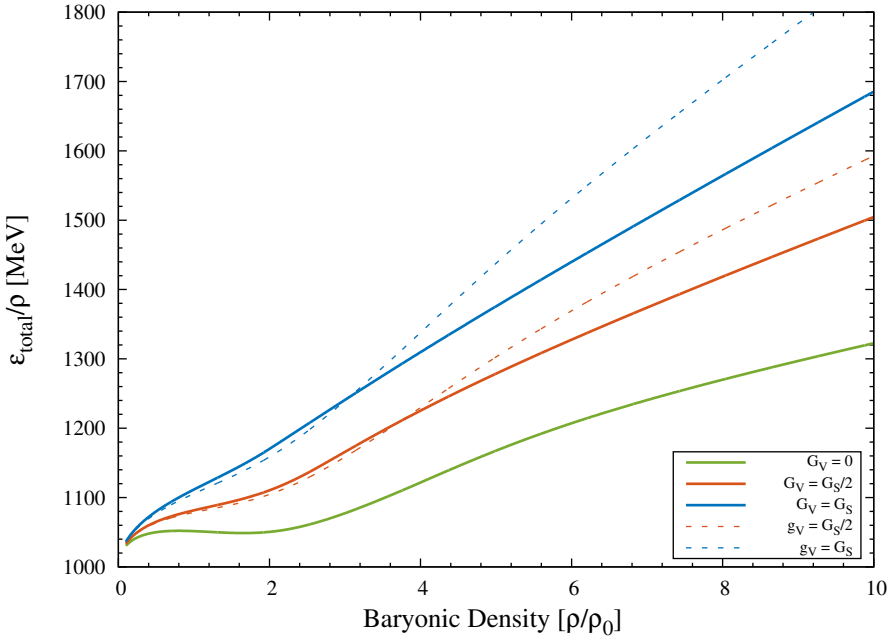

Figure 6.8.14: Same as Fig. 6.8.13, but for the parameter set HK.

The averaged energy per particle (including leptons) is shown as a function of

density in Figs. 6.8.13 and 6.8.14. Here there is a noticeable difference between the two parameter sets. Note the small change in scale between the two figures. The PS2 produces less energy per particle than the HK set. The impact of the t' Hooft term at low density causes considerable curvature—compare with the behaviour of quark masses in Figs. 6.8.7 and 6.8.8. Increased curvature is also present in the region where strange quarks are occurring. Albeit, with increasing strength of the vector interaction more energy per particle is produced for both parameter sets.

6.9 Summary

In this chapter, we began by introducing the NJL model, an effective low to intermediate energy model of QCD. A Fierz invariant NJL Lagrangian based on one gluon exchange was presented and then the mean field approximation was discussed in the path integral framework. The NJL effective potential and gap equations were presented and derived in App. B. Numerical results for model were presented and discussed. The results of the proper time regularised model developed in this chapter were compared to the three momentum regularised model with t' Hooft determinant term. The parameter set PS2 is preferred for modelling high density matter over PS1, because of the behaviour of the constituent quark mass as a function of chemical potential. For quark matter in beta equilibrium, the PS2 model produced overall qualitatively similar results to the HK model despite the different behaviour of the quark masses. Although, the PS2 model produced slightly more pressure, particularly at low density, as compared with the HK model. In the next chapter we will use hadronic QMC and NJL quark models to investigate hybrid stars.

7 Phase Transitions to Quark Matter

In this chapter we consider a transition from hadronic matter (modelled using the HF-QMC model) to quark matter (using the NJL model). We investigate the possibility of a smooth crossover transition in a purely phenomenological way, whereby we interpolate between hadronic and quark model equations of state (EoS).

7.1 Hybrid Stars and the Phase Transition to Quark Matter

It has long been thought that the densities reached inside the inner core of neutron stars may be sufficient to produce a phase transition from hadronic matter to deconfined quark matter forming hybrid stars. A transition to the chirally restored phase of QCD is also thought to occur at high density. It is unknown if these two transitions coincide and the form they may take. In understanding these transitions one would ideally like to use QCD directly, but as already described in detail in earlier chapters this is currently too difficult. For confinement, one typically resorts to using two phenomenological models which epitomise the key features of QCD in the two asymptotic regions of its phase diagram—one in the low density region modelling hadronic matter and the other modelling quark matter at intermediate to high density—and then construct a phase transition between the two. This means dissociation of hadrons does not occur naturally and is dependent on how we artificially construct the transition.

Various models have been used to describe each phase and different constructions in characterising the process of deconfinement have been investigated, such as the Maxwell [295, 297, 340–348] and Gibbs [291, 302, 304, 334, 349–357] constructions describing first order transitions and also interpolation/percolation constructions interpreting the transition to be of crossover type [282, 283, 334, 358–360]. The calculated properties of hybrid stars are considerably influenced by the choice of models and

type of construction used to describe the transition. In this section, we will discuss each of these constructions and how they relate to one another. However, in Sec. 7.2 we choose to investigate the possibility that the transition is described by a smooth crossover using a phenomenological interpolation procedure.

In chapters 5 and 6, we considered each phase to be in beta-equilibrium and also charge neutral. The requirement of charge neutrality effectively reduced each phase to a one component system controlled by the baryonic density or equivalently a baryonic chemical potential. Built on this foundation, one is naturally led to consider phase transitions in neutron stars modelled assuming a one component description, i.e., a Maxwell construction. This is the simplest possibility for constructing a phase transition and historically the most studied. In such a construction, looking at pressure versus baryonic chemical potential, one can infer the transition from hadronic to quark matter by where the curves for each phase meet. On either side of this point, the phase with the greatest pressure is the dominant phase. More precisely, the transition point in the Maxwell construction is identified by the following conditions of thermal, mechanical and one component chemical equilibrium

$$T_{HP} = T_{QP} \quad , \quad P_{HP} = P_{QP} \quad , \quad \mu_n^{HP} = \mu_n^{QP} \quad , \tag{7.1.1}$$

where in the quark phase the neutron chemical potential is defined as $\mu_n^{QP} = \mu_u + 2\mu_d$. This first order transition corresponds to a kink in the pressure versus neutron chemical potential plane and a constant pressure plateau in the pressure versus density plane. This plateau connects the hadronic phase to the quark phase. With this sudden jump in the density at constant pressure, the Maxwell construction does not allow for the possibility of a mixed phase where both hadrons and quarks can coexist together. For actual hybrid stars, in this construction, they will have a hadronic outer layer and dense quark core with no possibility for a mixed phase in between.

When modelling phase transitions in neutron stars using the Maxwell construction each phase is considered independently charge neutral. However, as was first pointed out by Glendenning [349], if a mixed phase exists then charge neutrality can be achieved globally rather than locally. To consider this possibility we are led to the Gibbs construction for a multi-component system. In the context of hybrid stars, we have a two component system corresponding to two conserved quantities, namely baryon number and charge. The removal of the unrealistic requirement of local charge neutrality has been found to have important consequences for hybrid EoS [349].

The Gibbs construction for a first order transition requires that thermal, mechanical and chemical equilibrium are implemented in the mixed phase region. Chemical equilibrium requires that the, now two, independent chemical potentials (the neutron and electron chemical potentials) of the two oppositely charged phases are equal. Outside of the coexistence region the phase with the greatest pressure is the persistent phase. As the hadronic phase is known to be the dominant phase at low density, one calculates the hadronic phase and uses the calculated neutron and electron chemical potentials as input into the quark phase calculation of the equation of state. Obviously, in the purely hadronic phase there is only one independent chemical potential owing to the requirement of charge neutrality, but in searching for a mixed phase where we do not require local charge neutrality, but rather global charge neutrality, we must

pass both the neutron and electron chemical potentials from the hadronic matter calculation to the quark matter calculation. If at some density the pressures of the two phases become equal, then a mixed phase is possible. If this mixed phase exists, it can potentially persist over a range of densities with the pressure increasing monotonically with density. In the mixed phase, hadronic matter will possess a charge and quark matter the opposite charge.

The Maxwell and Gibbs constructions described above are bulk constructions, treating both hadron and quark matter as uniform matter. Important finite size effects are neglected, such as the surface tension at the hadron-quark interface and also the Coulomb interaction. These effects have been shown to lead to the formation of geometrical structures forming phases commonly referred to as pasta or structured mixed phases. From more sophisticated calculations which take into account these effects, see for example Refs. [345, 361–367], it is known that these structures tend to smooth the pressure plateau seen in the Maxwell construction. Moreover, the Maxwell construction can be considered a limiting scenario where the surface tension is large and conversely for the Gibbs construction where it is taken to vanish.

These constructions describing first order transitions typically make it difficult to construct stiff hybrid EoS compatible with large neutron star mass observations, unless the hadronic EoS is already sufficiently stiff. However, some models have been able to produce massive hybrid stars compatible with observation, see for example [299, 334, 343, 347, 357].

The conventional first order constructions produce hybrid EoS which are typically softer than hadronic EoS. The EoS are softer because in order to implement the Maxwell and Gibbs constructions, the quark pressure must be less than the hadronic pressure at low neutron chemical potential, intersect at some point, and then remain above with increasing chemical potential. This requirement implicitly restricts the possible hybrid EoS to be softer than hadronic EoS in general.

Moreover, since no known model has a realistic description of the confinement mechanism this adds to the difficulty in providing a reasonable description of the matter in the transition region. Model derived hadronic and quark EoS may only provide adequate explanations of strongly interacting matter in respectively the low and high density limits. These models may, in fact, be unreliable in the intermediate transition region where the requirements of thermal, mechanical and chemical equilibrium are imposed. The requirement of mechanical equilibrium ($P_{\mathrm{Q}} = P_{\mathrm{H}}$) deserves special emphasis because models not including confinement would necessarily produce unnaturally large pressure. In some situations, to ensure a transition at a reasonable density, model parameters must be restricted or a bag constant introduced to lower the pressure [360]. Either of these choices will also affect the high density behaviour of the EoS [360]. We use the usual convention, where the pressure and the energy density vanish in vacuum. However, a bag constant could be introduced to produce non-zero values in vacuum. A larger positive value would lower the quark pressure helping to enable such a first order transition. For this reason, the Maxwell and Gibbs constructions could fail to capture essential features of the transition region accurately despite the models being otherwise reliable in their respective asymptotic limits.

In searching for the hadron–quark phase transition by the Maxwell and Gibbs

constructions, the implicit assumption is made that the transition is first order. This is generally assumed, but the hadron–quark transition may not be a first order transition in the interior of the QCD phase diagram. It may take the form of a crossover transition similar to what is predicted by lattice QCD at low density and high temperatures [368–371]. If deconfinement were to take the form of a crossover, we could parametrise our ignorance of the transition region by phenomenologically interpolating between the hadron and quark EoS. This possibility has recently received much attention from several groups [282, 283, 334, 359, 360].

An argument which suggests the possibility that the transition may be a crossover rather than a phase transition follows from the known extended nature of hadrons. With hadrons being a colour singlet cluster of confined quarks, an inference to be drawn from their nature is that a progressive transition to quark matter may occur where hadrons and quarks coexist and interact with one another. As the densities reached inside neutron stars are generally thought not to be greater than $10\rho_0$, the quarks are most likely not asymptotically free, but are rather still strongly interacting [282, 283]. It is well known that including a vector interaction among quarks can significantly stiffen an EoS [295], meaning that if a crossover transition to a stiff quark EoS occurred at low enough density, this would therefore offer a possible resolution between EoS with exotic degrees of freedom and the recent observations of massive neutron stars [282, 283].

Hybrid EoS were previously calculated using a Gibbs construction employing a Hartree QMC model and a simpler version of the NJL model without vector interactions in Refs. [351, 372]. More recently, a Gibbs construction was employed between a different variation of the Hartree-Fock QMC model and a bag model [357]. We will not consider the above constructions further. Instead, we will contemplate the possibility that the transition is actually a smooth crossover. This will be done using the Hartree–Fock Quark-Meson Coupling (QMC) model developed in Ch. 5 to describe the hadronic phase and the three flavour NJL model developed in Ch. 6 for the quark phase. In using these two models, quark degrees of freedom are influencing both regions with the latter also exemplifying chiral symmetry breaking. With both models employing quark degrees of freedom it is hoped that they will be more reliable in the transition region. In this region where hadrons and quarks are expected to coexist, it is likely that the quark substructure of hadrons would play an important role and their interaction with the external quarks to be strong. The QMC model has the advantage over models which employ point-like descriptions of hadrons by modelling the baryons as MIT bags. In addition to incorporating this structure which has been shown to be connected to many-body forces in a non-relativistic limit, it also includes its in-medium modification potentially making it more realistic by inclusion of this additional physics. Although, this is still a crude model of confinement and it still lacks an interaction between hadrons and the already deconfined external quarks.

In the next section we discuss the percolation picture of the hadron–quark transition. This kind of transition was, for example, recently investigated by Masuda *et al* [282, 283] using several hadronic models and the three momentum regularised NJL model. Their hadronic EoS were obtained using a G-matrix formulation employing various realistic potentials, such as the Argonne AV18 and Paris [69], Reid and Nijmegen [373] potentials supplemented with three-body forces. They also considered

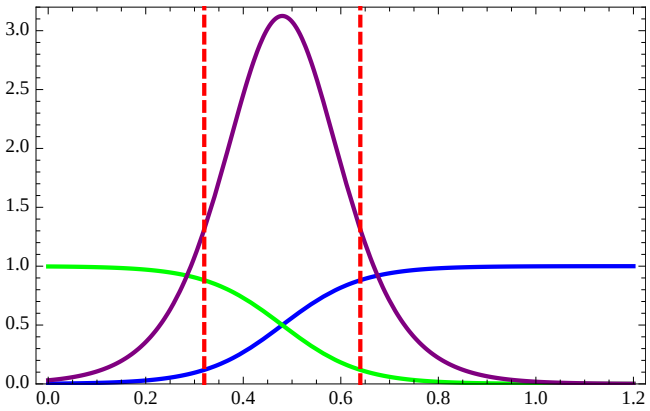

Figure 7.2.1: Interpolating functions $f_{\pm}(\rho)$ (blue/green) and $g_{+}(\rho)$ (purple) versus density (ρ) in units fm^{-3}. The red dashed vertical lines mark the chosen transition region $(\bar{\rho}, \Gamma) = (3\rho_0, \rho_0)$ with $\rho_0 = 0.16\text{fm}^{-3}$.

a relativistic mean field model SCL3$\Lambda\Sigma$ [374]. They concluded that massive hybrid stars ($M_{\text{NS}} \sim 2M_{\odot}$) could be produced using a percolation picture provided the quark matter EoS was stiff enough and the transition occurred at moderately low density ($\rho \sim 3\rho_0$), providing a possible reconciliation of exotic degrees of freedom with the Demorest and Antoniadis observations [202, 203]. We now examine this possibility using the Hartree–Fock QMC model and both the proper–time and three momentum regularised versions of the NJL model.

7.2 Interpolation Construction

If we assume that we understand how the low and high density matter behaves asymptotically, then we can parametrise our ignorance of the intermediate region where the phase transition occurs using an interpolating scheme. It should be understood that the choice of interpolating scheme is not unique. Masuda *et al* [282, 283] investigated two different interpolation constructions, pressure versus baryonic density and energy density versus baryonic density employing a hyperbolic tangent function. Hell and Weise [334] interpolated pressure as a function of energy density using a similar function. Alvarez Castillo *et al* [359] and Kojo *et al* [360] interpolated pressure as function of baryonic chemical potential using a gaussian and polynomial description, respectively. For each interpolation method, one thermodynamic variable was interpolated as a function of another, then the remaining variables were calculated from the interpolated variable. This results in additional thermodynamic corrections to the calculated variables beyond mere interpolation. These additional corrections are meant to preserve thermodynamic consistency between the variables, which may be important in applications to physical systems such as hybrid stars. However, since these corrections originate from a phenomenological interpolation it is not clear whether they are physically meaningful or simply an artefact of the interpolation construction used. Only a deeper understanding of QCD thermodynamics can answer this. For this reason, we show numerical results with and without this thermodynamic correction.

We follow Ref. [282] and interpolate energy density as a function of total baryonic density. To facilitate the transition between the hadron and quark EoS we introduce the following sigmoid interpolating functions

$$f_{\pm}(\rho) = \frac{1}{2}\left(1 \pm \tanh(X)\right) \quad , \tag{7.2.1}$$

where $X = \dfrac{\rho - \bar{\rho}}{\Gamma}$ and the transition region is chosen to be $\rho \in [\bar{\rho} - \Gamma, \bar{\rho} + \Gamma]$ with $(\bar{\rho}, \Gamma) = (3\rho_0, \rho_0)$ and $\rho_0 = 0.16\text{fm}^{-3}$. The transition from hadronic EoS to the quark EoS is centred about $\bar{\rho}$ with the width of the transition region determined by Γ. The interpolating functions are depicted in Fig. 7.2.1. These sigmoid functions are continuous, monotonic and differentiable, varying smoothly between the horizontal asymptotes of 0 and 1. There is no physical argument for these functions other than we want a smooth function to facilitate the transition from the hadronic EoS to the quark EoS producing a faux crossover transition. In this manner, two EoS based on different models, including complementary physics and aimed at describing matter in different density regimes, can be smoothly transitioned between in a reasonable, but phenomenological way. Alternative functions could of course be used, as long as they smoothly transitioned between the two EoS. Moreover, it is not necessary to use the hyperbolic tangent function to construct a sigmoid function, it is just a convenient choice as most programming languages have this as an inbuilt function. Other sigmoid functions utilising algebraic forms or the well known error function would produce very similar results.

The energy density is interpolated using Eq. (7.2.1) by

$$\epsilon(\rho) \;=\; \epsilon_{\text{HP}}(\rho) f_{-}(\rho) + \epsilon_{\text{QP}}(\rho) f_{+}(\rho) \quad . \tag{7.2.2}$$

Note that the functions $f_{\pm}(\rho)$ cannot be interpreted as the quark or hadronic matter volume fraction (as in a Gibbs construction mixed phase), they merely interpolate the energy density.

When the energy density is taken as the interpolated variable as a function of density, the pressure is then calculated from this interpolated energy density (Eq. (7.2.2)), using

$$P(\rho) = \rho^2 \frac{\partial(\epsilon/\rho)}{\partial \rho} \quad . \tag{7.2.3}$$

This leads to

$$P(\rho) = P_{\text{HP}}(\rho) f_{-}(\rho) + P_{\text{QP}}(\rho) f_{+}(\rho) + \Delta P \quad , \tag{7.2.4}$$

where the correction

$$\Delta P = \rho \left[\epsilon_{\text{QP}}(\rho) g_{+}(\rho) + \epsilon_{\text{HP}}(\rho) g_{-}(\rho)\right] \quad . \tag{7.2.5}$$

The functions $g_{\pm}(\rho)$ are the density derivatives of the interpolating functions,

$$g_{\pm}(\rho) = \frac{df_{\pm}(\rho)}{d\rho} = \pm \frac{2}{\Gamma} (e^{X} + e^{-X})^{-2} \quad . \tag{7.2.6}$$

Functions defined as the derivative of a sigmoid function are bell shaped curves because of the inherent "s" shape of all sigmoid functions. The density dependence of g_{+} is

shown in Fig. 7.2.1 , from this it can be inferred that the thermodynamic correction, ΔP, will only contribute significantly in the transition region. It is also dependent on the difference of the energy density between the two EoS. If a narrower transition region is chosen, then the bell curve will be more sharply peaked with a larger maximum producing a more substantial contribution to the pressure.

Using the above procedure we can easily construct many hybrid EoS. However, we cannot indiscriminately interpolate between hadronic and quark EoS. Rather we should also impose additional criteria to ensure we obtain a physically meaningful EoS. The requirements that the EoS be both stable and causal impose stringent constraints ruling out many possible interpolations.

In interpolating between the two EoS, the requirement of stability, i.e., the pressure gradient be greater than zero,

$$\frac{dP}{d\rho} > 0 \quad , \tag{7.2.7}$$

is very restrictive. Interpolated EoS that do not meet this requirement are not useful in modelling hybrid stars. Without the thermodynamic correction to the pressure it is clear from the interpolating functions and the EoS presented in earlier chapters will lead to an interpolated EoS that satisfies this constraint. However, the additional correction may induce inflection points in the EoS possibly leading to an instability.

By a causal EoS we simply mean an EoS where the speed of sound in matter, c_s, is less than the speed of light ($c = 1$):

$$c_s^2 = \frac{dP}{d\epsilon} < 1 \quad . \tag{7.2.8}$$

Here we simply calculate it from a high order polynomial fit to the EoS data file. Besides acting as a constraint, it is also a useful measure of the stiffness of an EoS.

7.3 Numerical Results and Discussion

Throughout this section the interpolations shown in figures, unless otherwise stated, are between the "Standard" or baseline scenario of the HF-QMC model and the PS2 and HK models incorporating a flavour dependent vector interaction with the transition region chosen to be $(\bar{\rho}, \Gamma) = (3\rho_0, \rho_0)$. Variations beyond these constructions are examined in Tables 7.3.1 and 7.3.2.

The interpolation of energy density as a function of density by Eq. (7.2.2) is shown in Fig. 7.3.1. The interpolated energy densities are compared to the quark and hadronic energy densities. There is a noticeable difference between PS2 and HK models, the HK models produce an energy density greater than the hadronic energy density for all values of the vector coupling. In the case of the PS2 model with no vector interaction the hadronic energy density is greater than the quark energy density for the density range shown. When the vector interaction is increased to half the scalar coupling, the hadronic energy density is greater than the quark energy density up until the density reaches $\rho \sim 0.7$ fm^{-3}, then the quark energy density is greater. The difference of the quark and hadronic energy density significantly affects the correction to the pressure to maintain thermodynamic consistency. It also dictates the sign of the correction as seen

from Eq. (7.2.5). A large separation of the quark and hadronic energy density curves indicates a larger correction is needed to maintain thermodynamic consistency—compare with Fig. 7.3.2. For all HK models, ΔP is positive and hence it will stiffen the EoS at the beginning of the transition region and soften towards the end. The strength of the vector interaction significantly influences the magnitude of ΔP and on increasing its strength ΔP is amplified considerably. As for the PS2 models, the sign of ΔP varies with density and the strength of the vector interaction. In the absence of the vector interaction, it is negative because of the density dependence of the difference of the quark and hadron energy densities. Thus, in contrast to HK models, it will soften the EoS at the beginning of the transition region and stiffen towards the end.

Figures 7.3.3 and 7.3.4 show pressure with and without the thermodynamic correction as a function of total baryonic density and energy density, respectively. As can be seen by comparing curves with and without the thermodynamic correction, the interpolated EoS is significantly affected by ΔP in the transition region. Without the thermodynamic correction, the transitions between the hadronic and all quark EoS occur smoothly without violating the constraints of thermodynamic stability and causality as would be expected from monotonic functions like those expressed in Eq. (7.2.1). Also, away from the transition region $(\bar{\rho}, \Gamma) = (3\rho_0, \rho_0)$ the interpolated EoS are almost equivalent to the un-interpolated hadronic and quark EoS. However, in plots (d) of Figs. 7.3.3 and 7.3.4, the correction to the pressure is so significant that the resulting EoS becomes unstable for HK models with $G_{\rm V} = G_{\rm S}/2$ and $G_{\rm V} = G_{\rm S}$. The greater the separation in the ϵ–ρ plane, the larger the correction ΔP, leading to more significant change in the pressure.

The speed of sound in matter squared is shown in Fig. 7.3.5 as a function of energy density. Interpolations between the hadronic EoS and quark models with both types of vector interaction are included in Fig. 7.3.5. On comparing with Fig. 7.3.4, it can be seen that as an EoS softens, sound slows down and as the EoS stiffens, sound speeds up. The speed of sound is a very good measure of the stiffness of an EoS. Without the thermodynamic correction the interpolated EoS with PS2 models are generally stiffer than those with HK models, particularly at low and intermediate density. It is also clear that the flavour independent vector interaction produces a stiffer EoS and hence faster sound than models incorporating the flavour dependent vector interaction. On inclusion of the thermodynamic correction, however, interpolated EoS with HK models incorporating a vector interaction are stiffer than their PS2 counterparts. The speed of sound is enhanced in the transition region for both PS2 and HK models. However, it is not as significant for the PS2 models. The EoS shown in Fig. 7.3.5 remain causal and most interpolated EoS examined in the tables also remain causal. However, there were a few exceptions. Those that did not meet the stability and causality requirements are indicated by an asterisks $(*)$ in Tables 7.3.1 and 7.3.2. In plot (d) of Fig. 7.3.5, the speed of sound becomes imaginary for HK models with $G_{\rm V} = G_{\rm S}/2$ and $G_{\rm V} = G_{\rm S}$, once again indicating an unstable EoS .

If an interpolated EoS was found to be unstable or to violate causality, that does not mean an interpolation between those particular hadronic and quark models is not possible in general. It simply means it is not possible to construct a consistent EoS in our current interpolation scheme. Equations of state that do not meet our requirements

of stability and causality with our chosen interpolation scheme are simply discarded. More detailed investigations on the dependence of the interpolation scheme are beyond the scope of this thesis and are left for future work.

Interpolated EoS which satisfied the two constraints were used as input to integrate the TOV equations[1]. The resulting M–R relations for several interpolations, with and without the thermodynamic correction, are shown in Fig. 7.3.6. All curves shown in Fig. 7.3.6 use the "Standard" or baseline scenario of the HF-QMC model, so all variations are a result of changes in the quark model and the thermodynamic correction ΔP. Without ΔP, interpolations with PS2 models are shown to produce massive hybrid stars, compatible with the Demorest and Antoniadis observations [202, 203], even in the absence of a vector interaction. However, for HK models only when $g_{\mathrm{V}} = G_{\mathrm{S}}$ is a sufficiently massive hybrid star, compatible with observations, actually produced. The only difference between these interpolated EoS is the quark model. The prediction of more massive hybrid stars is a result of the stiffer PS2 quark EoS at low and intermediate density. The softer HK models predict radii about 0.5 km smaller than PS2 models, but for both models increasing the vector coupling increases the radius only slightly.

Including ΔP has a significant impact on the M–R relationships for all models. Considering the interpolated EoS with the PS2 quark models, those with $G_{\mathrm{V}} = 0$ and $g_{\mathrm{V}} = G_{\mathrm{V}} = G_{\mathrm{S}}/2$ predict smaller maximum masses, whereas the $g_{\mathrm{V}} = G_{\mathrm{V}} = G_{\mathrm{S}}$ models produce more massive hybrid stars. In the absence of a vector interaction the interpolated EoS with the PS2 model no longer satisfies the constraints set by the observations of massive stars. More noticeable, however, is the separation of curves in terms of radii. The softening at the start of the transition region coming from the correction ΔP significantly reduces the radius, particularly for $G_{\mathrm{V}} = 0$. The other models also predict smaller radii than when ΔP was ignored. As for the interpolated EoS utilising the HK models, the maximum masses are considerably larger and radii are bigger because ΔP is always positive and larger in magnitude. The model with $G_{\mathrm{V}} = 0$ still does not meet the astrophysical constraints.

A summary of maximum mass configurations is presented in Table 7.3.1. To show the dependence of the interpolated EoS on the hadronic EoS we also included interpolations between the overly stiff variation of the HF-QMC model, where the cut-off used in the Fock terms is increased from $\Lambda = 0.9$ GeV to $\Lambda = 1.3$ GeV. From this table, it can be inferred that the properties of the maximum mass configurations of hybrid stars are affected by the hadronic model, but are mostly influenced by the quark model.

Table 7.3.2 summarises hybrid star properties under variation of the transition region, $\bar{\rho} \in \{3\rho_0, 4\rho_0, 5\rho_0\}$. As would naively be expected, pushing the centre of the transition region to higher density tends to produce a less stiff EoS for the majority of the interpolations which naturally translates to smaller maximum masses for hybrid stars. On delaying the transition to higher densities, it was found to be more difficult to construct a consistent EoS between the chosen hadronic and quark models. This was conspicuously evident for the HK models, partly owning to the greater separation in the ϵ–ρ plane of the hadronic and quark model curves, leading to a larger thermodynamic correction ΔP.

[1]The BPS EoS was attached at low density as in Ch. 5.

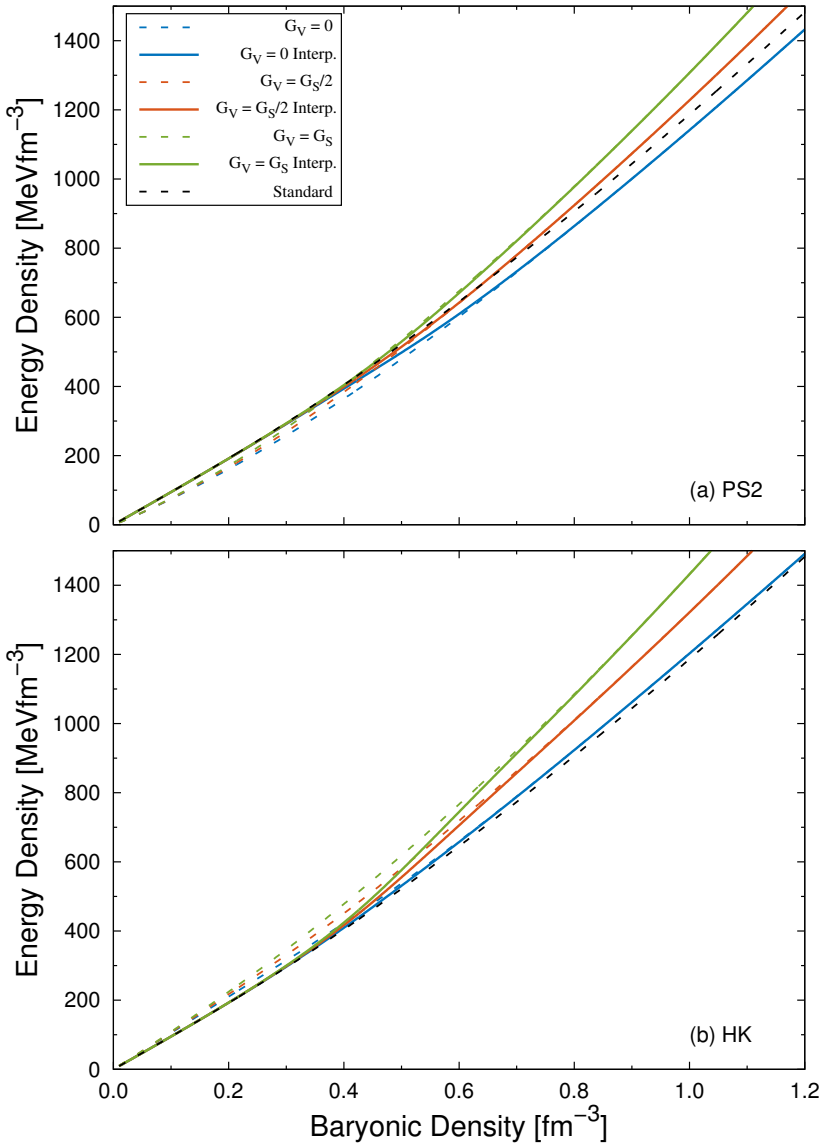

Figure 7.3.1: Energy density as a function of total baryonic density. For plot (a), the interpolation is between the "Standard" or baseline scenario of the HF-QMC model and the proper time regularised PS2 model with flavour dependent vector interaction. Similarly for plot (b), but with the three momentum regularised model with flavour dependent vector interaction. The crossover region is chosen to be $(\bar{\rho}, \Gamma) = (3\rho_0, \rho_0)$. Specific curves for both plots are indicated in the key of plot (a).

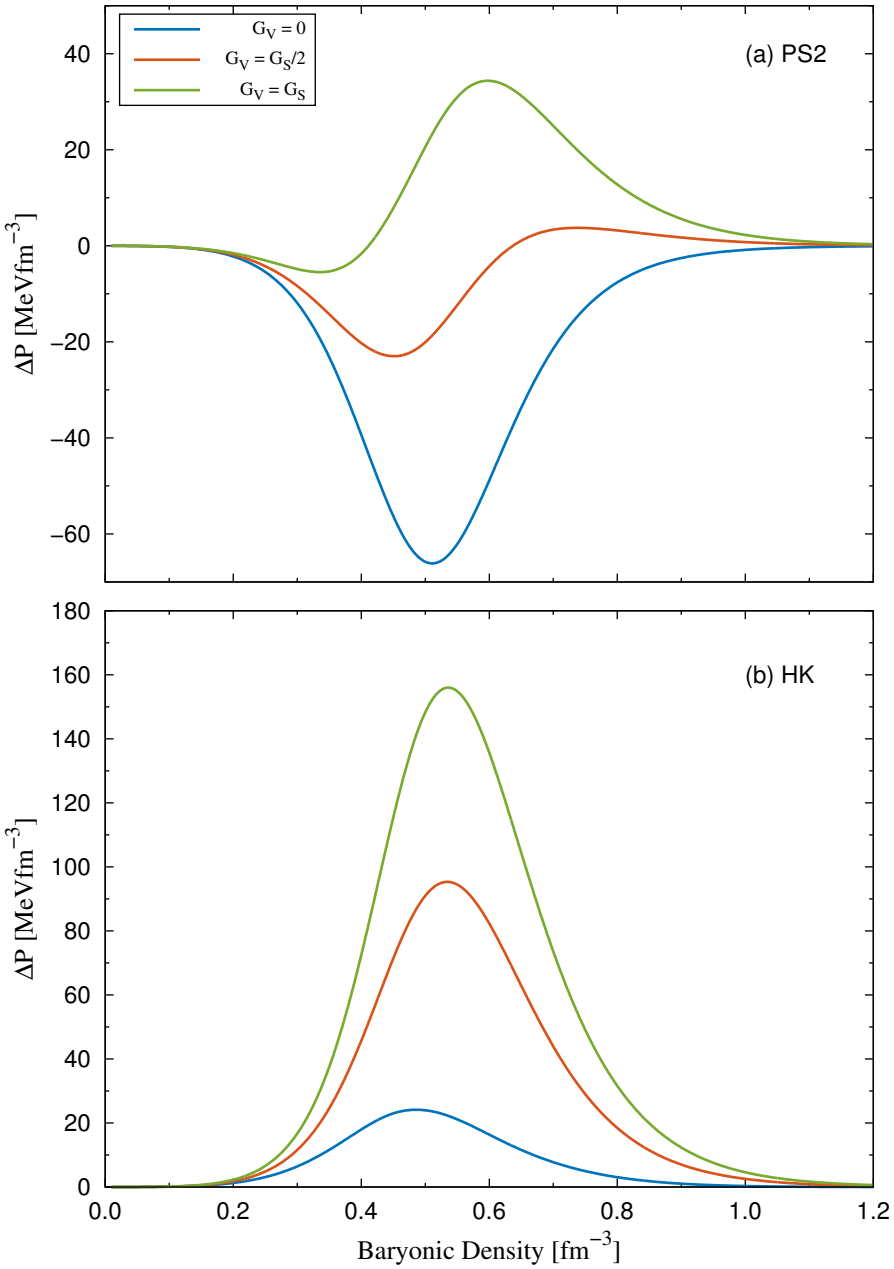

Figure 7.3.2: Thermodynamic correction ΔP as a function of total baryonic density as arising from the interpolation. For plot (a), the interpolation is between the "Standard" or baseline scenario of the HF-QMC model and the proper time regularised PS2 model with flavour dependent vector interaction. Similarly for plot (b), but with the three momentum regularised model with flavour dependent vector interaction. The crossover region is chosen to be $(\bar{\rho}, \Gamma) = (3\rho_0, \rho_0)$. Specific curves for both plots are indicated in the key of plot (a).

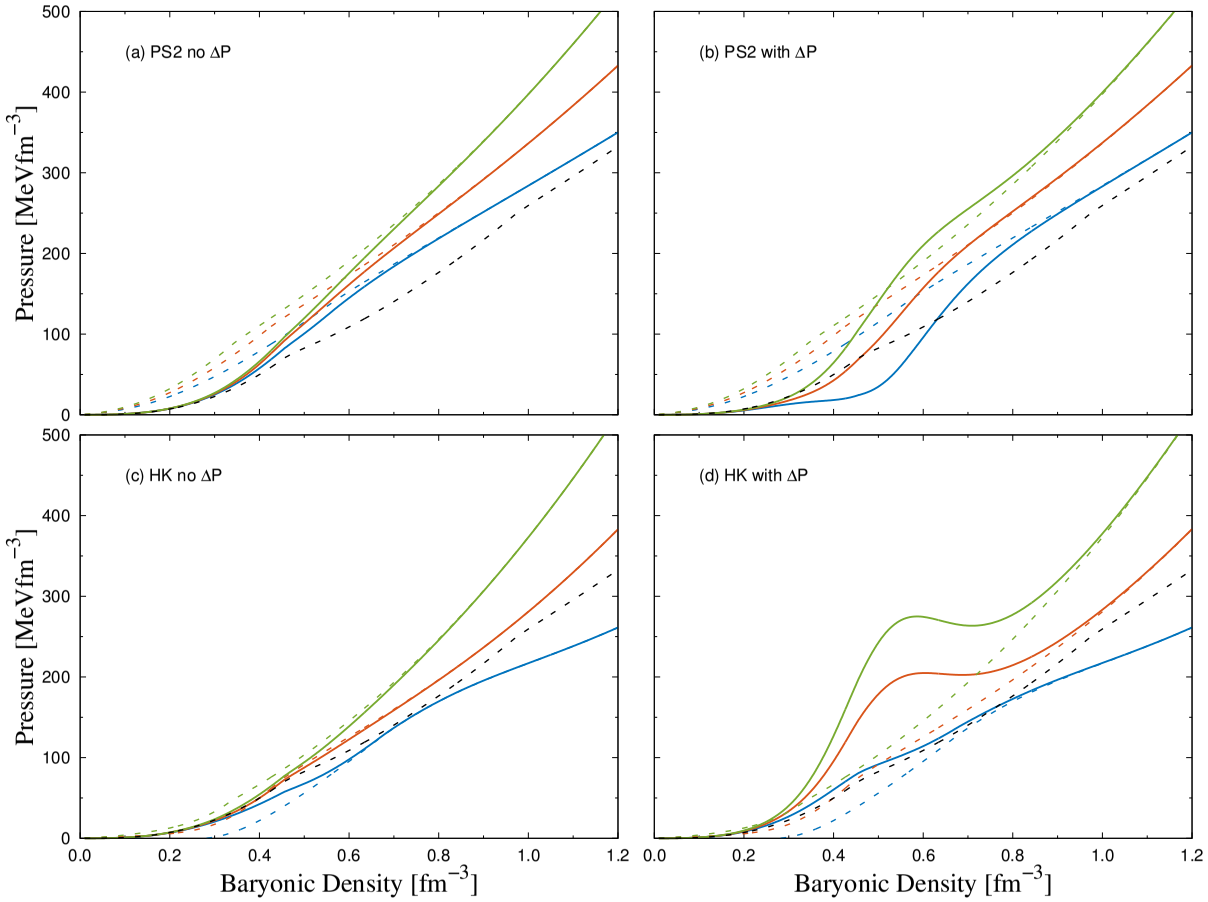

Figure 7.3.3: Pressure as a function of total baryonic density. For plots (a,b), the interpolation is between the "Standard" or baseline scenario of the HF-QMC model and the proper time regularised PS2 model with flavour dependent vector interaction. Similarly for plots (c,d), but with the three momentum regularised model with flavour dependent vector interaction. Plots (a,c) do not include the thermodynamic correction ΔP, whereas plots (b,d) include the correction for thermodynamic consistency. The crossover region is chosen to be $(\bar{\rho}, \Gamma) = (3\rho_0, \rho_0)$. Line types as in Fig. 7.3.1.

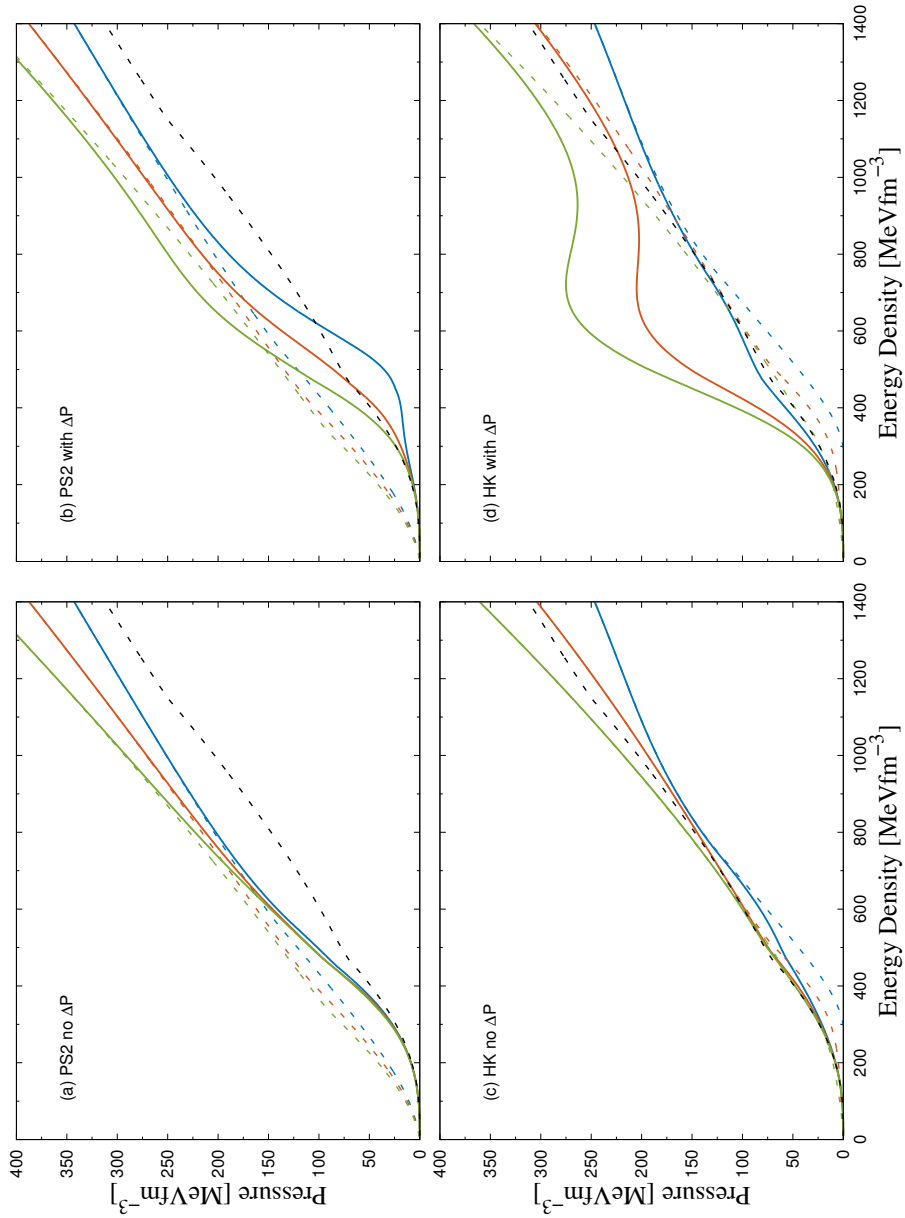

Figure 7.3.4: Pressure as a function of energy density. For plots (a,b), the interpolation is between the "Standard" or baseline scenario of the HF-QMC model and the proper time regularised PS2 model with flavour dependent vector interaction. Similarly for plots (c,d), but with the three momentum regularised model with flavour dependent vector interaction. Plots (a,c) do not include the thermodynamic correction ΔP, whereas plots (b,d) include the correction for thermodynamic consistency. The crossover region is chosen to be $(\bar{\rho}, \Gamma) = (3\rho_0, \rho_0)$. Line types as in Fig. 7.3.1.

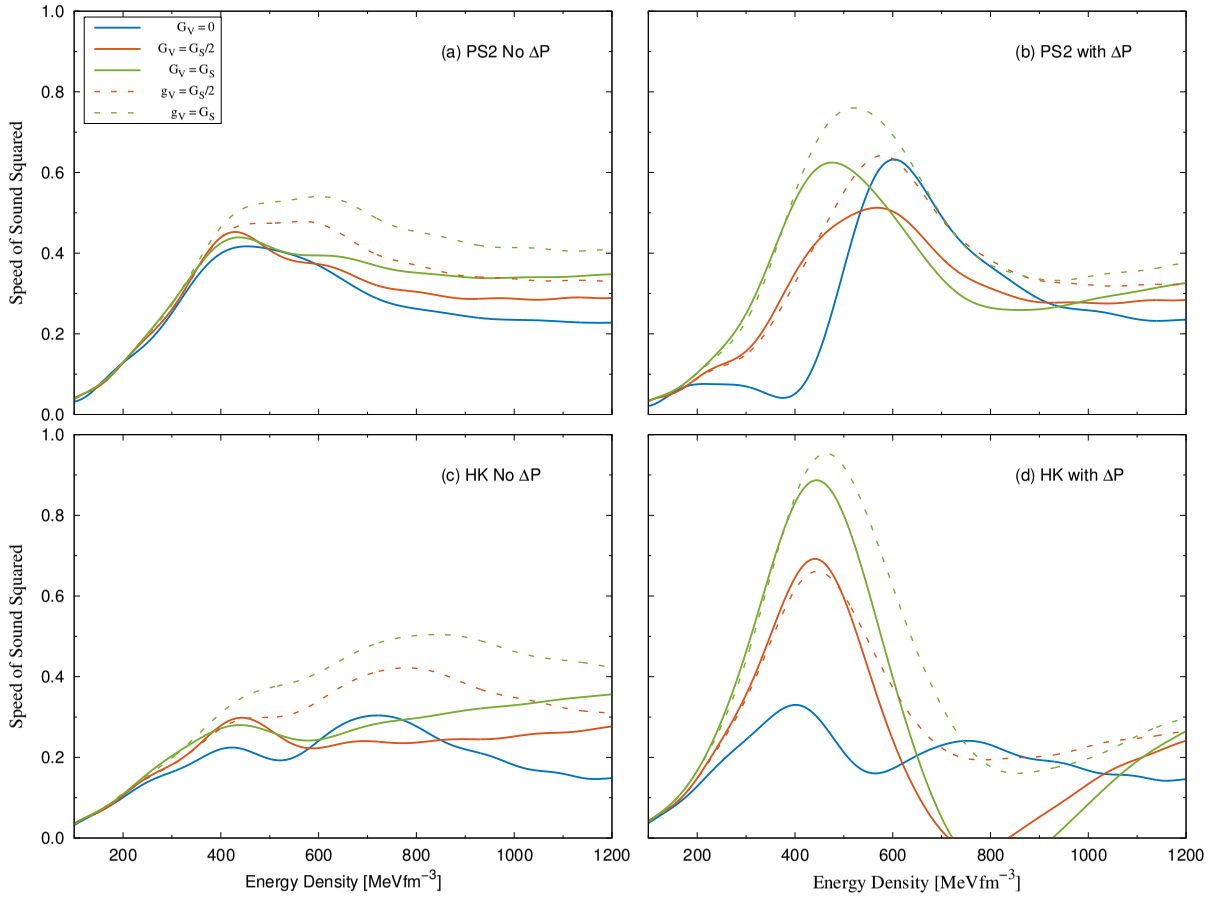

Figure 7.3.5: Speed of sound squared as a function of energy density. For plots (a,b), the interpolation is between the "Standard" or baseline scenario of the HF-QMC model and the proper time regularised PS2 model with flavour dependent (solid) and independent (dashed) vector interactions. Similarly for plots (c,d), but with the three momentum regularised model with flavour dependent (solid) and independent (dashed) vector interactions. Plots (a,c) do not include the thermodynamic correction ΔP, whereas plots (b,d) include the correction for thermodynamic consistency. The crossover region is chosen to be $(\bar{\rho}, \Gamma) = (3\rho_0, \rho_0)$. Specific curves for all plots are indicated in the key of plot (a).

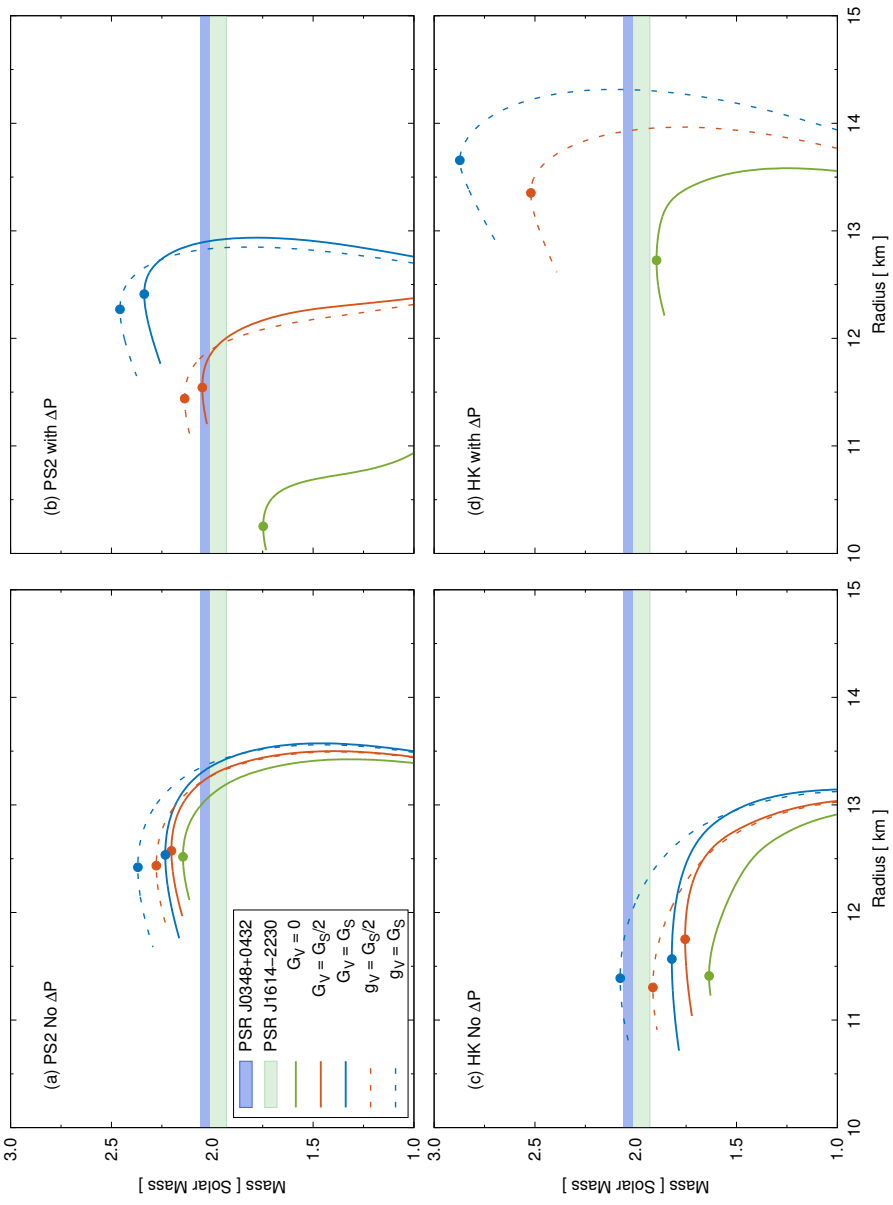

Figure 7.3.6: Neutron star mass as a function of radius. For plots (a,b), the interpolation is between the "Standard" or baseline scenario of the HF-QMC model and the proper time regularised PS2 model with flavour dependent (solid) and independent (dashed) vector interactions. Similarly for plots (c,d), but with the three momentum regularised model with flavour dependent (solid) and independent (dashed) vector interactions. Plots (a,c) do not include the thermodynamic correction ΔP, whereas plots (b,d) include the correction for thermodynamic consistency. The crossover region is chosen to be $(\bar{\rho}, \Gamma) = (3\rho_0, \rho_0)$. Specific curves for all plots are indicated in the key of plot (a).

Hadronic Model	Quark Model	G_V	Vector Int.	M_{max} $[M_\odot]$ No ΔP	M_{max} $[M_\odot]$ ΔP	R [km] No ΔP	R [km] ΔP	ρ_c^{max} $[\rho_0]$ No ΔP	ρ_c^{max} $[\rho_0]$ ΔP
Standard	PS2	0	-	2.15	1.75	12.52	10.25	5.50	7.54
Standard	PS2	$G_S/2$	dep.	2.20	2.05	12.57	11.54	5.18	5.90
Standard	PS2	$G_S/2$	indep.	2.28	2.14	12.44	11.44	5.28	5.94
Standard	PS2	G_S	dep.	2.23	2.34	12.54	12.41	5.00	4.98
Standard	PS2	G_S	indep.	2.37	2.46	12.42	12.27	5.02	5.02
Standard	HK	0	-	1.64	1.90	11.41	12.73	6.32	4.90
Standard	HK	$G_S/2$	dep.	1.76	$*$	11.75	$*$	5.40	$*$
Standard	HK	$G_S/2$	indep.	1.92	2.52	11.30	13.35	5.92	4.36
Standard	HK	G_S	dep.	1.82	$*$	11.57	$*$	5.38	$*$
Standard	HK	G_S	indep.	2.01	2.87	11.39	13.66	5.40	4.08
$\Lambda = 1.3$	PS2	0	-	2.19	1.73	12.74	10.24	5.34	7.68
$\Lambda = 1.3$	PS2	$G_S/2$	dep.	2.25	2.03	12.79	11.57	5.02	5.94
$\Lambda = 1.3$	PS2	$G_S/2$	indep.	2.32	2.12	12.64	11.46	5.14	5.98
$\Lambda = 1.3$	PS2	G_S	dep.	2.28	2.32	12.75	12.48	4.86	4.96
$\Lambda = 1.3$	PS2	G_S	indep.	2.40	2.44	12.61	12.31	4.90	5.02
$\Lambda = 1.3$	HK	0	-	1.69	1.89	11.73	12.95	5.96	4.66
$\Lambda = 1.3$	HK	$G_S/2$	dep.	1.81	$*$	12.12	$*$	5.04	$*$
$\Lambda = 1.3$	HK	$G_S/2$	indep.	1.95	2.52	11.56	13.47	5.70	4.28
$\Lambda = 1.3$	HK	G_S	dep.	1.87	$*$	11.97	$*$	5.00	$*$
$\Lambda = 1.3$	HK	G_S	indep.	2.11	2.87	11.62	13.73	5.24	4.04

Table 7.3.1: Hybrid star properties in the percolation picture. The crossover region is chosen to be $(\bar{\rho}, \Gamma) = (3\rho_0, \rho_0)$. An astericks $(*)$ indicates that a consistent EoS could not be constructed between that variation of hadronic and quark models with the chosen interpolation method.

Quark Model	$G_{\rm V}$	$\bar{\rho}$	$M_{\rm max}$ $[M_\odot]$		R [km]		$\rho_c^{\rm max}$ $[\rho_0]$	
			No ΔP	ΔP	No ΔP	ΔP	No ΔP	ΔP
PS2	0	$3\rho_0$	2.15	1.75	12.52	10.25	5.5	7.54
PS2	0	$4\rho_0$	1.98	$*$	11.84	$*$	6.18	$*$
PS2	0	$5\rho_0$	1.87	$*$	11.54	$*$	6.56	$*$
PS2	$G_{\rm S}/2$	$3\rho_0$	2.20	2.05	12.57	11.54	5.18	5.90
PS2	$G_{\rm S}/2$	$4\rho_0$	2.01	1.99	11.74	11.43	5.96	6.30
PS2	$G_{\rm S}/2$	$5\rho_0$	1.89	1.96	11.36	11.20	6.42	6.78
PS2	$G_{\rm S}$	$3\rho_0$	2.23	2.34	12.54	12.41	5.00	4.98
PS2	$G_{\rm S}$	$4\rho_0$	2.03	2.28	11.61	11.85	5.82	5.72
PS2	$G_{\rm S}$	$5\rho_0$	1.91	$*$	11.17	$*$	6.36	$*$
HK	0	$3\rho_0$	1.64	1.90	11.41	12.73	6.32	4.90
HK	0	$4\rho_0$	1.74	1.92	11.91	12.24	5.70	5.50
HK	0	$5\rho_0$	1.78	$*$	12.00	$*$	5.60	$*$
HK	$G_{\rm S}/2$	$3\rho_0$	1.76	$*$	11.75	$*$	5.40	$*$
HK	$G_{\rm S}/2$	$4\rho_0$	1.78	$*$	11.92	$*$	5.26	$*$
HK	$G_{\rm S}/2$	$5\rho_0$	1.79	$*$	11.93	$*$	5.38	$*$
HK	$G_{\rm S}$	$3\rho_0$	1.82	$*$	11.57	$*$	5.38	$*$
HK	$G_{\rm S}$	$4\rho_0$	1.82	$*$	11.59	$*$	5.38	$*$
HK	$G_{\rm S}$	$5\rho_0$	1.81	$*$	11.61	$*$	5.50	$*$

Table 7.3.2: Hybrid star properties in the percolation picture under variation of $\bar{\rho} \in \{3\rho_0, 4\rho_0, 5\rho_0\}$. The "Standard" or baseline scenario is used for the hadronic model and the flavour dependent vector interaction is used in each of the quark models. An astericks $(*)$ indicates that a consistent EoS could not be constructed between that variation of hadronic and quark models with the chosen interpolation method.

7.4 Summary

In this chapter we began by discussing phase transitions from hadronic matter to quark matter, with emphasis on the conventional first order treatments via the Maxwell and Gibbs constructions. How they are implemented, their properties and their shortcomings were highlighted. We then discussed modeling the transition as a smooth crossover, a possibility which has recently been given much consideration in the literature [282, 283, 334, 358–360]. Motivation for such a transition was discussed and one method for implementing this kind of transition was presented. The numerical results for the faux crossover construction between the HF-QMC and NJL models developed in earlier chapters were then presented and discussed.

The interpolation transitions for the "Standard" and the "$\Lambda = 1.3$ GeV" scenarios from Ch. 5 were shown. The latter was chosen so we could make a comparison with the "Standard" scenario and an overly stiff version of the model to see the effect the hadronic model has on the maximum neutron star mass in this kind of transition. It appears that the hadronic model only has a small affect on the maximum neutron star mass and it is mostly dependent on the quark model.

The affect of this interpolation method on the EoS of dense matter is shown in Fig. 7.3.3 and 7.3.4. At low and high density it can be seen to approach the assumed asymptotic limits, i.e. the hadronic and quark EoS, but in the intermediate region the pressure can be somewhat weakened or enhanced depending on ΔP. It produces a decrease in the pressure at the beginning of the transition region and increase towards the end for PS2 models and the opposite behaviour for HK models. This clearly comes from the density dependence of the difference between the energy densities of the two EoS (see Eq. (7.2.5)) and is therefore dependent on the two EoS we are interpolating between. Moreover, it suggests that the pressure in the transition region can potentially be outside the limits set by the hadronic and quark EoS and possibly have inflection points leading to an instability or violation of causality.

The main conclusion of this chapter is that the observations of large neutron stars can certainly be explained within such a construction using the HF-QMC and NJL models, if the quark model is sufficiently stiff and the transition occurred at low density, $\bar{\rho} \sim 3\rho_0$. This is in agreement with other recent works using similar and alternative methods to phenomenologically implement a faux crossover between hadronic and quark models.

Another important conclusion is that the correction ΔP (Eq. (7.2.5)) has a considerable influence on the interpolated EoS. As it arises from calculating the pressure from the phenomenologically interpolated energy density, its meaning is somewhat ambiguous. It is required for thermodynamic consistency, but on one hand it may merely be an artefact of our chosen interpolation scheme. On the other hand, it could be associated to non-perturbative physical effects in the transition region. More in depth work is certainly needed to understand the validity and importance of this term and the overall dependence on the interpolation scheme. Further insight can only come from more detailed analysis of QCD thermodynamics above $2\rho_0$. Moreover, future heavy ion collision experiments probing this region will certainly play an important role.

8
Summary and Outlook

In this final chapter, we summarise the content of our thesis and discuss possible future directions for the line of research presented here.

The underlying theme of this thesis was the calculation of the equation of state of strongly interacting matter at zero temperature and the modelling of cold neutron stars. The influence of quark degrees of freedom was especially emphasised with inclusion of their effects not only in the deconfined quark phase, but also the confined hadronic phase where they are usually neglected.

We began by exploring the hadronic equation of state for nuclear matter in the quark-meson coupling model, including full Fock terms. The equation of state for symmetric nuclear matter (SNM) and pure neutron matter (PNM) were calculated in a Hartree-Fock approximation of the quark-meson coupling (QMC) model. We included the effects of the four lightest mesons (σ, ω, ρ and π) and most notably the tensor interaction of the vector mesons. The results for a comprehensive set of nuclear matter properties, including K_0, L_0, K_{sym}, Q_0, $K_{\tau,v}$ and hyperon optical potentials at saturation density were studied in detail. We compared our numerical results with empirical data, CEFT and alternative models.

For most properties of nuclear matter, such as the incompressibility, we found good agreement with values extracted from empirical data for the majority of model variations considered. While the incompressibility was found to increase by the addition of the Fock terms in some cases and tended to lie at the mid to top end of the acceptable range, it serves as a useful constraint on the additional mass parameter, Λ, associated with the form factor that appears at the meson-baryon vertices (the latter only being needed when the Fock terms are computed). A modest variation of the nuclear matter observables with this parameter (which must lie above the masses of the exchanged mesons included in the theory) was found. However, hyperon optical potentials were not as accurately reproduced within the model. We found it necessary to phenomenologically rescale the hyperon scalar couplings to achieve agreement with accepted empirically extracted values.

The symmetry energy and its slope were noticeably influenced by the Fock terms, specifically curvature was introduced into these quantities through the tensor interaction. At saturation density we found in all cases that the isospin incompressibility is within accepted constraint limits and while the slope of the symmetry energy is on the larger side, it does lie within the broad limits reported by Tsang *et al.* [87].

The consistency found between the theoretical predictions of N^3LO chiral effective field theory and the QMC model studied here for PNM up to and around nuclear matter density is very satisfying. Beyond saturation density a slightly higher energy per particle as a function of density was found. As the QMC model naturally incorporates many-body effects it was not surprising to find that it produced a stiffer EoS than models lacking three-body forces, but it also predicted a somewhat stiffer EoS above saturation density than those that did.

Overall we found the Fock terms, especially the ρN tensor interaction, to have a significant affect on the EoS of nuclear matter. This is partly because the couplings of the model are fit to the saturation properties of SNM. The additional attraction from the Fock terms after contact subtraction leads to an increased ω vector coupling. It is increased because the delicate balance between the attractive and repulsive potentials leading to the saturation of nuclear matter is changed.

After constraining the Hartree-Fock QMC model at saturation density we then applied it to matter in generalised beta equilibrium (GBEM, including leptons and the entire spin-1/2 baryon octet). Here we have taken the view that hadrons remain the pertinent degrees of freedom, implicitly assuming no transition to more exotic matter occurs up to $\rho \sim 1.2$ fm^{-3}. The resulting EoS were then used as input to integrate the TOV equations and investigate the static properties of cold neutron stars.

At densities above three times nuclear matter density, the nucleon Fock terms were found to contribute significantly to the EoS and the corresponding attraction is what is responsible for the increased pressure and larger maximum stellar masses in several scenarios. On increasing form factor mass, Λ, the maximum stellar mass increases because of the increased vector coupling and pressure coming from the Fock terms. This increased pressure arises mainly from the ρ meson contribution. Even with the brief appearance of an additional hyperon in our baseline scenario, the value of $M_{\max}$ is still slightly larger than for the "Dirac Only" scenario because of the tensor interaction. We saw that the maximum neutron star mass, for the case of nuclear matter in beta-equilibrium where hyperons must appear, lies in the range 1.80 to $2.07 M_{\odot}$. Radii also tended to increase with Λ owing to the stiffer EoS. It was found that increasing the strength of the Fock terms could not be pushed too far. For the value of $\Lambda = 1.3$GeV the incompressibility is too high and radii are becoming too large.

The increased vector coupling produces a stiffer EoS making it easier to produce neutron stars with maximum masses compatible with observation. However, the simultaneous description of nuclear matter observables, hyperon optical potentials and massive neutron stars was difficult to achieve within the model. This, plus the dependence of the incompressibility and maximum mass on Λ, led us to conclude that the Hartree-Fock model used here with σ, ω, ρ and π mesons can only reproduce nuclear matter properties, phenomenological hypernuclear optical potentials and massive neutron star observations if there is significant rescaling of the hyperon coupling constants.

Allowing for the rescaling of hyperon couplings we conclude that the maximum mass allowed in the model lies in the range $1.8 - 2.1 M_\odot$.

With increasing density, hadrons begin to overlap and therefore are not likely to remain the relevant degrees of freedom. At some point they may dissociate into some form of quark matter. Whether or not the central densities achieved in neutron stars are sufficient to produce such a transition is uncertain. This possibility motivated us to study deconfined quark matter and the possibility of a deconfinement transition in neutron stars. Transitions to quark matter have been studied by many authors, see for example Refs. [282–284] for recent accounts.

We study deconfined quark matter using the three flavour Nambu–Jona-Lasinio model based on one-gluon exchange. The model is implemented by employing Schwinger's covariant method of proper time regularisation. Comparisons are made with the more commonly used three momentum regularised model with the t' Hooft determinant term. Two different parametrisations were considered, enforcing two different energy scales within the model. The parameter set PS2 ($M_\ell = 201$ MeV) was preferred for modelling high density matter over PS1 ($M_\ell = 400$ MeV), because of the behaviour of the constituent quark mass as a function of chemical potential. For quark matter in beta equilibrium, the PS2 model produced overall qualitatively similar results to the three momentum regularised model with t' Hooft determinant term using the HK parameter set despite the different behaviour of the quark masses. Although, the PS2 model produced slightly more pressure, particularly at low density, as compared with the HK model.

The inclusion of a flavour dependent vector interaction, which arises naturally after the application of Fierz transformations to the colour current interaction, was seen to significantly stiffen the quark matter EoS. A simpler flavour independent vector interaction was also considered and found to produce an even stiffer EoS. These vector interactions suggest slightly different species fractions in quark matter. For the flavour dependent interaction, the species fraction changes with increasing strength of the vector interaction because of the explicit dependence of the beta-equilibrium equations on the vector coupling. Whereas, the flavour independent vector interaction leaves the species fractions invariant.

For reasons outlined in Ch. 7, we chose to model the transition to quark matter as a smooth crossover. This possibility is particularly intriguing and has been given much consideration recently [282, 283, 334, 358–360]. Motivation for such a transition was discussed and one method for implementing this kind of transition was presented. Hybrid equations of state were constructed using this faux crossover construction and then the properties of hybrid stars were calculated.

The transition was implemented between the developed HF-QMC and NJL models. In particular, the interpolations were implemented for two variations of the HF-QMC model and the two NJL models with varying vector interactions. The "Standard" or baseline HF-QMC model scenario and an overly stiff version of the model, namely the "$\Lambda = 1.3$ GeV" scenario, were chosen to see what affect the hadronic model had on the maximum neutron star mass. It was found that the hadronic model only had a small affect and it was mostly dependent on the quark model.

In the faux crossover method implemented in Ch. 7, at low and high density the

interpolated EoS can be seen to approach the assumed asymptotic limits, i.e. the hadronic and quark EoS, but in the intermediate region the pressure can be somewhat weakened or enhanced depending on the thermodynamic correction ΔP. This correction results from requiring thermodynamic consistency and the density dependence of the difference between the energy densities of the two EoS. Therefore ΔP is dependent on the two EoS we are interpolating between. This correction has a considerable influence on the interpolated EoS, yet its meaning is somewhat ambiguous. It is required for thermodynamic consistency, but it may merely be an artefact of our chosen interpolation scheme. However, it could be associated to non-perturbative physical effects in the transition region. As already mentioned, more in depth work is certainly needed to understand the validity and importance of this term and the overall dependence on the interpolation scheme.

The enforcement of stability and causality constraints ruled out many possible constructions, although, it was concluded that the observations of large neutron stars by Demorest [202] and Antoniadis [203] can certainly be explained within this construction using the HF-QMC and NJL models, if the quark model is sufficiently stiff and the transition occurred at low density, $\bar{\rho} \sim 3\rho_0$. Our findings with the models used in this thesis are in agreement with other recent works using similar and alternative methods to phenomenologically implement a faux crossover between various hadronic and quark models [282, 283, 334, 358–360]. Moreover, the qualitative findings of the faux crossover construction used here should also extend to other hadronic and quark models.

We would now like to highlight an important point. The conceptual separation between the incompressibility at saturation density or the slope of the symmetry energy and 'stiffness' at higher densities is critical. It is the latter, i.e., the stiffness above saturation density, which leads to massive neutron stars.

There are many possible future directions for the research presented here. Probably the most pressing issue for enhancing the description of the hadronic sector, within this Hartree-Fock version of the QMC model, is reproducing the correct binding of hyperons in nuclear matter. Specifically, the under binding of Λ hyperons in nuclear matter and accounting for the known existence of Λ-hypernuclei without the need to phenomenologically rescale couplings. As the scalar couplings are dependent on the model of confinement it would be interesting to consider alternatives to bag models. A possible alternative to the bag model is, for example, the hadronised NJL model whereby one solves the Faddeev equation [318–320, 375]. It would also be important to investigate the combined effect of the tensor interaction and quark degrees of freedom have on not only ground state properties of finite nuclei, but also excited state properties, such as giant and pygmy resonances. Inclusion of additional meson degrees of freedom could also be considered. However, it is the treatment of the lightest mesons that is most important, and the inclusion of heavier mesons (e.g. δ, K^*, ...) would necessarily be more model dependent.

As a first step of modelling three flavour quark matter in the proper time regularised NJL model we have neglected superconducting phases and restricted ourself to the mean field approximation. From other investigations, it would seem to be important to extend this version of the model to superconducting matter (see for example Refs. [290–292, 294]) and to also include quantum fluctuations which lie beyond the leading order

mean field approximation [323].

The hybrid EoS developed here hinge on the assumption that the deconfinement transition is a crossover and that we can smoothly interpolate between hadronic and quark models, essentially parametrising our ignorance of the intermediate transition region. Determining whether it is indeed a crossover or not may be possible with upcoming HIC experiments probing even higher densities and greater asymmetries. If it were found to be a valid assumption, it would offer a possible resolution to the problem of exotic degrees of freedom and massive compact stars. However, more work would be needed to understand the interpolation dependence and the physical meaning behind corrections such as ΔP.

Understanding QCD, its thermodynamics (phase diagram and EoS), emergent phenomena and how to make the connection to traditional nuclear physics have long been very important and difficult open problems. In particular, the nature of confinement and how to connect the so-called non-perturbative and perturbative regimes of QCD will need to be better understood before we can finally say that we really understand the strong interaction and hence also its application to interesting physical systems like neutron stars and finite nuclei. Much research has been performed on these topics and they will continue to be avenues of intense research for the foreseeable future with a lively back and forth between theory and experiment. Nonetheless, the future is very bright for such investigations with numerous terrestrial experiments and astrophysical observations that will be carried out in the very near future. These are anticipated to shed new light, informing and inspiring further theoretical studies.

A

Hadronic Matter Supplemental Material

A.1 Bag Model Mass Parametrisations

We use the bag model mass parametrisation including one-gluon exchange as obtained in Ref. [188]. For the spin-1/2 octet baryons these parametrisations are as follows:

$$M_{\rm N}^* = M_{\rm N} - g_\sigma\sigma + (0.002143 + 0.10562R_N^{\rm free} - 0.01791(R_N^{\rm free})^2)(g_\sigma\sigma)^2 \quad , \tag{A.1.1}$$

$$\begin{aligned} M_\Lambda^* &= M_\Lambda - (0.6672 + 0.04638R_N^{\rm free} - 0.0022(R_N^{\rm free})^2)g_\sigma\sigma \\ &+ \quad (0.00146 + 0.0691R_N^{\rm free} - 0.00862(R_N^{\rm free})^2)(g_\sigma\sigma)^2 \quad , \end{aligned} \tag{A.1.2}$$

$$\begin{aligned} M_\Sigma^* &= M_\Sigma - (0.6653 - 0.08244R_N^{\rm free} + 0.00193(R_N^{\rm free})^2)g_\sigma\sigma \\ &+ \quad (0.00064 + 0.07869R_N^{\rm free} - 0.0179(R_N^{\rm free})^2)(g_\sigma\sigma)^2 \quad , \end{aligned} \tag{A.1.3}$$

$$\begin{aligned} M_\Xi^* &= M_\Xi - (0.3331 + 0.00985R_N^{\rm free} - 0.00287(R_N^{\rm free})^2)g_\sigma\sigma \\ &+ \quad (-0.00032 + 0.0388R_N^{\rm free} - 0.0054(R_N^{\rm free})^2)(g_\sigma\sigma)^2 \quad . \end{aligned} \tag{A.1.4}$$

A.2 Self-energy

In the nuclear matter rest frame the self-energy of a baryon can be written as [150]

$$\Sigma(k) = \Sigma^{\rm s}(k) + \gamma^0\Sigma^0(k) + \vec{\gamma}\cdot\vec{k}\Sigma^{\rm v}(k) \quad . \tag{A.2.1}$$

The individual functions can be obtained by taking the appropriate traces, such that

$$\Sigma^{\rm s}(k) = \frac{1}{4}{\rm Tr}\left[\Sigma(k)\right] \quad , \tag{A.2.2}$$

$$\Sigma^{0}(k) = \frac{1}{4}{\rm Tr}\left[\gamma^0\Sigma(k)\right] \quad , \tag{A.2.3}$$

$$\Sigma^{\rm v}(k) = -\frac{1}{4|\vec{k}|^2}{\rm Tr}\left[\vec{\gamma}\cdot\vec{k}\Sigma(k)\right] \quad . \tag{A.2.4}$$

A.3 Subtraction of Contact Terms

In the process to isolate and subtract the contact terms in the integrands, we neglect energy transfer, such that

$$q^2 = (p\,' - p)^2 = p'^2 + p^2 - 2p\,'\cdot p = 2M_B^{*2} - 2p\,'\cdot p \quad , \tag{A.3.1}$$

$$\Rightarrow p\,'\cdot p = M_B^{*2} - \frac{q^2}{2} \simeq M_B^{*2} + \frac{\vec{q}^2}{2} \quad . \tag{A.3.2}$$

A.3.1 Sigma Meson

For the σ meson we have

$$\begin{aligned} M_B^{*2} + E(\vec{p}\,')E(\vec{p}) - \vec{p}\,'\cdot\vec{p} &= M_B^{*2} + p'\cdot p \\ &\simeq 2M_B^{*2} + \frac{\vec{q}^2}{2} \quad . \end{aligned} \tag{A.3.3}$$

Therefore,

$$\begin{aligned} \frac{2M_B^{*2} + \frac{\vec{q}^2}{2}}{\vec{q}^2 + m_\sigma^2} &= \frac{2M_B^{*2}}{\vec{q}^2 + m_\sigma^2} + \frac{1}{2}\frac{\vec{q}^2}{\vec{q}^2 + m_\sigma^2} \\ &= \frac{2M_B^{*2}}{\vec{q}^2 + m_\sigma^2} + \frac{1}{2}(1 - \frac{m_\sigma^2}{\vec{q}^2 + m_\sigma^2}) \\ &= \frac{2M_B^{*2} - \frac{m_\sigma^2}{2}}{\vec{q}^2 + m_\sigma^2} + \frac{1}{2} \quad . \end{aligned} \tag{A.3.4}$$

The constant term $\frac{1}{2}$ is the contact term, which we multiply by the variable ξ. In all scenarios presented in the this thesis we use $\xi = 0$.

A.3.2 Vector Meson ($\eta = \omega/\rho$) Vector-Vector Term

For the vector meson, $\eta = \omega/\rho$, we have for the Vector-Vector term

$$\begin{aligned} 2M_B^{*2} - E(\vec{p}\,')E(\vec{p}) + \vec{p}\,'\cdot\vec{p} &= 2M_B^{*2} - p\,'\cdot p \\ &= M_B^{*2} + \frac{q\cdot q}{2} \end{aligned}$$

$$\simeq \quad M_B^{*2} - \frac{\vec{q}^2}{2} \quad . \tag{A.3.5}$$

Therefore,

$$\begin{aligned} \frac{M_B^{*2} - \frac{\vec{q}^2}{2}}{\vec{q}^2 + m_\eta^2} &= \frac{M_B^{*2}}{\vec{q}^2 + m_\eta^2} - \frac{1}{2}\frac{\vec{q}^2}{\vec{q}^2 + m_\eta^2} \\ &= \frac{M_B^{*2} + \frac{m_\eta^2}{2}}{\vec{q}^2 + m_\eta^2} - \frac{1}{2} \ , \end{aligned} \tag{A.3.6}$$

where the second term is multiplied by ξ.

A.3.3 Vector Meson ($\eta = \omega/\rho$) Vector-Tensor Term

For the vector meson, $\eta = \omega/\rho$, we have for the Vector-Tensor term

$$\begin{aligned} M_B^{*2} - E(\vec{p}\,')E(\vec{p}) + \vec{p}\,' \cdot \vec{p} &= M_B^{*2} - p\,' \cdot p \\ &= \frac{q \cdot q}{2} \\ &\simeq -\frac{\vec{q}^2}{2} \quad . \end{aligned} \tag{A.3.7}$$

Therefore,

$$-\frac{1}{2}\frac{\vec{q}^2}{\vec{q}^2 + m_\eta^2} = \frac{1}{2}\left(\frac{m_\eta^2}{\vec{q}^2 + m_\eta^2} - 1\right) \ , \tag{A.3.8}$$

where the second term is multiplied by ξ.

A.3.4 Vector Meson ($\eta = \omega/\rho$) Tensor-Tensor Term

For the vector meson, $\eta = \omega/\rho$, we have for the Tensor-Tensor term

$$\begin{aligned} &(5M_B^{*2} - E(\vec{p}\,')E(\vec{p}) + \vec{p}\,' \cdot \vec{p})(M_B^{*2} - E(\vec{p}\,')E(\vec{p}) + \vec{p}\,' \cdot \vec{p}) \\ &= (4M_B^{*2} + \frac{q \cdot q}{2})(\frac{q \cdot q}{2}) \\ &\simeq (4M_B^{*2} - \frac{\vec{q} \cdot \vec{q}}{2})(-\frac{\vec{q} \cdot \vec{q}}{2}) \quad . \end{aligned} \tag{A.3.9}$$

Therefore,

$$\begin{aligned} -\frac{\vec{q}^2}{2}\left(\frac{4M_B^{*2} - \frac{\vec{q}^2}{2}}{\vec{q}^2 + m_\eta^2}\right) &= -\frac{1}{2}(4M_B^{*2} - \frac{\vec{q}^2}{2})(1 - \frac{m_\eta^2}{\vec{q}^2 + m_\eta^2}) \\ &= (-2M_B^{*2} + \frac{\vec{q}^2}{4})(1 - \frac{m_\eta^2}{\vec{q}^2 + m_\eta^2}) \\ &= -2M_B^2 + \frac{2M_B^{*2}m_\eta^2}{\vec{q}^2 + m_\eta^2} + \frac{\vec{q}^2}{4} - \frac{m_\eta^2}{4}\frac{\vec{q}^2}{\vec{q}^2 + m_{\eta^2}} \end{aligned}$$

$$= (-2M_B^{*2} - \frac{m_\eta^2}{4} + \frac{\vec{q}^2}{4}) + \frac{2M_B^{*2}m_\eta^2}{\vec{q}^2 + m_\eta^2} + \frac{m_\eta^4}{4(\vec{q}^2 + m_\eta^2)} \quad , \tag{A.3.10}$$

where the term in the bracket is multiplied by ξ.

A.3.5 Pion Term

For the π meson term we have

$$E(\vec{p}\,')E(\vec{p}) - \vec{p}\,' \cdot \vec{p} - M_B^{*2} = M_B^{*2} - \frac{q \cdot q}{2} - M_B^{*2} \simeq \frac{\vec{q}^2}{2} \quad . \tag{A.3.11}$$

Therefore,

$$\frac{1}{2}\frac{\vec{q}^2}{\vec{q}^2 + m_\pi^2} = \frac{1}{2} - \frac{1}{2}\frac{m_\pi^2}{\vec{q}^2 + m_\pi^2} \quad , \tag{A.3.12}$$

where the first term is multiplied by ξ.

B

Quark Matter Supplemental Material

B.1 Supplementary Material on Path Integrals, Generating Functionals and the Stationary Phase Approximation

As discussed in introductory QFT texts (e.g. Refs. [253, 254]) a theory can be quantised by using either canonical or path integral quantisation. The former method can become unwieldy for complicated theories, whereas the latter presents several useful simplifications that make the treatment of intricate theories simpler. Using the path integral method one can also obtain non–perturbative information through bosonisation and the Schwinger–Dyson equations. As we are considering the NJL model viewed as a low energy effective theory of QCD, where nonperturbative effects are important, we will use the path integral method to quantise and derive the NJL thermodynamic potential and gap equations for the quarks. Before diving into their derivation in the NJL model we will briefly review basic properties of the path integral for bosons and fermions and explain a connection to the partition function.

B.1.1 The Generating Functional and Green's Functions in the Canonical Formalism

In statistical physics one usually exploits the partition function of a system to determine thermodynamical quantities and correlation functions. A similar tack can be taken in a QFT by introducing a generating functional $Z[J]$, where $J(x)$ is some source function. From this generating functional all the Green's functions of a theory can be obtained through functional differentiation. I will briefly review this and related ideas which are necessary for obtaining the EoS of quark matter—see Refs. [253, 254, 376–378] for extended discussions of the following material.

A source function $J(x)$ is introduced by coupling it linearly with a field $\phi(x)$ such that

$$\mathcal{L}[\phi(x)] \to \mathcal{L}[\phi(x)] + J(x)\phi(x) \tag{B.1.1}$$

or equivalently

$$\mathcal{H}[\phi(x)] \to \mathcal{H}[\phi(x)] - J(x)\phi(x) \quad . \tag{B.1.2}$$

This amounts to a new interaction term which induces excitations in the field $\phi(x)$ and hence its name source function. We decompose the Hamiltonian as

$$\mathcal{H}[\phi(x)] = \mathcal{H}_0[\phi(x)] + \mathcal{H}_I[\phi(x)] - J(x)\phi(x) \quad , \tag{B.1.3}$$

where $\mathcal{H}_0$ and $\mathcal{H}_I$ are the free and interacting parts of the Hamiltonian respectively, likewise for the Lagrangian. The generating functional of a QFT is akin to the partition function of statistical mechanics and is defined as

$$Z[J] = \langle\Omega|U(\infty,-\infty)|\Omega\rangle_J \quad , \tag{B.1.4}$$

where U is the time evolution operator and $|\Omega\rangle$ is the full interacting ground state. This amplitude tells us the probability that, in the presence of the source function $J(x)$, we start with no particles and finish with no particles. Eq. (B.1.4) is not normalised and should be normalised by dividing by $Z[J=0]$ defining the normalised generating functional $\mathcal{Z}[J]$. This normalization assures that in the absence of a source the persistence of the vacuum is absolute, that is $\mathcal{Z}[J=0]=1$. It also removes contributions due to particles spontaneously appearing and disappearing completely independent from the source function (i.e. vacuum contributions) and we will see that this normalization is necessary to obtain finite expressions.

The evolution operator can be written in terms of Dyson's exponential form

$$U(\infty,-\infty) = \mathrm{T}e^{i\int d^4x\{\mathcal{H}_I + J(x)\phi(x)\}} \quad , \tag{B.1.5}$$

where T is the time ordering operator, but with the understanding that the fields are in the Heisenberg picture. Then, by expanding the exponential in Eq.(B.1.5), the normalised generating functional can then be expressed as

$$\mathcal{Z}[J] = 1 + \sum_{n=1}^{\infty} \frac{i^n}{n!} \int d^4x_1 \dots d^4x_n J(x_1)\dots J(x_n)\langle\Omega|\mathrm{T}\phi_H(x_1)\dots\phi_H(x_n)|\Omega\rangle \quad . \tag{B.1.6}$$

Thus the n-point Green's functions are given simply by functional differentiation,

$$G^{(n)}(x_1,\dots,x_n) \equiv \langle\Omega|\mathrm{T}\phi_H(x_1)\dots\phi_H(x_n)|\Omega\rangle = \frac{1}{i^n}\frac{\delta^n\mathcal{Z}[J]}{\delta J(x_1)\dots\delta J(x_n)}\bigg|_{J=0} \quad . \tag{B.1.7}$$

The generating functional can be found by either relating it to the S-matrix via the the Gell-Mann-Low theorem or using the path integral, which will be discussed next.

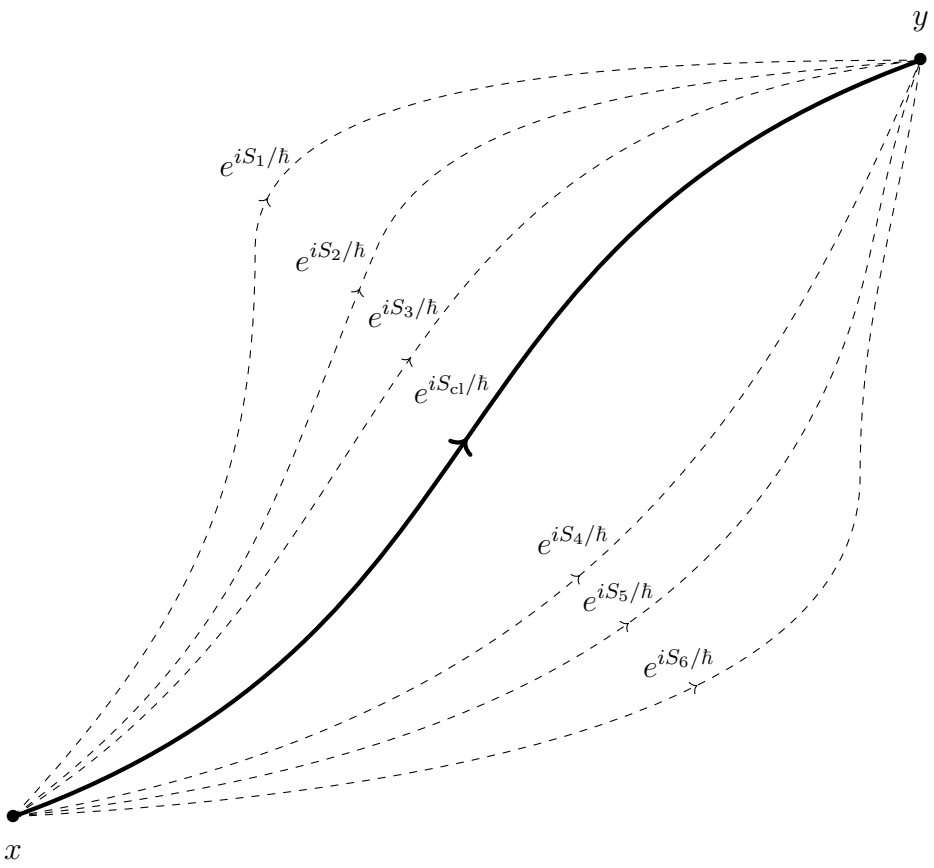

Figure 2.1.1: Schematic figure demonstrating the basis of the path integral method. The classical action $S_{\rm cl}$ is extremal.

B.1.2 The Path Integral Formalism

We will omit the usual spiel about path integrals and assume the reader is already familar with Feynman's path integration technique, where one sums over all possible (paths, field configurations) weighted by a phase factor $e^{iS/\hbar}$ where the S in the exponent is the action (c.f. Fig. B.1.2). The fields are taken to be in the Heisenberg picture and are not operators. The n–point correlations calculated in this formalism can be shown to be equivalent to the time ordered expectation values of the corresponding operators in the canonical formalism [253].

In this formalism the generating functional in terms of the path integral is

$$Z[J] = \int \mathcal{D}[\phi(x)]\ e^{i\int d^4x\ \mathcal{L}_0[\phi(x)]+\mathcal{L}_I[\phi(x)]+J(x)\phi(x)} \quad . \tag{B.1.8}$$

We can only really do Gaussian type path integrals explicitly. The free part of the Lagrangian can generally be put into this form. The interaction part of the Lagrangian is the part which causes some difficulty. In the NJL model under consideration, it is quartic in the quark fields. However, in certain cases we can transform the interacting part of the theory into something more palatable using Hubbard-Stratonovich transformations [316, 317]. These are discussed in Ch. 6.

B.1.3 Free Boson Theory

We begin with the path integral for the generating functional for a free boson scalar field theory. The Lagrangian for such a field ϕ is

$$\mathcal{L}_0[\phi(x)] = \frac{1}{2}(\partial_\mu \phi(x))^2 - \frac{1}{2}m^2\phi(x)^2 \quad . \tag{B.1.9}$$

The generating functional is then given by

$$\begin{aligned} Z_0[J] &= \int \mathcal{D}[\phi(x)]\ e^{i\int d^4x\{\mathcal{L}_0[\phi(x)]+J(x)\phi(x)\}} && \text{(B.1.10)} \\ &= \int \mathcal{D}[\phi(x)]\ e^{i\int d^4x\left\{\frac{1}{2}(\partial_\mu\phi(x))^2-\frac{1}{2}m^2\phi(x)^2+J(x)\phi(x)\right\}} \quad . && \text{(B.1.11)} \end{aligned}$$

Using integration by parts in the exponent and making the assumption that the field dies off at infinity (thus, allowing us to neglect the boundary term), results in

$$\begin{aligned} Z_0[J] &= \int \mathcal{D}[\phi(x)]\ e^{i\int d^4x\left\{-\frac{1}{2}\phi(x)\partial^2\phi(x)-\frac{1}{2}m^2\phi(x)^2+J(x)\phi(x)\right\}} && \text{(B.1.12)} \\ &= \int \mathcal{D}[\phi(x)]\ e^{i\int d^4x\left\{+\frac{1}{2}\phi(x)\left[-(\partial^2+m^2)\right]\phi(x))+J(x)\phi(x)\right\}} && \text{(B.1.13)} \\ &= \frac{N}{\sqrt{\mathrm{Det}(A(x,y))}} e^{-\frac{1}{2}\int d^4xd^4yJ(x)\left[iA^{-1}(x,y)\right]J(y)} \quad , && \text{(B.1.14)} \end{aligned}$$

where the last line can be obtained by simplifying to finite n dimensional vectors and matrices, diagonalising the matrix $A = -(\partial^2 + m^2)$, evaluating the separated Gaussian integrals and then taking the limit $n \to \infty$. The factor out front of the exponential in Eq. (B.1.14) is a product of an infinite constant and a potentially divergent determinant (product of an infinite number of eigenvalues), but normalization removes this divergent prefactor leaving

$$\mathcal{Z}_0[J] = e^{-\frac{1}{2}\int d^4xd^4yJ(x)i\Delta(x,y)J(y)} \quad , \tag{B.1.15}$$

where we have identified $iA^{-1}(x,y)$ with the scalar boson propagator $i\Delta(x,y)$—i.e. the two-point Green's function, which can be readily seen as correct by Eq. (B.1.7).

Note if we are only interested in the equilibrium properties, then we will be led to consider the natural logarithm of the unnormalised generating functional and set the source function to zero, which gives

$$\begin{aligned} \mathrm{Log}\left(Z[J=0]\right) &= \mathrm{Log}\left[\frac{N}{\sqrt{\mathrm{Det}\left(A(x,y)\right)}}\right] && \text{(B.1.16)} \\ &= \mathrm{Log}(N) - \frac{1}{2}\mathrm{Log}\left[\mathrm{Det}\left(A(x,y)\right)\right] && \text{(B.1.17)} \\ &= \mathrm{Log}(N) - \frac{1}{2}\mathrm{Tr}\left[\mathrm{Log}\left(A(x,y)\right)\right] \quad . && \text{(B.1.18)} \end{aligned}$$

Note that the Log$N$ term is a constant and hence has no effect on the equilibrium properties. In the last line we made use of the property # 4 in App. B.5.

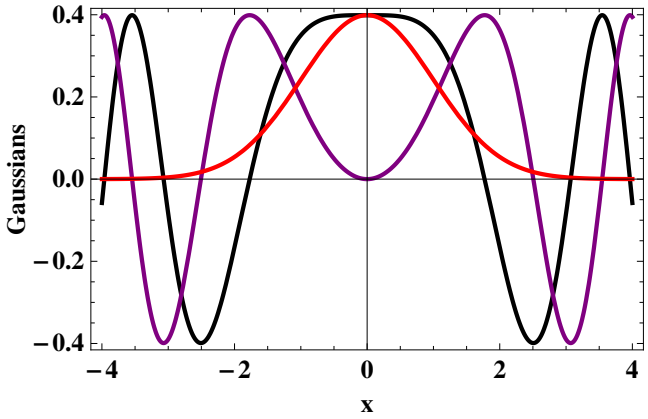

Figure 2.1.2: (Red) Eq. (B.1.19), (Black) Real part of Eq. (B.1.20) and (Purple) Imaginary part of Eq. (B.1.20).

B.1.4 Stationary and Saddle Point Approximation

Before considering the stationary and saddle point approximation to path integrals we will consider the Gaussian or normal distribution function

$$f_{\mathbb{R}}(x) = \frac{1}{\sqrt{2\pi}\sigma}\int_{-\infty}^{\infty} dx \exp\left(-\frac{(x-\mu)^2}{2\sigma^2}\right) \tag{B.1.19}$$

and a complex generalisation

$$f_{\mathbb{C}}(x) = \frac{1}{\sqrt{2\pi}\sigma}\int_{-\infty}^{\infty} dx \exp\left(+i\frac{(x-\mu)^2}{2\sigma^2}\right) \quad , \tag{B.1.20}$$

where μ is the mean, σ is the standard deviation and σ^2 is the variance. Eq. (B.1.19) and Eq. (B.1.20) are respectively simple models of Euclidean and Minkowski path integrals. The behaviour of the integrands is depicted in Fig. (B.1.4). The real Gaussian has a maximum at its mean and contributes significantly when $|x-\mu| \leq \sigma$ i.e. close to its mean value. Its complex counterpart has both real and imaginary parts which are also depicted in Fig. (B.1.4). This phase factor does not vary much about its stationary point i.e when $|x-\mu| \leq \sigma$, beyond which it fluctuates rapidly. These rapidly fluctuating contributions cancel, meaning that the most significant contribution comes from the domain close to the mean. These observations are the basis for the stationary phase and saddle point approximations to the Minkowski and Euclidean path integrals. These methods are generalisations of Laplace's method and are discussed in [322] for ordinary integrals and in [310] for path integrals.

We will not discuss the application of these methods to ordinary integrals like the analogue models in Eqs. (B.1.19) and (B.1.20), instead we simply refer the reader to Ref. [322] and apply a stationary phase analysis to a simple quantum field theory.

Consider a scalar bosonic theory whose generating functional is given by

$$Z[J] = \int \mathcal{D}\phi \exp\left(\frac{i}{\hbar}\left[S[\phi] + J\cdot\phi\right]\right) \quad , \tag{B.1.21}$$

where S is te action and we use the following dot notation

$$J \cdot \varphi \quad = \int d^4x \; J(x)\varphi(x) \quad . \tag{B.1.22}$$

Equation (B.1.21) is the same as Eq. (B.1.10) with the exception that we have kept $\hbar$ explicit instead of making use of natural units by setting $\hbar = 1$. By analogy to the arguments given above for the analogue of the Minkowski path integral it is obvious that as $\hbar \to 0$, the semi-classical limit, the dominant contribution comes from the critical points, $\phi^a_{(\mathrm{c})}$, which are the solutions to

$$\left.\frac{\delta S}{\delta \phi(x)}\right|_{\phi=\phi^a_{(\mathrm{c})}} + J = 0 \quad . \tag{B.1.23}$$

Away from a stationary point the integrand fluctuates rapidly, effectively cancelling all contributions, leading only to an asymptotically small contribution.

In general, there may be multiple stationary points. Assuming that this set of stationary points is finite and that each one can be isolated in some neighbourhood $U_a \subset \mathbb{R}^{1,3}$, where $U_i \cap U_j = \emptyset$ for $i \neq j$. From this assumption, the generating functional can be written as

$$Z[J] = \sum_{a=1,\ldots,k} \int_{U_a} \mathcal{D}\phi \; \exp\left(\frac{i}{\hbar}\left[S[\phi] + J \cdot \phi\right]\right) + \quad \text{asymptotically small contributions} \quad . \tag{B.1.24}$$

The exponent in the phase factor can be expanded about each stationary point by considering, $\phi = \phi^a_{(\mathrm{c})} + \hbar^{1/2}\phi^a_{(\mathrm{q})}$, where the $\hbar^{1/2}\phi^a_{(\mathrm{q})}$ describes small quantum fluctuations about the stationary point $\phi^a_{(\mathrm{c})}$, such that

$$S[\phi(x)] + J(x)\cdot\phi(x) \quad = \quad S[\phi^a_{(\mathrm{c})}(x)] + J(x)\cdot\phi^a_{(\mathrm{c})}(x) \tag{B.1.25}$$

$$+ \hbar^{1/2}\left(\int d^4x \; \phi^a_{(\mathrm{q})}(x)\left(\left.\frac{\delta S}{\delta\phi(x)}\right|_{\phi=\phi^a_{(\mathrm{c})}} + J(x)\right)\right)$$

$$+ \frac{\hbar}{2}\int d^4x \int d^4y \left(\phi^a_{(\mathrm{q})}(x)\left.\frac{\delta^2 S}{\delta\phi(x)\delta\phi(y)}\right|_{\phi=\phi^a_{(\mathrm{c})}}\phi^a_{(\mathrm{q})}(y)\right)$$

$$+ \quad \ldots \quad .$$

(B.1.26)

We allow each region U_a to extend to the whole of Minkowski space $\mathbb{R}^{1,3}$. The first two terms in Eq. (B.1.25) are no longer integrated over all the field configurations as the $\phi^a_{(\mathrm{c})}$ are just constant points in the space of all field configurations. The third term in parentheses is zero by the classical equations of motion, i.e Eq. (B.1.23). These observations lead to the following expression for the generating functional upon truncating to second order

$$Z[J] \quad = \quad \sum_{a=1,\ldots,k} \exp\left(\frac{i}{\hbar}(S[\phi^a_{(\mathrm{c})}] + J\cdot\phi^a_{(\mathrm{c})})\right) \tag{B.1.27}$$

$$\times \int \mathcal{D}(\hbar^{1/2}\phi^a_{(\mathrm{q})}) \exp\left(\frac{i}{\hbar}\left[\frac{\hbar}{2}\int d^4x \int d^4y \left(\phi^a_{(\mathrm{q})} \frac{\delta^2 S}{\delta\phi(x)\delta\phi(y)}\bigg|_{\phi=\phi^a_{(\mathrm{c})}} \phi^a_{(\mathrm{q})}\right)\right]\right) ,$$

where we have made use of the invariance of the measure under translations ($\mathcal{D}\phi = \mathcal{D}(\phi^a_{(\mathrm{c})} + \hbar^{1/2}\phi^a_{(\mathrm{q})}) = \mathcal{D}(\hbar^{1/2}\phi^a_{(\mathrm{q})})$). This simplifies the generating functional, $Z[J]$, to a Gaussian integral over $\phi^a_{(\mathrm{q})}$. Performing the integration yields

$$Z[J] = \tilde{\mathcal{N}} \sum_{a=1,\ldots,k} \exp\left(\frac{i}{\hbar}(S[\phi^a_{(\mathrm{c})}] + J\cdot\phi^a_{(\mathrm{c})})\right)\left[\mathrm{Det}\left(\frac{\delta^2 S}{\delta\phi(x)\delta\phi(y)}\bigg|_{\phi=\phi^a_{(\mathrm{c})}}\right)\right]^{-1/2} , \tag{B.1.28}$$

where Det is a functional determinant. Eq. (B.1.28) is basically a resummation of 1-loop graphs. The Hessian of the action is an operator and its inverse defines a propagator for the quantum fluctuation $\phi_{(\mathrm{q})}$. In terms of the NJL model this corresponds to the propagators of the auxiliary fields, i.e., the mesons. Making use of the operator identity $\mathrm{Log}\left[\mathrm{Det}\left(\hat{\mathcal{O}}\right)\right] = \mathrm{Tr}\left[\mathrm{Log}\left(\hat{\mathcal{O}}\right)\right]$ we have

$$Z[J] = \tilde{\mathcal{N}} \sum_{a=1,\ldots,k} \exp\left(\frac{i}{\hbar}(S[\phi^a_{(\mathrm{c})}] + J\cdot\phi^a_{(\mathrm{c})}) + \frac{i\hbar}{2}\mathrm{Tr}\left[\mathrm{Log}\left(\frac{\delta^2 S}{\delta\phi(x)\delta\phi(y)}\bigg|_{\phi=\phi^a_{(\mathrm{c})}}\right)\right]\right) , \tag{B.1.29}$$

For simplicity in our NJL model calculations using the Lagrangian given by Eq. (6.3.8), we assume that there is only one unique critical point. Given that the bosonised form of this Lagrangian is at most quadratic in the auxiliary fields, we will assume that the critical point can be uniquely determined by physical considerations. In higher-order multi-quark interactions other critical points may appear and make important contributions [379].

B.1.5 The Connected Generating Functional and the Effective Action

The connected generating functional $W[J]$ is related to the generating functional $Z[J]$ by

$$Z[J] = e^{iW[J]} . \tag{B.1.30}$$

Clearly, if the exponential is expanded in a functional Taylor series then every connected and disconnected graph is generated as every disconnected graph is a product of connected graphs. It just remains to show the expansion coefficients are correct [253]. The connected generating functional is then calculated by taking the logarithm

$$W[J] = -i\mathrm{Log}Z[J] . \tag{B.1.31}$$

Taking the first functional derivative with respect to the source function J and setting the source to zero we obtain the expectation value of the field ϕ, that is

$$\frac{\delta W[J]}{\delta J(x)} = -i\frac{1}{Z[J]}\frac{\delta Z[J]}{\delta J(x)}\bigg|_{J=0} = \langle\phi(x)\rangle . \tag{B.1.32}$$

The second order functional derivatives with respect to the source functions give rise to the two point connected Green's functions and so on,

$$G^{(n)}_{\text{conn}}(x_1,\ldots,x_n) = \langle\phi(x_1),\ldots,\phi(x_n)\rangle_{\text{conn}} = -i^{n+1}\frac{\delta W[J]}{\delta J(x_1)\ldots J(x_2)}\bigg|_{J=0} \quad . \tag{B.1.33}$$

A new object can be obtained from the connected generating functional by refraining from setting the source function to zero, such that

$$\frac{\delta W[J]}{\delta J(x)} = -i\frac{1}{Z[J]}\frac{\delta Z[J]}{\delta J(x)} = \langle\phi(x)\rangle[J] \equiv \varphi(x) \quad , \tag{B.1.34}$$

where $\varphi(x)$ is commonly referred to as a background field. It is a classical function of space-time, but a functional of the source function J. The situation can be inverted and the source function, J, can be thought of a functional of φ instead. Using this background field we can obtain yet another generating functional $\Gamma[\varphi]$ via a Legendre transformation,

$$\Gamma[\varphi] = W[J] - J\cdot\varphi \quad . \tag{B.1.35}$$

This new generating functional, Γ, is called the effective action and is the generating functional for the one particle irreducible (1PI) graphs[1]. It is a functional of the classical field φ only. Performing functional differentiation with respect to φ, one obtains

$$\frac{\delta\Gamma[\varphi]}{\delta\varphi(x)} = -J(x) \quad . \tag{B.1.36}$$

Evaluating Eq. (B.1.36) at $\varphi(x) = \langle\phi(x)\rangle$ implies the source function is zero and that the Euler-Lagrange equations can be obtained by extremising the effective action

$$\frac{\delta\Gamma[\varphi]}{\delta\varphi(x)}\bigg|_{\varphi=\langle\phi\rangle} = 0 \quad . \tag{B.1.37}$$

The Hessian of the effective action gives the inverse propagator

$$\frac{\delta^2\Gamma[\varphi]}{\delta\varphi(x)\delta\varphi(y)}\bigg|_{\varphi=\langle\phi\rangle} = \Delta^{-1}(x-y) \quad . \tag{B.1.38}$$

More generally, the n-point 1PI correlation functions can be obtained from higher-order functional differentiations,

$$G^{(n)}_{\text{1PI}}(x_1,\ldots,x_n) = \langle\phi(x_1,\ldots,x_n)\rangle_{\text{1PI}} = i\frac{\delta^n\Gamma[\varphi]}{\delta\varphi(x_1)\ldots\delta\varphi(x_n)}\bigg|_{\varphi=\langle\phi\rangle} \quad . \tag{B.1.39}$$

The relationships between the action, S; and the generating functional, $Z[J]$; the connected generating functional, $W[J]$; and the effective action, $\Gamma[\varphi]$; are summarised in Fig. (B.1.5).

[1] a.k.a. proper vertices

Moreover, with this generating functional we can define an effective potential. The effective action can be generally written as

$$\Gamma[\varphi] = \int d^4x \left[f(\varphi)\partial_\mu\varphi\partial^\mu\varphi - V_{\text{eff}}(\varphi) + \text{ higer order derivative terms} \right] \quad , \tag{B.1.40}$$

where $V_{\text{eff}}(\varphi)$ is called the effective potential. Simplifying to a constant field configuration $\varphi(x) = \varphi_{(\text{const})}$

$$\Gamma[\varphi_{(\text{const})}] = \int d^4x \left[-V_{\text{eff}}(\varphi_{(\text{const})}) \right] = -V_{\text{eff}}(\varphi_{(\text{const})}) V_{\mathbb{R}^{1,3}} \quad , \tag{B.1.41}$$

where $V_{\mathbb{R}^{1,3}}$ denotes the space-time volume.

To calculate the effective action and potential one generally needs to choose an approximation scheme. The effective action is related to the original generating functional by

$$e^{\frac{i}{\hbar}\{\Gamma[\varphi] + J\cdot\varphi\}} = \mathcal{N} \int \mathcal{D}\phi \; e^{\frac{i}{\hbar}\{S[\phi] + J\cdot\phi\}} \quad . \tag{B.1.42}$$

As can be seen in Eq. (B.1.42), $\Gamma[\varphi]$, includes the quantum effects due to the functional integration. To extract useful information from this equation we consider the effective action expanded in a power series of $\hbar$:

$$\Gamma[\varphi] = \sum_{n=0}^{\infty} \hbar^n \Gamma_{(n)}[\varphi] \tag{B.1.43}$$

on the left hand side of Eq. (B.1.42) and we perform a stationary phase analysis (described in Sec. B.1.4 on the right hand side and equate powers of $\hbar$. The leading term for the (quantum) effective action is simply the (classical) action,

$$\Gamma_{(0)}[\phi^{(\text{c})}] = S[\phi^{(\text{c})}] \quad , \tag{B.1.44}$$

where to this order $\varphi = \phi^{(\text{c})} = \langle\phi\rangle$. This order of approximation corresponds to the mean field approximation.

B.1.6 Connection to QFTs at Finite Temperature and Statistical Mechanics

The subtle connection between QFT and statistical mechanics can be understood rather simply [376]. To explain their relation to one another we will introduce the method known as the Matsubara or imaginary time formalism. It requires the introduction of the concepts of imaginary time and Wick rotations allowing us to map a zero temperature QFT to a statistical (finite temperature or thermal) field theory. We will not develop the finite temperature formalism fully, and we merely note that other methods do exist to generalise QFTs to finite temperature, such as the real time formalism, but as we are only interested in the equilibrium properties of (the zero temperature limit of) the quark matter EoS the Matsubara formalism will suffice. It is introduced to elucidate the connection between the generating functional in a zero temperature

General Unnormalised Generating functional:

$$Z[J]$$

Normalised Generating Functional:

$$\mathcal{Z}[J] = \frac{Z[J]}{Z[0]}$$

Connected Generating Functional:

$$W[J] = -i\mathrm{Log}Z[J]$$

Effective action or Generating Functional for 1PI graphs:

$$\Gamma[\varphi] = W[J] - J \cdot \varphi$$

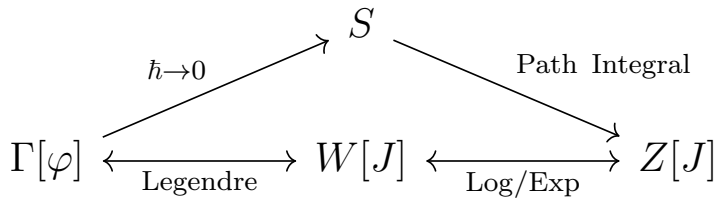

Figure 2.1.3: Summary of generating functionals of interest and their interrelations.

QFT, its partition function and to make a connection to the more familiar statistical mechanics.

As discussed in the previous sections the generating functional contains all the information of a QFT. To study the statistical behaviour of a quantum system in thermal equilibrium the analogous quantity, the partition function, is introduced. An appropriate ensemble is first chosen and the density matrix is defined. From this the partition function can then be defined. The partition function in which we are interested in this thesis is the grand canonical partition function, as we will be taking both the chemical potential of any conserved charges and the temperature to be fixed (the temperature will be taken to be zero, but for the moment we will consider the temperature to be finite). For the grand canonical ensemble the density matrix is

$$\rho(\beta) = e^{-\beta(\hat{H}-\mu\hat{N})} \tag{B.1.45}$$

where β is the inverse equilibrium temperature, $\beta = \dfrac{1}{k_B T}$ and k_B is the Boltzmann constant, which we take to be unity. The $\hat{H}$ is the Hamiltonian describing the system, $\hat{N}_i$ are the number operators of the conserved charges and the μ_i are the associated chemical potentials. The grand canonical partition function is in general given by

$$Z = \mathrm{Tr}\rho(\beta) = \mathrm{Tr}\left[e^{-\beta(\hat{H}-\mu_i\hat{N}_i)}\right] \quad , \tag{B.1.46}$$

where the trace, Tr, stands for the "sum" over all expectation values in any complete basis. In a QFT the trace is an integral over an infinite dimensional basis. From this partition function all the equilibrium thermodynamical variables and correlation functions can be determined and as such it is also referred as a generating functional.

The generating functional and partition function are defined in terms of an exponential evolution operator and an exponential Boltzmann like factor. In QFT this exponential is complex taking the form $e^{-i\hat{H}t/\hbar}$, whereas in statistical mechanics it is real, $\sim e^{-\beta\hat{H}}$. The similarity between these two theories, by which both their generating functionals are dependent on exponential functions, motivates the transformations

$$\frac{it}{\hbar} \longleftrightarrow \frac{1}{k_B T} \quad , \tag{B.1.47}$$

mapping a QFT onto a statistical (thermal) field theory or vice versa. In this way imaginary time ($\tau \equiv it$) in a QFT behaves as inverse temperature in a statistical field theory.

It is important to realise that imaginary time is not introduced by simply multiplying by i, but rather performing a rotation of t or equivalently p^0 in the complex plane by $-\pi/2$ or $\pi/2$ respectively. These rotations are depicted in Figs. B.1.6 and B.1.6. This analytic continuation into the complex plane is called a Wick rotation, a Wick rotated QFT a Euclidean quantum field theory, its action the Euclidean action, and so on. The rotation changes the signature of metric from Minkowski $(+,-,-,-)$ to Euclidean $(+,+,+,+)$. The transition to imaginary time (or Euclidean space) has important consequences such as the path integral appears to have better convergence and be better defined. Moreover, we no longer need to introduce the Feynman $i\epsilon$ in the propagators because there is no longer a pole for real values of momentum and energy.

Upon the identification $\Delta\tau = i\Delta t = \beta$, the imaginary time integral is integrated only over a finite interval on the imaginary axis and by definition of the partition function, the trace imposes the evolution of the initial state back to the same state. For a real scalar boson theory, this results in a restriction on the possible field configurations to be periodic in τ with period β. Conversely, due to the anti-commuting nature of fermions their field configurations are restricted to be anti-periodic. This compactification in the imaginary time coordinate means that the Fourier expansions of the fields will only depend on a discrete set of frequencies, where the (anti-)periodicity restricts the frequencies to be

$$\omega_n = \begin{cases} \dfrac{2n\pi}{\beta} & \text{bosons} \\ \dfrac{(2n+1)\pi}{\beta} & \text{fermions} \end{cases} \quad . \tag{B.1.48}$$

That is, only even modes contribute for bosons and only odd modes contribute for fermions. It is also important to realise that in using the Matsubara formalism to generalise a zero temperature QFT to finite temperature there is no longer a time, time has been traded for finite temperature. In this formalism we can work out the Finite temperature Green's functions, thermal averages and even do perturbation theory, but it is only relevant for a system in thermodynamic equilibrium. It is assumed that one can rotate back, but this may not always be well defined. See Table B.1.6 for a summary of changes that occur upon rotation.

Table 2.1.1: Transformations upon Wick rotation and various definitions.

Minkowski	Euclidean
$g_{\mu\nu}$	$-\delta_{\mu\nu}$
t	$-i\tau$
$\vec{x}$	$\vec{x}$
$x^\mu \equiv (t, \vec{x})$	$x^\mu_E \equiv (\tau, \vec{x})$
x^2	$-x^2_E$
d^4x	$-id^4x_{\mathrm{E}}$
p^0	ip^4
$\vec{p}$	$\vec{p}$
$p^\mu \equiv (p^0, \vec{p})$	$p^\mu_E \equiv (p^4, \vec{p})$
d^4p	id^4p_{E}
p^2	$-p^2_{\mathrm{E}}$
V^0	$-iV_4$
$\vec{V}$	$\vec{V}$
$V^\mu \equiv (V^0, \vec{V})$	$V^\mu_E \equiv (V^4, \vec{V})$
iS	$-S_{\mathrm{E}}$
$Z[J] \equiv \int \mathcal{D}\phi e^{\frac{i}{\hbar}S[\phi]} \equiv e^{\frac{iW}{\hbar}}$	$Z_{\mathrm{E}}[J] \equiv \int \mathcal{D}\phi e^{-\frac{1}{\hbar}S_E[\phi]} \equiv e^{\frac{W_E}{\hbar}}$
$W[J] \equiv -i\hbar \mathrm{Log} Z[J]$	$W_E[J] \equiv \hbar \mathrm{Log} Z_E[J]$
$\varphi(x) \equiv \dfrac{\delta W}{\delta J(x)}$	$\varphi_E(x) \equiv \dfrac{\delta W_E}{\delta J(x)}$
$\Gamma[\varphi] \equiv W[J] - J \cdot \varphi$	$\Gamma_E[\varphi] \equiv J \cdot \varphi - W_E[J]$
$\Gamma^{1-\mathrm{loop}}[\varphi] \equiv S[\varphi] + \dfrac{i\hbar}{2}\mathrm{Tr}\left[\mathrm{Log}\left(S''[\varphi]\right)\right]$	$\Gamma^{1-\mathrm{loop}}_E[\varphi] \equiv S_E[\varphi] + \dfrac{\hbar}{2}\mathrm{Tr}\left[\mathrm{Log}\left(S''_E[\varphi]\right)\right]$

To obtain the equilibrium quantities of interest, such as the internal energy, pressure and density, one uses the usual methods of statistical mechanics obtaining the thermodynamic potential, which is analogous to the zero temperature effective potential. At zero temperature we do not have the restriction to a finite imaginary time interval and therefore do not have to worry about the considerations of discrete frequency modes due to the compactification that occurs at finite temperature. Alternatively, if we instead mapped our QFT to a thermal field theory by the method described above and obtained the thermodynamical variables through the partition function, and then took the zero temperature limit, this would reduce to the same result at our level of approximation in the calculation of the quark matter EoS using the NJL model. Moreover, the thermal Green's functions and thermal averages would also reduce to their zero temperature counter parts.

B.1.7 Free Fermion Theory

The free fermions are described by the following Lagrangian density

$$\mathcal{L}_0 = \bar{\psi}(i\partial\!\!\!/ - m)\psi \quad , \tag{B.1.49}$$

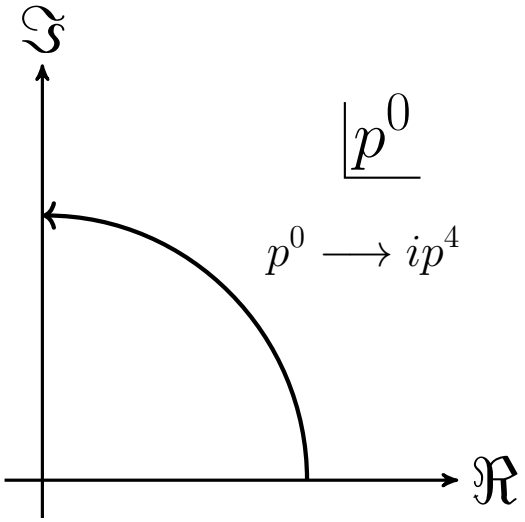

Figure 2.1.4: Wick rotation in momentum space.

where ψ and its adjoint $\bar{\psi} = \psi^\dagger \gamma^0$ are four component Dirac spinors, $\not{\partial} = \gamma^\mu \partial_\mu$ and γ^μ are the Dirac matrices [253]. The equation of motion, the Dirac equation, is obtained from the Euler-Lagrange equation.

Using the standard methods, the conjugate momentum of the field ψ is found to be $\pi_\psi = i\psi^\dagger$ and therefore must be treated independently from ψ. By Noether's theorem this Lagrangian has the conserved current $j^\mu = \bar{\psi}\gamma^\mu\psi$ due to a $U(1)$ invariance. The associated conserved charge is

$$Q = \int d^3x j^0 = \psi^\dagger \psi \quad . \tag{B.1.50}$$

Fermions obey the Pauli exclusion principle and as a consequence the fields ψ and $\bar{\psi}$ anti-commute. In the path integral formulation, these fields are interpreted as Grassmann numbers. We will not review the basic results involving fermionic path integrals and instead refer the reader to Refs. [253] and [376]. In a similar way in which the scalar boson generating functional is derived, the fermion generating functional can also be derived. It is important to note that the fields ψ and $\bar{\psi}$ couple to different sources $\bar{\eta}(x)$ and $\eta(x)$, respectively. In the case of anti-commuting Grassman numbers the useful finite dimensional identity which can be generalised to an infinite number of dimensions is

$$\int d\eta_1^\dagger d\eta_1 \ldots d\eta_N^\dagger d\eta_N e^{\eta^\dagger D \eta} = \mathrm{Det} D \quad , \tag{B.1.51}$$

where D is an $N \times N$ matrix. The unnormalised generating functional is

$$\begin{aligned} Z[\eta, \bar{\eta}] &= \int \mathcal{D}[\psi(x)]\mathcal{D}[\bar{\psi}(x)] \qquad (B.1.52) \\ &\quad \times \exp\left(i \int d^4x \left[\bar{\psi}(x)(i\not{\partial} - m)\psi(x) + \bar{\eta}(x)\psi(x) + \bar{\psi}(x)\eta(x) \right] \right) \\ &= \mathrm{Det}(S^{-1}) \exp\left(-i \int d^4x d^4y \; \bar{\eta}(x)(i\not{\partial} - m)^{-1}\eta(y) \right) \quad . \qquad (B.1.53) \end{aligned}$$

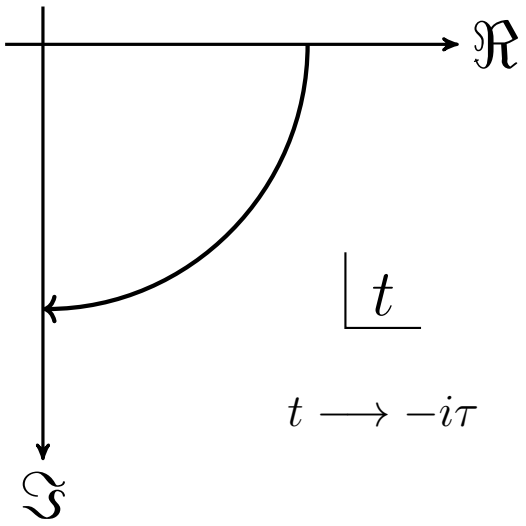

Figure 2.1.5: Wick rotation in configuration space.

Eq. (B.1.53) can be normalised by dividing by $Z[\eta = 0, \bar{\eta} = 0]$. For reference the normalised generating functional is

$$\mathcal{Z}[\eta, \bar{\eta}] = \exp\left(-i \int d^4x d^4y \; \bar{\eta}(x) S(x-y) \eta(y)\right) \quad , \tag{B.1.54}$$

where we introduced the Fermion propagator $S(x-y) = (i\partial\!\!\!/ - m)^{-1}$.

B.2 Symmetry Lie Group and Lie Algebra Conventions

SU(N) generators G_a, $a = 1, \ldots, N^2 - 1$ satisfy the commutation relations

$$[G_a, G_b] = i f_{abc} G_c \quad , \tag{B.2.1}$$

where f_{abc} are the structure constants of the group. These generators form the associated Lie algebra $\mathfrak{su}(N)$ with the Lie bracket defined by the commutator. These generators are normalised such that $\mathrm{Tr}[G_a G_b] = 2\delta_{ab}$ and are commonly supplemented by

$$G_0 = \sqrt{\frac{2}{N}} \mathbb{1}_N \quad . \tag{B.2.2}$$

Specifically, the SU(2) generators τ_a, Pauli matrices, are given by

$$\tau_1 = \begin{bmatrix} 0 & 1 \\ 1 & 0 \end{bmatrix}, \quad \tau_2 = \begin{bmatrix} 0 & -i \\ i & 0 \end{bmatrix}, \quad \tau_3 = \begin{bmatrix} 1 & 0 \\ 0 & -1 \end{bmatrix} \quad . \tag{B.2.3}$$

These are supplemented by $\tau_0 = \mathbb{1}_2$.

The SU(3) generators $t_a(\lambda_a)$ for colour(flavour), are given by

$$\lambda_1 = \begin{bmatrix} 0 & 1 & 0 \\ 1 & 0 & 0 \\ 0 & 0 & 0 \end{bmatrix}, \qquad \lambda_2 = \begin{bmatrix} 0 & -i & 0 \\ i & 0 & 0 \\ 0 & 0 & 0 \end{bmatrix}, \qquad \lambda_3 = \begin{bmatrix} 1 & 0 & 0 \\ 0 & -1 & 0 \\ 0 & 0 & 0 \end{bmatrix}, \tag{B.2.4}$$

$$\lambda_4 = \begin{bmatrix} 0 & 0 & 1 \\ 0 & 0 & 0 \\ 1 & 0 & 0 \end{bmatrix}, \qquad \lambda_5 = \begin{bmatrix} 0 & 0 & -i \\ 0 & 0 & 0 \\ i & 0 & 0 \end{bmatrix}, \qquad \lambda_6 = \begin{bmatrix} 0 & 0 & 0 \\ 0 & 0 & 1 \\ 0 & 1 & 0 \end{bmatrix}, \tag{B.2.5}$$

$$\lambda_7 = \begin{bmatrix} 0 & 0 & 0 \\ 0 & 0 & -i \\ 0 & i & 0 \end{bmatrix}, \quad \lambda_8 = \frac{1}{\sqrt{3}} \begin{bmatrix} 1 & 0 & 0 \\ 0 & 1 & 0 \\ 0 & 0 & -2 \end{bmatrix} \quad . \tag{B.2.6}$$

$$\tag{B.2.7}$$

and are referred to as the Gell–Mann matrices. These matrices which generate SU(3) can be supplemented by $\lambda_0 = \sqrt{\frac{2}{3}}\mathbb{1}_3$.

B.3 Fierz Transformations

A number of textbooks and review articles derive Fierz transformations, we refer the reader to Ref. [310]. Fierz transformations for the Dirac space portion of the interaction vertices in the $q\bar{q}$–channel are given by

$$\begin{bmatrix} (\mathbb{1}_{N_\mathrm{D}})_{ij}(\mathbb{1}_{N_\mathrm{D}})_{kl} \\ (i\gamma_5)_{ij}(i\gamma_5)_{kl} \\ (\gamma_\alpha)_{ij}(\gamma^\alpha)_{kl} \\ (\gamma_\mu\gamma_5)_{ij}(\gamma^\mu\gamma_5)_{kl} \\ (\sigma_{\mu\nu})_{ij}(\sigma^{\mu\nu})_{kl} \end{bmatrix} = \begin{bmatrix} 1/4 & -1/4 & 1/4 & -1/4 & 1/8 \\ -1/4 & 1/4 & 1/4 & -1/4 & -1/8 \\ 1 & 1 & -1/2 & -1/2 & 0 \\ -1 & -1 & -1/2 & -1/2 & 0 \\ 3 & -3 & 0 & 0 & -1/2 \end{bmatrix} \begin{bmatrix} (\mathbb{1}_{N_\mathrm{D}})_{il}(\mathbb{1}_{N_\mathrm{D}})_{kj} \\ (i\gamma_5)_{il}(i\gamma_5)_{kj} \\ (\gamma_\alpha)_{il}(\gamma^\alpha)_{kj} \\ (\gamma_\mu\gamma_5)_{il}(\gamma^\mu\gamma_5)_{kj} \\ (\sigma_{\mu\nu})_{il}(\sigma^{\mu\nu})_{kj} \end{bmatrix} . \tag{B.3.1}$$

General SU(N) Fierz transformations for the colour and flavour space portions of the interaction vertices are given by

$$\begin{bmatrix} (\mathbb{1}_N)_{ij}(\mathbb{1}_N)_{kl} \\ (\lambda_a)_{ij}(\lambda_a)_{kl} \end{bmatrix} = \begin{bmatrix} 1/N & 1/2 \\ 2(\frac{N^2-1}{N^2}) & -1/N \end{bmatrix} \begin{bmatrix} (\mathbb{1}_N)_{il}(\mathbb{1}_N)_{kj} \\ (\lambda_a)_{il}(\lambda_a)_{kj} \end{bmatrix} \quad . \tag{B.3.2}$$

B.4 Useful Functional Formulas

Given a functional $F = F[f(x)]$, then consider its value as $f(x) \to f(x) + \delta\eta(x)$. The functional Taylor expansion in powers of the perturbation is

$$\begin{aligned} F[f(x)+\delta\eta(x)] &= F[f(x)] + \int d^4x\ \delta\eta(x)\frac{\delta F[f(x)]}{\delta f(x)} \\ &\quad + \frac{1}{2}\int d^4x d^4y\ \delta\eta(x)\frac{\delta^2 F[f(x)]}{\delta f(x)\delta f(y)}\delta\eta(y) + \ \ldots \end{aligned} \tag{B.4.1}$$

A functional Taylor expansion is used in the stationary phase approximation.

The following formulas are useful for determining meson propagators:

$$\frac{\delta}{\delta f(y)}\mathrm{Tr}\left[\mathrm{Log}\left(\hat{\mathcal{O}}[f(x)]\right)\right] = \mathrm{Tr}\left[\hat{\mathcal{O}}^{-1}[f(x)]\frac{\delta\hat{\mathcal{O}}[f(x)]}{\delta f(y)}\right] \tag{B.4.2}$$

and

$$\begin{aligned}\frac{\delta^2}{\delta f(z)\delta f(y)}\mathrm{Tr}\left[\mathrm{Log}\left(\hat{\mathcal{O}}[f(x)]\right)\right] &= \frac{\delta}{\delta f(z)}\mathrm{Tr}\left[\hat{\mathcal{O}}^{-1}[f(x)]\frac{\delta\hat{\mathcal{O}}[f(x)]}{\delta f(y)}\right] &\text{(B.4.3)}\\ &= -\mathrm{Tr}\left[\hat{\mathcal{O}}^{-1}[f(x)]\frac{\delta\hat{\mathcal{O}}[f(x)]}{\delta f(z)}\hat{\mathcal{O}}^{-1}[f(x)]\frac{\delta\hat{\mathcal{O}}[f(x)]}{\delta f(y)}\right]\\ &\quad +\mathrm{Tr}\left[\hat{\mathcal{O}}^{-1}[f(x)]\frac{\delta^2\hat{\mathcal{O}}[f(x)]}{\delta f(z)\delta f(y)}\right] . &\text{(B.4.4)}\end{aligned}$$

B.5 Useful Properties Involving Determinants

In the following $a \in \mathbb{F}$ where $\mathbb{F}$ is a field (in the abstract algebra sense of the word) considered usually to be either $\mathbb{R}$ or $\mathbb{C}$, $\mathbb{1}_N$ is an identity matrix of dimension N and A, B are non-singular matrices. The following properties also generalise to operators.

1. $\mathrm{Det}(AB) = \mathrm{Det}A.\mathrm{Det}B$
2. $\mathrm{Det}(a\mathbb{1}_N) = a^N$
3. $\mathrm{Det}(a\mathbb{1}_N \otimes \mathbb{1}_M) = \mathrm{Det}(a\mathbb{1}_{NM}) = a^{NM}$, where the tensor product for matrices is simply the Kronecker product.
4. $$\begin{aligned}\mathrm{Det}\left(\hat{\mathcal{O}}\right) &= \prod_i \lambda_i &\text{(B.5.1)}\\ &= \mathrm{Exp}\left[\mathrm{Log}\left(\prod_i \lambda_i\right)\right] &\text{(B.5.2)}\\ &= \mathrm{Exp}\left[\sum_i \mathrm{Log}\left(\lambda_i\right)\right] &\text{(B.5.3)}\\ &= \mathrm{Exp}\left[\mathrm{Tr}\left(\mathrm{Log}\left\{\hat{\mathcal{O}}\right\}\right)\right] &\text{(B.5.4)}\end{aligned}$$

   where $\hat{\mathcal{O}}$ is a non-singular operator and λ_i are its eigenvalues, obtaining

$$\mathrm{Log}\left[\mathrm{Det}\left(\hat{\mathcal{O}}\right)\right] = \mathrm{Tr}\left[\mathrm{Log}\left(\hat{\mathcal{O}}\right)\right] \quad . \tag{B.5.5}$$

B.6 Schwinger's Proper Time Regularisation

Schwinger's proper time regularisation scheme [321] is a two step process. It begins with the identification

$$\mathrm{Log}A = -\int d\tau \ \frac{e^{-\tau A}}{\tau} \quad . \tag{B.6.1}$$

Taking the partial derivative with respect to A on both sides of Eq. (B.6.1) one can show that

$$\frac{1}{A} = \int d\tau \ e^{-\tau A} \quad , \tag{B.6.2}$$

$$\frac{1}{A^2} = \int d\tau \ \tau e^{-\tau A} \quad , \tag{B.6.3}$$

and so on. Using the principle of mathematical induction one can extend this to

$$\frac{1}{A^n} = \frac{1}{(n-1)!}\int d\tau \ \tau^{n-1} e^{-\tau A} \quad . \tag{B.6.4}$$

This way of rewriting the above terms does not regularise the integrals appearing in NJL model calculations, but it puts them into a form where terms may easily be combined and then regularised. Upon making use of one of the above identifications the integrand is then multiplied by a regulating function, $r_{\mathrm{UV}}(\tau)$, which we will take to be a straightforward step function,

$$r_{\mathrm{UV}}(\tau) = \Theta\left(\tau - \frac{1}{\Lambda^2_{\mathrm{UV}}}\right) \quad . \tag{B.6.5}$$

This is the most common form [290, 291, 310, 315, 380, 381], although alternative forms for the regulating function could be considered [310]. It should also be noted that the model could be regularised at the level of the action in this way, instead of regulating each divergent expression as it appears by the above substitutions [310]. At our level of approximation both approaches are equivalent.

B.7 Effective Potential Derivation

B.7.1 Effective Potential in Vacuum

In vacuum the mean field effective potential is calculated from Eqs. (6.4.15), (6.4.39) and (6.4.37). As a function of the constituent quark masses, or equivalently the quark condensates, the effective potential takes the form

$$V^{\mathrm{NJL}}_{\mathrm{MF}}(M_u, M_d, M_s) = i\mathrm{Tr}\left[\mathrm{Log}\left(S^{-1}\right)\right] + 2G_{\mathrm{S}}\sum_{i\in\{u,d,s\}}(\rho^{\mathrm{s}}_i)^2 \tag{B.7.1}$$

$$= i\sum_{i\in\{u,d,s\}}\mathrm{Tr}\left[\mathrm{Log}\left(S_i^{-1}\right)\right] + 2G_{\mathrm{S}}\sum_{i\in\{u,d,s\}}(\rho^{\mathrm{s}}_i)^2 \quad , \tag{B.7.2}$$

where the last trace is a functional trace over configuration space and also over Dirac and colour spaces. The first trace is also over flavour space, but as S^{-1} is diagonal, Eq. (6.4.7), this amounts to just a sum over flavours. Diagonality follows from

Eq. (6.4.7), Eq. (6.4.44) and the fact that only $S_u^{(c)}$, $S_d^{(c)}$ and $S_s^{(c)}$ are non-zero. In Eq. (B.7.1) we also made use of

$$\sum_{a=0}^{8} \frac{(S_a^{(c)})^2}{4G_S} = \sum_{a=0}^{8} G_S \langle \bar{\psi} \lambda_a \psi \rangle^2 = 2G_S \sum_{i \in \{u,d,s\}} \langle \bar{\psi}_i \psi_i \rangle^2 = 2G_S \sum_{i \in \{u,d,s\}} (\rho_i^s)^2 \quad . \tag{B.7.3}$$

Using property # 4 of App. B.5, the fact that the our expressions are degenerate in colour[2] and the following result that the determinant in Dirac space of the inverse propagator is

$$\mathrm{Det}_D(\not{p} - M_i) = \mathrm{Det}_D \begin{pmatrix} -M_i & 0 & p^0 - p^3 & -p^1 + ip^2 \\ 0 & -M_i & -p^1 + ip^2 & p^0 + p^3 \\ p^0 + p^3 & p^1 - ip^2 & -M_i & 0 \\ p^1 + ip^2 & p^0 - p^3 & 0 & -M_i \end{pmatrix} = (p^2 - M_i^2)^2 \quad , \tag{B.7.4}$$

the first term in Eq. (B.7.2) can be written as

$$i \sum_{i \in \{u,d,s\}} \mathrm{Tr} \left[\mathrm{Log} \left(S_i^{-1} \right) \right] = i \sum_{i \in \{u,d,s\}} N_C \int \frac{d^4p}{(2\pi)^4} \mathrm{Log}(p^2 - M_i^2)^2 \tag{B.7.5}$$

$$= 2iN_C \sum_{i \in \{u,d,s\}} \int \frac{d^4p}{(2\pi)^4} \mathrm{Log}(p^2 - M_i^2) \quad . \tag{B.7.6}$$

This term is divergent and must be regularised. Eq. (B.7.2) can now be written as

$$V_{MF}^{NJL}(M_u, M_d, M_s) = 2iN_C \sum_{i \in \{u,d,s\}} \int \frac{d^4p}{(2\pi)^4} \mathrm{Log}(p^2 - M_i^2) + 2G_S \sum_{i \in \{u,d,s\}} (\rho_i^s)^2 \, . \tag{B.7.7}$$

B.7.2 Effective Potential at Finite Density

At finite density the mean field effective potential is calculated in the same manner as in the case of the vacuum. The additional term in the Lagrangian, Eq. (6.6.1), and the vector interactions which now contributes, lead to the following expression for the quark inverse propagator in momentum space for each flavour i

$$S_i^{-1}(p) = (p_0 + \tilde{\mu}_i)\gamma^0 - \vec{p} \cdot \vec{\gamma} - m_i + 4G_S \rho_i^s \quad , \tag{B.7.8}$$

where we have introduced the "reduced" chemical potential

$$\tilde{\mu}_i = \mu_i - 4G_V \langle \psi_i^\dagger \psi_i \rangle \quad . \tag{B.7.9}$$

The vector interaction reduces the chemical potential. The modification of the quark propagator leads to additional terms in the effective potential. The constituent quark masses or equivalently the the quark condensates are modified due to the appearance

[2] or equivalently do the tensor product between Dirac and colour space terms and use property # 3 of App. (B.5) and standard property of logarithms that $\mathrm{Log} a^x = x \mathrm{Log} a$

of these new terms in the effective potential. The mean field or leading contribution to the effective potential is now given by the following function

$$V_{\rm MF}^{\rm NJL}(\{M_i\},\{\mu_i\}) = i\sum_{i\in\{u,d,s\}}{\rm Tr}\left[{\rm Log}\left(S_i^{-1}\right)\right] + 2G_{\rm S}\sum_{i\in\{u,d,s\}}(\rho_i^{\rm s})^2 - 2G_{\rm V}\sum_{i\in\{u,d,s\}}(\rho_i^{\rm v})^2 \tag{B.7.10}$$

$$= i\sum_{i\in\{u,d,s\}}{\rm Log}\left[{\rm Det}\left(S_i^{-1}\right)\right] + 2G_{\rm S}\sum_{i\in\{u,d,s\}}(\rho_i^{\rm s})^2 - 2G_{\rm V}\sum_{i\in\{u,d,s\}}(\rho_i^{\rm v})^2 \quad , \tag{B.7.11}$$

where we have followed the same arguments used in the case of the vacuum effective potential. The trace is once again a functional trace over configuration space and also over Dirac and colour indices. This expression is still degenerate in colour and combined with the result that the determinant in Dirac space of the inverse propagator is now

$${\rm Det}_{\rm D}(\not{p} - M_i + \gamma^0\tilde{\mu}_i) = ((p^0+\tilde{\mu}_i)^2 - \vec{p}^{\,2} - M_i^2)^2 \quad , \tag{B.7.12}$$

the first term in Eq. (B.7.11) can be written as

$$i\sum_{i\in\{u,d,s\}}{\rm Tr}\left[{\rm Log}\left(S_i^{-1}\right)\right] = i\sum_{i\in\{u,d,s\}}{\rm LogDet}S_i^{-1} \tag{B.7.13}$$

$$= 2iN_{\rm C}\sum_{i\in\{u,d,s\}}\int\frac{d^4p}{(2\pi)^4}{\rm Log}\left[(p^0+\tilde{\mu}_i)^2 - \vec{p}^{\,2} - M_i^2\right] \quad . \tag{B.7.14}$$

To further simplify this term we symmetrise. This can be done because we integrate over both positive and negative values of p^0, so that:

$$\begin{aligned}
&2\int\frac{d^4p}{(2\pi)^4}{\rm Log}\left[(p^0+\tilde{\mu}_i)^2 - \vec{p}^{\,2} - M_i^2\right] \\
&= \int\frac{d^4p}{(2\pi)^4}{\rm Log}\left[(p^0+\tilde{\mu}_i)^2 - \vec{p}^{\,2} - M_i^2\right] \\
&\qquad + \int\frac{d^4p}{(2\pi)^4}{\rm Log}\left[(p^0+\tilde{\mu}_i)^2 - \vec{p}^{\,2} - M_i^2\right] \\
&= \int\frac{d^4p}{(2\pi)^4}{\rm Log}\left[(p^0+\tilde{\mu}_i)^2 - \vec{p}^{\,2} - M_i^2\right] \\
&\qquad + \int\frac{d^4p}{(2\pi)^4}{\rm Log}\left[(-p^0+\tilde{\mu}_i)^2 - \vec{p}^{\,2} - M_i^2\right] \\
&= \int\frac{d^4p}{(2\pi)^4}{\rm Log}\left[\left((p^0+\tilde{\mu}_i)^2 - \vec{p}^{\,2} - M_i^2\right).\left((-p^0+\tilde{\mu}_i)^2 - \vec{p}^{\,2} - M_i^2\right)\right] .
\end{aligned} \tag{B.7.15}$$

Introducing $E_{p,i} = \sqrt{\vec{p}^{\,2} + M_i^2}$ and expanding the square brackets out and then re-grouping the terms, in the following way

$$\left((p^0+\tilde{\mu}_i)^2 - \vec{p}^{\,2} - M_i^2\right).\left((-p^0+\tilde{\mu}_i)^2 - \vec{p}^{\,2} - M_i^2\right)$$

$$
\begin{aligned}
&= \left((p^0+\tilde{\mu}_i)^2 - E_{p,i}\right).\left((-p^0+\tilde{\mu}_i)^2 - E_{p,i}\right) \\
&= \left((E_{p,i}-\tilde{\mu}_i) - p^0\right)\left((E_{p,i}-\tilde{\mu}_i) + p^0\right)\left((E_{p,i}+\tilde{\mu}_i) - p^0\right)\left((E_{p,i}+\tilde{\mu}_i) + p^0\right) \\
&= \left((E_{p,i}-\tilde{\mu}_i)^2 - (p^0)^2\right)\left((E_{p,i}+\tilde{\mu}_i)^2 - (p^0)^2\right) \\
&= \left((p^0)^2 - (E_{p,i}-\tilde{\mu}_i)^2\right)\left((p^0)^2 - (E_{p,i}+\tilde{\mu}_i)^2\right) \qquad \text{(B.7.16)}
\end{aligned}
$$

Substituting Eq. (B.7.16) back into Eq. (B.7.15) and adding and subtracting the vacuum contribution we obtain

$$
\begin{aligned}
i\sum_{i\in\{u,d,s\}} \mathrm{Tr}\left[\mathrm{Log}\left(S_i^{-1}\right)\right] &= 2iN_{\mathrm{C}}\sum_{i\in\{u,d,s\}}\int\frac{d^4p}{(2\pi)^4}\mathrm{Log}\left[(p^0+\tilde{\mu}_i)^2 - \vec{p}^{\,2} - M_i^2\right] \\
&= iN_{\mathrm{C}}\sum_{i\in\{u,d,s\}}\int\frac{d^4p}{(2\pi)^4}\mathrm{Log}\left[\left((p^0)^2 - (E_{p,i}-\tilde{\mu}_i)^2\right).\right. \\
&\qquad\qquad \left.\left((p^0)^2 - (E_{p,i}+\tilde{\mu}_i)^2\right)\right] \\
&= iN_{\mathrm{C}}\sum_{i\in\{u,d,s\}}\int\frac{d^4p}{(2\pi)^4}\mathrm{Log}\left[\left((p^0)^2 - (E_{p,i}-\tilde{\mu}_i)^2\right)\right] \\
&\quad + iN_{\mathrm{C}}\sum_{i\in\{u,d,s\}}\int\frac{d^4p}{(2\pi)^4}\mathrm{Log}\left[\left((p^0)^2 - (E_{p,i}+\tilde{\mu}_i)^2\right)\right] \\
&= iN_{\mathrm{C}}\sum_{i\in\{u,d,s\}}\int\frac{d^4p}{(2\pi)^4}\mathrm{Log}\left[\left((p^0)^2 - (E_{p,i}-\tilde{\mu}_i)^2\right)\right] \\
&\quad + iN_{\mathrm{C}}\sum_{i\in\{u,d,s\}}\int\frac{d^4p}{(2\pi)^4}\mathrm{Log}\left[\left((p^0)^2 - (E_{p,i}+\tilde{\mu}_i)^2\right)\right] \\
&\quad + 2iN_{\mathrm{C}}\sum_{i\in\{u,d,s\}}\int\frac{d^4p}{(2\pi)^4}\mathrm{Log}\left[(p^0)^2 - E_{p,i}^2\right] \\
&\quad - 2iN_{\mathrm{C}}\sum_{i\in\{u,d,s\}}\int\frac{d^4p}{(2\pi)^4}\mathrm{Log}\left[(p^0)^2 - E_{p,i}^2\right] \\
&= iN_{\mathrm{C}}\sum_{i\in\{u,d,s\}}\int\frac{d^4p}{(2\pi)^4}\mathrm{Log}\left[\frac{(p^0)^2 - (E_{p,i}-\tilde{\mu}_i)^2}{(p^0)^2 - E_{p,i}^2}\right] \\
&\quad + iN_{\mathrm{C}}\sum_{i\in\{u,d,s\}}\int\frac{d^4p}{(2\pi)^4}\mathrm{Log}\left[\frac{(p^0)^2 - (E_{p,i}+\tilde{\mu}_i)^2}{(p^0)^2 - E_{p,i}^2}\right] \\
&\quad + 2iN_{\mathrm{C}}\sum_{i\in\{u,d,s\}}\int\frac{d^4p}{(2\pi)^4}\mathrm{Log}\left[p^2 - M_i^2\right] \quad . \qquad \text{(B.7.17)}
\end{aligned}
$$

The last integral is simply the vacuum contribution. The first two integrals contain the finite density contribution to the effective potential. Using [382]

$$
\int dp^0\ \mathrm{Log}\left[\frac{(p^0)^2 - a^2 + i\epsilon}{(p^0)^2 - b^2 + i\epsilon}\right] = 2\pi i\left(|a| - |b|\right) \qquad \text{(B.7.18)}
$$

we can perform the integration over p^0 and obtain the Fermi contribution to be

$$\begin{aligned} V^{\rm NJL}_{\rm Fermi}(\{M_i\},\{\mu_i\}) &= iN_{\rm C}\sum_{i\in\{u,d,s\}}\int\frac{d^4p}{(2\pi)^4}{\rm Log}\left[\frac{(p^0)^2-(E_{p,i}-\tilde{\mu}_i)^2}{(p^0)^2-E^2_{p,i}}\right] \\ &\quad +iN_{\rm C}\sum_{i\in\{u,d,s\}}\int\frac{d^4p}{(2\pi)^4}{\rm Log}\left[\frac{(p^0)^2-(E_{p,i}+\tilde{\mu}_i)^2}{(p^0)^2-E^2_{p,i}}\right] \qquad \text{(B.7.19)} \\ &= -N_{\rm C}\sum_{i\in\{u,d,s\}}\int\frac{d^3p}{(2\pi)^3}\ (|E_{p,i}-\tilde{\mu}_i|+|E_{p,i}+\tilde{\mu}_i|-2|E_{p,i}|) \\ &\qquad \text{(B.7.20)} \\ &= -2N_{\rm C}\sum_{i\in\{u,d,s\}}\int\frac{d^3p}{(2\pi)^3}\,\Theta(\tilde{\mu}_i-E_{p,i})(\tilde{\mu}_i-E_{p,i}) \quad . \qquad \text{(B.7.21)} \end{aligned}$$

This term is not divergent and does not need to be regularised as it is cut off by the step function. Although the model should only be considered valid below the UV cut off.

Eq. (B.7.11) can now be written as

$$V^{\rm NJL}_{\rm MF}(\{M_i\},\{\mu_i\}) = V^{\rm NJL}_{\rm div}(\{M_i\},\{\mu_i\}) + V^{\rm NJL}_{\rm fin}(\{M_i\},\{\mu_i\}) \quad . \qquad \text{(B.7.22)}$$

where

$$V^{\rm NJL}_{\rm div}(\{M_i\},\{\mu_i\}) = 2iN_{\rm C}\sum_{i\in\{u,d,s\}}\int\frac{d^4p}{(2\pi)^4}{\rm Log}(p^2-M_i^2) + 2G_{\rm S}\sum_{i\in\{u,d,s\}}(\rho^{\rm s}_i)^2 \qquad \text{(B.7.23)}$$

and for the finite density contribution we have

$$\begin{aligned} V^{\rm NJL}_{\rm fin}(\{M_i\},\{\mu_i\}) &= V^{\rm NJL}_{\rm Fermi}(\{M_i\},\{\mu_i\}) - 2G_{\rm V}\sum_{i\in\{u,d,s\}}(\rho^{\rm v}_i)^2 \qquad \text{(B.7.24)} \\ &= V^{\rm NJL}_{\rm Fermi}(\{M_i\},\{\mu_i\}) - \sum_{i\in\{u,d,s\}}\frac{(\tilde{\mu}_i-\mu_i)^2}{8G_{\rm V}} \quad . \qquad \text{(B.7.25)} \end{aligned}$$

To calculate the equation of state at finite density we redefine the effective potential by subtracting a constant, so that the mean field pressure ($P_{\rm MF} = -V_{\rm MF}$) is by definition zero in vacuum. This subtraction is performed by,

$$V_{\rm MF}(\{M_i\},\{\mu_i\}) \equiv V^{\rm NJL}_{\rm MF}(\{M_i\},\{\mu_i\}) - V^{\rm NJL}_{\rm MF}(\{M_i=M_{i0}\},\{\mu_i=0\}) \quad , \qquad \text{(B.7.26)}$$

where we now relabel the vacuum values of the constituent quark masses, condensates and densities with a subscript zero. The final expression at finite density is then

$$V_{\rm MF}(\{M_i\},\{\mu_i\}) = V_{\rm div}(\{M_i\},\{\mu_i\}) + V_{\rm fin}(\{M_i\},\{\mu_i\}) \quad , \qquad \text{(B.7.27)}$$

where $V^{\rm NJL}_{\rm fin}(\{M_i\},\{\mu_i\})$ is still given by Eq. (B.7.25), as we only subtracted the vacuum contribution. We have just dropped the NJL superscript for convenience and simplicity of notation. The divergent contribution breaks up into three pieces

$$V_{\rm div}(\{M_i\},\{\mu_i\}) = V^{\rm vac}_{\rm div}(\{M_i\},\{\mu_i\}) + 2G_{\rm S}\sum_{i\in\{u,d,s\}}(\rho^{\rm s}_i)^2 - 2G_{\rm S}\sum_{i\in\{u,d,s\}}(\rho^{\rm s}_{i0})^2 \qquad \text{(B.7.28)}$$

$$= V_{\rm div}^{\rm vac}(\{M_i\},\{\mu_i\}) + \sum_{i\in\{u,d,s\}} \frac{(M_i-m_i)^2}{8G_{\rm S}} - \sum_{i\in\{u,d,s\}} \frac{(M_{i0}-m_i)^2}{8G_{\rm S}} \quad , \tag{B.7.29}$$

where the first is the divergent vacuum contribution (quark loop term) and is

$$V_{\rm div}^{\rm vac}(\{M_i\},\{\mu_i\}) = 2iN_c \sum_{i\in\{u,d,s\}} \int \frac{d^4k}{(2\pi)^4}\ {\rm Log}\left[\frac{k^2-M_i^2+i\epsilon}{k^2-M_{i0}^2+i\epsilon}\right] \quad . \tag{B.7.30}$$

In App. (B.7.3) it is evaluated in our chosen regularisation scheme, Schwinger's proper time method.

B.7.3 Divergent Part of the Effective Potential

The first term of the divergent part of the vacuum contribution to the effective potential is given by

$$V_{\rm div}^{\rm vac}(M_u,M_d,M_s) = 2iN_c \sum_{i\in\{u,d,s\}} \int \frac{d^4k}{(2\pi)^4}\ {\rm Log}\left[\frac{k^2-M_i^2+i\epsilon}{k^2-M_{i0}^2+i\epsilon}\right] \tag{B.7.31}$$

To evaluate we perform a Wick rotation in the p^0 plane (see Table (B.1.6)), which means we no longer have a need for the $i\epsilon$ terms, giving

$$V_{\rm div}^{\rm vac}(M_u,M_d,M_s) = -6 \sum_{i\in\{u,d,s\}} \int \frac{d^4k_{\rm E}}{(2\pi)^4}\ {\rm Log}\left[\frac{-k_{\rm E}^2-M_i^2}{-k_{\rm E}^2-M_{i0}^2}\right] \quad . \tag{B.7.32}$$

Eq. (B.7.32) is now in Euclidean momentum space. Assuming isotropy we make use of the 4 dimensional hyperspherical symmetry. That is, to evaluate Eq. (B.7.32) further we use the volume of a four dimensional hypersphere in momentum space, $V_{4D} = \frac{1}{2}\pi^2 k_{\rm E}^4$, thus the Euclidean space measure is $d^4k_{\rm E} = 2\pi^2 k_{\rm E}^3 dk_{\rm E}$ and

$$V_{\rm div}^{\rm vac}(M_u,M_d,M_s) = -6 \sum_{i\in\{u,d,s\}} \int_0^\infty \frac{2\pi^2}{(2\pi)^4} dk_{\rm E} k_{\rm E}^3\ {\rm Log}\left[\frac{k_{\rm E}^2+M_i^2}{k_{\rm E}^2+M_{i0}^2}\right] \tag{B.7.33}$$

$$= -\frac{3}{4\pi^2} \sum_{i\in\{u,d,s\}} \int_0^\infty dk_{\rm E} k_{\rm E}^3\ \left[{\rm Log}\left(k_{\rm E}^2+M_i^2\right) - {\rm Log}\left(k_{\rm E}^2+M_{i0}^2\right)\right] \quad . \tag{B.7.34}$$

As noted earlier this is divergent. We make the proper time replacement

$${\rm Log}A \longrightarrow -\int_{-\infty}^{\infty} \frac{d\tau}{\tau}\ e^{-\tau A} \tag{B.7.35}$$

and impose a UV cutoff, $\Lambda_{\rm UV}$, to regularise the vacuum contribution,

$$V_{\rm div}^{\rm vac}(M_u,M_d,M_s) = \frac{3}{4\pi^2} \sum_{i\in\{u,d,s\}} \int_0^\infty dk_{\rm E} k_{\rm E}^3\ \left[\int_{\frac{1}{\Lambda_{\rm UV}^2}}^\infty \frac{d\tau}{\tau}\ \left(e^{-\tau\left(k_{\rm E}^2+M_i^2\right)} - e^{-\tau\left(k_{\rm E}^2+M_{i0}^2\right)}\right)\right] \quad . \tag{B.7.36}$$

Next we interchange the order of integrations and perform the momentum integral,

$$V_{\rm div}^{\rm vac}(M_u,M_d,M_s) = \frac{3}{4\pi^2}\sum_{i\in\{u,d,s\}}\int_{\frac{1}{\Lambda_{\rm UV}^2}}^{\infty}\left[\frac{d\tau}{\tau}\left(e^{-\tau M_i^2}-e^{-\tau M_{i0}^2}\right)\int_0^{\infty}dk_{\rm E}k_{\rm E}^3\,e^{-\tau k_{\rm E}^2}\right] \tag{B.7.37}$$

$$= \frac{3}{4\pi^2}\sum_{i\in\{u,d,s\}}\int_{\frac{1}{\Lambda_{\rm UV}^2}}^{\infty}\frac{d\tau}{\tau}\left(e^{-\tau M_i^2}-e^{-\tau M_{i0}^2}\right)\cdot\frac{1}{2\tau^2} \tag{B.7.38}$$

$$= \frac{3}{8\pi^2}\sum_{i\in\{u,d,s\}}\int_{\frac{1}{\Lambda_{\rm UV}^2}}^{\infty}\frac{d\tau}{\tau^3}\left(e^{-\tau M_i^2}-e^{-\tau M_{i0}^2}\right) \tag{B.7.39}$$

$$= \frac{3}{8\pi^2}\sum_{i\in\{u,d,s\}}\left[M_i^4\Gamma(-2,\frac{M_i^2}{\Lambda_{\rm UV}^2})-M_{i0}^4\Gamma(-2,\frac{M_{i0}^2}{\Lambda_{\rm UV}^2})\right]\quad, \tag{B.7.40}$$

where $\Gamma(a,z)$ is the incomplete gamma function. Eq. (B.7.40) can also be written in terms of the exponential integral $\mathrm{Ei}(x)$,

$$V_{\rm div}^{\rm vac}(M_u,M_d,M_s) = \frac{3}{16\pi^2}\sum_{i\in\{u,d,s\}}\left[\left(e^{-M_i^2/\Lambda_{\rm UV}^2}\Lambda_{\rm UV}^4(1-\frac{M_i^2}{\Lambda_{\rm UV}^2})-M_i^4\mathrm{Ei}(-\frac{M_i^2}{\Lambda_{\rm UV}^2}\right)\right.$$
$$\left.-\left(e^{-M_{i0}^2/\Lambda_{\rm UV}^2}\Lambda_{\rm UV}^4(1-\frac{M_{i0}^2}{\Lambda_{\rm UV}^2})-M_{i0}^4\mathrm{Ei}(-\frac{M_{i0}^2}{\Lambda_{\rm UV}^2}\right)\right]. \tag{B.7.41}$$

B.8 The Gap Equation

B.8.1 The Gap Equation in Vacuum

In vacuum the quark propagator for flavour i is

$$S_i(p)\equiv S_{\rm F}^i(p)=\frac{1}{\not{p}-M_i+i\epsilon}\quad, \tag{B.8.1}$$

where the subscript F indicates the usual Feynman propagator. The $i\epsilon$ term will disappear on rotation to Euclidean momentum space as it will no longer be needed, because the propagator no longer has poles for real momentum and energy. The gap equation is given by

$$M_i=m_i-4G_{\rm S}\langle\bar{\psi}_i\psi_i\rangle\quad. \tag{B.8.2}$$

Using Eq. (B.8.1) one can the can write the quark condensate for flavour i as

$$\langle\bar{\psi}_i\psi_i\rangle = -i\mathrm{Tr}S_i \tag{B.8.3}$$

$$= -i\mathrm{Tr}\int\frac{d^4p}{(2\pi)^4}\frac{1}{\not{p}-M_i+i\epsilon} \tag{B.8.4}$$

$$= -i\mathrm{Tr}\int\frac{d^4p}{(2\pi)^4}\frac{\not{p}+M_i}{p^2-M_i^2+i\epsilon} \tag{B.8.5}$$

$$= -4iN_{\rm C}M_i \int \frac{d^4p}{(2\pi)^4}\frac{1}{p^2-M_i^2+i\epsilon} \quad . \tag{B.8.6}$$

We now Wick rotate making use of the properties summarised in Table B.1.6. The condensate becomes

$$\langle\bar{\psi}_i\psi_i\rangle = -4(i)^2N_{\rm C}M_i \int \frac{d^4p_{\rm E}}{(2\pi)^4}\frac{1}{-p_{\rm E}^2-M_i^2} \quad . \tag{B.8.7}$$

Thus, in Euclidean momentum space the quark condensate takes the following form

$$\langle\bar{\psi}_i\psi_i\rangle = -\frac{N_{\rm C}M_i}{2\pi^2}\int_0^\infty dp_{\rm E}\ \frac{p_{\rm E}^3}{p_{\rm E}^2+M_i^2} \quad , \tag{B.8.8}$$

which is divergent. It is regularised using Schwinger's proper time regularisation scheme

$$\begin{aligned}
\langle\bar{\psi}_i\psi_i\rangle &= -\frac{N_{\rm C}M_i}{2\pi^2}\int_0^\infty dp_{\rm E}\ \frac{p_{\rm E}^3}{p_{\rm E}^2+M_i^2} && \text{(B.8.9)}\\
&= -\frac{N_{\rm C}M_i}{2\pi^2}\int_0^\infty dp_{\rm E}\ p_{\rm E}^3\int_{\frac{1}{\Lambda_{\rm UV}^2}}^\infty d\tau e^{-\tau\left(p_{\rm E}^2+M_i^2\right)} && \text{(B.8.10)}\\
&= -\frac{N_{\rm C}M_i}{2\pi^2}\int_{\frac{1}{\Lambda_{\rm UV}^2}}^\infty d\tau\int_0^\infty dp_{\rm E}\ p_{\rm E}^3 e^{-\tau\left(p_{\rm E}^2+M_i^2\right)} && \text{(B.8.11)}\\
&= -\frac{N_{\rm C}M_i}{2\pi^2}\int_{\frac{1}{\Lambda_{\rm UV}^2}}^\infty d\tau\frac{e^{-\tau M_i^2}}{2\tau^2} \quad . && \text{(B.8.12)}
\end{aligned}$$

Finally the vacuum gap equation is written as

$$\begin{aligned}
M_i &= m_i + 4G_{\rm S}\frac{N_{\rm C}M_i}{2\pi^2}\int_{\frac{1}{\Lambda_{\rm UV}^2}}^\infty d\tau\frac{e^{-\tau M_i^2}}{2\tau^2} && \text{(B.8.13)}\\
&= m_i + \frac{3G_{\rm S}M_i}{\pi^2}\int_{\frac{1}{\Lambda_{\rm UV}^2}}^\infty d\tau\frac{e^{-\tau M_i^2}}{\tau^2} \quad , && \text{(B.8.14)}
\end{aligned}$$

where we have used $N_{\rm C}=3$. This expression can also be obtained from

$$\frac{\partial V_{\rm MF}^{\rm NJL}}{\partial M_i} = 0 \quad , \tag{B.8.15}$$

where $V_{\rm MF}^{\rm NJL}$ is given by Eq. (B.7.7).

B.8.2 The Gap Equation at Finite Density

The quark propagator in-medium is

$$\begin{aligned}
S_i(p) &= S_{\rm F}^i(p) + S_{\rm D}^i(p) && \text{(B.8.16)}\\
&= \frac{1}{\not{p}-M_i} + i\frac{\pi}{E_{p,i}}(\not{p}+M_i)\Theta(\mu_i-E_{p,i})\delta(p_0-E_{p,i}) \quad . && \text{(B.8.17)}
\end{aligned}$$

The gap equation is given by

$$M_i = m_i - 4G_{\rm S}\langle\bar{\psi}_i\psi_i\rangle \quad , \tag{B.8.18}$$

where the condensate for flavour i is

$$\langle\bar{\psi}_i\psi_i\rangle = -i{\rm Tr}S_i = -i{\rm Tr}S_{\rm F}^i - i{\rm Tr}S_{\rm D}^i \quad . \tag{B.8.19}$$

The first term in Eq. (B.8.19) is the vacuum contribution calculated in App. B.8.1. The second term is evaluated as follows

$$\begin{aligned} -i{\rm Tr}S_{\rm D}^i &= -i{\rm Tr}\left[i\frac{\pi}{E_{p,i}}(\not{p}+M_i)\Theta(\mu_i-E_{p,i})\delta(p_0-E_{p,i})\right] && \text{(B.8.20)}\\ &= 2N_{\rm C}\int\frac{d^3p}{(2\pi)^3}\frac{M_i}{E_{p,i}}\Theta(\mu_i-E_{p,i}) && \text{(B.8.21)}\\ &= \frac{M_iN_{\rm C}}{2\pi^2}\left[\mu_i\sqrt{\mu_i^2-M_i^2}-M_i^2{\rm Log}\left[\frac{\mu_i+\sqrt{\mu_i^2-M_i^2}}{M_i}\right]\right] \quad . && \text{(B.8.22)} \end{aligned}$$

The resulting expression for the in-medium gap equation is

$$\begin{aligned} M_i &= m_i + \frac{3G_{\rm S}M_i}{\pi^2}\int_{\frac{1}{\Lambda_{UV}^2}}^{\infty}d\tau\frac{1}{\tau^2}e^{-\tau M_i^2} && \text{(B.8.23)}\\ &\quad - \frac{2G_{\rm S}M_iN_{\rm C}}{\pi^2}\left[\mu_i\sqrt{\mu_i^2-M_i^2}-M_i^2{\rm Log}\left[\frac{\mu_i+\sqrt{\mu_i^2-M_i^2}}{M_i}\right]\right] . && \text{(B.8.24)} \end{aligned}$$

Note that the Fermi contribution is finite, although the expression as a whole should be viewed as only valid below the UV cut-off. In the presence of a vector interaction the chemical potential is replaced by the reduced chemical potential. This expression can also be obtained from

$$\frac{\partial V_{\rm MF}}{\partial M_i} = 0 \quad , \tag{B.8.25}$$

where $V_{\rm MF}$ is given by Eq. (B.7.27).

B.9 Pion Polarisation Function

Here we outline the calculation of the pion polarisation graph in the proper time regularisation scheme. It is worth noting that we are considering objects in a direct product space

$$\text{Dirac} \otimes \text{Flavour} \otimes \text{Colour} \quad , \tag{B.9.1}$$

so that when the interaction is the same for say all colours we have an N_c-fold degeneracy. This can be seen from the more general trace formula ${\rm Tr}[\hat{A}\otimes\hat{B}\otimes\hat{C}] = {\rm Tr}[\hat{A}]{\rm Tr}[\hat{B}]{\rm Tr}[\hat{C}]$, where $\hat{A},\hat{B},\hat{C}$ are operators in the above 3 spaces.

The pion polarisation function is

$$\frac{1}{i}\Pi_\pi(k^2) = 6\int \frac{d^4p}{(2\pi)^4}\frac{\mathrm{Tr}\left[i\gamma_5(\not p+\frac{\not k}{2}+M)i\gamma_5(\not p-\frac{\not k}{2}+M)\right]}{((p+\frac{k}{2})^2-M^2)((p-\frac{k}{2})^2-M^2)} \quad , \tag{B.9.2}$$

where the traces over colour and flavour have been performed. The Dirac trace is evaluated as follows

$$\begin{aligned}\mathrm{Tr}\left[\gamma_5(\not p+\frac{\not k}{2}+M)\gamma_5(\not p-\frac{\not k}{2}+M)\right] &= \mathrm{Tr}\left[\gamma_5\not p\gamma_5\not p\right]-\frac{1}{2}\mathrm{Tr}\left[\gamma_5\not p\gamma_5\not k\right]\\ &\quad+\mathrm{Tr}\left[\gamma_5\not p\gamma_5 M\right]+\frac{1}{2}\mathrm{Tr}\left[\gamma_5\not k\gamma_5\not p\right]\\ &\quad-\frac{1}{2}\mathrm{Tr}\left[\gamma_5\not k\gamma_5\right]+\frac{1}{2}\mathrm{Tr}\left[\gamma_5\not k\gamma_5 M\right]\\ &\quad+\mathrm{Tr}\left[\gamma_5 M\gamma_5\not p\right]-\frac{1}{2}\mathrm{Tr}\left[\gamma_5 M\gamma_5\not k\right]\\ &\quad+\mathrm{Tr}\left[\gamma_5 M\gamma_5 M\right] \quad .\end{aligned} \tag{B.9.3}$$

Using the fact that the trace of an odd number of gamma matrices is zero, $\gamma_5^2 = \mathbb{1}_D$, $\gamma_\mu\gamma_\nu = -\gamma_\nu\gamma_\mu$ and $Tr[\not a\not b] = 4a\cdot b$ we arrive at the following

$$\mathrm{Tr}\left[\gamma_5(\not p+\frac{\not k}{2}+M)\gamma_5(\not p-\frac{\not k}{2}+M)\right] = 4(M^2-p^2+\frac{k^2}{4}) \quad . \tag{B.9.4}$$

This evaluation of the trace can be substituted back into the polarisation equation and we can continue with the calculation of the pion polarisation graph. The next step is to write the denominator in terms of partial fractions. That is,

$$\frac{1}{ab} = \frac{(a+b)}{(a+b)}.\frac{1}{ab} = \frac{\frac{a}{ab}+\frac{b}{ab}}{a+b} = \frac{\frac{1}{a}+\frac{1}{b}}{a+b}$$

$$a = (p+\frac{1}{2}k)^2-M^2 \tag{B.9.5}$$

$$b = (p-\frac{1}{2}k)^2-M^2 \tag{B.9.6}$$

$$a+b = (p+\frac{1}{2}k)^2-M^2+(p-\frac{1}{2}k)^2-M^2 \tag{B.9.7}$$

$$= 2(p^2+\frac{1}{4}k^2-M^2) \quad . \tag{B.9.8}$$

Note that the trace evaluated above in Eq. (B.9.4) can be rewritten as

$$4(M^2-p^2+\frac{k^2}{4}) = 4((M^2-p^2-\frac{k^2}{4})+\frac{1}{2}k^2) \quad . \tag{B.9.9}$$

The first term on the RHS of Eq. (B.9.9) is the same as $(-2)\times$ the denominator. Thus the polarisation function becomes

$$\frac{1}{i}\Pi_\pi(p) = 12\int\frac{d^4p}{(2\pi)^4}\left(\frac{1}{(p+\frac{1}{2}k)^2-M^2}+\frac{1}{(p-\frac{1}{2}k)^2-M^2}\right)$$

$$-24\int\frac{d^4p}{(2\pi)^4}\left(\frac{k^2/2}{((p-\frac{1}{2}k)^2-M^2)((p+\frac{1}{2}k)^2-M^2)}\right) \quad . \text{(B.9.10)}$$

In the first term of Eq. (B.9.10) we have two integrals. It is possible to shift the momentum in the first $p \to p' = p + \frac{1}{2}k$ and the momentum in the second to $p \to p'' = p - \frac{1}{2}k$, then we can relabel p such that the first term is just

$$\text{Term 1} = 2\times 12\int\frac{d^4p}{(2\pi)^4}\frac{1}{p^2-M^2} \quad . \text{(B.9.11)}$$

This integral is common in the NJL model, also appearing in the gap equation for example. For this reason we evaluate it explicitly here in our chosen regularisation scheme, proper time regularisation. First we will need to Wick rotate from Minkowski space to Euclidean space, giving

$$\begin{aligned}
\text{Term 1} &= i24\int\frac{d^4p_E}{(2\pi)^4}\frac{1}{-p_E^2-M^2} &\text{(B.9.12)}\\
&= -i24\int\frac{d^4p_E}{(2\pi)^4}\frac{1}{p_E^2+M^2} &\text{(B.9.13)}\\
&= -i24\frac{1}{(2\pi)^4}\int 2\pi^2 p_E^3 dp_E\frac{1}{p_E^2+M^2}\\
&= -i\frac{3}{\pi^2}\int_0^\infty dp_E p_E^3\frac{1}{p_E^2+M^2} \quad . &\text{(B.9.14)}
\end{aligned}$$

Using the proper time replacement for regulating the divergent integral term 1 becomes

$$\begin{aligned}
\text{Term 1} &= -i\frac{3}{\pi^2}\int_0^\infty dp_E\ p_E^3\ \int_{1/\Lambda_{UV}^2}^\infty d\tau\ e^{-\tau(p_E^2+M^2)} &\text{(B.9.15)}\\
&= -i\frac{3}{\pi^2}\int_{1/\Lambda_{UV}^2}^\infty d\tau\ e^{-\tau M^2}\int_0^\infty dp_E\ p_E^3\ e^{-\tau p_E^2} \quad . &\text{(B.9.16)}
\end{aligned}$$

Using

$$\int_0^\infty dp_E\ p_E^3\ e^{-\tau p_E^2} = \frac{1}{2\tau^2} \quad , \text{(B.9.17)}$$

we thus have

$$\text{Term 1} = -i\frac{3}{\pi^2}\int_{1/\Lambda_{UV}^2}^\infty d\tau\ \frac{e^{-\tau M^2}}{2\tau^2} \quad . \text{(B.9.18)}$$

Term 2 of Eq. (B.9.10) is

$$\text{Term 2} = -24\frac{k^2}{2}\int\frac{d^4p}{(2\pi)^4}\ \frac{1}{((p+\frac{1}{2}k)^2-M^2)((p-\frac{1}{2}k)^2-M^2)} \quad . \text{(B.9.19)}$$

Now we use the Feynman parameter trick to obtain

$$\text{Term 2} = -24\frac{k^2}{2}\int\frac{d^4p}{(2\pi)^4}\ \int_0^1\frac{dx}{\left[x((p+\frac{1}{2}k)^2-M^2)+(1-x)((p-\frac{1}{2}k)^2-M^2)\right]^2}$$

(B.9.20)

and simplifying the denominator we have

$$\begin{aligned}\text{Denominator} &= \Big[x(p^2+\frac{1}{4}k^2+p\cdot k-M^2)+p^2-p\cdot k \\ &\qquad +\frac{1}{4}k^2-M^2-x(p^2-p\cdot k+\frac{1}{4}k^2-M^2)\Big]^2 \\ &= \Big[xp\cdot k+p^2-p\cdot k+\frac{1}{4}k^2-M^2+xp\cdot k\Big]^2 \quad . \end{aligned} \tag{B.9.21}$$

To simplify the denominator we shift the momentum $p \to p - xk + \frac{1}{2}k$, such that

$$\begin{aligned}(\text{Denominator})^{1/2} &= 2xp\cdot k+p^2-p\cdot k+\frac{1}{4}k^2-M^2 \\ &= 2x(p-xk+\frac{1}{2}k)\cdot k \\ &\quad +(p-xk+\frac{1}{2}k)^2 \\ &\quad -(p-xk+\frac{1}{2}k)\cdot k \\ &\quad +\frac{1}{4}k^2 \\ &\quad -M^2 \\ &= p^2+k^2(x-x^2)-M^2 \quad . \end{aligned} \tag{B.9.22}$$

Next we substitute Eq. (B.9.22) back into term 2, Eq. (B.9.20), and Wick rotate into Euclidean space

$$\text{Term 2} = -\frac{24\times 2\pi^2}{16\pi^4}\frac{k^2}{2}\; i\; \int_0^1 dx \int_0^\infty \frac{dp_E p_E^3}{\left(p_E^2+k^2(x^2-x)+M^2\right)^2} \quad . \tag{B.9.23}$$

What now remains is to use proper time regularisation, yielding

$$\begin{aligned}\text{Term 2} &= -\frac{3k^2 i}{2\pi^2}\int_0^1 dx \int_0^\infty dp_E\; p_E^3 \int_{1/\Lambda_{UV}^2}^\infty d\tau\; \tau e^{-\tau\left[p_E^2+k^2(x^2-x)+M^2\right]} \\ &= -\frac{3k^2 i}{2\pi^2}\int_0^1 dx \int_{1/\Lambda_{UV}^2}^\infty d\tau\; \tau e^{-\tau\left[k^2(x^2-x)+M^2\right]} \int_0^\infty dp_E\; p_E^3 e^{-\tau p_E^2} \\ &= -\frac{3k^2 i}{4\pi^2}\int_0^1 dx \int_{1/\Lambda_{UV}^2}^\infty d\tau\; \frac{e^{-\tau\left[k^2(x^2-x)+M^2\right]}}{\tau} \quad . \end{aligned} \tag{B.9.24}$$

The polarisation function for the pion is finally given by

$$\frac{1}{i}\Pi_\pi(k^2) = -\frac{3i}{\pi^2}I_1(M^2) - \frac{3k^2 i}{4\pi^2}I_2(k^2,M^2) \quad , \tag{B.9.25}$$

where

$$I_1(M^2) = \int_{1/\Lambda_{UV}^2}^{\infty} d\tau \; \frac{e^{-\tau M^2}}{2\tau^2} \tag{B.9.26}$$

and

$$I_2(k^2, M^2) = \int_0^1 dx \int_{1/\Lambda_{UV}^2}^{\infty} d\tau \; \frac{e^{-\tau\left[k^2(x^2-x)+M^2\right]}}{\tau} \quad . \tag{B.9.27}$$

Eqs. (B.9.26) and (B.9.27) can be evaluated numerically.

B.10 Pion-quark Coupling

From Eq. (B.9.25) it can be shown that the pion-quark coupling is given by

$$\begin{aligned} \frac{1}{g_{\pi qq}^2} &= \left.\frac{\partial \Pi_\pi}{\partial q^2}\right|_{q^2=m_\pi^2} \\ &= \frac{3}{4\pi^2}\int_0^1 dx \int_{1/\Lambda_{\rm UV}^2}^{\infty} d\tau \left[\frac{1}{\tau} - m_\pi^2(x^2-x)\right] e^{-\tau(m_\pi^2(x^2-x)+M^2)} \end{aligned} \quad , \tag{B.10.1}$$

where x is a Feynman parameter.

B.11 Pion Decay Constant

To calculate the pion decay constant we take as our starting point the matrix element, Eq. (2.2.11),

$$\langle 0|\bar{\psi}(0)\gamma^\mu\gamma_5\frac{\lambda_a}{2}\psi(0)|\pi_b\rangle = i f_\pi q^\mu \delta_{ab} \quad . \tag{B.11.1}$$

Performing the flavour and colour traces we obtain

$$iq^\mu f_\pi = -g_{\pi qq} N_{\rm C} \int \frac{d^4p}{(2\pi)^4} {\rm Tr}\left[\gamma^\mu\gamma_5 S_\ell(p+\frac{1}{2}q)\gamma_5 S_\ell(p-\frac{1}{2}q)\right] . \tag{B.11.2}$$

The Dirac trace is performed by the usual methods and can be shown to be

$${\rm Tr}\left[\gamma^\mu\gamma_5(\not{p}+\frac{\not{q}}{2}+M)\gamma_5(\not{p}-\frac{\not{q}}{2}+M)\right] = -4Mq^\mu \quad . \tag{B.11.3}$$

On substitution of this result (Eq. (B.11.3)) into Eq. (B.11.2), we see that the pion decay constant can be expressed as

$$f_\pi = -ig_{\pi qq} 4N_{\rm C} M \int \frac{d^4p}{(2\pi)^4} \frac{1}{\left((p+q/2)^2 - M^2 + i\epsilon\right)\left((p-q/2)^2 - M^2 + i\epsilon\right)} \tag{B.11.4}$$

Using Feynman's parameter trick

$$\frac{1}{AB} = \int_0^1 \frac{dx}{\left[xA + (1-x)B\right]^2} \tag{B.11.5}$$

to re-express the integral in Eq. (B.11.4) and shifting the momentum $p \to p+q/2-xq$, Eq. (B.11.4) becomes

$$f_\pi = -ig_{\pi qq}4N_{\rm C}M\int\frac{d^4p}{(2\pi)^4}\int_0^1\frac{dx}{\left[p^2+q^2(x-x^2)-M^2+i\epsilon\right]^2} \quad . \tag{B.11.6}$$

Wick rotating and implementing proper time regularisation we obtain the final expression for the pion decay constant

$$\begin{aligned} f_\pi &= -ig_{\pi qq}4N_{\rm C}Mi\int\frac{d^4p_E}{(2\pi)^4}\int_0^1\frac{dx}{\left[-p_E^2+q^2(x-x^2)-M^2\right]^2} \\ &= g_{\pi qq}4N_{\rm C}M\int\frac{d^4p_E}{(2\pi)^4}\int_0^1\frac{dx}{\left[p_E^2+q^2(x^2-x)+M^2\right]^2} \\ &= g_{\pi qq}4N_{\rm C}M\int_0^\infty\frac{2\pi^2p_E^3dp_E}{16\pi^4}\int_0^1\frac{dx}{\left[p_E^2+q^2(x^2-x)+M^2\right]^2} \\ &= g_{\pi qq}\frac{N_{\rm C}M}{2\pi^2}\int_0^1dx\int_{1/\Lambda_{\rm UV}^2}^\infty d\tau\tau\int_0^\infty dp_E\ p_E^3e^{-\tau\left(p_E^2+q^2(x^2-x)+M^2\right)} \\ &= g_{\pi qq}\frac{N_{\rm C}M}{4\pi^2}\int_0^1dx\int_{1/\Lambda_{\rm UV}^2}^\infty d\tau\ \frac{e^{-\tau\left(q^2(x^2-x)+M^2\right)}}{\tau} \quad . \end{aligned} \tag{B.11.7}$$

B.12 Three Momentum Regularised NJL Model with t' Hooft Term

In the main body of the thesis, for comparison purposes, we also present results using the three flavour NJL model with the so called t' Hooft determinant term. This NJL model is regularised using the simpler non-covariant three momentum regularisation scheme. This model was used for example in Ref. [282] to investigate hybrid stars. Our definition of the couplings is slightly different from Ref. [282]. The Lagrangian density under investigation here is explicitly given by

$$\mathcal{L}_{\rm TM} = \mathcal{L}_{\rm NJL}+\mathcal{L}_{\rm det} \quad , \tag{B.12.1}$$

where $\mathcal{L}_{\rm NJL}$ is given by Eq. (6.3.8) and

$$\mathcal{L}_{\rm det} = -G_{\rm D}\left[\det{}_{\rm F}\left[\bar\psi\left(1+\gamma_5\right)\psi\right]+\det{}_{\rm F}\left[\bar\psi\left(1-\gamma_5\right)\psi\right]\right] \quad . \tag{B.12.2}$$

The determinant $\det_{\rm F}$ is a flavour determinant and as such it mixes quarks of different flavours.

Following the same methods and notation as used in earlier sections, the effective mean field potential for this NJL model can be shown to be

$$V_{\rm MF}^{\rm TM}\left(\{M_i\},\{\mu_i\}\right) = -2N_{\rm C}\sum_{i\in\{u,d,s\}}\int\frac{d^3p}{(2\pi)^3}E_i\Theta(\Lambda-|\vec p|)$$

$$
\begin{aligned}
&-2N_{\rm C}\sum_{i\in\{u,d,s\}}\int\frac{d^3p}{(2\pi)^3}\Theta(\tilde{\mu}_i-E_i)(\tilde{\mu}_i-E_i)\\
&+2G_{\rm S}\sum_{i\in\{u,d,s\}}(\rho_i^{\rm s})^2-4G_{\rm D}\rho_u^{\rm s}\rho_d^{\rm s}\rho_s^{\rm s}-2G_{\rm V}\sum_{i\in\{u,d,s\}}(\rho_i^{\rm v})^2-V_0^{\rm TM}
\end{aligned}
\tag{B.12.3}
$$

where $E_i=\sqrt{\vec{p}^2+M_i^2}$. The constant vacuum term subtracted in Eq. (B.12.3) to give zero pressure in vacuum is

$$
V_0^{\rm TM}=2G_{\rm S}\sum_{i\in\{u,d,s\}}(\rho_{0i}^{\rm s})^2-4G_{\rm D}\rho_{0u}^{\rm s}\rho_{0d}^{\rm s}\rho_{0s}^{\rm s}-2N_{\rm C}\sum_{i\in\{u,d,s\}}\int\frac{d^3p}{(2\pi)^3}E_{0i}\Theta(\Lambda-|\vec{p}|)\quad,
\tag{B.12.4}
$$

where the subscript 0 means the vacuum value i.e $E_{0i}=\sqrt{\vec{p}^2+M_{0i}^2}$. The constituent quark masses are given by

$$
M_i=m_i-4G_{\rm S}\rho_i^{\rm s}+2G_{\rm D}\rho_j^{\rm s}\rho_k^{\rm s}\quad,
\tag{B.12.5}
$$

where the subscripts (i,j,k) are a cyclic permutation of (u,d,s). The scalar condensate of quark i is

$$
\rho_i^{\rm s}=-\frac{3}{\pi^2}\int_{\rm p_F^i}^{\Lambda}dp\;p^2\frac{M_i}{E_i}
\tag{B.12.6}
$$

and its Fermi momentum in the presence of a vector interaction is $p_{\rm F}^i=\sqrt{\tilde{\mu}_i^2-M_i^2}\Theta(\tilde{\mu}_i-M_i)$.

Bibliography

[1] E. Rutherford. The magnetic and electric deviation of easily absorbed rays from radium. *Philos.Mag.*, (6)5:177, 1903.

[2] E. Rutherford and T Royds. Spectrum of the radium emanation. *Philos.Mag.*, (6)16:313–317, 1908.

[3] E. Rutherford. The scattering of alpha and beta particles by matter and the structure of the atom. *Philos.Mag.*, (6)21:669–688, 1911.

[4] H. Geiger and E. Marsden. On a diffuse reflection of the α-particles. *Proceedings of the Royal Society of London. Series A*, 82(557):495–500, 1909.

[5] Lloyd A. Young. Interaction of nuclear particles. *Phys. Rev.*, 47:972–972, Jun 1935.

[6] J. M. B. Kellogg, I. I. Rabi, N. F. Ramsey, and J. R. Zacharias. An electrical quadrupole moment of the deuteron: The radiofrequency spectra of HD and D molecules in a magnetic field. *Phys. Rev.*, 57:677–695, Apr 1940.

[7] Milton G. White. Scattering of high energy protons in hydrogen. *Phys. Rev.*, 49:309–316, Feb 1936.

[8] M. A. Tuve, N. P. Heydenburg, and L. R. Hafstad. The scattering of protons by protons. *Phys. Rev.*, 50:806–825, Nov 1936.

[9] L. R. Hafstad, N. P. Heydenburg, and M. A. Tuve. The scattering of protons by protons. *Phys. Rev.*, 53:239–246, Feb 1938.

[10] G. Breit, E. U. Condon, and R. D. Present. Theory of scattering of protons by protons. *Phys. Rev.*, 50:825–845, Nov 1936.

[11] Hideki Yukawa. On the interaction of elementary particles. *Proc.Phys.Math.Soc.Jap.*, 17:48–57, 1935.

[12] Wolfgang Pauli. *Meson theory of nuclear forces, Second ed.* New York : Interscience Publishers, 1946.

[13] Seth H. Neddermeyer and Carl D. Anderson. Note on the nature of cosmic-ray particles. *Phys. Rev.*, 51:884–886, May 1937.

[14] J. C. Street and E. C. Stevenson. New evidence for the existence of a particle of mass intermediate between the proton and electron. *Phys. Rev.*, 52:1003–1004, Nov 1937.

[15] C. M. G. Lattes, G. P. S. Occhialini, and C. F. Powell. Observations on the tracks of slow mesons in photographic emulsions. *Nature*, 160:453–456, Oct 1947.

[16] G. P. S. Occhialini and C. F. Powell. Nuclear disintegrations produced by slow charged particles of small mass. *Nature*, 159:186–190, Feb 1947.

[17] E. Gardner and C.M.G. Lattes. Production of mesons by the 184-inch berkeley cyclotron. *Science*, 107:270–271, Mar 1948.

[18] G. P. S. Occhialini and C. F. Powell. The artificial production of mesons. *Nature*, 161:551–552, Apr 1948.

[19] Mituo Taketani, Seitaro Nakamura, and Muneo Sasaki. On the method of the theory of nuclear forces. *Progress of Theoretical Physics*, 6(4):581–586, 1951.

[20] Junji Iwadare, Shoichiro Otsuki, Ryozo Tamagaki, and Wataro Watari. Two-nucleon problem with pion theoretical potential, I: Determination of coupling constant and deuteron problem. *Progress of Theoretical Physics*, 16(5):455–471, 1956.

[21] Junji Iwadare, Shoichiro Otsuki, Ryozo Tamagaki, and Wataro Watari. Determination of the pion coupling constant in nuclear forces. *Progress of Theoretical Physics*, 15(1):86–88, 1956.

[22] S. Machida, S. numa, and M. Taketani. On the fourth-order nuclear potential. *Progress of Theoretical Physics*, 6(5):904–905, 1951.

[23] M. Taketani, S. Machida, and S. numa. Meson theory of nuclear forces. *Progress of Theoretical Physics*, 6(4):638–639, 1951.

[24] Mitsuo Taketani, Shigeru Machida, and Shoroku O-numa. The meson theory of nuclear forces, I: The deuteron ground state and low energy neutron-proton scattering. *Progress of Theoretical Physics*, 7(1):45–56, 1952.

[25] Mituo Taketani, Seitaro Nakamura, and Muneo Sasaki. On the method of the theory of elementary particles. *Progress of Theoretical Physics*, 5(4):730–734, 1950.

[26] M. Taketani, S. numa, and S. Koide. On the nuclear forces and the ground state of deuteron. *Progress of Theoretical Physics*, 6(4):635–637, 1951.

[27] David Y. Wong. One-meson contribution to the deuteron quadrupole moment. *Phys. Rev. Lett.*, 2:406–407, May 1959.

[28] Norman K. Glendenning and Gustav Kramer. Nucleon-nucleon triplet-even potentials. *Phys. Rev.*, 126:2159–2168, Jun 1962.

[29] K. A. Brueckner and K. M. Watson. Nuclear forces in pseudoscalar meson theory. *Phys. Rev.*, 92:1023–1035, Nov 1953.

[30] R. Machleidt. The meson theory of nuclear forces and nuclear matter. , : , 1985.

[31] Abraham Klein. On the concept of potential in quantum field theory. *Progress of Theoretical Physics*, 20(3):257–266, 1958.

[32] J. L. Gammel and R. M. Thaler. Spin-orbit coupling in the proton-proton interaction. *Phys. Rev.*, 107:291–298, Jul 1957.

[33] J. L. Gammel and R. M. Thaler. Spin-orbit coupling in the neutron-proton interaction. *Phys. Rev.*, 107:1337–1340, Sep 1957.

[34] P. S. Signell and R. E. Marshak. Semiphenomenological two-nucleon potential. *Phys. Rev.*, 109:1229–1239, Feb 1958.

[35] B. C. Maglicc, L. W. Alvarez, A. H. Rosenfeld, and M. L. Stevenson. Evidence for a T=0 three-pion resonance. *Phys. Rev. Lett.*, 7:178–182, Sep 1961.

[36] C. Alff, D. Berley, D. Colley, N. Gelfand, U. Nauenberg, D. Miller, J. Schultz, J. Steinberger, T. H. Tan, H. Brugger, P. Kramer, and R. Plano. Production of pion resonances in π^+p interactions. *Phys. Rev. Lett.*, 9:322–324, Oct 1962.

[37] R. Machleidt, K. Holinde, and C. Elster. The Bonn meson exchange model for the nucleon nucleon interaction. *Phys.Rept.*, 149:1–89, 1987.

[38] Murray Gell-Mann. The eightfold way: A theory of strong interaction symmetry. CTSL-20, TID-12608, 1961.

[39] G Zweig. An $SU(3)$ model for strong interaction symmetry and its breaking; Version 1. Technical Report CERN-TH-401, CERN, Geneva, Jan 1964.

[40] NN-online. http://nn-online.org.

[41] INS DAC - Institute for Nuclear Studies Data Analysis Center. http://http://gwdac.phys.gwu.edu.

[42] Robert Jastrow. On charge independence and high energy scattering. *Phys. Rev.*, 79:389–389, Jul 1950.

[43] Robert Jastrow. On the nucleon-nucleon interaction. *Phys. Rev.*, 81:165–170, Jan 1951.

[44] Robert Jastrow. On the hard sphere model of the nucleon. *Phys. Rev.*, 81:636–636, Feb 1951.

[45] David Y. Wong and H. Pierre Noyes. Electrostatic corrections to nucleon-nucleon dispersion relations. *Phys. Rev.*, 126:1866–1872, Jun 1962.

[46] Leon Heller, Peter Signell, and N. R. Yoder. Charge symmetry, charge independence, and the nucleon-nucleon scattering lengths. *Phys. Rev. Lett.*, 13:577–579, Nov 1964.

[47] E. M. Henley and L. K. Morrison. Scattering lengths and charge independence. *Phys. Rev.*, 141:1489–1493, Jan 1966.

[48] S. N. Biswas, Aditya Kumar, and R. P. Saxena. Deviations from charge independence in $n - p$ and in $n - n$ scattering lengths by S-matrix methods. *Phys. Rev.*, 142:1141–1144, Feb 1966.

[49] J. L. Gammel, R. S. Christian, and R. M. Thaler. Calculation of phenomenological nucleon-nucleon potentials. *Phys. Rev.*, 105:311–319, Jan 1957.

[50] T. Hamada and I.D. Johnston. A potential model representation of two nucleon data below 315-MeV. *Nucl.Phys.*, 34:382–403, 1962.

[51] K. E. Lassila, M. H. Hull, H. M. Ruppel, F. A. McDonald, and G. Breit. Note on a nucleon-nucleon potential. *Phys. Rev.*, 126:881–882, Apr 1962.

[52] M. Lacombe, B. Loiseau, J. M. Richard, R. Vinh Mau, J. Côté, P. Pirès, and R. de Tourreil. Parametrization of the Paris N–N potential. *Phys. Rev. C*, 21:861–873, Mar 1980.

[53] Jr. Reid, Roderick V. Local phenomenological nucleon-nucleon potentials. *Annals Phys.*, 50:411–448, 1968.

[54] R. B. Wiringa, R. A. Smith, and T. L. Ainsworth. Nucleon-nucleon potentials with and without $\Delta(1232)$ degrees of freedom. *Phys. Rev. C*, 29:1207–1221, Apr 1984.

[55] R. B. Wiringa, V. G. J. Stoks, and R. Schiavilla. Accurate nucleon-nucleon potential with charge-independence breaking. *Phys. Rev. C*, 51:38–51, Jan 1995.

[56] V. G. J. Stoks, R. A. M. Klomp, C. P. F. Terheggen, and J. J. de Swart. Construction of high-quality NN potential models. *Phys. Rev. C*, 49:2950–2962, Jun 1994.

[57] R. Machleidt. High-precision, charge-dependent bonn nucleon-nucleon potential. *Phys. Rev. C*, 63:024001, Jan 2001.

[58] J.D. Walecka. Theoretical nuclear and subnuclear physics. *Oxford Stud.Nucl.Phys.*, 16:1–610, 1995.

[59] K. Holinde. The short range part of the NN interaction: quark - gluon versus meson exchange. *Nucl.Phys.*, A415:477–496, 1984.

[60] C. Elster and K. Holinde. NN scattering phase shifts: quark-gluon versus meson exchange. *Phys.Lett.*, B136:135–138, 1984.

[61] C. Elster and K. Holinde. Nucelon anti-nucleon interaction: quark-gluon versus meson exchange. *Phys.Lett.*, B149:293–298, 1984.

[62] G.Q. Liu, M. Swift, Anthony William Thomas, and K. Holinde. The role of nucleon structure in the NN interaction: Effects of pion exchange between quarks. *Nucl.Phys.*, A556:331–354, 1993.

[63] B. Ter Haar and R. Malfliet. Nucleons, mesons and deltas in nuclear matter. A relativistic Dirac-Bruckner approach. *Phys.Rept.*, 149:207–286, 1987.

[64] E.N.E. van Dalen, C. Fuchs, and Amand Faessler. The relativistic Dirac-Brueckner approach to asymmetric nuclear matter. *Nucl.Phys.*, A744:227–248, 2004.

[65] F. de Jong and H. Lenske. Asymmetric nuclear matter in the relativistic Bruckner Hartree-Fock approach. *Phys.Rev.*, C57:3099–3107, 1998.

[66] B. D. Day and R. B. Wiringa. Brueckner-Bethe and variational calculations of nuclear matter. *Phys. Rev. C*, 32:1057–1062, Sep 1985.

[67] J. Cugnon, P. Deneye, and A. Lejeune. Neutron matter properties in an extended Bruckner approach. *Z.Phys.*, A328:409–415, 1987.

[68] I. Bombaci and U. Lombardo. Asymmetric nuclear matter equation of state. *Phys. Rev. C*, 44:1892–1900, Nov 1991.

[69] M. Baldo, G. F. Burgio, and H.-J. Schulze. Hyperon stars in the Brueckner-Bethe-Goldstone theory. *Phys. Rev. C*, 61:055801, Apr 2000.

[70] I. Vidaña, A. Polls, A. Ramos, L. Engvik, and M. Hjorth-Jensen. Hyperon-hyperon interactions and properties of neutron star matter. *Phys. Rev. C*, 62:035801, Jul 2000.

[71] W. Zuo, A. Lejeune, U. Lombardo, and J.F. Mathiot. Microscopic three-body force for asymmetric nuclear matter. *Eur.Phys.J.*, A14:469–475, 2002.

[72] K. Sumiyoshi, K. Oyamatsu, and H. Toki. Neutron star profiles in the relativistic Bruckner-Hartree-Fock theory. *Nucl. Phys.*, A595:327–345, 1995.

[73] A. Akmal, V. R. Pandharipande, and D. G. Ravenhall. Equation of state of nucleon matter and neutron star structure. *Phys. Rev. C*, 58:1804–1828, Sep 1998.

[74] Abhishek Mukherjee and V. R. Pandharipande. Variational theory of hot nucleon matter. *Phys. Rev. C*, 75:035802, Mar 2007.

[75] A. Fabrocini and S. Fantoni. Correlated basis function results for the Argonne models of nuclear matter . *Physics Letters B*, 298(34):263 – 266, 1993.

[76] C. Bisconti, F. Arias de Saavedra, G. Co', and A. Fabrocini. Ground states of medium-heavy doubly-closed-shell nuclei in correlated-basis function theory. *Phys. Rev. C*, 73:054304, May 2006.

[77] Y. Dewulf, W. H. Dickhoff, D. Van Neck, E. R. Stoddard, and M. Waroquier. Saturation of nuclear matter and short-range correlations. *Phys. Rev. Lett.*, 90:152501, Apr 2003.

[78] T. Frick and H. Müther. Self-consistent solution to the nuclear many-body problem at finite temperature. *Phys. Rev. C*, 68:034310, Sep 2003.

[79] B. S. Pudliner, V. R. Pandharipande, J. Carlson, Steven C. Pieper, and R. B. Wiringa. Quantum Monte Carlo calculations of nuclei with $A \lesssim 7$. *Phys. Rev. C*, 56:1720–1750, Oct 1997.

[80] K.E. Schmidt and S. Fantoni. A quantum Monte Carlo method for nucleon systems. *Physics Letters B*, 446(2):99 – 103, 1999.

[81] J. Carlson, J. Morales, V. R. Pandharipande, and D. G. Ravenhall. Quantum Monte Carlo calculations of neutron matter. *Phys. Rev. C*, 68:025802, Aug 2003.

[82] S. Gandolfi, A. Yu. Illarionov, S. Fantoni, F. Pederiva, and K. E. Schmidt. Equation of state of superfluid neutron matter and the calculation of the S01 pairing gap. *Phys. Rev. Lett.*, 101:132501, Sep 2008.

[83] S. Gandolfi, A. Yu. Illarionov, K. E. Schmidt, F. Pederiva, and S. Fantoni. Quantum Monte Carlo calculation of the equation of state of neutron matter. *Phys. Rev. C*, 79:054005, May 2009.

[84] K. Hebeler and A. Schwenk. Chiral three-nucleon forces and neutron matter. *Phys. Rev. C*, 82:014314, Jul 2010.

[85] K. Hebeler, J. M. Lattimer, C. J. Pethick, and A. Schwenk. Constraints on neutron star radii based on chiral effective field theory interactions. *Phys. Rev. Lett.*, 105:161102, Oct 2010.

[86] Steven C. Pieper, V. R. Pandharipande, R. B. Wiringa, and J. Carlson. Realistic models of pion-exchange three-nucleon interactions. *Phys. Rev. C*, 64:014001, Jun 2001.

[87] M. B. Tsang, J. R. Stone, F. Camera, P. Danielewicz, S. Gandolfi, K. Hebeler, C. J. Horowitz, Jenny Lee, W. G. Lynch, Z. Kohley, R. Lemmon, P. Möller, T. Murakami, S. Riordan, X. Roca-Maza, F. Sammarruca, A. W. Steiner, I. Vidaña, and S. J. Yennello. Constraints on the symmetry energy and neutron skins from experiments and theory. *Phys. Rev. C*, 86:015803, Jul 2012.

[88] Anthony William Thomas and Wolfram Weise. *The structure of the nucleon.* Wiley-VCH Verlag Berlin, 2001.

[89] W. Greiner, S. Schramm, and E. Stein. *Quantum chromodynamics*. Springer-Verlag Berlin Heidelberg, 2002.

[90] Yuval Ne'eman. Derivation of strong interactions from a gauge invariance. *Nucl.Phys.*, 26:222–229, 1961.

[91] Samuel S.M.Wong. *Introductory nuclear physics*. Wiley-VCH Verlag GmbH & Co. KGaA, 1998.

[92] A. Hosaka and H. Toki. *Quarks, baryons and chiral symmetry*. World Scientific, 2001.

[93] Bertrand Delamotte. A hint of renormalization. *Am.J.Phys.*, 72:170–184, 2004.

[94] Alain Connes and Dirk Kreimer. Hopf algebras, renormalization and noncommutative geometry. *Commun.Math.Phys.*, 199:203–242, 1998.

[95] Dirk Kreimer. On the Hopf algebra structure of perturbative quantum field theories. *Adv.Theor.Math.Phys.*, 2:303–334, 1998.

[96] Alain Connes and Matilde Marcolli. *Noncommutative geometry, quantum fields and motives*. Providence, R.I. : American Mathematical Society, 2008.

[97] F. J. Dyson. Divergence of perturbation theory in quantum electrodynamics. *Phys. Rev.*, 85:631–632, Feb 1952.

[98] Charles Angas Hurst. Perturbation expansions in quantum field theory. *Rept.Math.Phys.*, 57:121–129, 2006.

[99] Charles Angas Hurst. An example of a divergent perturbation expansion in field theory. *Proc.Cambridge Phil.Soc.*, 48:625, 1952.

[100] Charles Angas Hurst. The enumeration of graphs in the Feynman-Dyson technique. *Proc.Roy.Soc.Lond.*, A214:44, 1952.

[101] David J. Gross and Frank Wilczek. Ultraviolet behavior of non-abelian gauge theories. *Phys. Rev. Lett.*, 30:1343–1346, Jun 1973.

[102] H. David Politzer. Reliable perturbative results for strong interactions? *Phys. Rev. Lett.*, 30:1346–1349, Jun 1973.

[103] Jerome I. Friedman and Henry W. Kendall. Deep inelastic electron scattering. *Ann.Rev.Nucl.Part.Sci.*, 22:203–254, 1972.

[104] Richard E. Taylor. Deep inelastic scattering: The early years. *Rev. Mod. Phys.*, 63:573–595, Jul 1991.

[105] Henry W. Kendall. Deep inelastic scattering: Experiments on the proton and the observation of scaling. *Rev. Mod. Phys.*, 63:597–614, Jul 1991.

[106] Jerome I. Friedman. Deep inelastic scattering: Comparisons with the quark model. *Rev. Mod. Phys.*, 63:615–627, Jul 1991.

[107] T. Massam. The quark hunters' progress. , : , 1968.

[108] R. Machleidt and D.R. Entem. Chiral effective field theory and nuclear forces. *Phys.Rept.*, 503:1–75, 2011.

[109] Kris Heyde. *Basic ideas and concepts in nuclear physics: An introductory approach*. Taylor & Francis, Inc., 2004.

[110] L.N. Savushkin and H. Toki. *The atomic nucleus as a relativistic system*. Springer-Verlag Berlin Heidelberg, 2004.

[111] N.K. Glendenning. *Compact stars: Nuclear physics, particle physics, and general relativity*. Springer-Verlag, New York, Berlin, Heidelberg., 1997.

[112] C.J. Horowitz, E.F. Brown, Y. Kim, W.G. Lynch, R. Michaels, et al. A way forward in the study of the symmetry energy: experiment, theory, and observation. *arXiv*, 1401.5839:1, 2014.

[113] C. J. Horowitz and J. Piekarewicz. Neutron radii of ^{208}Pb and neutron stars. *Phys. Rev. C*, 64:062802, Nov 2001.

[114] C. J. Horowitz and J. Piekarewicz. Neutron star structure and the neutron radius of ^{208}Pb. *Phys. Rev. Lett.*, 86:5647–5650, Jun 2001.

[115] J. R. Stone, N. J. Stone, and S. A. Moszkowski. Incompressibility in finite nuclei and nuclear matter. *Phys. Rev. C*, 89:044316, Apr 2014.

[116] J.P. Blaizot. Nuclear compressibilities. *Physics Reports*, 64(4):171 – 248, 1980.

[117] J. Treiner, H. Krivine, O. Bohigas, and J. Martorell. Nuclear incompressibility: From finite nuclei to nuclear matter. *Nuclear Physics A*, 371(2):253 – 287, 1981.

[118] R.C. Nayak, J.M. Pearson, M. Farine, P. Gleissl, and M. Brack. Leptodermous expansion of finite-nucleus incompressibility. *Nuclear Physics A*, 516(1):62 – 76, 1990.

[119] B. Alex Brown. Neutron radii in nuclei and the neutron equation of state. *Phys. Rev. Lett.*, 85:5296–5299, Dec 2000.

[120] Satoshi Yoshida and Hiroyuki Sagawa. Neutron skin thickness and equation of state in asymmetric nuclear matter. *Phys. Rev. C*, 69:024318, Feb 2004.

[121] S. Typel and B. Alex Brown. Neutron radii and the neutron equation of state in relativistic models. *Phys. Rev. C*, 64:027302, Jun 2001.

[122] R.J. Furnstahl. Neutron radii in mean field models. *Nucl.Phys.*, A706:85–110, 2002.

[123] M. Baldo, C. Maieron, P. Schuck, and X. Vinas. Low densities in nuclear and neutron matters and in the nuclear surface. *Nucl.Phys.*, A736:241–254, 2004.

[124] Z. H. Li and H.-J. Schulze. Neutron star structure with modern nucleonic three-body forces. *Phys. Rev. C*, 78:028801, Aug 2008.

[125] T.W. Donnelly, J. Dubach, and Ingo Sick. Isospin dependences in parity violating electron scattering. *Nucl.Phys.*, A503:589, 1989.

[126] C. J. Horowitz, S. J. Pollock, P. A. Souder, and R. Michaels. Parity violating measurements of neutron densities. *Phys. Rev. C*, 63:025501, Jan 2001.

[127] M N Harakeh and A Van der Woude. *Giant resonances: fundamental high-frequency modes of nuclear excitation.* Oxford studies in nuclear physics. Oxford Univ. Press, Oxford, 2002.

[128] Zhongyu Ma, Nguyen Van Giai, Hiroshi Toki, and Marcelle L'Huillier. Compressibility of nuclear matter and breathing mode of finite nuclei in relativistic random phase approximation. *Phys. Rev. C*, 55:2385–2388, May 1997.

[129] D. Vretenar, T. Nikšić, and P. Ring. A microscopic estimate of the nuclear matter compressibility and symmetry energy in relativistic mean-field models. *Phys. Rev. C*, 68:024310, Aug 2003.

[130] G. Colò, N. Van Giai, J. Meyer, K. Bennaceur, and P. Bonche. Microscopic determination of the nuclear incompressibility within the nonrelativistic framework. *Phys. Rev. C*, 70:024307, Aug 2004.

[131] B. K. Agrawal, S. Shlomo, and V. Kim Au. Nuclear matter incompressibility coefficient in relativistic and nonrelativistic microscopic models. *Phys. Rev. C*, 68:031304, Sep 2003.

[132] N. Ryezayeva, T. Hartmann, Y. Kalmykov, H. Lenske, P. von Neumann-Cosel, V. Yu. Ponomarev, A. Richter, A. Shevchenko, S. Volz, and J. Wambach. Nature of low-energy dipole strength in nuclei: The case of a resonance at particle threshold in ^{208}Pb. *Phys. Rev. Lett.*, 89:272502, Dec 2002.

[133] I. Poltoratska, P. von Neumann-Cosel, A. Tamii, T. Adachi, C.A. Bertulani, et al. Pygmy dipole resonance in ^{208}Pb. *Phys.Rev.*, C85:041304, 2012.

[134] A. Zilges, S. Volz, M. Babilon, T. Hartmann, P. Mohr, et al. Concentration of electric dipole strength below the neutron separation energy in N=82 nuclei. *Phys.Lett.*, B542:43, 2002.

[135] P. Adrich, A. Klimkiewicz, M. Fallot, K. Boretzky, T. Aumann, D. Cortina-Gil, U. Datta Pramanik, Th. W. Elze, H. Emling, H. Geissel, M. Hellström, K. L. Jones, J. V. Kratz, R. Kulessa, Y. Leifels, C. Nociforo, R. Palit, H. Simon, G. Surówka, K. Sümmerer, and W. Waluś. Evidence for pygmy and giant dipole resonances in ^{130}Sn and ^{132}Sn. *Phys. Rev. Lett.*, 95:132501, Sep 2005.

[136] A. Klimkiewicz, N. Paar, P. Adrich, M. Fallot, K. Boretzky, T. Aumann, D. Cortina-Gil, U. Datta Pramanik, Th. W. Elze, H. Emling, H. Geissel, M. Hellström, K. L. Jones, J. V. Kratz, R. Kulessa, C. Nociforo, R. Palit, H. Simon, G. Surówka, K. Sümmerer, D. Vretenar, and W. Waluś. Nuclear symmetry energy and neutron skins derived from pygmy dipole resonances. *Phys. Rev. C*, 76:051603, Nov 2007.

[137] D. Savran, M. Fritzsche, J. Hasper, K. Lindenberg, S. Müller, V. Yu. Ponomarev, K. Sonnabend, and A. Zilges. Fine structure of the pygmy dipole resonance in ^{136}Xe. *Phys. Rev. Lett.*, 100:232501, Jun 2008.

[138] O. Wieland, A. Bracco, F. Camera, G. Benzoni, N. Blasi, S. Brambilla, F. C. L. Crespi, S. Leoni, B. Million, R. Nicolini, A. Maj, P. Bednarczyk, J. Grebosz, M. Kmiecik, W. Meczynski, J. Styczen, T. Aumann, A. Banu, T. Beck, F. Becker, L. Caceres, P. Doornenbal, H. Emling, J. Gerl, H. Geissel, M. Gorska, O. Kavatsyuk, M. Kavatsyuk, I. Kojouharov, N. Kurz, R. Lozeva, N. Saito, T. Saito, H. Schaffner, H. J. Wollersheim, J. Jolie, P. Reiter, N. Warr, G. deAngelis, A. Gadea, D. Napoli, S. Lenzi, S. Lunardi, D. Balabanski, G. LoBianco, C. Petrache, A. Saltarelli, M. Castoldi, A. Zucchiatti, J. Walker, and A. Bürger. Search for the pygmy dipole resonance in ^{68}Ni at 600MeV/nucleon. *Phys. Rev. Lett.*, 102:092502, Mar 2009.

[139] D. Vretenar, N. Paar, P. Ring, and G.A. Lalazissis. Collectivity of the low lying dipole strength in relativistic random phase approximation. *Nucl.Phys.*, A692:496–517, 2001.

[140] D. Sarchi, P.F. Bortignon, and G. Col. Dipole states in stable and unstable nuclei. *Physics Letters B*, 601(12):27 – 33, 2004.

[141] P.-G. Reinhard and W. Nazarewicz. Information content of the low-energy electric dipole strength: Correlation analysis. *Phys. Rev. C*, 87:014324, Jan 2013.

[142] P.-G. Reinhard and W. Nazarewicz. Information content of a new observable: The case of the nuclear neutron skin. *Phys. Rev. C*, 81:051303, May 2010.

[143] J. Piekarewicz, B. K. Agrawal, G. Colò, W. Nazarewicz, N. Paar, P.-G. Reinhard, X. Roca-Maza, and D. Vretenar. Electric dipole polarizability and the neutron skin. *Phys. Rev. C*, 85:041302, Apr 2012.

[144] J. Piekarewicz. Pygmy resonances and neutron skins. *Phys. Rev. C*, 83:034319, Mar 2011.

[145] J. Piekarewicz. Pygmy dipole resonance as a constraint on the neutron skin of heavy nuclei. *Phys. Rev. C*, 73:044325, Apr 2006.

[146] Andrea Carbone, Gianluca Colò, Angela Bracco, Li-Gang Cao, Pier Francesco Bortignon, Franco Camera, and Oliver Wieland. Constraints on the symmetry energy and neutron skins from pygmy resonances in ^{68}Ni and ^{132}Sn. *Phys. Rev. C*, 81:041301, Apr 2010.

[147] Christian Fuchs. Kaon production in heavy ion reactions at intermediate energies. *Prog.Part.Nucl.Phys.*, 56:1–103, 2006.

[148] Pawel Danielewicz, Roy Lacey, and William G. Lynch. Determination of the equation of state of dense matter. *Science*, 298:1592–1596, 2002.

[149] Bao-An Li, Lie-Wen Chen, and Che Ming Ko. Recent progress and new challenges in isospin physics with heavy-ion reactions. *Phys.Rept.*, 464:113–281, 2008.

[150] Brian D. Serot and John Dirk Walecka. The relativistic nuclear many body problem. *Adv.Nucl.Phys.*, 16:1–327, 1986.

[151] Brian D. Serot and John Dirk Walecka. Recent progress in quantum hadrodynamics. *Int.J.Mod.Phys.*, E6:515–631, 1997.

[152] Y.K. Gambhir, editor. *Mean field description of nuclei*. Narosa Pub., 2006.

[153] L. I. Schiff. Nonlinear meson theory of nuclear forces. I. neutral scalar mesons with point-contact repulsion. *Phys. Rev.*, 84:1–9, Oct 1951.

[154] L. I. Schiff. Nonlinear meson theory of nuclear forces. II. Nonlinearity in the meson-nucleon coupling. *Phys. Rev.*, 84:10–11, Oct 1951.

[155] M. H. Johnson and E. Teller. Classical field theory of nuclear forces. *Phys. Rev.*, 98:783–787, May 1955.

[156] Hans-Peter Duerr. Relativistic effects in nuclear forces. *Phys. Rev.*, 103:469–480, Jul 1956.

[157] J.D. Walecka. A theory of highly condensed matter. *Annals Phys.*, 83:491–529, 1974.

[158] R. J. Furnstahl, Robert J. Perry, and Brian D. Serot. Two-loop corrections for nuclear matter in the walecka model. *Phys. Rev. C*, 40:321–353, Jul 1989.

[159] Norman K. Glendenning. Vacuum polarization effects on nuclear matter and neutron stars. *Nucl.Phys.*, A493:521, 1989.

[160] Pierre A.M. Guichon, Hrayr H. Matevosyan, N. Sandulescu, and Anthony William Thomas. Physical origin of density dependent force of the skyrme type within the quark meson coupling model. *Nucl.Phys.*, A772:1–19, 2006.

[161] J. Rikovska-Stone, Pierre A.M. Guichon, Hrayr H. Matevosyan, and Anthony William Thomas. Cold uniform matter and neutron stars in the quark-mesons-coupling model. *Nucl.Phys.*, A792:341–369, 2007.

[162] É. Massot and G. Chanfray. Relativistic chiral Hartree-Fock description of nuclear matter with constraints from nucleon structure and confinement. *Phys. Rev. C*, 78:015204, Jul 2008.

[163] J. Hu, H. Toki, W. Wen, and H. Shen. The role of the form factor and short-range correlation in the relativistic Hartree-Fock model for nuclear matter. *The European Physical Journal A*, 43(3):323–334, 2010.

[164] J. Boguta and A.R. Bodmer. Relativistic calculation of nuclear matter and the nuclear surface. *Nucl.Phys.*, A292:413–428, 1977.

[165] A.R. Bodmer. Relativistic mean field theory of nuclei with a vector meson self-interaction. *Nucl.Phys.*, A526:703–721, 1991.

[166] Y. Sugahara and H. Toki. Relativistic mean field theory for unstable nuclei with nonlinear sigma and omega terms. *Nucl.Phys.*, A579:557–572, 1994.

[167] G. A. Lalazissis, J. König, and P. Ring. New parametrization for the Lagrangian density of relativistic mean field theory. *Phys. Rev. C*, 55:540–543, Jan 1997.

[168] G. A. Lalazissis, T. Nikšić, D. Vretenar, and P. Ring. New relativistic mean-field interaction with density-dependent meson-nucleon couplings. *Phys. Rev. C*, 71:024312, Feb 2005.

[169] B. G. Todd-Rutel and J. Piekarewicz. Neutron-rich nuclei and neutron stars: A new accurately calibrated interaction for the study of neutron-rich matter. *Phys. Rev. Lett.*, 95:122501, Sep 2005.

[170] Simona Malace, David Gaskell, Douglas W. Higinbotham, and Ian Cloet. The Challenge of the EMC Effect: existing data and future directions. *Int. J. Mod. Phys.*, E23:1430013, 2014.

[171] P. N. Bogolioubov. Sur un modle quarks quasi-indpendants. *Ann. Inst. Henri Poincare*, 8:163, 1967.

[172] A. Chodos, R. L. Jaffe, K. Johnson, and C. B. Thorn. Baryon structure in the bag theory. *Phys. Rev. D*, 10:2599–2604, Oct 1974.

[173] A. Chodos, R. L. Jaffe, K. Johnson, C. B. Thorn, and V. F. Weisskopf. New extended model of hadrons. *Phys. Rev. D*, 9:3471–3495, Jun 1974.

[174] Anthony William Thomas. Chiral symmetry and the bag model: A new starting point for nuclear physics. *Adv.Nucl.Phys.*, 13:1–137, 1984.

[175] Thomas A. DeGrand, R.L. Jaffe, K. Johnson, and J.E. Kiskis. Masses and other parameters of the light hadrons. *Phys.Rev.*, D12:2060, 1975.

[176] A. Hosaka and H. Toki. Chiral bag model for the nucleon. *Phys. Rept.*, 277:65–188, 1996.

[177] H. Shen and H. Toki. Quark mean field model for nuclear matter and finite nuclei. *Phys. Rev. C*, 61:045205, Mar 2000.

[178] H. Toki, U. Meyer, A. Faessler, and R. Brockmann. Quark mean field model for nucleons in nuclei. *Phys. Rev.*, C58:3749–3752, 1998.

[179] H. Shen and H. Toki. Study of Lambda hypernuclei in the quark mean field model. *Nucl. Phys.*, A707:469–476, 2002.

[180] J. N. Hu, A. Li, H. Toki, and W. Zuo. Extended quark mean-field model for neutron stars. *Phys. Rev.*, C89(2):025802, 2014.

[181] Pierre A.M. Guichon. A possible quark mechanism for the saturation of nuclear matter. *Phys.Lett.*, B200:235, 1988.

[182] Pierre A.M. Guichon, Koichi Saito, Evgenii N. Rodionov, and Anthony William Thomas. The role of nucleon structure in finite nuclei. *Nucl.Phys.*, A601:349–379, 1996.

[183] G. Krein, Anthony William Thomas, and Kazuo Tsushima. Fock terms in the quark meson coupling model. *Nucl.Phys.*, A650:313–325, 1999.

[184] K. Saito and Anthony William Thomas. A quark - meson coupling model for nuclear and neutron matter. *Phys.Lett.*, B327:9–16, 1994.

[185] Koichi Saito. Relationship between quark meson coupling model and quantum hadrodynamics. *Prog.Theor.Phys.*, 108:609–614, 2002.

[186] P. A. M. Guichon and A. W. Thomas. Quark structure and nuclear effective forces. *Phys. Rev. Lett.*, 93:132502, Sep 2004.

[187] K. Saito, Kazuo Tsushima, and Anthony William Thomas. Nucleon and hadron structure changes in the nuclear medium and impact on observables. *Prog.Part.Nucl.Phys.*, 58:1–167, 2007.

[188] Pierre A.M. Guichon, Anthony W. Thomas, and Kazuo Tsushima. Binding of hypernuclei in the latest quark-meson coupling model. *Nucl.Phys.*, A814:66–73, 2008.

[189] S.L. Shapiro and S.A. Teukolsky. *Black holes, white dwarfs, and neutron stars: The physics of compact objects*. John-Wiley & Sons, Inc., 1983.

[190] James B. Hartle. *Gravity : an introduction to Einstein's general relativity*. San Francisco : Addison-Wesley, 2003.

[191] P. Haensel, A.Y. Potekhin, and D.G. Yakovlev. *Neutron stars 1: Equation of state and structure*. Springer-Verlag New York, 2007.

[192] J.M. Lattimer and M. Prakash. The physics of neutron stars. *Science*, 304:536–542, 2004.

[193] James M. Lattimer and Maddapa Prakash. Neutron star observations: Prognosis for equation of state constraints. *Phys.Rept.*, 442:109–165, 2007.

[194] James M. Lattimer and M. Prakash. What a two solar mass neutron star really means. *arXiv*, 1012.3208:1, 2010.

[195] W. Baade and F. Zwicky. Remarks on super-novae and cosmic rays. *Phys. Rev.*, 46:76–77, Jul 1934.

[196] A. Hewish, S. J. Bell, J. D. H. Pilkington, P. F. Scott, and R. A. Collins. Observation of a rapidly pulsating radio source. *Nature*, 217:709–713, 1968.

[197] Andrew W. Steiner, James M. Lattimer, and Edward F. Brown. The equation of state from observed masses and radii of neutron stars. *Astrophys.J.*, 722:33–54, 2010.

[198] Valery Suleimanov, Juri Poutanen, Mikhail Revnivtsev, and Klaus Werner. Neutron star stiff equation of state derived from cooling phases of the x-ray burster 4U 1724-307. *Astrophys.J.*, 742:122, 2011.

[199] Andrew W. Steiner, James M. Lattimer, and Edward F. Brown. The neutron star mass-radius relation and the equation of state of dense matter. *Astrophys.J.*, 765:L5, 2013.

[200] James M. Lattimer and Yeunhwan Lim. Constraining the symmetry parameters of the nuclear interaction. *Astrophys.J.*, 771:51, 2013.

[201] James M. Lattimer and Andrew W. Steiner. Neutron star masses and radii from quiescent low-Mass x-ray binaries. *Astrophys.J.*, 784:123, 2014.

[202] Paul Demorest, Tim Pennucci, Scott Ransom, Mallory Roberts, and Jason Hessels. Shapiro delay measurement of a two solar mass neutron star. *Nature*, 467:1081–1083, 2010.

[203] John Antoniadis, Paulo C.C. Freire, Norbert Wex, Thomas M. Tauris, Ryan S. Lynch, et al. A massive pulsar in a compact relativistic binary. *Science*, 340:6131, 2013.

[204] James B. Hartle. Slowly rotating relativistic stars. I. Equations of structure. *ApJ.*, 150:1005, 1967.

[205] Kip S. Hartle, James B.; Thorne. Slowly rotating relativistic stars. II. Models for neutron stars and supermassive stars. *ApJ,*, 153:807, 1968.

[206] Nikolaos Stergioulas. Rotating stars in relativity. *Living Rev.Rel.*, 6:3, 2003.

[207] A. Bauswein and H.-T. Janka. Measuring neutron-star properties via gravitational waves from neutron-star mergers. *Phys. Rev. Lett.*, 108:011101, Jan 2012.

[208] A. Bauswein, H.-T. Janka, K. Hebeler, and A. Schwenk. Equation-of-state dependence of the gravitational-wave signal from the ring-down phase of neutron-star mergers. *Phys. Rev. D*, 86:063001, Sep 2012.

[209] A. Bauswein, R. Oechslin, and H.-T. Janka. Discriminating strange star mergers from neutron star mergers by gravitational-wave measurements. *Phys. Rev. D*, 81:024012, Jan 2010.

[210] A. Bauswein, N. Stergioulas, and H.-T. Janka. Revealing the high-density equation of state through binary neutron star mergers. *Phys. Rev. D*, 90:023002, Jul 2014.

[211] A.E. Broderick, M. Prakash, and J.M. Lattimer. Effects of strong magnetic fields in strange baryonic matter. *Phys.Lett.*, B531:167–174, 2002.

[212] A. Broderick, M. Prakash, and J.M. Lattimer. The equation of state of neutron star matter in strong magnetic fields. *Astrophys.J.*, 537:351, 2000.

[213] Christian Y. Cardall, Madappa Prakash, and James M. Lattimer. Effects of strong magnetic fields on neutron star structure. *Astrophys.J.*, 554:322–339, 2001.

[214] P. Yue and H. Shen. Neutron star matter in the quark-meson coupling model in strong magnetic fields. *Phys.Rev.*, C74:045807, 2006.

[215] P. Yue and H. Shen. Quark-meson coupling model for antikaon condensation in neutron star matter with strong magnetic fields. *Phys.Rev.*, C77:045804, 2008.

[216] P. Yue, F. Yang, and H. Shen. Properties of hyperonic matter in strong magnetic fields. *Phys.Rev.*, C79:025803, 2009.

[217] A. Rabhi, P.K. Panda, and C. Providencia. Warm and dense stellar matter under strong magnetic fields. *Phys.Rev.*, C84:035803, 2011.

[218] M. Zeilik and S. A. Gregory. *Introductory astronomy and astrophysics*. Saunders college publishing, 1998.

[219] Richard C. Tolman. Static solutions of Einstein's field equations for spheres of fluid. *Phys. Rev.*, 55:364–373, Feb 1939.

[220] J. R. Oppenheimer and G. M. Volkoff. On massive neutron cores. *Phys. Rev.*, 55:374–381, Feb 1939.

[221] A. G. Cameron. Neutron star models. *ApJ.*, 130:884, 1959.

[222] Edward Farhi and R. L. Jaffe. Strange matter. *Phys. Rev. D*, 30:2379–2390, Dec 1984.

[223] Edward Witten. Cosmic Separation of Phases. *Phys.Rev.*, D30:272–285, 1984.

[224] D. J. Scalapino. π^- condensate in dense nuclear matter. *Phys. Rev. Lett.*, 29:386–388, Aug 1972.

[225] A. B. Migdal. π condensation in nuclear matter. *Phys. Rev. Lett.*, 31:257–260, Jul 1973.

[226] D.B. Kaplan and A.E. Nelson. Strange goings on in dense nucleonic matter. *Phys.Lett.*, B175:57–63, 1986.

[227] P. Haensel and M. Proszynski. On the neutron star transition to a pion-condensed configuration. *Physics Letters B*, 96(34):233 – 237, 1980.

[228] P. Haensel and M. Proszynski. Pion condensation in cold dense matter and neutron stars. *Astrophys.J.*, 258:306–320, 1982.

[229] Arkady B. Migdal, A.I. Chernoutsan, and I.N. Mishustin. Pion condensation and dynamics of neutron stars. *Phys.Lett.*, B83:158–160, 1979.

[230] S. Barshay, G. Vagradov, and G.E. Brown. Possibility of a phase transition to a pion condensate in neutron stars. *Phys.Lett.*, B43:359–361, 1973.

[231] D.B. Kaplan and A.E. Nelson. Kaon condensation in dense matter. *Nucl.Phys.*, A479:273, 1988.

[232] Jens O. Andersen. Bose-Einstein condensation in dense quark matter. *Nucl.Phys.*, A820:171C–174C, 2009.

[233] J. Carlson, H. Heiselberg, and V. R. Pandharipande. Kaon condensation in dense matter. *Phys. Rev. C*, 63:017603, Dec 2000.

[234] Jens O. Andersen. Pion and kaon condensation at finite temperature and density. *Phys. Rev. D*, 75:065011, Mar 2007.

[235] Jens O. Andersen and Lars E. Leganger. Kaon condensation in the color-flavor-locked phase of quark matter, the Goldstone theorem, and the 2PI Hartree approximation. *Nucl.Phys.*, A828:360–389, 2009.

[236] D. P. Menezes, P. K. Panda, and C. Providência. Kaon condensation in the quark-meson coupling model and compact stars. *Phys. Rev. C*, 72:035802, Sep 2005.

[237] C. Y. Ryu, C. H. Hyun, S. W. Hong, and B. T. Kim. Kaon condensation and composition of neutron star matter in a modified quark-meson coupling model. *Phys. Rev. C*, 75:055804, May 2007.

[238] V.K. Magas, J. Yamagata-Sekihara, S. Hirenzaki, E. Oset, and A. Ramos. Latest results for the antikaon–nucleon optical potential. *Few-Body Systems*, 50(1-4):343–345, 2011.

[239] E Oset, M Kaskulov, E Hernandez, A Ramos, V K Magas, J Yamagata-Sekihara, S Hirenzaki, D Gamermann, R Molina, L Tolos, and L Roca. Selected topics on hadrons in nuclei. *Journal of Physics: Conference Series*, 312(2):022006, 2011.

[240] A.W. Thomas, D.L. Whittenbury, J.D. Carroll, K. Tsushima, and J.R. Stone. Equation of state of dense matter and consequences for neutron stars. *EPJ Web Conf.*, 63:03004, 2013.

[241] S. Weissenborn, D. Chatterjee, and J. Schaffner-Bielich. Hyperons and massive neutron stars: Vector repulsion and SU(3) symmetry. *Phys. Rev. C*, 85:065802, Jun 2012.

[242] S. Weissenborn, D. Chatterjee, and J. Schaffner-Bielich. Hyperons and massive neutron stars: The role of hyperon potentials. *Nucl.Phys.*, A881:62–77, 2012.

[243] S. Weissenborn, D. Chatterjee, and J. Schaffner-Bielich. Hyperons and massive neutron stars: Vector repulsion and strangeness. *Nucl.Phys.*, A914:421–426, 2013.

[244] D. L. Whittenbury, J. D. Carroll, A. W. Thomas, K. Tsushima, and J. R. Stone. Quark-meson coupling model, nuclear matter constraints, and neutron star properties. *Phys. Rev. C*, 89:065801, Jun 2014.

[245] Tsuyoshi Miyatsu, Tetsuya Katayama, and Koichi Saito. Effects of Fock term, tensor coupling and baryon structure variation on a neutron star. *Phys.Lett.*, B709:242–246, 2012.

[246] A. Bouyssy, J.-F. Mathiot, Nguyen Van Giai, and S. Marcos. Relativistic description of nuclear systems in the Hartree-Fock approximation. *Phys. Rev. C*, 36:380–401, Jul 1987.

[247] L. D. Miller. Elastic electron scattering formalism for relativistic nuclear models. *Phys. Rev. C*, 14:706–717, Aug 1976.

[248] L. D. Miller. State-dependent equivalent local potentials for the Dirac equation. *Phys. Rev. C*, 12:710–712, Aug 1975.

[249] L. D. Miller. Exchange potentials in relativistic Hartree-Fock theory of closed-shell nuclei. *Phys. Rev. C*, 9:537–554, Feb 1974.

[250] C.J. Horowitz and Brian D. Serot. Properties of nuclear and neutron matter in a relativistic hartree-fock theory. *Nuclear Physics A*, 399(2):529 – 562, 1983.

[251] Stefan Scherer and Matthias R. Schindler. A primer for chiral perturbation theory. *Lect.Notes Phys.*, 830:pp.1–338, 2012.

[252] J. J. de Swart. The octet model and its Clebsch-Gordan coefficients. *Rev. Mod. Phys.*, 35:916–939, Oct 1963.

[253] M. Kaku. *Quantum field theory: A modern introduction.* Oxford Univ. Press, 1993.

[254] Michael E. Peskin and Daniel V. Schroeder. *An Introduction to quantum field theory.* Westview Press, 1995.

[255] Tsuyoshi Miyatsu and Koichi Saito. Neutron star properties in the chiral quark-meson coupling model. *Few Body Syst.*, 54:1591–1594, 2013.

[256] J. Beringer et al. Review of Particle Physics (RPP). *Phys.Rev.*, D86:010001, 2012.

[257] R.A. Williams and C. Puckett-Truman. Extended vector meson dominance model for the baryon octet electromagnetic form-factors. *Phys.Rev.*, C53:1580–1588, 1996.

[258] Thomas A. Rijken, M.M. Nagels, and Yasuo Yamamoto. Baryon-baryon interactions: Nijmegen extended-soft-core models. *Prog.Theor.Phys.Suppl.*, 185:14–71, 2010.

[259] Michel Farine, J.M. Pearson, and F. Tondeur. Nuclear-matter incompressibility from fits of generalized Skyrme force to breathing-mode energies . *Nuclear Physics A*, 615(2):135 – 161, 1997.

[260] I. Tews, T. Krger, K. Hebeler, and A. Schwenk. Neutron matter at next-to-next-to-next-to-leading order in chiral effective field theory. *Phys.Rev.Lett.*, 110(3):032504, 2013.

[261] K. Hebeler and R.J. Furnstahl. Neutron matter based on consistently evolved chiral three-nucleon interactions. *Phys.Rev.*, C87(3):031302, 2013.

[262] Isaac Vidaña, Constan ça Providência, Artur Polls, and Arnau Rios. Density dependence of the nuclear symmetry energy: A microscopic perspective. *Phys. Rev. C*, 80:045806, Oct 2009.

[263] S. Gandolfi, J. Carlson, and Sanjay Reddy. Maximum mass and radius of neutron stars, and the nuclear symmetry energy. *Phys. Rev. C*, 85:032801, Mar 2012.

[264] K. Hebeler, J.M. Lattimer, C.J. Pethick, and A. Schwenk. Constraints on neutron star radii based on chiral effective field theory interactions. *Phys.Rev.Lett.*, 105:161102, 2010.

[265] Pawel Danielewicz, Roy Lacey, and William G. Lynch. Determination of the equation of state of dense matter. *Science*, 298:1592–1596, 2002.

[266] J.R. Stone and P.-G. Reinhard. The Skyrme interaction in finite nuclei and nuclear matter. *Prog.Part.Nucl.Phys.*, 58:587–657, 2007.

[267] M. Dutra, O. Lourenço, J. S. Sá Martins, A. Delfino, J. R. Stone, and P. D. Stevenson. Skyrme interaction and nuclear matter constraints. *Phys. Rev. C*, 85:035201, Mar 2012.

[268] M. Dutra, O. Loureno, B.V. Carlson, A. Delfino, D.P. Menezes, et al. Relativistic mean-field models and nuclear matter constraints. *AIP Conf.Proc.*, 1529:238, 2013.

[269] Hiroyuki Sagawa, Satoshi Yoshida, Guo-Mo Zeng, Jian-Zhong Gu, and Xi-Zhen Zhang. Isospin dependence of incompressibility in relativistic and nonrelativistic mean field calculations. *Phys. Rev. C*, 76:034327, Sep 2007.

[270] Lie-Wen Chen, Bao-Jun Cai, Che Ming Ko, Bao-An Li, Chun Shen, et al. High-order effects on the incompressibility of isospin asymmetric nuclear matter. *Phys.Rev.*, C80:014322, 2009.

[271] Gordon Baym, Christopher Pethick, and Peter Sutherland. The ground state of matter at high densities: Equation of state and stellar models. *Astrophys.J.*, 170:299–317, 1971.

[272] Richard C. Tolman. Effect of inhomogeneity on cosmological models. *Proceedings of the National Academy of Sciences*, 20(3):169–176, 1934.

[273] F.S. Kitaura, Hans-Thomas Janka, and W. Hillebrandt. Explosions of O-Ne-Mg cores, the Crab supernova, and subluminous type II-P supernovae. *Astron.Astrophys.*, 450:345–350, 2006.

[274] Philipp Podsiadlowski, J.D.M. Dewi, P. Lesaffre, J.C. Miller, W.G. Newton, et al. The Double pulsar J0737-3039: Testing the neutron star equation of state. *Mon.Not.Roy.Astron.Soc.*, 361:1243–1249, 2005.

[275] J.D. Carroll. The quark-meson coupling model as a description of dense matter. *AIP Conf.Proc.*, 1374:205–207, 2011.

[276] Sebastien Guillot, Mathieu Servillat, Natalie A. Webb, and Robert E. Rutledge. Measurement of the radius of neutron stars with high S/N quiescent low-mass x-ray binaries in globular clusters. *Astrophys.J.*, 772:7, 2013.

[277] E. Massot, J. Margueron, and G. Chanfray. On the maximum mass of hyperonic neutron stars. *Europhys.Lett.*, 97:39002, 2012.

[278] Tetsuya Katayama, Tsuyoshi Miyatsu, and Koichi Saito. EoS for massive neutron stars. *Astrophys.J.Suppl.*, 203:22, 2012.

[279] Tsuyoshi Miyatsu and Koichi Saito. Effect of gluon and pion exchanges on hyperons in nuclear matter. *Prog.Theor.Phys.*, 122:1035–1044, 2010.

[280] J. Schaffner-Bielich. Strangeness in compact stars. *Nucl.Phys.*, A835:279–286, 2010.

[281] Fridolin Weber. Strange quark matter and compact stars. *Prog.Part.Nucl.Phys.*, 54:193–288, 2005.

[282] Kota Masuda, Tetsuo Hatsuda, and Tatsuyuki Takatsuka. Hadron-quark crossover and massive hybrid stars. *PTEP*, 2013(7):073D01, 2013.

[283] Kota Masuda, Tetsuo Hatsuda, and Tatsuyuki Takatsuka. Hadron-quark crossover and massive hybrid stars with strangeness. *Astrophys.J.*, 764:12, 2013.

[284] David Blaschke, David E. Alvarez Castillo, Sanjin Benic, Gustavo Contrera, and Rafal Lastowiecki. Nonlocal PNJL models and heavy hybrid stars. *PoS*, ConfinementX:249, 2012.

[285] Yoichiro Nambu and G. Jona-Lasinio. Dynamical model of elementary particles based on an analogy with superconductivity. I. *Phys.Rev.*, 122:345–358, 1961.

[286] Yoichiro Nambu and G. Jona-Lasinio. Dynamical model of elementary particles based on an analogy with superconductivity. II. *Phys.Rev.*, 124:246–254, 1961.

[287] John Bardeen, L.N. Cooper, and J.R. Schrieffer. Theory of superconductivity. *Phys.Rev.*, 108:1175–1204, 1957.

[288] John Bardeen, L.N. Cooper, and J.R. Schrieffer. Microscopic theory of superconductivity. *Phys.Rev.*, 106:162, 1957.

[289] R.M. Davidson and E. Ruiz Arriola. Parton distributions functions of pion, kaon and eta pseudoscalar mesons in the NJL model. *Acta Phys.Polon.*, B33:1791–1808, 2002.

[290] S. Lawley, Wolfgang Bentz, and Anthony William Thomas. The phases of isospin asymmetric matter in the two flavor NJL model. *Phys.Lett.*, B632:495–500, 2006.

[291] S. Lawley, Wolfgang Bentz, and Anthony William Thomas. Nucleons, nuclear matter and quark matter: A unified NJL approach. *J.Phys.*, G32:667–680, 2006.

[292] F. Neumann, M. Buballa, and M. Oertel. Mixed phases of color superconducting quark matter. *Nucl.Phys.*, A714:481–501, 2003.

[293] Stefan B. Rüster, Verena Werth, Michael Buballa, Igor A. Shovkovy, and Dirk H. Rischke. Phase diagram of neutral quark matter: Self-consistent treatment of quark masses. *Phys. Rev. D*, 72:034004, Aug 2005.

[294] D. Blaschke, S. Fredriksson, H. Grigorian, A. M. Öztaş, and F. Sandin. Phase diagram of three-flavor quark matter under compact star constraints. *Phys. Rev. D*, 72:065020, Sep 2005.

[295] T. Klahn, D. Blaschke, F. Sandin, C. Fuchs, A. Faessler, H. Grigorian, G. Ropke, and J. Trumper. Modern compact star observations and the quark matter equation of state. *Phys. Lett.*, B654:170–176, 2007.

[296] Shotaro Imai, Hiroshi Toki, and Wolfram Weise. Quark-Hadron Matter at Finite Temperature and Density in a Two-Color PNJL model. *Nucl. Phys.*, A913:71–102, 2013.

[297] D Blaschke, T Klähn, R astowiecki, and F Sandin. How strange are compact star interiors? *Journal of Physics G: Nuclear and Particle Physics*, 37(9):094063, September 2010.

[298] T. Klahn, D. Blaschke, and F. Weber. Exploring hybrid star matter at NICA and FAIR. *Phys.Part.Nucl.Lett.*, 9:484–487, 2012.

[299] T. Klähn, R. Łastowiecki, and D. Blaschke. Implications of the measurement of pulsars with two solar masses for quark matter in compact stars and heavy-ion collisions: A Nambu-Jona-Lasinio model case study. *Phys. Rev. D*, 88:085001, Oct 2013.

[300] C.H. Lenzi, A.S. Schneider, C. Providencia, and R.M. Marinho. Compact stars with a quark core within NJL model. *Phys.Rev.*, C82:015809, 2010.

[301] Fridolin Weber, Milva Orsaria, and Rodrigo Negreiros. Impact of rotation on the structure and composition of neutron stars. , : , 2013.

[302] M Orsaria, H Rodrigues, F Weber, and G A Contrera. Quark-hybrid matter in the cores of massive neutron stars. *Phys. Rev. D*, 87(2):23001, January 2013.

[303] M Orsaria, H Rodrigues, F Weber, and G A Contrera. Quark deconfinement in high-mass neutron stars. *Physical Review C*, 89(1):015806, January 2014.

[304] Klaus Schertler, Stefan Leupold, and Jurgen Schaffner-Bielich. Neutron stars and quark phases in the NJL model. *Phys.Rev.*, C60:025801, 1999.

[305] Peng-Cheng Chu, Xin Wang, Lie-Wen Chen, and Mei Huang. Quark magnetar in the three-flavor Nambu–Jona–Lasinio model with vector interactions and a magnetized gluon potential. *Phys. Rev. D*, 91:023003, Jan 2015.

[306] U. Vogl and W. Weise. The Nambu and Jona Lasinio model: Its implications for hadrons and nuclei. *Prog.Part.Nucl.Phys.*, 27:195–272, 1991.

[307] S.P. Klevansky. The Nambu-Jona-Lasinio model of quantum chromodynamics. *Rev.Mod.Phys.*, 64:649–708, 1992.

[308] Tetsuo Hatsuda and Teiji Kunihiro. QCD phenomenology based on a chiral effective Lagrangian. *Phys.Rept.*, 247:221–367, 1994.

[309] G. Ripka. Introduction to Nambu-Jona-Lasinio models of hadrons. *Czech.J.Phys.*, 46:721–750, 1996.

[310] G. Ripka. *Quarks bound by chiral fields: The quark-structure of the vacuum and of light mesons and baryons*. Oxford Univ. Press, 1997.

[311] Michael Buballa. NJL model analysis of quark matter at large density. *Phys.Rept.*, 407:205–376, 2005.

[312] Alexander A. Osipov, Brigitte Hiller, Alex H. Blin, and Joao da Providencia. Effects of eight-quark interactions on the hadronic vacuum and mass spectra of light mesons. *Annals Phys.*, 322:2021–2054, 2007.

[313] Alexander A. Osipov, Brigitte Hiller, and Joao da Providencia. Multi-quark interactions with a globally stable vacuum. *Phys.Lett.*, B634:48–54, 2006.

[314] Dietmar Ebert, Thorsten Feldmann, and Hugo Reinhardt. Extended NJL model for light and heavy mesons without q - anti-q thresholds. *Phys.Lett.*, B388:154–160, 1996.

[315] Wolfgang Bentz and Anthony William Thomas. The stability of nuclear matter in the Nambu-Jona-Lasinio model. *Nucl.Phys.*, A696:138–172, 2001.

[316] R. L. Stratonovich. . *Doklady Akad. Nauk S.S.S.R.*, 115:1097, 1957. [translation: Soviet Phys. Doklady 2, 416 (1958)].

[317] J. Hubbard. Calculation of partition functions. *Phys. Rev. Lett.*, 3:77–78, Jul 1959.

[318] N. Ishii, W. Bentz, and K. Yazaki. Faddeev approach to the nucleon in the Nambu-Jona-Lasinio (NJL) model. *Phys.Lett.*, B301:165–169, 1993.

[319] N. Ishii, W. Bentz, and K. Yazaki. Solution of the relativistic three quark Faddeev equation in the Nambu-Jona-Lasinio (NJL) model. *Phys.Lett.*, B318:26–31, 1993.

[320] N. Ishii, W. Bentz, and K. Yazaki. Baryons in the NJL model as solutions of the relativistic Faddeev equation. *Nucl.Phys.*, A587:617–656, 1995.

[321] Julian Schwinger. On gauge invariance and vacuum polarization. *Phys. Rev.*, 82:664–679, Jun 1951.

[322] C. M. Bender and S. A. Orszag. *Advanced mathematical methods for scientists and engineers*. 1978.

[323] M. Oertel, M. Buballa, and J. Wambach. Meson loop effects in the NJL model at zero and nonzero temperature. *Phys.Atom.Nucl.*, 64:698–726, 2001.

[324] R. Kaminski, G. Mennessier, and S. Narison. Gluonium nature of the $\sigma/f_0(600)$ from its coupling to $K\bar{K}$. *Phys.Lett.*, B680:148–153, 2009.

[325] R.J. Crewther and Lewis C. Tunstall. Origin of $\Delta I = 1/2$ rule for kaon decays: QCD infrared fixed point. *arXiv*, 1203.1321:1, 2012.

[326] R.J. Crewther and Lewis C. Tunstall. Infrared fixed point in the strong running coupling: Unraveling the $\Delta I = 1/2$ puzzle in K-decays. *Mod.Phys.Lett.*, A28:1360010, 2013.

[327] J. Crewther, R. and Lewis C. Tunstall. $\Delta I = 1/2$ rule for kaon decays derived from QCD infrared fixed point. *Phys. Rev. D*, 91:034016, Feb 2015.

[328] R.J. Crewther and Lewis C. Tunstall. Chiral-scale perturbation theory about an infrared fixed point. *EPJ Web Conf.*, 73:03006, 2014.

[329] R.J. Crewther. Status of the U(1) problem. *Riv.Nuovo Cim.*, 2N8:63–117, 1979.

[330] R.J. Crewther. Chirality selection rules and the U(1) problem. *Phys.Lett.*, B70:349, 1977.

[331] R.J. Crewther. Effects of topological charge in gauge theories. *Acta Phys.Austriaca Suppl.*, 19:47–153, 1978.

[332] Veljko Dmitrasinovic and H. Toki. Light hadron spectra in the constituent quark model with the Kobayashi-Kondo-Maskawa-'t Hooft effective UA(1) symmetry breaking interaction. *Annals Phys.*, 321:355–401, 2006.

[333] E. E. Salpeter and H. A. Bethe. A relativistic equation for bound-state problems. *Phys. Rev.*, 84:1232–1242, Dec 1951.

[334] Thomas Hell and Wolfram Weise. Dense baryonic matter: Constraints from recent neutron star observations. *Phys. Rev. C*, 90:045801, Oct 2014.

[335] GSL project contributors. GSL - GNU scientific library - GNU project - free software foundation (FSF). http://www.gnu.org/software/gsl/, 2010.

[336] Shinji Maedan. Influence of current mass on the spatially inhomogeneous chiral condensate. *Prog.Theor.Phys.*, 123:285–302, 2010.

[337] Nino M. Bratovic, Tetsuo Hatsuda, and Wolfram Weise. Role of vector interaction and axial anomaly in the PNJL modeling of the QCD phase diagram. *Phys.Lett.*, B719:131–135, 2013.

[338] Thomas Hell, Kouji Kashiwa, and Wolfram Weise. Impact of vector-current interactions on the QCD phase diagram. *J.Mod.Phys.*, 4:644–650, 2013.

[339] A.V. Friesen, Yu. L. Kalinovsky, and V.D. Toneev. Impact of the vector interaction on the phase structure of QCD matter. *arXiv*, 1412.6872: , 2014.

[340] A. Rosenhauer and E.F. Staubo. Hybrid stars and the equation of state. *Nuclear Physics B - Proceedings Supplements*, 24(2):156–159, 1991.

[341] David Blaschke, Thomas Klähn, and Fredrik Sandin. Equation of state at high densities and modern compact star observations. *Journal of Physics G: Nuclear and Particle Physics*, 35(1):014051, January 2008.

[342] B. K. Agrawal. Equations of state and stability of color-superconducting quark matter cores in hybrid stars. *Phys. Rev. D*, 81:023009, Jan 2010.

[343] Luca Bonanno and Armen Sedrakian. Composition and stability of hybrid stars with hyperons and quark color-superconductivity. *Astronomy & Astrophysics*, 539:A16, March 2012.

[344] C. H. Lenzi and G. Lugones. Hybrid stars in the light of the massive pulsar PSR J16142230. *The Astrophysical Journal*, 759(1):57, 2012.

[345] Domenico Logoteta, Constança Providência, and Isaac Vidaña. Formation of hybrid stars from metastable hadronic stars. *Physical Review C*, 88(5):055802, November 2013.

[346] S. Plumari, G. F. Burgio, V. Greco, and D. Zappalà. Quark matter in neutron stars within the field correlator method. *Physical Review D*, 88(8):083005, October 2013.

[347] Sanjin Benić. Heavy hybrid stars from multi-quark interactions. *The European Physical Journal A*, 50(7):111, July 2014.

[348] Thomas Klahn and Tobias Fischer. Vector interaction enhanced bag model for astrophysical applications. *arXiv*, 1503.07442: , 2015.

[349] Norman K. Glendenning. First order phase transitions with more than one conserved charge: Consequences for neutron stars. *Phys.Rev.*, D46:1274–1287, 1992.

[350] Wolfgang Bentz, T. Horikawa, N. Ishii, and Anthony William Thomas. Phase transition from nuclear matter to color superconducting quark matter. *Nucl. Phys.*, A720:95–130, 2003.

[351] J.D. Carroll, D.B. Leinweber, A.G. Williams, and A.W. Thomas. Phase transition from QMC hyperonic matter to deconfined quark matter. *Phys.Rev.*, C79:045810, 2009.

[352] A. G. Grunfeld, D. B. Blaschke, D. Gómez Dumm, T. Klähn, and N. N. Scoccola. Nonlocality effects in the phase diagram of neutral quark matter. *Physics of Particles and Nuclei*, 39(7):1040–1043, December 2008.

[353] Jun Xu, Lie-Wen Chen, Che Ming Ko, and Bao-An Li. Isospin- and momentum-dependent effective interactions for the baryon octet and the properties of hybrid stars. *Physical Review C*, 81(5):055803, May 2010.

[354] Guo Yun Shao. Evolution of proto-neutron stars with the hadron-quark phase transition. *Physics Letters, Section B: Nuclear, Elementary Particle and High-Energy Physics*, 704(4):343–346, 2011.

[355] Domenico Logoteta, Ignazio Bombaci, Constança Providência, and Isaac Vidaña. Chiral model approach to quark matter nucleation in neutron stars. *Physical Review D*, 85(2):023003, January 2012.

[356] Domenico Logoteta, Constança Providência, Isaac Vidaña, and Ignazio Bombaci. Quark matter nucleation with a microscopic hadronic equation of state. *Physical Review C*, 85(5):055807, May 2012.

[357] Tsuyoshi Miyatsu, Myung-ki Cheoun, and Koichi Saito. Equation of state for neutron stars with hyperons and quarks in relativistic Hartree-Fock approximation. *arXiv*, 1506.05552:1–37, 2015.

[358] M Asakawa and T Hatsuda. What thermodynamics tells us about the QCD plasma. *Phys. Rev. D*, 55(7):4488–4491, 1997.

[359] D.E. Alvarez Castillo, Sanjin Benić, David Blaschke, and Rafa astowiecki. Crossover transition to quark matter in heavy hybrid stars. *Acta Physica Polonica B Proceedings Supplement*, 7(1):203, 2014.

[360] Toru Kojo, Philip D. Powell, Yifan Song, and Gordon Baym. Phenomenological QCD equation of state for massive neutron stars. *Physical Review D*, 91(4):045003, February 2015.

[361] H. Heiselberg, C. J. Pethick, and E. F. Staubo. Quark matter droplets in neutron stars. *Phys. Rev. Lett.*, 70:1355–1359, 1993.

[362] N. K. Glendenning and S. Pei. Crystalline structure of the mixed confined - deconfined phase in neutron stars. *Phys. Rev.*, C52:2250–2253, 1995.

[363] N. K. Glendenning. Phase transitions and crystalline structures in neutron star cores. *Phys. Rept.*, 342:393–447, 2001.

[364] Tomoki Endo, Toshiki Maruyama, Satoshi Chiba, and Toshitaka Tatsumi. Hadron-quark matter phase transition in neutron stars. In *International summer school and workshop on hot points in astrophysics and cosmology Dubna, Russia, august 2-13, 2004*, 2005.

[365] Toshiki Maruyama, Toshitaka Tatsumi, Dmitri N. Voskresensky, Tomonori Tanigawa, Tomoki Endo, and Satoshi Chiba. Finite size effects on kaonic pasta structures. *Phys. Rev.*, C73:035802, 2006.

[366] Toshiki Maruyama, Toshitaka Tatsumi, Dmitri .N. Voskresensky, Tomonori Tanigawa, and Satoshi Chiba. Nuclear pasta structures and the charge screening effect. *Phys. Rev.*, C72:015802, 2005.

[367] Toshiki Maruyama, Satoshi Chiba, Hans-Josef Schulze, and Toshitaka Tatsumi. Hadron-quark mixed phase in hyperon stars. *Physical Review D*, 76(12):123015, December 2007.

[368] C. Bernard, T. Burch, C. DeTar, J. Osborn, Steven Gottlieb, E. B. Gregory, D. Toussaint, U. M. Heller, and R. Sugar. QCD thermodynamics with three flavors of improved staggered quarks. *Phys. Rev. D*, 71:034504, Feb 2005.

[369] Y. Aoki, G. Endrodi, Z. Fodor, S.D. Katz, and K.K. Szabo. The order of the quantum chromodynamics transition predicted by the standard model of particle physics. *Nature*, 443:675–678, 2006.

[370] M. Cheng, N. H. Christ, S. Datta, J. van der Heide, C. Jung, F. Karsch, O. Kaczmarek, E. Laermann, R. D. Mawhinney, C. Miao, P. Petreczky, K. Petrov, C. Schmidt, and T. Umeda. Transition temperature in QCD. *Phys. Rev. D*, 74:054507, Sep 2006.

[371] A. Bazavov, T. Bhattacharya, M. Cheng, C. DeTar, H.-T. Ding, Steven Gottlieb, R. Gupta, P. Hegde, U. M. Heller, F. Karsch, E. Laermann, L. Levkova, S. Mukherjee, P. Petreczky, C. Schmidt, R. A. Soltz, W. Soeldner, R. Sugar, D. Toussaint, W. Unger, and P. Vranas. Chiral and deconfinement aspects of the QCD transition. *Phys. Rev. D*, 85:054503, Mar 2012.

[372] J.D. Carroll. *Applications of the octet baryon quark-meson coupling model to hybrid stars*. PhD thesis, University of Adelaide, 2009.

[373] B. Friedman and V.R. Pandharipande. Hot and cold, nuclear and neutron matter. *Nuclear Physics A*, 361(2):502 – 520, 1981.

[374] K. Tsubakihara, H. Maekawa, H. Matsumiya, and A. Ohnishi. Λ hypernuclei and neutron star matter in a chiral SU(3) relativistic mean field model with a logarithmic potential. *Phys. Rev. C*, 81:065206, Jun 2010.

[375] Manuel E. Carrillo-Serrano, Ian C. Cloët, and Anthony W. Thomas. Su(3)-flavor breaking in octet baryon masses and axial couplings. *Phys. Rev. C*, 90:064316, Dec 2014.

[376] Joseph I. Kapusta. *Finite temperature field theory*. Cambridge Univ. Press., 1989.

[377] R.J. Rivers. *Path integral methods in quantum field theory*. Cambridge Univ. Press., 1987.

[378] M.S. Swanson. *Path integrals and quantum processes*. New York : Academic Press, 1992.

[379] Brigitte Hiller, Alexander A. Osipov, Veronique Bernard, and Alex H. Blin. Functional integral approaches to the bosonization of effective multi-quark interactions with $U_{\rm A}(1)$ breaking. *SIGMA*, 2:026, 2006.

[380] Wolfgang Bentz, T. Horikawa, N. Ishii, and Anthony William Thomas. Description of nucleons, nuclear matter and quark matter in an effective quark theory. *Prog.Theor.Phys.Suppl.*, 151:176–180, 2003.

[381] Manuel E. Carrillo-Serrano, Ian C. Clot, and Anthony W. Thomas. SU(3)-flavour breaking in octet baryon masses and axial couplings. *Phys.Rev.*, C90:064316, 2014.

[382] Sarah Howie. *A unified approach to nuclear matter and quark matter*. PhD thesis, University of Adelaide, Department of physics, 2006.